UNIVERSITÀ DEGLI STUDI FIRENZE

DOTTORATO DI RICERCA IN
Scienze Chimiche

CICLO XXVI

COORDINATORE Prof. Andrea Goti

Waste polymeric materials valorization through microwave assisted pyrolysis

Settore Scientifico Disciplinare CHIM/04

Dottorando
Dott. *Undri Andrea*

Tutore
Prof. *Frediani Piero*

Coordinatore
Prof. Goti Andrea

Anni 2011/2013

This work is for
my best supporters,
my family

Contents

List of Figures

List of Tables

List of Equations

Acknowledgements

I would like to thank Cooperativa Autotrasportatori Fiorentini – CAF Scral and Fondazione Ente Cassa di Risparmio di Pistoia e Pescia for financial support;.

I would particularly like to thank my PhD supervisor Piero Frediani and every member of the research group of industrial chemistry at Department of Chemistry – University of Florence, Luca Rosi, Marco Frediani, and my colleague for great support and scientific contribution to this thesis.

I am very grateful to Franco Berruti, Cedric Briens, Mamdouh Abou-Zaid, and the people at ICFAR (Institute for Chemicals and Fuels from Alternative Resources) - Western University, London, Canada, for hosting me during a fruitful period of scientific collaboration focused on development of an analytical method for bio-oil characterization.

Many thanks also to Maurizio Passaponti of University of Florence for CHN analysis and his glassware masterpieces.

Abstract

Microwave assisted pyrolysis (MAP) was exploited to convert several classes of waste polymers into a solid, a liquid, and a gas with promising application as energy, power, and chemical sources. The polymeric materials tested were: tires, high density poly(ethylene) (HDPE), poly(propylene) (PP), poly(styrene) (PS), multilayer packaging beverage (WMP), wood pellets (WP), poly(lactic acid) (PLA), and corn-derived plastic bags (CDP).

Pyrolysis experiments were carried out in a batch laboratory scale reactor, using a microwave (MW) oven operating at 2.45 GHz, an energy output up to 6KW, and for some pyrolysis a fractionating system, directly connected to the pyrolysis oven. The presence of a fractionating system minimized the influence of different MW powers enhancing the residence time and usually improving the quality of the liquid product.

MAP of tire might be run without the addition of a MW absorber. The liquid obtained showed a reduced density (from 0.92 to 0.88 g/cm^3), and viscosity (from 3.92 to 1.25 cP) when working with the fractionating system. Furthermore aromatic and olefinic compounds were formed in high amount. Different tire affected the MAP results: Tires containing a large amount of aromatics (styrene copolymers) were pyrolyzed faster than tire containing large amount of natural rubber. X-ray diffraction of solid from MAP of tire showed two different crystalline forms of ZnS, spharelite or wurtzite present due to the different pyrolysis condition. The presence of these compounds suggested that tires were heated to a temperature higher than the usually accounted.

MAP of polyolefins, HDPE, PP, and PS was performed using different MW absorbers (tire, carbon, or Fe) and MW power, obtaining a high quality liquid fraction with tailoring properties. From HDPE a mixture of linear alkanes, the corresponding 1-alkenes, and a very low amount of aromatics was obtained. On the contrary liquids from MAP of PP contained a mixture of methyl branched alkanes and alkenes, some aromatics and dienes. From MAP of PS a clear and low viscosity liquids were always collected (yield 91.6 wt%) together with low amount of gas (3.0 wt %) and solid (0.9 wt %). Using a MW power of 3 KW the

styrene in the liquid was increased up to 65.98 %.

MAP of WMP might by run with or without a MW absorber, and five products were always collected: char, gas, unscratched Al, and two liquid fractions. The organic liquid phase contained large amount of hydrocarbons, useful as fuel or the source of chemicals. The other liquid phase contained large amount of water and oxygenated organic compounds, such as acetic acid, 2-hydroxypropan-2-one and levoglucosan.

MAP of WP might be run without a MW absorber but the pyrolysis could not be completed in a short time. WP were converted into a char which preserved their former shape and a two phase liquid. These latter phases were characterized using an innovative chromatographic methodology.

MAP of PLA was performed using different MW absorbers (tire, carbon, or Fe) and MW power, obtaining a liquid rich in lactide (the cyclic dimer of lactic acid) and other oxygenated hydrocarbons. The collected lactide was enantiopure and it was collected, separate, and directly purified from the liquid. Up to 9 wt% of initial PLA was recovered as L-lactide.

MAP CDP was performed using different MW absorbers (carbon or Fe) and MW power, obtaining a liquid and large amount of gas accordingly to the pyrolysis conditions. The liquid after centrifugation was separate in three phases, upper, medium, and lower. Medium fractions were mainly composed of water (70 wt%), acids, alcohols, and anydrosugars and their pyrolysis products. Upper and lower fractions showed close properties and composition except that the lower fraction was a wax. Indeed the lower fraction was composed of oligomers and the upper phase was composed by the pyrolyzed products of these oligomers. It contained large amount of aromatic acid and phthalates and their derivatives.

1. Introduction

Polymers are well-established constituent of almost any object from everyday life to professional uses. In the 20th century their wide exploitation has been reached due to key characteristics of plastic-made items such as great adaptability of properties, low energy demand for production, and low final price. In late '80s due to these features plastics overcame steel volumetric production for the first time in history. [1]

Nowadays our lifestyle will not be possible without polymers, or rather great changes of it will be necessary. In this polymer related society plastic items are produced from raw chemical feedstock, used for whatever application, and disposed in various ways, as expected. Indeed living matter for a sound and healthy society should be the preservation and valorization of its energy, matter, and "environment" feedstock otherwise this actual lifestyle is hardly sustainable.

The ceaseless claim for raw materials and energy, together with large production of wastes are the two faces of the same coin. Plastics require petroleum or biomasses derived monomer together with energy for their synthesis. So it is possible to say that plastics store up matter and energy used for their production. At the end of their life plastic-made items are disposed and their matter and energy contents could be lost if they are not properly valorized. So far a closed loop life-cycle for a plastic item must be achieved (Figure 1.1)

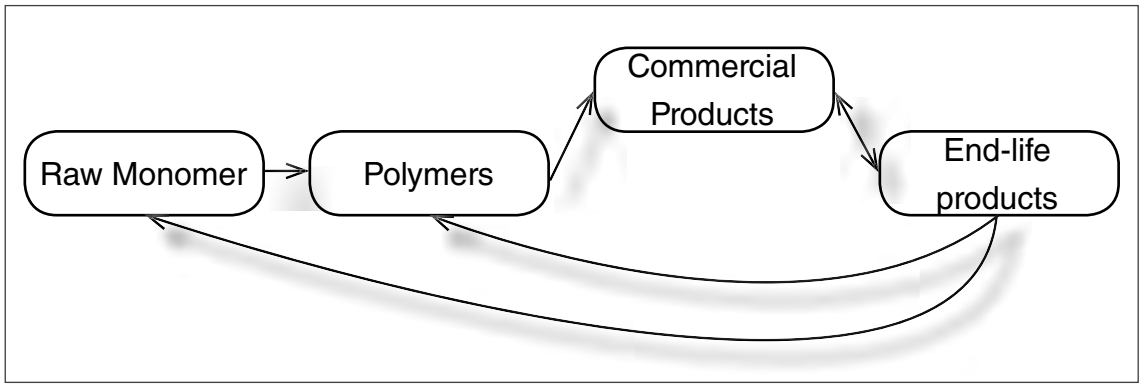

Figure 1.1. Ideal closed loop cycle for plastic items.

Waste plastics should be the source of matter and/or energy, instead of merely waste, for renewed products to minimize the use of fresh raw material.

Many efforts are bestowed on waste valorization through reuse and recycling processes. In the next sections are addressed the features of the main polymers actually produced together with the technologies available for their disposal. A more detailed review is reported for pyrolysis processes because pyrolysis is a promising technology and its study is the main subject of this work.

1.1. Main polymers

Polymers are macromolecules made of repeating structural units, from few hundreds to thousands units per each molecule itself. Aside from this general definition with “polymer” is outlined a wide-range of compounds. So far many classifications are possible when speaking of polymers, anyway a first distinction can be done between natural and synthetic polymers.

Natural polymers are parts of our everyday life from very ancient time; such as: cellulose, natural rubber, wool, silk, amber, polysaccharides, and ribonucleic acids; even if it is far from being complete.

Synthetic polymers also comprise an extremely broad number of different macromolecules even if obtained from the same monomer; some of the main classes are listed: poly(ethylene) (PE), poly(propylene) (PP), poly(vinylchloride) (PVC), poly(styrene) (PS), poly(ethylene terephthalate) (PET), poly(urethane) (PUR), poly(lactic acid) (PLA), and poly(carbonate) (PC).

Polymers in both classes are seldom used in item manufacturing as pure macromolecules but more frequently with the addition of inorganic/organic compounds or mixed/blended with other materials accordingly to desired final properties and application. For instance any PVC contains always different amount of phthalates as plasticizers. Tires are even more complex items because they are realized using different polymers, inorganics, and metal wires. The list could be far much longer than this.

All these polymers have large market share and in Table 1.1 are listed the 2011 European production. In 2011 the turnover increases for European polymer market and it is worthy of note an increment of 0.3% even if the financial crisis was spreading.[2]

Table 1.1. 2011 European productions of the main polymer classes.

Polymer	Production ($\times 10^9$ Kg)	Production (%)
PE	13.6	29
PP	8.9	19
PVC	5.2	11
PS	3.5	7.5
PET	3.1	6.5
PUR	3.3	7
Others	9.4	20
TOTAL	**47**	**100**

In the following sections a brief description of some of the previously cited polymers is reported. A detailed description of their synthesis and characterization can be found in the literature reported in each section.

1.1.1. Poly(ethylene): Production and use

Ethylene polymers enclose a large number of PE plastics which could include other alkenes monomer, as minor compounds, into their structure. These PEs are synthetized through radical or catalytic polymerizations. According to the polymerization reaction completely different PEs could be obtained. Branching degree is used as a discriminating parameters for PEs classification.

High pressure polymerization processes led to spontaneous branch formation which could be linear or branched alkyl groups. This PE is called low density poly(ethylene), LDPE, its branches vary also within the same PE molecule from methyl group to thousand carbon atoms.

Catalytic polymerization of ethylene produces PE polymers without branches at all, it is widely known as high density poly(ethylene), HDPE. Catalyzed polymerization can be used also to introduce branching intentionally, even with total control on the branching distribution, by polymerizing ethylene together with low amount of terminal alkenes. Among these the most produced PE is linear low density poly(ethylene), LLDPE. In Figure 1.2 is reported a schematic structure of these three cited PEs, the main features are maximized to enhance differences among them.

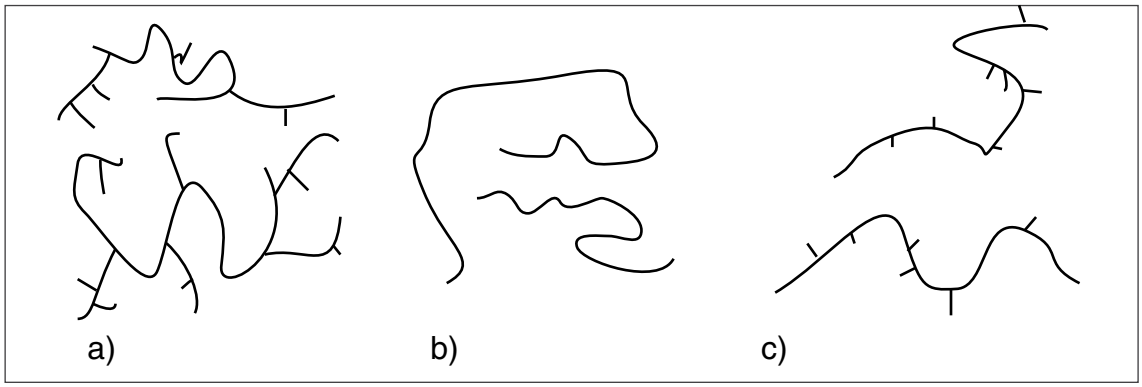

Figure 1.2. Schematic structure of PE. a) LDPE; b) HDPE; c) LLDPE.

LDPE and LLDPE are white translucent solids and rather flexible; as films they are transparent and the white color is slightly perceptible. However HDPE is a more rigid, white opaque solid and it forms film with turbid appearance.

PE is not soluble in any solvent at room temperature, but above its melting point it becomes soluble in aromatics and chlorinated hydrocarbons. It may also swell in some solvent like xylenes. In Table 1.2 are listed some of the main properties of PEs.

Table 1.2. Properties of LDPE, LLDPE, and HDPE

Property	LDPE	LLDPE	HDPE
Density (Kg/m^3)	924.3	922.0	961.0
Crystallinity (%)	40	40	67
Temperature of fusion (K)	383	395	404
M_w	200,000	158,100	136,300
M_n	44,200	35,800	18,400
Tensile rupture strength (MPa)	12.0	25.3	21.1
Elongation at ropture (%)	653	811	906

A brief list of the several polymerization technologies is reported below.

- Polymerization in supercritical ethylene: it is carried out at high ethylene pressure (60 – 350 MPa) and at a temperature (473 – 623 K), above PE melting point, the mixture of supercritical ethylene and molten PE work as polymerization medium. This process can be done with radical initiators (oxygen or organic peroxides), Ziegler catalysts, and metallocene catalysts; it allows to synthetize copolymers with polar monomers.
- Polymerization in solution: aliphatic, aromatic and chlorinated solvent together with Ziegler and/or metallocene-based catalysts are employed in this process. A draw-back is the solvent removal at the end of polymerization.
- Slurry polymerization: this process shows high versatility and convenience. It is the first commercial polymerization process for HDPE and it is performed in hydrocarbon slurry (usually light alkane).
- Gas phase polymerization: Ziegler or metallocene supported over a polymeric matrix can be used as catalyst in this process. The supported catalyst forms a bed inside gas-phase reactor and it is mechanically agitated or a fluidized-bed technique is employed.

PE properties, such as density, crystallinity, and molecular weight, may be adjusted following few means. Temperature controls density in free radical polymerization of LDPE and molecular weight in radical polymerization and with Philips catalyst. Molecular hydrogen can act as chain transfer agent and it may be used to control the molecular weight in Ziegler catalysis. Post polymerization reactions can modify PE physical properties such as stiffness, hardness, and impact strength.[3]

HDPE, LDPE, and LLDPE are used in several applications and the main market areas are briefly listed below. Worthy of note is the difference market of each PE: film for LDPE and LLDPE (usually sold in the same market) and structural application for HDPE.

- Film: LDPE is the preferred packaging material due to its transparency,

toughness, and adaptability to contents shape. HDPE can be processed but the final appearance is not usually accepted by final users. LDPE is produced by film blowing process at 433- 453 K. Apart for packaging issues LDPE films are used for impermeable or stabilizing membranes in civil engineering constructions. Additives are used such as UV stabilizer in finished product.

- Extrusion coating: LDPE is used for coating purpose of cardboard, paper and aluminum for multi-layer packaging, and for low level impurities applications.[4]
- Blow-molding: HDPE is actually the preferred material for containers because it merges stress crack resistance with higher rigidity than LDPE, so low bottle weight is obtained. They are used for detergent, milk, but also fuel and solvent storage and transportation.
- Injection molding: it is used for a large variety of products such as caps, lids, housewares, toys, and industrial containers. LDPE and HDPE are both used. LLDPE can be used only if they have narrow molecular mass distribution.
- Extrusion, pipe: the use for pipes is one of the few engineering applications where a continuous stress is applied. Indeed it is used for water and natural gas distribution systems. They are manufactured with HDPE.
- Extrusion, wire and cable insulation: LDPE is used as insulator for high frequency and telephone cables due to its dielectric properties.

1.1.2. Poly(propylene): Production and use

Nowadays propene derived polymers are widely used due to monomer low price and appealing finish product properties.[5]

PP is produced in three type accordingly to PP tacticity: isotactic (is the most produced PP, tough semi-crystalline material used as engineering plastic), syndiotactic (semi-crystalline, used as engineering material), and atactic (amorphous material used as binder for plastic and inorganics in construction industry); detailed description is reported in Figure 1.3.

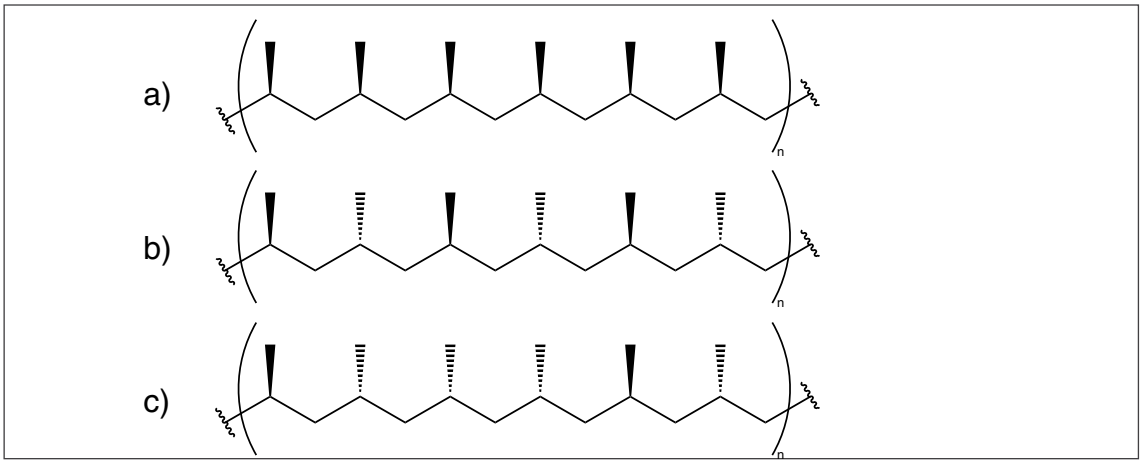

Figure 1.3. Three classes of PP: a) isotactic; b) syndiotactic; c) atactic.

Two catalytic systems are actually used for isotactic PP synthesis: based on

$TiCl_4$ supported (Ziegler-Natta), and metallocene catalyst. Syndiotactic PP is produced only through metallocene catalysis.

PP can be obtained with various technologies; the main two are briefly described below:

- Polymerization in slurry: two approaches are actually in use; the first one uses propene as reaction medium. While the second uses a non-reactive hydrocarbon as diluent.
- Polymerization in gas-phase: fluidized bed gas-phase technology employs either supported Ziegler-Natta or metallocene catalyst.

Isotactic PP is a rigid semi-crystalline plastic with a density of 0.903 g/cm^3 and a melting point of 438 K. It is less stiff but shows higher tensile properties than HDPE. Isotactic PP is used as competing material in other engineering thermoplastics, such as acrylonitrile-butadiene-styrene rubber (ABS).

PP obtained with metallocene catalysis showed small fraction of chemical defects.

Syndiotactic PP is a rigid semi-crystalline plastic with a density of 0.88 g/cm^3. It has a low melting point (403 K), crystallinity and tensile strength than isotactic PP. However, syndiotactic PP has exceptional softness, high clarity and gloss, together with good scratch resistance.

Atactic PP is an amorphous material with a glass transition temperature (T_g) of 293 K. It is always present in small quantities (1 – 5%) in PP produced with Ziegler–Natta catalysts. Amorphous PP is separate by solvent extraction. It modifies their properties improving their low temperature performance, processability and optical properties, but decreases stiffness and long-term ageing properties.[6]

Isotactic PP is processed by injection molding into articles with complex profiles such as internal trim in cars, household items, toys, and rigid packaging. It is also used for melt spun fibers and nonwoven fibers production, for rugs and wall-to-wall carpeting (melt spun fiber); hygiene products and single-use clothes (nonwoven fiber).

Syndiotactic PP cover a small market volume, it is used for sheet, film, and injection molding applications or in blending with other polymers.

Atactic PP is used for modified bitumen roofing, as an adhesive and a sealant, where enhance bitumen flexibility and ultraviolet resistance are mandatory.

1.1.3. Poly(styrene): Production and use

PS is a thermoplastic polymer and due to its properties PS can be used in an extremely wide range of applications. PS is commercialized as amorphous transparent resin. At ambient temperature is a clear glass polymer due to phenyl group presence which raises the T_g slightly over 373 K. Over that temperature PS is a viscous liquid which can be easily processed by extrusion or injection-

molding techniques.[7]

PS is synthetized using continuous bulk polymerization plants, the polymerization easily occurred because styrene, PS monomer, is extremely reactive and polymers are obtained just by heating without the addition of initiators.

Performance enhancement of PS materials are obtained by the addition of processing aids, antistatic agent, UV stabilizers, glass fibers, or by copolymerization with other monomers such as acrylonitrile and/or butadiene. These materials are not discussed in this brief review.

PS is employed in packaging applications (such as disposable tumblers, television cabinets, meat and food trays, and egg cartons) and in building industry as rigid foam insulator.

As already outlined styrene is extremely reactive, indeed it can work as electron donor as well as electron acceptor. So it can be polymerized through radical, cationic, or anionic mechanisms, or by coordination propagation steps. Anyway industrial polymerization is carried out by self-started free radical mechanism. The propagation mechanism for the chain growth proceeds by addition of monomer to the radical chain end. Growing chain is mainly terminated by coupling reactions. If a proper control of temperature is not achieved radical degradation of newly formed PS may occur, a more detail discussion is reported in Section 1.3. A good control of molecular weight may be achieved by controlling temperature obtaining PS with average masses between 100,000 and 400,000.

Other polymerization processes such as, cationic, anionic, and catalytic, may produce PS with interesting properties but few commercial applications are known.

Successful large scale use of PS is explained because a tailor made product may be achieved at very low cost if compared with other competitive materials.

1.1.4. Poly(lactic acid): Production and use

Lactic acid is a yearly renewable feedstock which was polymerized for the first time to a high molecular weight polymer in 1932 through ring opening polymerization (ROP) of cyclic dimeric ester of lactic acid, the lactide.[8] Anyway it has found large scale applications only in recent years.

Both lactic acid stereoisomers can be polymerized with good stereoisomeric control in poly(lactic acid) (PLA) allowing a control on the final polymer properties.

PLA is an aliphatic polyester, thermoplastic, with a T_g about 333 K, and a melting point of 453 K for homopolymers. It is stable up to 473 K and it usually shows high crystallinity, mechanical and chemical resistance, and permeability to aqueous vapors.[9]

Amorphous PLA is soluble in common solvents such as tetrahydrofuran (THF), chlorinated hydrocarbons, and benzene.[10]

PLA is obtained by polymerization of lactic acid following two main strategies.

The direct condensation of lactic acid yields a low molecular weight polymer which does not find any use in almost any application due to its glassy-brittle nature. Anyway these short chains of PLA can be heated giving a reverse polymerization to yield the lactide, and this cyclic ester can be used to synthetize high molar weight (M_w) PLA (M_w about 100,000) in the presence of a catalyst such as stannous octoate. In the second strategy lactic acid in the presence of a catalyst is azeotropically dehydrated to a high-boiling aprotic solvent at reduced pressures, obtaining PLA with Mw greater than 300,000.[11] In Figure 1.4 are summarized the main synthetic pathways. Other polymerization processes are available; their detailed description can be found in literature.[11,12]

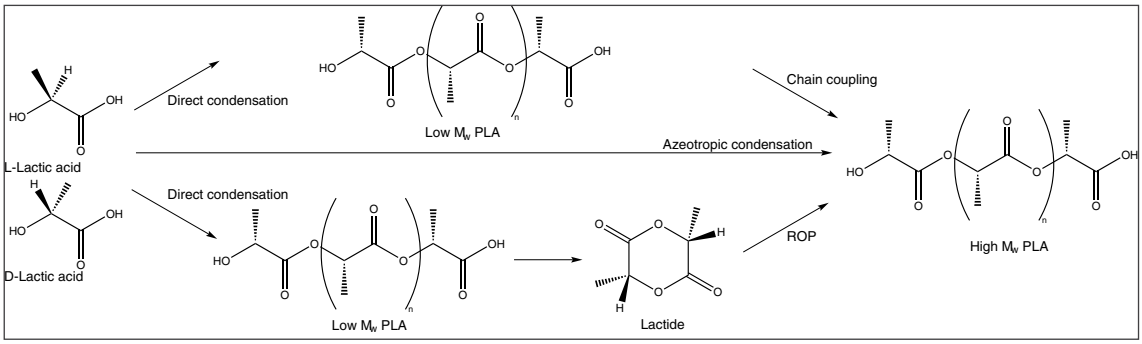

Figure 1.4. The three possible pathway for PLA synthesis.

PLA is used in several application, the main are listed below:

- Medical application: its use is limited to sutures and orthopedic (bone) fixation.[12]
- Packaging: in food-contact applications.[13]
- Coating: for instance of paper due to easy formation of films.
- Fiber: they already found application in dresses as replacement of other polyesters[14] and also for more specific applications.[15]
- Agricultural: for various application such as weed prevention nets, vegetation nets, vegetation pots, ropes, and binding tape.[11]

1.1.5. Tire: Production and use

Tires are extremely complex items which comprise a blend of several polymeric, organic, and inorganic materials to give the feature mandatory for traction of vehicles. Composition of tire is tuned to fulfill some specific requirement for traction accordingly to the large variety of tire classes which are available on the market. The main property requirements are listed:[16]

- Load carrying capacity
- Damping of road irregularities
- Adhesion to the road
- Transfer of longitudinal and lateral forces

- Immediate steering response
- Dimensional stability
- Structural resistance
- Low energy consumption
- Low noise generation

A tire is essentially a cord–rubber composite and in Figure 1.5 is reported a schematic view of tire section.

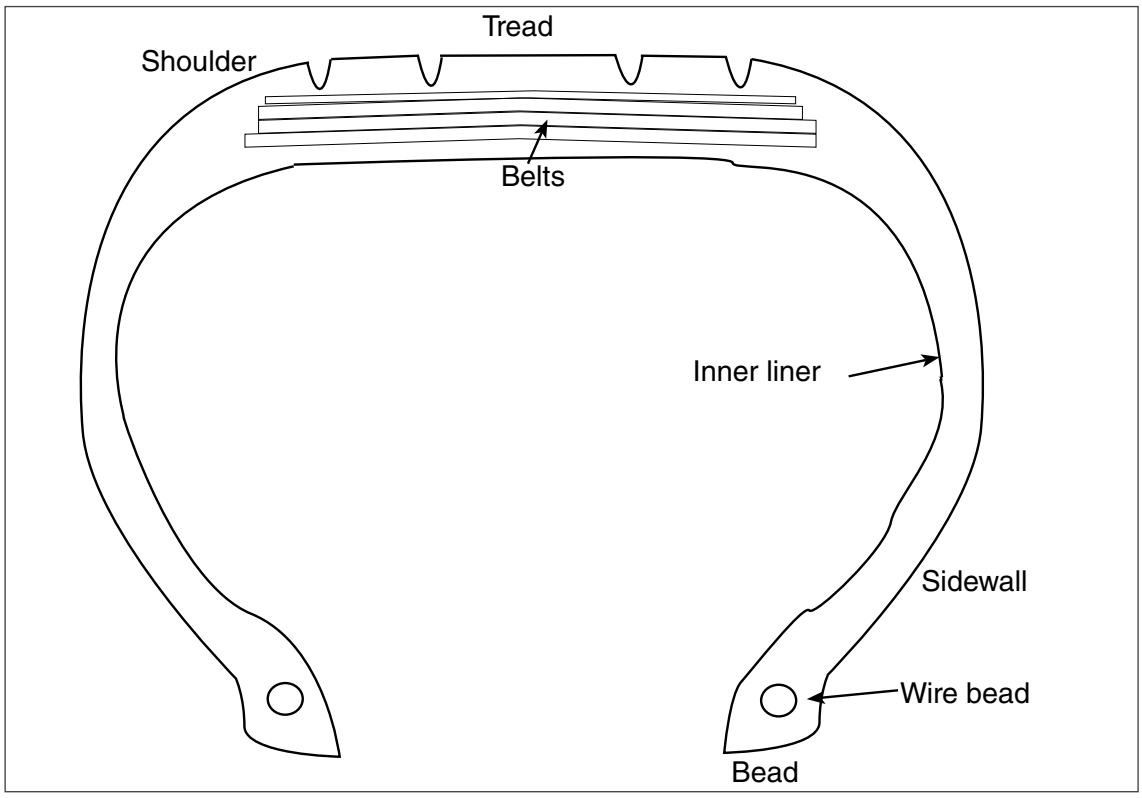

Figure 1.5. Schematic cut view of a tire.

Tires have plies of reinforcing cords extending transversely from bead to bead, on top of which it is located a belt below the tread. The belt cords have low extensibility and are made of steel and fabric depending on tire application.[17]

Aside from steel wires and fabric cords tires comprise a polymeric matrix, inorganic fillers, and additives for manufacturing issue and for enhancing finish product characteristics. The formulation of tire consists of four main components: polymers, filler or other reinforcing agents, stabilizer, and vulcanization systems. Other secondary components may be included, such as: resins, oil, and/or short fiber. [17]

There are five classes of polymers used in tire manufacturing: natural rubber, synthetic polyisoprene rubber, styrene-butadiene and acrylonitrile-butadiene copolymers, poly(butadiene), and butyl rubber (poly(isobutene) copolymerized with small amounts of isoprene).

Carbon blacks, clays, and silica constitute the filler or reinforcement system. Optimization of the amount of these materials in a formulation depends on the

application for which the component is designed.

The stabilizer and antioxidant protects the compounds from aging and oxidation to improve the long-term durability of the tire.

The vulcanization process and its design are mandatory because a not-vulcanized rubber is not very elastic, it does not kept its shape after a large deformation, and can be sticky. After vulcanization the polymeric matrix form a network where sulfur is the crosslinking agent increasing retractile forces and reducing the permanent deformation after removal of the deforming force.[17] Vulcanization process usually needs accelerators (such as: tetramethylthiuramdisulphide and mercaptobenzothiazole) and activators (such as zinc oxide and stearic acid) to improve the final network characteristics.

In Table 1.3 are reported the main components of a car and a truck tire.[18]

Table 1.3. Main components of a representative car and truck tire.

	Car		Truck	
Tire composition	**New (%)**	**Used (%)**	**New (%)**	**Used (%)**
Polymers	48	47	45	43
Carbon black	22	21.5	22	21
Steel	15	16.5	25	27
Fabric	5	5.5	-	-
ZnO	1.2	1	2.2	2
Sulfur	1	1	1	1
Other	8	7.5	6	6

1.1.6. Multi-layer packaging: Production and use

In the last decades the pressing demand for more specific packaging application has been focused on multi materials. They can merge their feature to achieve surprisingly useful final characteristics. Among the vast series of composites multi-layer items are exploited for beverage packaging due to their gas barrier and potentially aseptic properties.[4,19]

In Figure 1.6 are reported two magnified schematic views of multi-layer packages (MLP) sheets.

They are differentiated by the presence of an aluminum foil used as long-term barrier against gas permeation. Indeed for short-life packaging this foil is not present.

The paper layer is considerably thick, and it represents almost the whole sheet thickness. It is obtained by overlapping perpendicular thick layer of Kraft paper. The paper contains little amounts of hemicellulose and its color is pale-brown. The finish print design and images are in situ directly directly polymerized by UV assisted polymerization in the presence of radical initiators. In Table 1.4 are listed the main constituent of a referring paint for this application.[19]

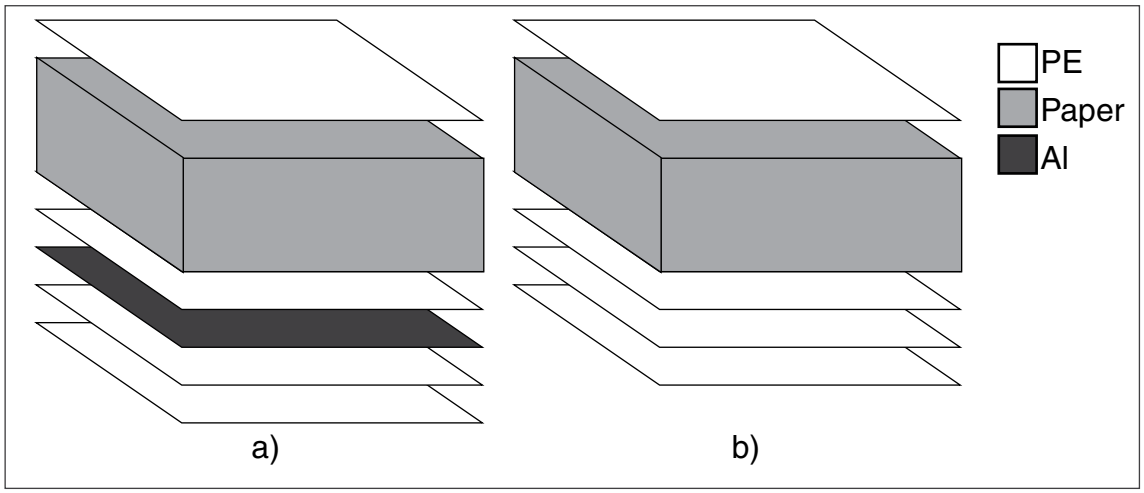

Figure 1.6. Schematic views of MLP: a) with aluminum foil; b) without aluminum foil.

Table 1.4. Composition of a referring paint.[19]

Component	Amount (%)
Bisphenol A epoxyacrilate	44.0
Neopentyl glycol propoxylate diacrylate	30.9
Dimethylpropan tetraacrilate	3.2
Benzophenone	6.0
Acrilated amine	9.9
Bentonite	0.4
ZnO	3.6

The PE employed is LDPE for its transparency and ability to form films, as reported in Section 1.1.1 and insolubility into the liquid inside the container.

1.1.7. Automotive shredder residue: Production and use

End-of-life vehicles (ELV) were recycled since 1958 recovering useful materials such as metals and re-sales used parts.[20] However ELVs comprise four classes of materials: ferrous and non-ferrous metals, polymers, and other materials. Their distribution among ELVs varies according to vehicle designs but the non-metal fraction may represent up to 20 wt% of ELVs. This fraction is ground and scraps with dimension of few centimeters are collected. They are called automotive shredder residue (ASR) and also known as car-fluff.[20] Usually ASRs are made of polymers (rubber, PEs, and PUR foams), textiles, metals, cable, dirt, wood, and so call fines (the smallest particles). ASR are heavily contaminated by chlorine, chromium, and lead compounds.[21,22]

1.1.8. Biomasses, wood: Production and use

Wood is the most available natural and renewable resource, furthermore its composition and appealing properties makes wood an economic valuable product. Wood is exploited as raw material for pulp, structural timber, sawn wood, panels, furniture and other purposes but its use for energy production is limited in industrialized countries. The total phytomass of the earth is estimated to be 1.24×10^{12} t, among which 80% is attributed to wood.[23]

Wood is defined as the inner tissue of stems, branches, and roots of perennial plants. It is a transport system for water and its solutes, a storage tissue for reserve material, and provides the plant with mechanical stability.

The main components of wood are assembled into wood cell walls; they are cellulose, hemicellulose, and lignin. The amount of cellulose in European wood is 41 – 43 %, while lignin and hemicellulose contents are strongly dependent of wood species and growth conditions (22 – 27 % and 25 – 35% respectively).

Lignin is a cross-linked macromolecule made up of phenylpropane units, which are linked together by at least ten different C–C and C–O bonds (Figure 1.7). The irregular structure of lignin arises from its biosynthesis, in which the last step is a non-enzymatic, random recombination of phenoxy radicals.

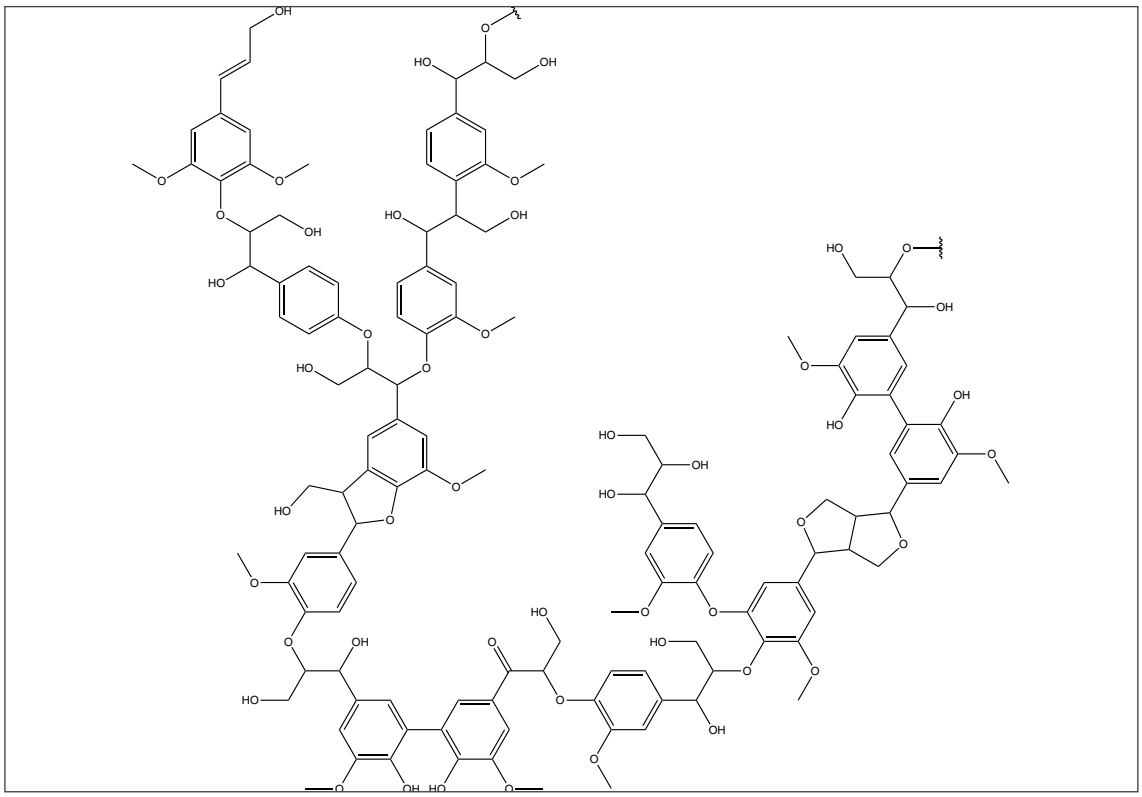

Figure 1.7. Lignin general structure

Cellulose is the most important wood component having linear long chains of β-(1,4)-glycosidically bonded D-glucose units, in the form of pyranose rings (Figure 1.8). The Mw of native cellulose is between 1,800,000 and 2,500,000. In

industrial pulp however, cellulose is degraded to M_w values of 180,000 – 540,000.

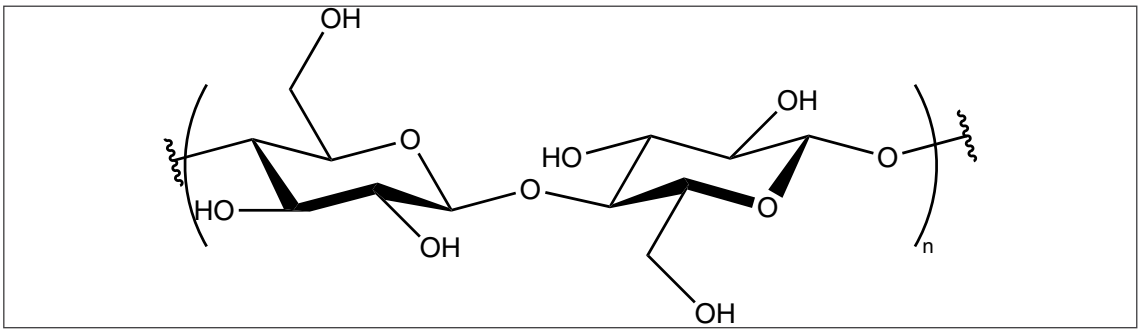

Figure 1.8. Cellulose repeting unit.

Hemicelluloses are polysaccharides that differ from cellulose due to the presence of several branched sugar moieties, which have lower molecular masses than cellulose. The two main types of hemicelluloses are xylans and glucomannans (Figure 1.9). Structural differences also exist between hemicelluloses form different wood species.

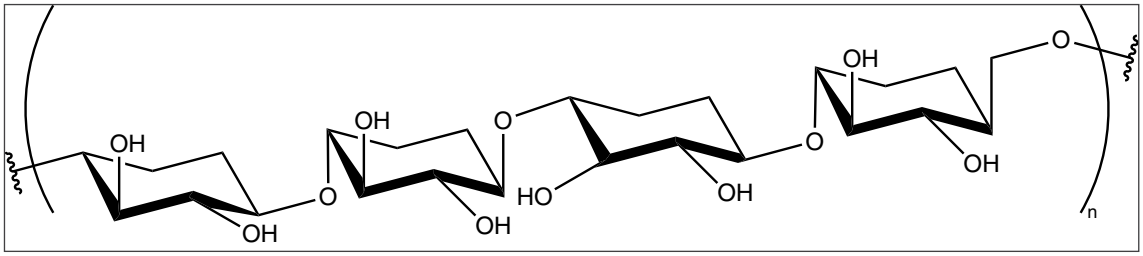

Figure 1.9. Hemicellulose general structure.

1.1.9. MaterBi: Production and use

Europe introduced measures on management of packaging waste through the directive 85/339/EEC in 1985. Anyway it was too vague to find any effect on national policies. Only in 2005 the revision through Directive 94/62/EC and the introduction of EN 13432:2000 clarified the characteristics of bio-material. From 2011 these directives were adopted in Italy and as acknowledgment the PE based shopping bags were forbidden and must be replaced by bio-degradable bags.

Actually a bio-plastic material (MaterBi®) from vegetable is largely used, especially from corn starch to gether with other bio-polymers such as PLA. Its production require starch destructurization, complexation, and addition of compatibilizers, in the presence of specific synthetic and/or natural polymers, plasticizer, and other additives.[24,25] This great variability of processing brings different type of so called grades of bio-polymers with a wide range of properties which allows their use in various field.[26]

1.2. Waste management

The concept of waste is defined in several ways and an unambiguous definition is not easy to propose because a waste for someone could be still useful for others. Two definition of waste are reported.

> "materials that are not prime products (that is, products produced for the market) for which the generator has no further use in terms of his/her own purposes of production, transformation or consumption, and of which he/she wants to dispose. Wastes may be generated during the extraction of raw materials, the processing of raw materials into intermediate and final products, the consumption of final products, and other human activities. Residuals recycled or reused at the place of generation are excluded. See also biological waste, solid waste, industrial wastes and household waste."[27]

> "waste shall mean any substance or object in the categories set out in […] which the holder discards or intends or is required to discard."[28]

Wastes comprise a wide assortment of materials, items, and stuffs in solid, liquid, and gaseous phases. Even so the discussion is focused on solid waste management and routes for waste valorization.

Indeed since the 1970s the practice of waste management, which initially was targeted to their collection and disposal, started to gain interest regarding recycling and reuse of wastes collected.

Initially the policy proposed was focused on reducing waste generation by putting emphasis of three R rule: reduction, reuse, and recycle. Anyway wastes were produced and incinerated or landfilled if no other options were available.

Today these policies are consolidated and they try to evolve in a more efficient system to achieve the final goal of zero waste; the key elements foreseen for this objective are listed as follow:[29]

- investment in community for waste reduction and resource recovery;
- participation of citizens in recycling;
- product redesign to make waste non-toxic and reusable;
- extension of producer's responsibility beyond initial sale that will enhance buy-back programs;
- end of subsidies to enterprises that uses virgin resources only.

Nowadays the waste management is considerably enhanced but the way to obtain zero waste is still long.

Waste is primarily generated from three different sources: households, commercial establishments, and health care or research institutions. The composition of these

wastes may vary considerably among different neighborhood and period of the year. In Table 1.5 is reported a typical garbage composition in the United States.[29]

Table 1.5. Typical garbage composition in the United States.

Component	Range (wt%)
Food waste	4.4-15.3
Garden waste	12.5-24.2
Glass	6.5-10.9
Iron and aluminium	4.0-9.0
Moisture	27.1-35.0
Other combustible	1.6-12.1
Other noncombustible	1.8-11.1
Paper	41.6-53.5
Plastic	0.76-5.7

As outlined before when a waste is generated few options are available recycling, incineration, composting, and landfilling.

When choosing the way to dispose an item must be kept in mind that this item is produced using energy and raw material and they are partially stored in it. If it is disposed in landfills its energy and material content are completely lost. So far landfilling should be avaoided because nothing is recovered form a waste displaced into the ground.

Recycling can be defined as the process by which waste materials are separated from unrecoverable wastes and/or remanufactured into usable or marketable materials.[30] However recycling is not always worthwhile depending if the emissions, energy consumption, and environmental pollution caused by collection and reprocessing are lower than those required to manufacture new products from raw materials.

Recycling of polymeric materials can be a challene and a worthwhile recycling because it allows both reducing the amount of waste by recirculation of recovered materials and opening new market areas. In Figure 1.10 is reported a schematic diagram for plastic waste recycling.

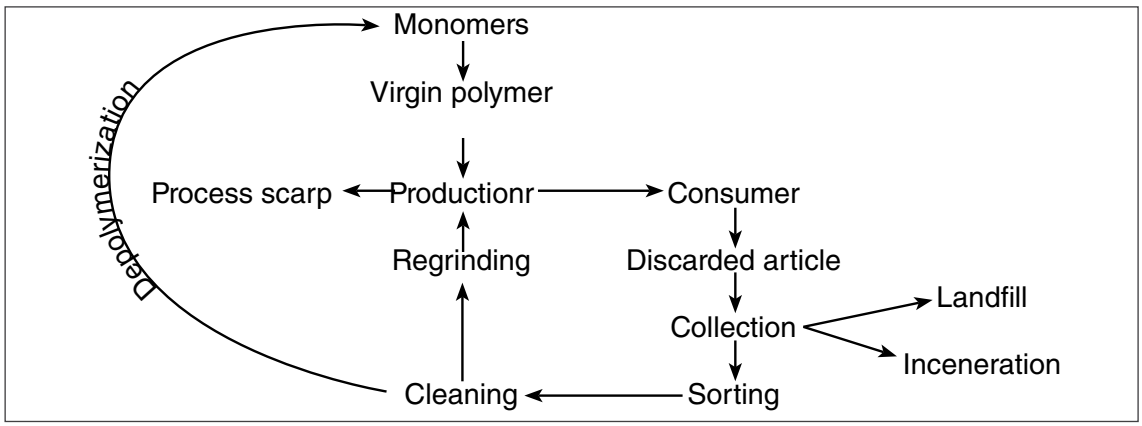

Figure 1.10. A general scheme for plastics recycling.

Anyway plastic recycling shows the same problems arouse for the other wastes and a complete recycling is far from to be reached. Mixed, polluted, finely divided, or strongly bonded materials are hardly recycled and strong efforts are spent to upgrade the actual technologies for achieve their worthwhile recycling.

Currently plastic recycling are achieved with optimal results if it is possible to sort and clean a single plastic component from waste stream.[31] Only thermoplastic polymers can be reprocessed by using them directly or more often mixed with virgin polymer of the same type. This is the best way to safeguard the energy and hydrocarbons required for their synthesis. This is called Primary Recycling. From a long time it is carried out in industries which produce and process plastics mainly for economic reasons. Indeed recovered materials have a price up to 70% of the new one. [31] Anyway some technical problem may be encountered in primary recycling. [31]

- Degradation of the material due to repeated processing followed by a drop of its properties.
- Contamination (such as a grey material from plastics of different colors).
- Handling of low density item such as foams.

Recycling of mixed and composite wastes, where polymers are not separable, is more difficult than single thermoplastic polymers. Indeed mixed plastic can enter into the material recycling system if large quantities are available with a constant composition. Anyway the reprocessing of mixed plastics by molding shows some limitations. Only thermoplastic are able to melt and their miscibility among different type of plastics is poor and frequently they are completely immiscible.[31]

Nevertheless these procedures can be applied for a limited number of times and they are not applicable to some plastic waste (such as: contaminated, degraded from previous recycling, composite materials, filled plastic, thermosetting plastics, and elastomers).[32] Anyway recycling of these materials is still possible but it can be achieved by breaking down polymer structures to smaller compounds. Several technologies are able to break a polymer chain and they can be applied to recover the starting monomer or hydrocarbons in agreement with polymer characteristics and technology employed: hydrolysis, alcoholysis, aminolysis, hydrogenation, or pyrolysis are available. These processes were thoroughly investigated and some of them are patented.[33-35]

Hydrolysis may allow recovering the starting compounds used for polymer synthesis. Water molecules may hydrolyze the linkage points in polymers back-bone. Hydrolysable plastics are polyamides, polyesters, polycarbonates, poly(urea) s, and polyurethanes. Strong reaction conditions are required in order to obtain an efficient hydrolysis.[36]

Alcoholysis works like hydrolysis but the cleavage of back-bone chains is done by an alcohol. In this way the alcohol derivatives of the starting monomer is obtained.

Alcoholysis can be performed also with diols and the products may contain terminal hydroxyl groups.[37] Polymers such as polyolefins are not hydrolysable, they are stable in hydrolysis conditions.

Hydrogenation process breaks the carbon bonds in polyolefin through hydrogenolysis. As expected alkanes are the main products. Furthermore almost any polymer can be decomposed and any sorting operation can be avoided. Hydrogenation proceeds slowly so strong reaction conditions (773 K and 400 bar) and a catalyst are required to improve the efficiency but the life of the catalyst is short.[31]

Pyrolysis is thoroughly described in Section 1.3.

Incineration is also a possible recycling path if any other reuse for plastic waste is not possible. In this way the chemical content used to produce and manufacture the plastic is lost. Anyway the energy content of plastic, regarded as calorific value, is high as a fuel and higher than coal.[31,38] So far plastic waste can be employed as feedstock for power station to produce electricity. However incineration may leak some pollutants into the environment.

Landfilling is the worst possible outcome for a plastic waste. Its energy and chemical content are completely lost, their low density and long degradation time cause a rapid and long term filling of dumping sites. Anyway dumping sites can be seen as a future source of materials by mining them.[39]

A detailed description of waste management and disposal can be found in literature.[29-31,38]

1.3. Pyrolysis

Pyrolysis is a high temperature treatment (starting from 600 K, for biomasses, 700 K, for plastics) which breaks polymeric macromolecules giving compounds having a lower molecular weight. It is usually performed in an inert, not oxidizing, environment and three classes of products are obtained: a gas (volatile), a liquid/ wax (condensable), and a char (inorganic compounds such as fillers stable to pyrolysis conditions).[40]

Thermoplastics, thermosetting polymers, elastomers, composite materials, and heavily soiled or aged plastics can be recycled through pyrolysis. Furthermore mixed waste stream, which are not easy separated, can be pyrolyzed. Products obtained may show less economic value than those from hydrogenation nut the process is less expensive.[31]

Nevertheless a pyrolysis process shows sound advantages compared to other chemical recycling technologies. Pyrolysis does not require any source of hydrogen or a catalyst (even if it can be used) such as for hydrogenation; the energy and chemical content present in the waste is preserved together with a reduction of gas production up to 20 fold and toxic oxidized species (dioxins and NO_x) are not formed if compared to incineration. The pollutants, if they do not pyrolyze, are concentrated into the char.[31]

Pyrolysis is an endothermic process which requires large amount of energy to break down polymers bond and an efficient heat transfer system to overcome the poor thermal conductivity of polymers. It is driven by free radical reactions like thermal cracking processes.[41]

Several technologies were developed to convert efficiently any sort of polymers structure into useful products; it is achieved by different heating technology, apparatus design, and sometimes using catalysts.

The heat transfer from the source to the polymer covers a mandatory issue in a pyrolysis system due to poor thermal conductivity of polymer. The heating source may be internal or external to the pyrolysis reactor. An internal source can be realized when the polymers are partially oxidated to fulfill the energy requirement.[42] The external sources may be realized if the reactor is heated by an electric oven or by any other equipment where an external combustion is run and the heat is transferred to the polymeric material by a heating transport system. The efficient transfer of heat is improved by adjusting the apparatus design such as fixed,[43] fluidized,[44] or conical spouted bed,[45] autoclave,[46] and rotary kiln[47] reactors. Other technologies transfer heat to polymers in different way such as plasma[48] or microwave radiation (MW). MW nature and application in pyrolysis field are discussed in next Sections. In Figure 1.11 is reported a schematic pyrolysis system.

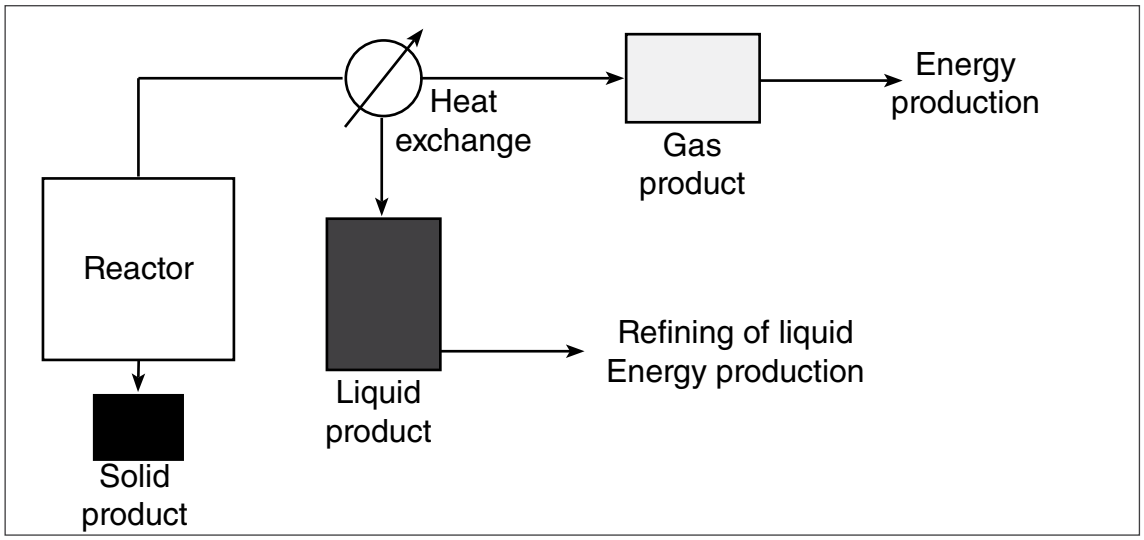

Figure 1.11. A schematic pyrolysis unit.

The pyrolysis process is characterized by several parameters which play decisive roles on products properties such as: feed size,[49] temperature, and residence time in the reactor.[50]

Feed size determines how the polymer is heated, due to its poor thermal conductivity. If large pieces are pyrolyzed a gradient of temperature between the outside and the inside parts of the samples is always observed. Smaller seizes are faster and more uniformly heated. Anyway small pieces of plastic require a pretreatment and an accurate milling/chopping process.

Temperature can be kept constant or varied during the experiment. Together with the residence time of vapors inside the reactor it is a roughly indication of how energy is transferred to the polymer.

In the next paragraphs a brief literature review of pyrolysis in classical heating experiments is reported.

1.3.1. Polyolefins

PE and PP are the most produced polyolefins thus they are largely investigated in pyrolysis experiment. The main product collected from polyolefin pyrolysis is a high or low viscous liquid depending on the reaction conditions.

Polyolefin pyrolysis is driven by a series of radical homolytic bonds cleavage and the main products in PE pyrolysis are linear alkanes, their corresponding 1-alkenes (from C1 to C54), cyclic, and aromatic compounds.[51] Usually in classical pyrolysis, when the heat transfer is not optimal, the main product form PE is a wax or a high viscous liquid, semi-solid at room temperature.

Meanwhile PP pyrolysis gives branched alkanes, and alkenes together with aromatic compounds.[52] Furthermore PP may be used as starting material for production of carbon nanotubes, using a catalyst and specific pyrolysis conditions.[53,54]

The cleavage of C-C bonds requires a higher activation energy for PE than PP,[45] respectively 225 kJ mol^{-1} and 176 kJ mol^{-1}. The lower energy requirement, for PP, is connected with the presence of tertiary carbon atoms in the main chain which are easily broken giving tertiary radical intermediates more stable than secondary one formed by PE.

In a fluidized bed reactor (characterized by a very efficient heat transfer) PE, and PP are pyrolyzed giving waxes, low viscosity liquid,[51, 55] and even BTX,[56] while in a conical spouted bed reactor (heat transfer is less efficient) a wax is the sole product.[45] In Figure 1.12 and Figure 1.13 are reported the main reactions involved in polyolefin pyrolysis.

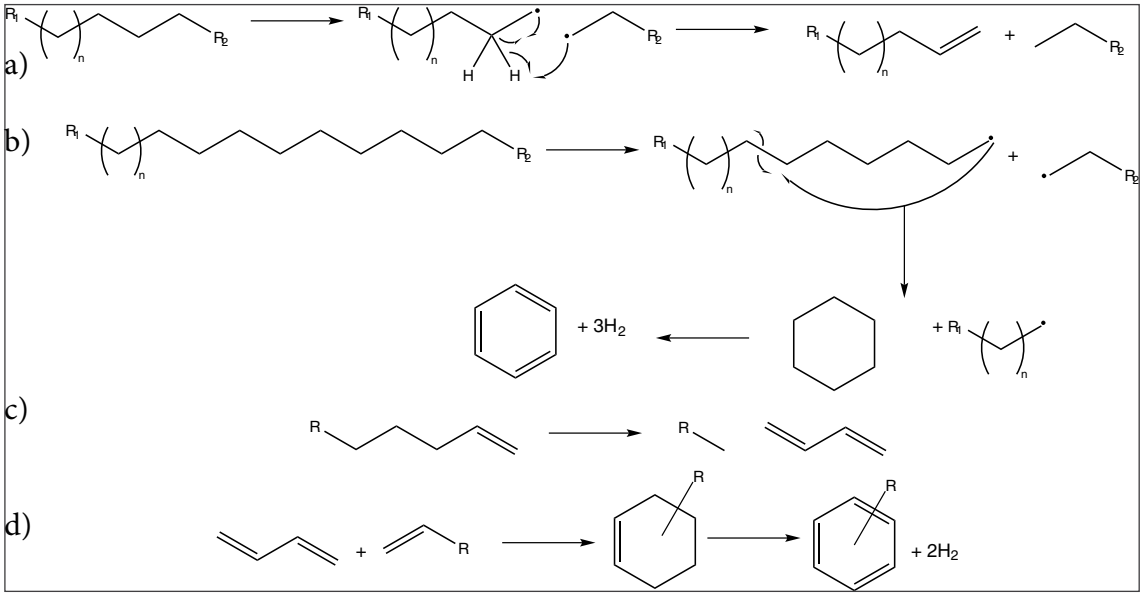

Figure 1.12. Pyrolysis of PE, main reactions and products. a) C-C bond cleavage with alkane and 1-alkene formation; b) chain end radical formation followed by a ring formation and a dehydrogenation reaction; c) dialkene formation; d) Diels-Alder followed by a dehydrogenation reaction.

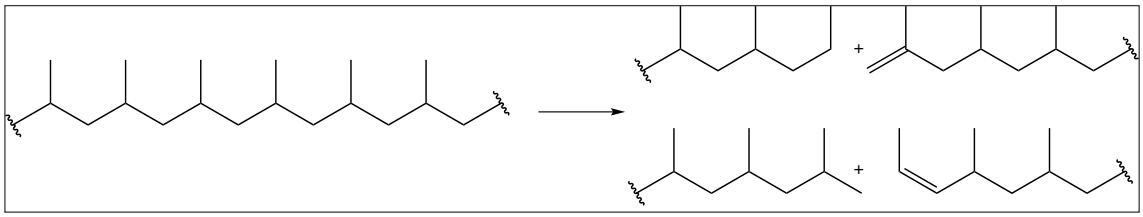

Figure 1.13. Pyrolysis of PP, main reactions and products; It is highlighted the formation of 1- or 2- alkenes.

High grade products, especially connected with the liquid fraction, may be obtained using a catalytic system such as: zeolites,[57-60] basic salts,[61] and Zigler-Natta catalyst,[44, 62] but the catalyst must be very frequently regenerated.

1.3.2. Poly(styrene)

Pyrolysis of PS allow the valorization of the phenyl moiety widely present. Indeed PS may be converted into single ring aromatic compounds, together with low amount of char and gas, if appropriate pyrolysis conditions are employed.[50,63-65]

As reported for PE and PP, also PS pyrolysis is driven by free radical reactions that may act with three different competitive paths accordingly to radical formed: chain-end, near chain-end, or random internal position. So far the fate of these radicals is: β-scission to give an alkene and a smaller radical, hydrogen transfer from another molecule to form a dead chain and a new radical, or intra-molecular hydrogen radical transfer with the formation of an alkene and an alkane.[66, 67] Pyrolysis of PS is already active at 623 K, and the main product is a dark viscous liquid rich in single ring aromatic compounds (benzene, toluene, ethylbenzene, and styrene). In Figure 1.14 is reported a schematic degradation pathway for a PS macromolecule.

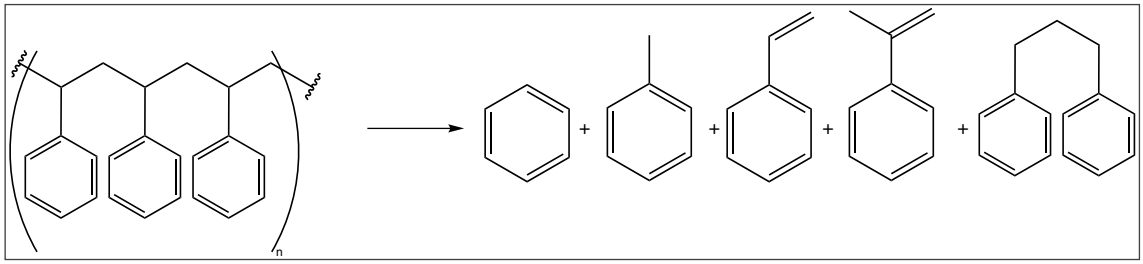

Figure 1.14. Pyrolysis of PS and formation of its degradation products.

Char formation improves when pyrolysis temperature raises.[50] The char is formed by condensation between neighboring phenyl moieties. Anyway different pyrolysis behavior is observed for different classes of PS (virgin, expanded, and compacted from containers), especially for what concerning the composition and distribution of aromatics in the liquid fraction.[68]

The use of a catalyst may improve the production of some specific aromatic compounds, such as styrene.[69-74] Furthermore catalytic degradation of PS may lead to the formation of molecular hydrogen in a two steps process in the presence of a Ni catalyst.[75] Styrene improvements were also achieved using different fluidizing medium, such as quartz sand in a fluidized bed reactor,[63] light-cycle-oil,[76] or tar pitches.[77]

1.3.3. Poly(lactic acid) (PLA)

The thermal degradation of PLA is a complex process in which a wide number of reactions are involved in relation to the pyrolysis condition and to the presence of a catalyst or salts. PLA is reactive towards thermal treatments in much more pronounced way than other polyester from renewable source.[78,79]

The primary pyrolysis products are CO, CO_2, methylketene, acetaldehyde, H_2O,

cyclic oligomers, and lactide.[80] The main reaction routes for non-radical reactions are backbiting inter-esterification reactions involving OH chain ends. There are two main pyrolysis mechanisms for polyesters: cis-elimination and trans-esterification (Figure 1.15). Over 570 K radical reactions may occur, they are assumed to start with either an alkyl-oxygen or an acyl-oxygen homolysis (Figure 1.16). If residual tin is present different route are available and larger amount of lactide is formed.[81]

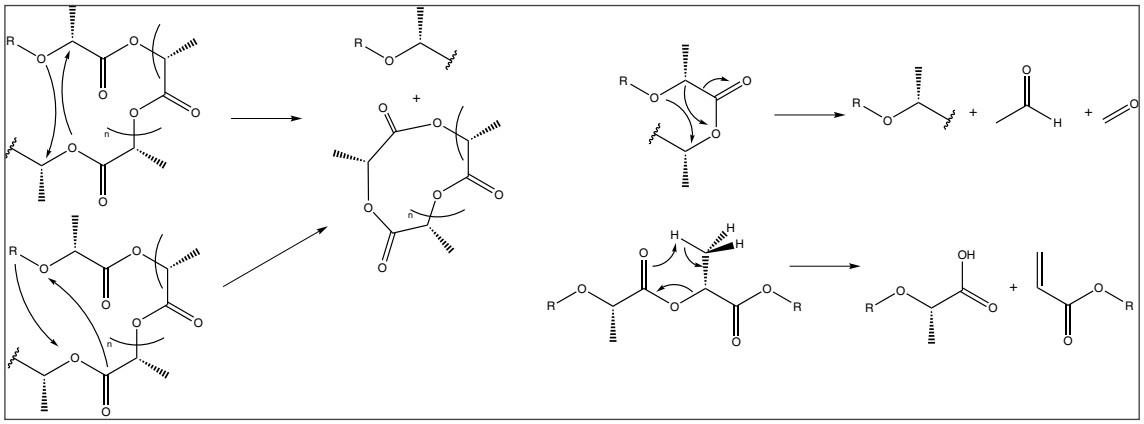

Figure 1.15. Possible non-radical reactions involving PLA pyrolysis.

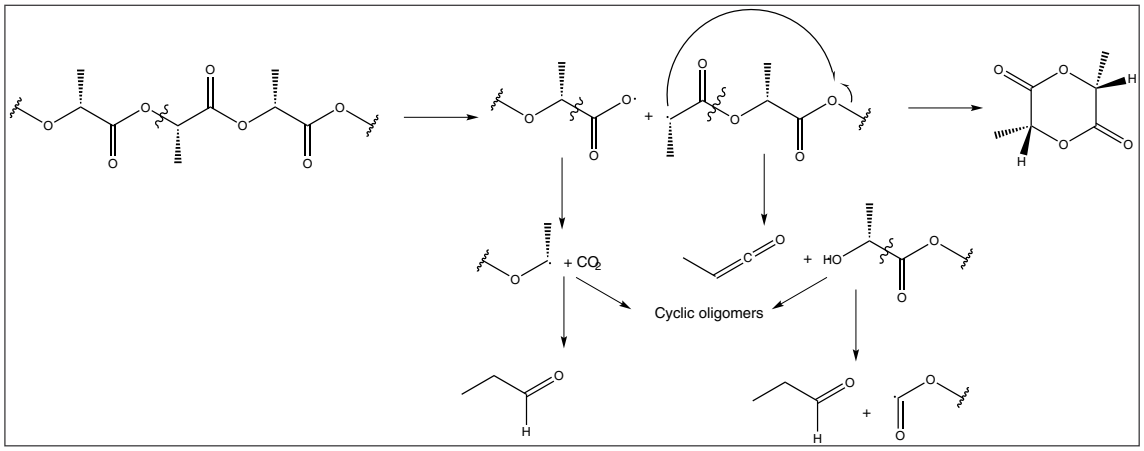

Figure 1.16. Possible pathways for radical reactions for pyrolysis of PLA.

The increasing presence of residue tin catalyst in PLA increases the unzipping reaction rate to yield lactide and lowered the decomposition temperature.[82] Furthermore if a purified PLA is pyrolyzed the formation of enantiopure lactide is reduced and diastereoisomers and cyclic oligomers are formed.[83]

The pyrolysis of PLA is influenced by the different chain-end at the carboxyl group, the presence of a metal ion (such as calcium or magnesium) end/or capped types.[84, 85] In this case the control over temperature seems to be mandatory to control the stereochemistry of lactides obtained.[86]

In addition pyrolysis of PLA can be performed with comparable results using virgin PLA or the reprocessed one.[87]

PLA can be pyrolyzed also in the presence of other polymers and metal oxides with negligible effects on its pyrolysis behavior and low racemization of the lactide

formed.[88] However PLA interactions are reported in co-pyrolysis with different materials such as biomasses. Biomasses pyrolysis formed water (an unwanted degradation product in pyrolysis of biomasses) which could hydrolyze ester bonds in PLA. Thus PLA is hydrolyzed to lactic acid and the water content in liquid from biomasses is reduced.[89]

1.3.4. Wood

Pyrolysis of wood-derived materials is exploited mainly to obtain raw liquid fuels which undergo to catalytic upgrading.[90, 91]

Kinetics and thermal decomposition mechanisms for the pyrolysis of plant biomass and its constituents have been extensively studied. In contrast, few studies have focused on the use of catalysts for biomass cracking (in situ upgrading) to generate chemicals. The pyrolysis of wood produces a wide number of substances and their amounts are markedly dependent on the process variables and whether a hardwood or softwood is pyrolyzed.

Permanent gases contain CO_2, CO, CH_4 and low amounts of H_2 and C_2 hydrocarbons.[92, 93] The composition of the liquid (Figure 1.17) is highly dependent on the severity of the thermal treatment (temperature and residence time of the vapors) and the presence of char. During the pyrolysis process when the temperature is below 673 – 773 K primary vapors (oxygenates) are formed; at higher temperature (up to 1123 K) hydrocarbon or secondary tars are formed; above 1123 – 1273 K aromatic or tertiary tars are collected.[94,95] The amount of mixed oxygenated compounds increases with temperature: phenolic ethers, alkyl phenols, heterocyclic, and ethers. Polyaromatic hydrocarbons (PAH) are also formed.[91] Liquid products contain also an appreciable amount of water from both the moisture content of the feed and decomposition reactions.

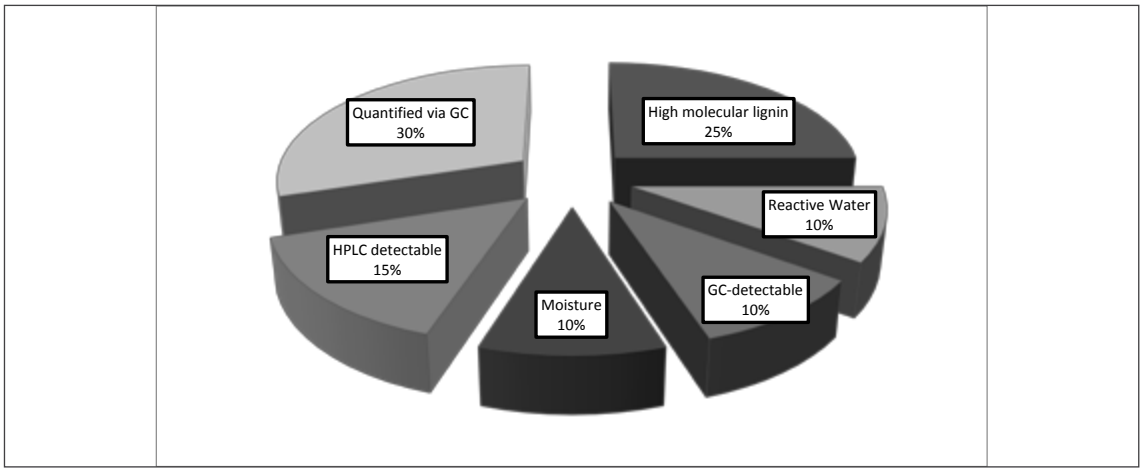

Figure 1.17. Typical composition of a liquid from pyrolysis of wood.[96]

Pyrolysis of wood is extensively studied and several detailed review are now available.[91,96-98]

1.3.5. MaterBi

To the best of our knowledge pyrolysis of starch-based plastics is not exploited. The thermal behavior of these plastics is studied in blend with synthetic polymers. The blend is buried in soil and the tests are performed by the means of TGA.[99-104]

Anyway some researches were performed on the pyrolysis of starch and starch materials. The main products were similar to those obtained in the pyrolysis of cellulosic materials such as anydrosugars and other oxygenated compounds.[105-108]

1.3.6. Tire

Pyrolysis of tire allows the formation of three worthwhile products: a gas (H_2, CO, CO_2, H_2S, and volatile hydrocarbons), a liquid (condensable hydrocarbons), and a carbonaceous char (carbon and inorganic compounds such as fillers or their derivatives stable to pyrolysis conditions). The non-condensable fraction contains C1 – C4 hydrocarbons, hydrogen, and other inorganics (CO_x, nitrogen, and H_2S) and may show a high heating value among 30 – 40 MJ Nm^{-3} which is connected with reaction conditions.[46] The condensable fraction, the liquid, contains a wide amount of hydrocarbons from the pyrolysis of the polymeric matrix such as limonene, benzene, toluene, xylenes, and phenyl derivatives.[109, 110] The char contains carbon and inorganic fillers which are not pyrolyzed, they are widely investigated for active carbon production[111-118] or inks for printing issue.[119]

The amounts and characteristics of the three products are affected by several experimental variables: apparatus design, type of heating, composition and size of tire stock, temperature, residence time, and the eventual presence of a catalytic system.

A wide selection of layout for pyrolysis is reported such as autoclave[46, 109, 120-123], fixed-bed reactor[43, 124-129], moving-bed reactor[130-133], and rotary kiln.[47] As expected the choice of a specific apparatus allow controlling the other parameters. For instance moving-bed or fluidized bed show good heat transfer to the polymeric matrix but require a small feed size and short residence time.

Until now only the conventional heating technologies show promising worthwhile application to large scale plant and they are the only discussed in this section.

Pyrolysis starts over 770 K; below this temperature degradation products are not formed.

The brand of tire may also play an important role because different brand has different composition and the polymer used in their manufacturing could be completely different. Thus different gas and liquid yield and composition are expected due to different polymers degradation.

The main parameters of several reported pyrolysis experiment are listed in Table 1.6.[134]

Table 1.6. Main parameters and yield for pyrolysis of tire.

Tire size (mm)	Time (min)	T (K)	Yield of liquid (wt%)	Pressure (Pa)	Other	Ref.
1.5-2.0	60	823 923 1073	47.4-55.6 45.4-56.0 47.2-55.1	101,325		43
13-15	198-246	723 823 923	43.0 44.6 42.9	81,000-91,000	Rotary klin reactor	47
20-30	30	573 773 973	4.8 38.0 38.5	n.r.		109
20-30	30	573 773 973	4.8 38.8 38.5	101,325	Fluidized bed pyrolysis	120
2 6 10 16 20	n.r.	733	75.5 66.5 60.5 60.0 64.0	n.r.		125
25 x 30	60	773	56.1-60.1	n.r.		126
n.r.	143	773	65	101,325	Steam pyrolysis	131
13.9 <15.6	437 780 600	773 773-843 783-843	57.5 56.5 40.9	12,000 13,000 10,000		138
1.0-1.4	n.r.	723 773 873 723 773 873	42.0 41.5 40.0 49.0 45.0 40.0	101,325	Fluidized bed pyrolysis. CBV Y-Zeolite; catalyst to feed ratio 1:1. ZSM-5 zeolite; catalyst to feed ratio 1:1.	140

n.r.: not reported.

The yield may be influenced by the way they are calculated (for instance if metal wire are counted or not). Anyway yield of liquid never exceeds 55 wt%, and yield of gas may reach 55 wt% in relation to the pyrolysis condition.

The mechanism for hydrocarbons formation is quite complex and many reactions are involved, anyway some general reaction route are proposed; they are reported in Figure 1.18 and Figure 1.19.

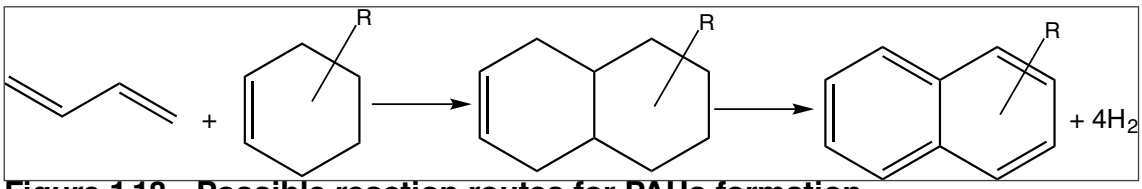

Figure 1.18. Possible reaction routes for PAHs formation.

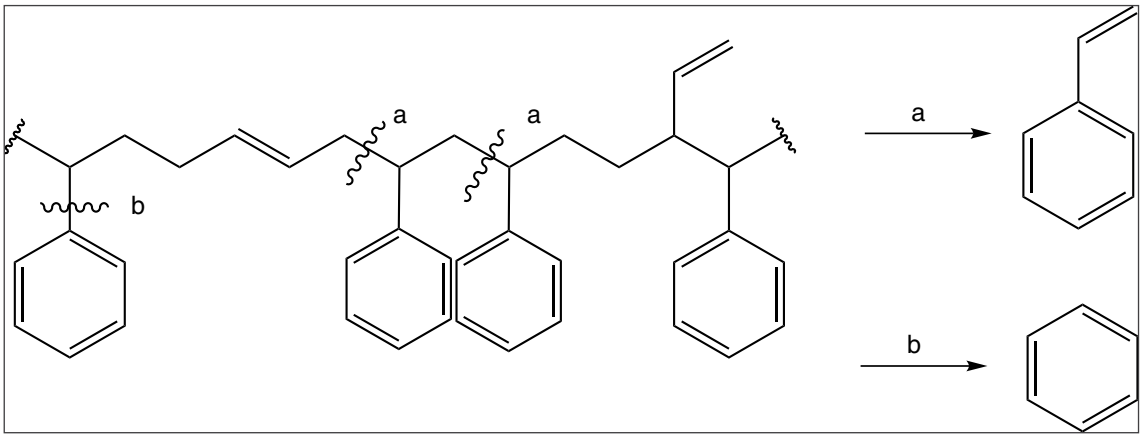

Figure 1.19. Possible reaction routes for aromatics formation.

Limonene is a typical polyisoprene degradation product; its formation may follow the route reported in Figure 1.20.[135-138]

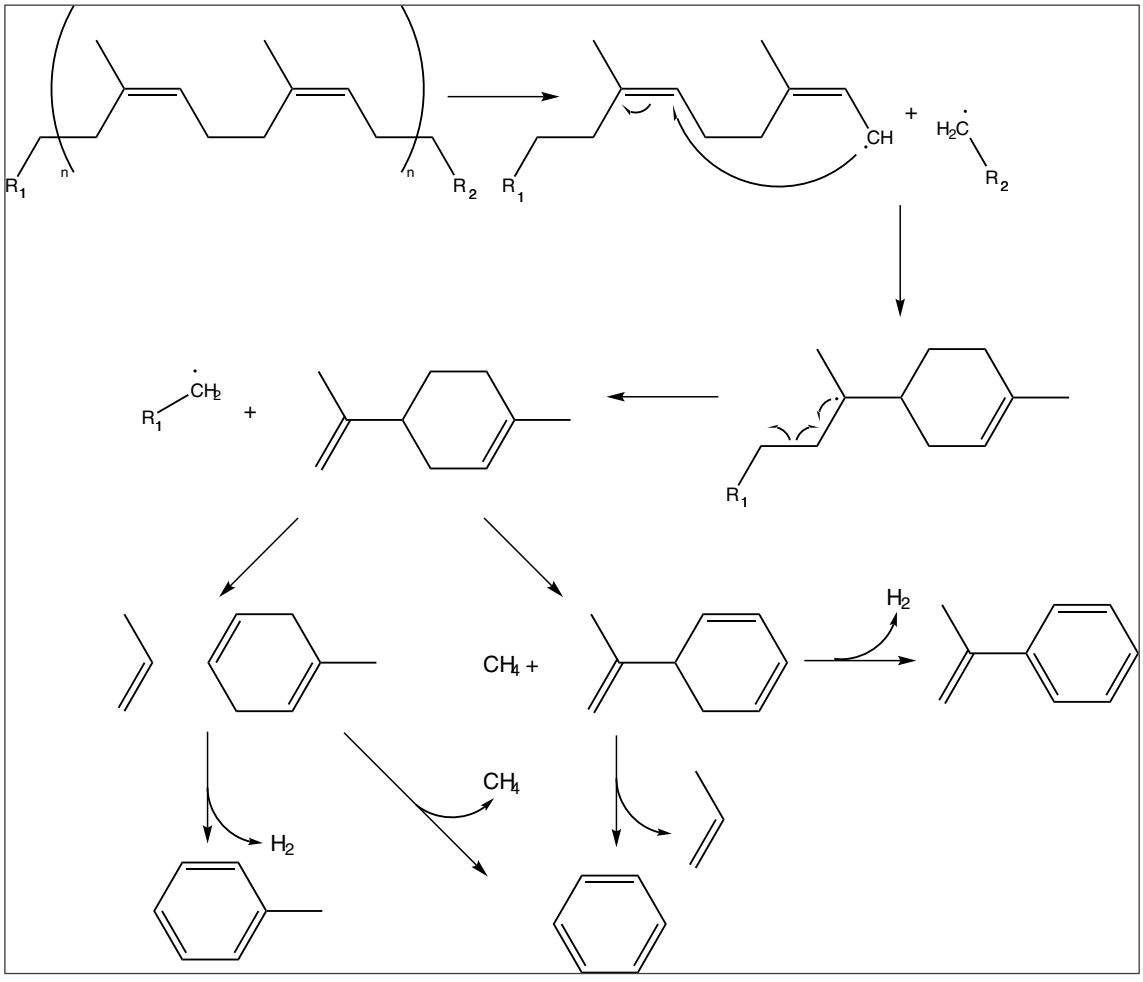

Figure 1.20. Possible reaction route for limonene formation and pyrolysis.

A catalytic system may be employed for upgrading the liquid. It may modify yield and quality of the products. The main effects are enhancement of aromatics formation[139-142], pyrolysis efficiency[143, 144], and hydrogen production.[145]

1.3.7. Multi-layer packaging (MLP)

Pyrolysis of MLP is investigated in both nitrogen[146] and oxygen environment.[147, 148] These materials contain paper, PE, and sometimes metals and other inorganics in their structure such as aluminum foil (Section 1.1.7). Pyrolysis behavior of MLP was mainly investigated by thermo gravimetric analysis (TGA)[149] showing negligible influence during pyrolysis between cellulose, PE degradation products, and aluminum. Indeed the products formed were accounted for the separate pyrolysis of cellulose and PE. In fact kinetics study indicates two clear different stages during pyrolysis which correspond to the degradation of cellulose and PE.[147, 150-152]

Details on PE pyrolysis can be found in Section 1.3.1.

During cellulose pyrolysis several successive reactions may take place. Cellulose undergo in a first step to a back biting reaction of polysaccharide to anydrosugars, among which the main component is levoglucosan (1,6-anhydro-β-D-glucopyranose), and oxygenated compounds such as furans, aldehydes, alcohols, and aromatics accordingly to reaction conditions.[153-157] These latter compounds may be formed also through levoglucosan and other anydrosugars pyrolysis.[156]

At the same time more efforts are exploited in researching the pyrolysis behavior of lignocellulosic materials in the presence of synthetic polymers. On the contrary to the pyrolysis of MAP the findings reported show a significant interaction between paper and PE ensuing an increase of char yield when slow heating and long running process is employed.[158] Sharypov et al. report in several studies strong interactions between degradation products of synthetic and natural polymers in an autoclave reactor at 670 K.[159-161] Other interactions between synthetic polymers such as PP and wood-derived materials are reported by Jakab et al. They observe a shift of PP pyrolysis temperature to lower values.[162] Rutkowski and Kubacki investigated the co-pyrolysis of cellulose and PS. They obtained a liquid in high yield and having a better quality than the product from pure biomass.[163]

These results evidence an interaction between pyrolysis product from wood-derived materials and synthetic polymers if the radicals formed during polymers degradation are present in large amount or stay in strict contact for longer time with the pyrolysis products of biomasses. Indeed PP and PS has lower activation energy and radicals are formed easily than PE, which need long reaction time to show interaction with paper.[158]

1.3.8. Automotive shredder residue (ASR)

ASR shows a composition extremely variable and their pyrolysis products show extremely variable characteristics. Pyrolysis of ASR was investigated with TGA[164] and laboratory scale systems.[165, 166] A brief illustration of the main technologies employed together with the products yield is reported in Table 1.7.[21]

Table 1.7. Technologies and relative yields used in pyrolysis of ASR.

T (K)	Solid (%)	Liquid (%)	Gas (%)	Other	Ref.
773	47.5	35	7.7	Conventional pyrolysis; tubular reactor	165
873	37.5	43	5.8		
973	33	55	8.5		
1073	25	53	12.2		
773	55	25.7	5.8	Fast pyrolysis	
873	52.3	30	11.5		
973	39	21.2	24.1		
1073	37	21.8	34		
673	69.4	7.1	23.5	Autoclave, light ASR	166
573	63.6	10.3	26.1		
973	58.8	8.8	32.4		
673	54.1	25.5	20.4	Autoclave, heavy ASR	
573	39.4	29.0	31.6		
973	38.3	20.2	41.5		

Liquid and solid from ASR pyrolysis contain carcinogenic compounds, chlorine containing materials, and metal compounds which may jeopardize the further use of these products.[164]

The gas fraction as expected contains hydrogen, methane, propane, acetylene, and butane. They have high energy content and can be safely used as heat source for the process.[167]

Improvements in products characteristics are obtained by a preliminary mechanical sorting followed by a catalytic pyrolysis.[168] Pretreatments seem to be mandatory to collect products with more affordable characteristics.[169]

Pyrolysis of ASR can be performed also to produce hydrogen in the presence of a catalytic system.[170]

Reference

1. Kaminsky, W.; Predel, M.; Sadiki, A., Feedstock recycling of polymers by pyrolysis in a fluidised bed. *Polym. Degrad. Stabil.* **2004**, 85, 1045-1050.
2. Plasticeurope Plastics – the Facts 2012 An analysis of European plastics production, demand and waste data for 2011. http://www.plasticseurope.org/Document/plastics-the-facts-2012.aspx?Page=DOCUMENT&FoIID=2 (Accessed: 26.02.2013),
3. Whiteley, K. S., Polyethylene. In *Ullmann's Encyclopedia of Industrial Chemistry*, Wiley-VCH Verlag GmbH & Co. KGaA: 2000.
4. Weikert, R. J. Method of making aseptic packaging. US 4,021,283, 1977.
5. Heggs, T. G., Polypropylene. In *Ullmann's Encyclopedia of Industrial Chemistry*, Wiley-VCH Verlag GmbH & Co. KGaA: 2000.
6. Benedikt, G. M.; Goodall, B. L., *Metallocene Catalyzed Polymers*. William Andrew Publishing: Norwich, NY, 1998; p 394.
7. Maul, J.; Frushour, B. G.; Kontoff, J. R.; Eichenauer, H.; Ott, K.-H.; Schade, C., Polystyrene and Styrene Copolymers. In *Ullmann's Encyclopedia of Industrial Chemistry*, Wiley-VCH Verlag GmbH & Co. KGaA: 2000.
8. Carothers, W. H.; Dorough, G. L.; Natta, F. J. v., Studies of polymerization and ring formation. x. the reversible polymerization of six-membered cyclic esters. J. Am. Chem. Soc. **1932**, 54, 761-772.
9. Spinu, M.; Jackson, C.; Keating, M. Y.; Gardner, K. H., Material Design in Poly(Lactic Acid) Systems: Block Copolymers, Star Homo- and Copolymers, and Stereocomplexes. *J. Macromol. Sci. A* **1996**, 33, 1497-1530.
10. Hartmann, M. H., *High Molecular Weight Polylactic Acid Polymers. In Biopolymers from Renewable Resources*, Kaplan, D., Ed. Springer Berlin Heidelberg: **1998**; pp 367-411.
11. Garlotta, D., A Literature Review of Poly(Lactic Acid). *J. Polym. Environ.* **2001**, 9, (2), 63-84.
12. Poly(Lactic Acid): Synthesis, Structures, Properties, Processing, and Applications. John Wiley & Sons, Inc.: Canada, **2010**; p 522.
13. Datta, R.; Tsai, S.-P.; Bonsignore, P.; Moon, S.-H.; Frank, J. R., Technological and economic potential of poly(lactic acid) and lactic acid derivatives. *FEMS Microbiol. Rev.* **1995**, 16, 221-231.
14. Vink, E. T. H.; Rábago, K. R.; Glassner, D. A.; Springs, B.; O'Connor, R. P.; Kolstad, J.; Gruber, P. R., The Sustainability of NatureWorks™ Polylactide Polymers and Ingeo™ Polylactide Fibers: an Update of the Future. *Macromol. Biosci.* **2004**, 4, 551-564.
15. Li, D.; Frey, M. W.; Baeumner, A. J., Electrospun polylactic acid nanofiber membranes as substrates for biosensor assemblies. *J. Membr. Sci.* **2006**, 279, 354-363.
16. Overhoff, D., Tires. In *Ullmann's Encyclopedia of Industrial Chemistry*, Wiley-VCH Verlag GmbH & Co. KGaA: 2000.
17. Mark, J. E.; Erman, B.; Eirich, F. R., *Science and Technology of Rubber*. 3 ed.; Elsevier Academic Press: Burlington, 2005.
18. Sharma, V. K.; Mincarini, M.; Fortuna, F.; Cognini, F.; Cornacchia, G., Disposal of waste tyres for energy recovery and safe environment—Review. *Energ. Convers. Manage.* **1998**, 39, 511-528.
19. Petrucci, G., Tecnologia di produzione e confezionamento dei contenitori di poliaccoppiato e problematiche connesse alla cessione di isopropiltioxantone agli

alimenti. *Il Bollettino degli Esperti Ambientali* **2007**, 1, 16-22.
20. Vermeulen, I.; Van Caneghem, J.; Block, C.; Baeyens, J.; Vandecasteele, C., Automotive shredder residue (ASR): Reviewing its production from end-of-life vehicles (ELVs) and its recycling, energy or chemicals' valorisation. *J. Hazard. Mater.* **2011**, 190, 8-27.
21. Harder, M. K.; Forton, O. T., A critical review of developments in the pyrolysis of automotive shredder residue. *J. Anal. Appl. Pyrolysis* **2007**, 79, 387-394.
22. Morselli, L.; Santini, A.; Passarini, F.; Vassura, I., Automotive shredder residue (ASR) characterization for a valuable management. *Waste Manage.* **2010**, 30, 2228-2234.
23. Nimz, H. H.; Schmitt, U.; Schwab, E.; Wittmann, O.; Wolf, F., Wood. In *Ullmann's Encyclopedia of Industrial Chemistry*, Wiley-VCH Verlag GmbH & Co. KGaA: 2000.
24. Bastioli, C., Properties and applications of Mater-Bi starch-based materials. *Polym. Degrad. Stabil.* **1998**, 59, 263-272.
25. Haque, M. M.-U.; Alvarez, V.; Paci, M.; Pracella, M., Processing, compatibilization and properties of ternary composites of Mater-Bi with polyolefins and hemp fibres. *Compos. Part. A: Appl. S.* **2011**, 42, 2060-2069.
26. La Mantia, F. P.; Morreale, M., Green composites: A brief review. *Compos. Part. A: Appl. S.* **2011**, 42, 579-588.
27. Division, U. N. S. Environment Glossary. http://unstats.un.org/unsd/environmentgl/gesform.asp?getitem=1178 (Accessed: 22.04.2013),
28. 75/442/EEC, EuropeanUnion, 1975
29. Bagchi, A., Waste Management, Solid. In *Kirk-Othmer Encyclopedia of Chemical Technology*, John Wiley & Sons, Inc.: 2000.
30. Boerner, C.; Chilton, K.; Updated by, S., Recycling. In *Kirk-Othmer Encyclopedia of Chemical Technology*, John Wiley & Sons, Inc.: 2000.
31. Kaminsky, W., Plastic, Recycling. In *Ullmann's Encyclopedia of Industrial Chemistry*, Wiley-VCH, Ed. Wiley-VCH: Verlag GmbH & Co. KGaA, 2000; Vol. A 21.
32. Fletcher, B. L.; Mackay, M. E., A model of plastics recycling: does recycling reduce the amount of waste? *Resour. Conserv. Recy.* **1996**, 17, 141-151.
33. Frediani, P.; Rosi, L.; Frediani, M.; Undri, A.; Occhialini, S.; Meini, S. Production Of Hydrocarbons From Pyrolysis of Tyres. WO2012110991, 2012.
34. Frediani, P.; Rosi, L.; Frediani, M.; Undri, A.; Occhialini, S. Production of Hydrocarbons from Copyrolysis of Plastic and Tyre Material with Microwave Heating. WO2012110990, 2012.
35. Dai, S. A.; Lin, C.-H.; Lin, H.-y.; Liao, W.-Z. Process for producing bis-alkoxylated diols of bisphenol a from spent polycarbonate discs(PC) or PC waste. US20070978561, 2008.
36. Grause, G.; Buekens, A.; Sakata, Y.; Okuwaki, A.; Yoshioka, T., Feedstock recycling of waste polymeric material. *J. Mater. Cycles Waste Manage.* **2011**, 13, 265-282.
37. Kim, D.; Kim, B.-k.; Cho, Y.; Han, M.; Kim, B.-S., Kinetics of Polycarbonate Glycolysis in Ethylene Glycol. *Ind. Eng. Chem. Res.* **2008**, 48, 685-691.
38. Khait, K., Recycling, Plastics. In *Encyclopedia of Polymer Science and Technology*, John Wiley & Sons, Inc.: 2002.
39. Bosmans, A.; Vanderreydt, I.; Geysen, D.; Helsen, L., The crucial role of Waste-to-Energy technologies in enhanced landfill mining: a technology review. *J. Clean. Prod.* **2012**, 55, 10-23.
40. Feedstock Recycling and Pyrolysis of Waste Plastics. John Wiley & Sons,

Ltd: 2006.
41. Panda, A. K.; Singh, R. K.; Mishra, D. K., Thermolysis of waste plastics to liquid fuel A suitable method for plastic waste management and manufacture of value added products—A world prospective. *Renew. Sust. Energ. Rev.* **2010**, 14, 233-248.
42. Conesa, J. A.; Martin-Gullon, I.; Font, R.; Jauhiainen, J., Complete Study of the Pyrolysis and Gasification of Scrap Tires in a Pilot Plant Reactor. *Environ. Sci. Technol.* **2004**, 38, 3189-3194.
43. Ucar, S.; Karagoz, S.; Ozkan, A. R.; Yanik, J., Evaluation of two different scrap tires as hydrocarbon source by pyrolysis. *Fuel* **2005**, 84, 1884–1892.
44. Kaminsky, W.; Zorriqueta, I.-J. N., Catalytical and thermal pyrolysis of polyolefins. *J. Anal. Appl. Pyrol.* **2007**, 79, 368-374.
45. Aguado, R.; Olazar, M.; José, M. J. S.; Gaisàn, B.; Bilbao, J., Wax Formation in the Pyrolysis of Polyolefins in a Conical Spouted Bed Reactor. *Energy Fuels* **2002**, 16, 1429-1437.
46. Laresgoiti, M. F.; Marco, I. d.; Torres, A.; Caballero, B.; Cabrero, M. A.; Chomòn, M. J., Chromatographic analysis of the gases obtained in tyre pyrolysis. *J. Anal. Appl. Pyrol.* **2000**, 55, 43-54.
47. Li, S.-Q.; Yao, Q.; Chi, Y.; Yan, J.-H.; Cen, K.-F., Pilot-Scale Pyrolysis of Scrap Tires in a Continuous Rotary Kiln Reactor. *Ind. Eng. Chem. Res.* **2004**, 43, 5133-5145.
48. Tang, L.; Huang, H., Thermal plasma pyrolysis of used tires for carbon black recovery. *J. Mater. Sci.* **2005**, 40, 3817-3819.
49. Meng, X.; Xu, C.; Li, L.; Gao, J., Cracking Performance and Feed Characterization Study of Catalytic Pyrolysis for Light Olefin Production. *Energy Fuels* **2011**, 25, 1357-1363.
50. Onwudili, J. A.; Insura, N.; Williams, P. T., Composition of products from the pyrolysis of polyethylene and polystyrene in a closed batch reactor: Effects of temperature and residence time. *J. Anal. Appl. Pyrol.* **2009**, 86, 293-303.
51. Mastral, F. J.; Esperanza, E.; Garcìa, P.; Juste, M., Pyrolysis of high-density polyethylene in a fluidised bed reactor. Influence of the temperature and residence time. *J. Anal. Appl. Pyrol.* **2002**, 63, 1-15.
52. Wong, H.-W.; Kruse, T. M.; Woo, O. S.; Broadbelt, L. J., Tertiary resource recovery from waste polymers via pyrolysis: polypropylene. *Prepr. Symp. - Am. Chem. Soc., Div. Fuel Chem.* **2000**, 45, 480-484.
53. Mishra, N.; Das, G.; Ansaldo, A.; Genovese, A.; Malerba, M.; Povia, M.; Ricci, D.; Di Fabrizio, E.; Di Zitti, E.; Sharon, M.; Sharon, M., Pyrolysis of waste polypropylene for the synthesis of carbon nanotubes. *J. Anal. Appl. Pyrol.* **2012**, 94, 91-98.
54. Liu, J.; Jiang, Z.; Yu, H.; Tang, T., Catalytic pyrolysis of polypropylene to synthesize carbon nanotubes and hydrogen through a two-stage process. *Polym. Degrad. Stabil.* **2011**, 96, 1711-1719.
55. Kaminsky, W.; Schlesselmann, B.; Simon, C., Olefins from polyolefins and mixed plastics by pyrolysis. *J. Anal. Appl. Pyrol.* **1995**, 32,19-27.
56. Jung, S.-H.; Cho, M.-H.; Kang, B.-S.; Kim, J.-S., Pyrolysis of a fraction of waste polypropylene and polyethylene for the recovery of BTX aromatics using a fluidized bed reactor. *Fuel Process. Technol.* **2010**, 91, 277-284.
57. Zhao, W.; Hasegawa, S.; Fujita, J.; Yoshii, F.; Sasaki, T.; Makuuchi, K.; Sun, J.; Nishimoto, S.-i., Effects of zeolites on the pyrolysis polypropylene. *Polym. Degrad. Stabil.* **1996**, 53, 129-135.

58. Elordi, G.; Olazar, M.; Lopez, G.; Artetxe, M.; Bilbao, J., Continuous Polyolefin Cracking on an HZSM-5 Zeolite Catalyst in a Conical Spouted Bed Reactor. *Ind. Eng. Chem. Res.* **2011**, 50, 6061-6070.
59. Arandes, J. M.; Torre, I.; Castano, P.; Olazar, M.; Bilbao, J., Catalytic Cracking of Waxes Produced by the Fast Pyrolysis of Polyolefins. *Energy Fuels* **2007**, 21, 561-569.
60. Arandes, J. M.; Torre, I.; Azkoiti, M. J.; Castano, P.; Bilbao, J.; Lasa, H. d., Effect of catalyst properties on the cracking of polypropylene pyrolysis waxes under FCC conditions. *Catal.Today* **2008**, 133-135, 413-419.
61. Tekin, K.; Akal; n, M. K.; Kad; Ç; Karagöz, S., Catalytic degradation of waste polypropylene by pyrolysis. *J. Energy Inst.* **2012**, 85, 150-155.
62. Donaj, P. J.; Kaminsky, W.; Buzeto, F.; Yang, W., Pyrolysis of polyolefins for increasing the yield of monomers' recovery. *Waste Manage.* **2012**, 32, 840-846.
63. Williams, P. T.; Williams, E. A., Interaction of Plastics in Mixed-Plastics Pyrolysis. *Energy Fuels* **1999**, 13, 188-196.
64. Park, B.-I.; Bozzelli, J.; Booty, M.; Bernhard, M. J.; Mesuere, K.; Pettigrew, C. A.; Shi, J.-C.; Simonich, S. L., Polymer Pyrolysis and Oxidation Studies in a Continuous Feed and Flow Reactor: Cellulose and Polystyrene. *Environ. Sci. Technol.* **1999**, 33, 2584-2592.
65. Kiran, N.; Ekinci, E.; Snape, C. E., Recyling of plastic wastes via pyrolysis. *Resour. Conserv. Recy.* **2000**, 29, 273-283.
66. Poutsma, M. L., Further considerations of the sources of the volatiles from pyrolysis of polystyrene. *Polym. Degrad. Stabil.* **2009**, 94, 2055-2064.
67. Snegirev, A. Y.; Talalov, V. A.; Stepanov, V. V.; Harris, J. N., Formal kinetics of polystyrene pyrolysis in non-oxidizing atmosphere. *Thermochim. Acta* **2012**, 548, 17-26.
68. Mo, Y.; Zhao, L.; Chen, C.-L.; Tan, G. Y. A.; Wang, J.-Y., Comparative pyrolysis upcycling of polystyrene waste: thermodynamics, kinetics, and product evolution profile. *J.Therm. Anal. Calorim.* **2013**, 111, 781-788.
69. Puente, G. d. l.; Sedran, U., Recycling polystyrene into fuels by means of FCC: performance of various acidic catalysts. *Appl. Catal., B* **1998**, 19, 305-311.
70. Marczewski, M.; Kaminska, E.; Marczewska, H.; Godek, M.; Rokicki, G.; Sokolowski, J., Catalytic decomposition of polystyrene. The role of acid and basic active centers. *Appl. Catal., B* **2013**, 129, 236-246.
71. Park, J. J.; Park, K.; Kim, J.-S.; Maken, S.; Song, H.; Shin, H.; Park, J.-W.; Choi, M.-J., Characterization of Styrene Recovery from the Pyrolysis of Waste Expandable Polystyrene. *Energy Fuels* **2003**, 17, 1576-1582.
72. Williams, P. T.; Bagri, R., Hydrocarbon gases and oils from the recycling of polystyrene waste by catalytic pyrolysis. *Int. J. Energ. Res.* **2004**, 28, 31-44.
73. Wu, C.; Williams, P. T., Pyrolysis-gasification of plastics, mixed plastics and real-world plastic waste with and without Ni-Mg-Al catalyst. *Fuel* **2010**, 89, 3022-3032.
74. Sun, H.; Rosenthal, C.; Schmidt, L. D., Oxidative Pyrolysis of Polystyrene into Styrene Monomers in an Autothermal Fixed-Bed Catalytic Reactor. *ChemSusChem* **2012**, 5, 1883-1887.
75. Acomb, J. C.; Nahil, M. A.; Williams, P. T., Thermal processing of plastics from waste electrical and electronic equipment for hydrogen production. *J. Anal. Appl. Pyrol.*, In Press, http://dx.doi.org/10.1016/j.jaap.2012.09.014.
76. Arandes, J. M.; Erena, J.; Azkoiti, M. J.; Olazar, M.; Bilbao, J., Thermal recycling of polystyrene and polystyrene-butadiene dissolved in a light cycle oil. *J.*

Anal. Appl. Pyrol. **2003**, 70, 747-760.
77. Andreikov, E. I.; Amosova, I. S.; Dikovinkina, Y. A.; Krasnikova, O. V.; Pervova, M. G., Pyrolysis of polystyrene in coal tar and ethylene tar pitches. *Russ. J. Appl. Chem.* **2012**, 85, 89-97.
78. Aoyagi, Y.; Yamashita, K.; Doi, Y., Thermal degradation of poly[(R)-3-hydroxybutyrate], poly[ε-caprolactone], and poly[(S)-lactide]. *Polym. Degrad. Stabil.* **2002**, 76, 53-59.
79. Sivalingam, G.; Madras, G., Thermal degradation of binary physical mixtures and copolymers of poly(ε-caprolactone), poly(D, L-lactide), poly(glycolide). *Polym. Degrad. Stabil.* **2004**, 84, 393-398.
80. Kopinke, F. D.; Mackenzie, K., Mechanistic aspects of the thermal degradation of poly(lactic acid) and poly(β-hydroxybutyric acid). J. *Anal. Appl. Pyrol.* **1997**, 40–41, 43-53.
81. Kopinke, F.-D.; Remmler, M.; Mackenzie, K.; Milder, M.; Wachsen, Thermal decomposition of biodegradable polyesters -II. Poly(lactic acid). *Polym. Degrad. Stabil.* **1996**, 53, 329-342.
82. Nishida, H.; Mori, T.; Hoshihara, S.; Fan, Y.; Shirai, Y.; Endo, T., Effect of tin on poly(l-lactic acid) pyrolysis. *Polym. Degrad. Stabil.* **2003**, 81, 515-523.
83. Mori, T.; Nishida, H.; Shirai, Y.; Endo, T., Effects of chain end structures on pyrolysis of poly(L-lactic acid) containing tin atoms. *Polym. Degrad. Stabil.* **2004**, 84, 243-251.
84. Fan, Y.; Nishida, H.; Hoshihara, S.; Shirai, Y.; Tokiwa, Y.; Endo, T., Pyrolysis kinetics of poly(l-lactide) with carboxyl and calcium salt end structures. *Polym. Degrad. Stabil.* **2003**, 79, 547-562.
85. Fan, Y.; Nishida, H.; Mori, T.; Shirai, Y.; Endo, T., Thermal degradation of poly(L-lactide): effect of alkali earth metal oxides for selective L,L-lactide formation. *Polymer* **2004**, 45, 1197-1205.
86. Fan, Y.; Nishida, H.; Shirai, Y.; Endo, T., Racemization on thermal degradation of poly(l-lactide) with calcium salt end structure. *Polym. Degrad. Stabil.* **2003**, 80, 503-511.
87. Badia, J. D.; Santonja-Blasco, L.; Martínez-Felipe, A.; Ribes-Greus, A., A methodology to assess the energetic valorization of bio-based polymers from the packaging industry: Pyrolysis of reprocessed polylactide. *Bioresour. Technol.* **2012**, 111, 468-475.
88. Omura, M.; Tsukegi, T.; Shirai, Y.; Nishida, H.; Endo, T., Thermal Degradation Behavior of Poly(Lactic Acid) in a Blend with Polyethylene. *Ind. Eng. Chem. Res.* **2006**, 45, 2949-2953.
89. Cornelissen, T.; Yperman, J.; Reggers, G.; Schreurs, S.; Carleer, R., Flash co-pyrolysis of biomass with polylactic acid. Part 1: Influence on bio-oil yield and heating value. *Fuel* **2008**, 87, 1031-1041.
90. Vitolo, S.; Seggiani, M.; Frediani, P.; Ambrosini, G.; Politi, L., Catalytic upgrading of pyrolytic oils to fuel over different zeolites. *Fuel* **1999**, 78, 1147-1159.
91. Di Blasi, C., Modeling chemical and physical processes of wood and biomass pyrolysis. *Progr. Energ. Combust.* **2008**, 34, 47-90.
92. Blasi, C. D.; Branca, C., Kinetics of Primary Product Formation from Wood Pyrolysis. *Ind. Eng. Chem. Res.* **2001**, 40, 5547-5556.
93. Di Blasi, C.; Branca, C.; Santoro, A.; Gonzalez Hernandez, E., Pyrolytic behavior and products of some wood varieties. *Combust. Flame* **2001**, 124, 165-177.
94. Morf, P.; Hasler, P.; Nussbaumer, T., Mechanisms and kinetics of

homogeneous secondary reactions of tar from continuous pyrolysis of wood chips. *Fuel* **2002**, 81, 843-853.
95. Branca, C.; Giudicianni, P.; Di Blasi, C., GC/MS Characterization of Liquids Generated from Low-Temperature Pyrolysis of Wood. *Ind. Eng. Chem. Res.* **2003**, 42, 3190-3202.
96. Mohan, D.; Pittman, C. U.; Steele, P. H., Pyrolysis of Wood/Biomass for Bio-oil: A Critical Review. *Energy Fuels* **2006**, 20, 848-889.
97. Bridgwater, A. V., Renewable fuels and chemicals by thermal processing of biomass. *Chem. Eng. J.* **2003**, 91, 87-102.
98. Bridgwater, A. V.; Peacocke, G. V. C., Fast pyrolysis processes for biomass. *Renew. Sust. Energ. Rev.* **2000**, 4, 1-73.
99. Ramis, X.; Cadenato, A.; Salla, J. M.; Morancho, J. M.; Vallés, A.; Contat, L.; Ribes, A., Thermal degradation of polypropylene/starch-based materials with enhanced biodegradability. *Polym. Degrad. Stabil.* **2004**, 86, 483-491.
100. Cadenato, A.; Ramis, X.; Salla, J. M.; Morancho, J. M.; Contat-Rodrigo, L.; Vallés-Lluch, A.; Ribes-Greus, A., Calorimetric studies of PP/Mater-Bi blends aged in soil. *J. Appl. Polym. Sci.* **2006**, 100, 3446-3453.
101. Vallés-Lluch, A.; Contat-Rodrigo, L.; Ribes-Greus, A., Degradation studies of LDPE–Mater-Bi blends annealed and aged in soil. *J. Appl. Polym. Sci.* **2002**, 86, 405-413.
102. Alvarez, V. A.; Ruseckaite, R. A.; Vázquez, A., Degradation of sisal fibre/ Mater Bi-Y biocomposites buried in soil. *Polym. Degrad. Stabil.* **2006**, 91, 3156-3162.
103. Moriana-Torró, R.; Contat-Rodrigo, L.; Santonja-Blasco, L.; Ribes-Greus, A., Thermal characterisation of photo-oxidized HDPE/Mater-Bi and LDPE/Mater-Bi blends buried in soil. *J. Appl. Polym. Sci.* **2008**, 109, 1177-1188.
104. Buckley, J.; Halliday, A.; Lewis, A.; Druminski, D.; Shivkumar, S., Mechanical properties and degradation of commercial biodegradable plastic bags. *Annu. Tech. Conf. - Soc. Plast. Eng.* **2011**, 69th, 1032-1039.
105. Yang, Z.; Liu, X.; Yang, Z.; Zhuang, G.; Bai, Z.; Zhang, H.; Guo, Y., Preparation and formation mechanism of levoglucosan from starch using a tubular furnace pyrolysis reactor. *J. Anal. Appl. Pyrol.* **2013**, 102, 83-88.
106. Patwardhan, P. R.; Satrio, J. A.; Brown, R. C.; Shanks, B. H., Product distribution from fast pyrolysis of glucose-based carbohydrates. *J. Anal. Appl. Pyrol.* **2009**, 86, 323-330.
107. Gómez-Martínez, D.; Barneto, A. G.; Martínez, I.; Partal, P., Modelling of pyrolysis and combustion of gluten–glycerol-based bioplastics. *Bioresour. Technol.* **2011**, 102, 6246-6253.
108. Choi, S.-S.; Kim, M.-C.; Kim, Y.-K., Influence of silica on formation of levoglucosan from carbohydrates by pyrolysis. *J. Anal. Appl. Pyrol.* **2011**, 90, 56-62.
109. Laresgoiti, M. F.; Caballero, B. M.; de Marco, I.; Torres, A.; Cabrero, M. A.; Chomón, M. J., Characterization of the liquid products obtained in tyre pyrolysis. *J. Anal. Appl. Pyrol.* **2004**, 71, 917-934.
110. Frigo, S.; Seggiani, M.; Puccini, M.; Vitolo, S. Liquid fuel production from waste tyre pyrolysis and its utilisation in a Diesel engine. *Fuel* **2014**, 116, 399-408.
111. Hofman, M.; Pietrzak, R., Adsorbents obtained from waste tires for NO_2 removal under dry conditions at room temperature. *Chem. Eng. J.* **2011**, 170, 202–208.
112. Lòpez, G.; Olazar, M.; Artetxe, M.; Amutio, M.; Elordi, G.; Bilbao, J., Steam

activation of pyrolytic tyre char at different temperatures. *J. Anal. Appl. Pyrol.* **2009**, 85, 539-543.
113. Aranda, A.; Murillo, R.; Garcìa, T.; Callén, M. S.; Mastral, A. M., Steam activation of tyre pyrolytic carbon black: Kinetic study in a thermobalance. *Chem. Eng. J.* **2007**, 126, 79-85.
114. Zabaniotou, A.; Madau, P.; Oudenne, P. D.; Jung, C. G.; Delplancke, M.-P.; Fontana, A., Active carbon production from used tire in two-stage procedure: industrial pyrolysis and bench scale activation with H_2O–CO_2 mixture. *J. Anal. Appl. Pyrol.* **2004**, 72, 289-297.
115. Mui, E. L. K.; Ko, D. C. K.; McKay, G., Production of active carbons from waste tyres – a review. *Carbon* **2004**, 42, 2789-2805.
116. Ko, D. C. K.; Mui, E. L. K.; Lau, K. S. T.; McKay, G., Production of activated carbons from waste tire – process design and economical analysis. *Waste Manage.* **2004**, 24, 875–888.
117. Zabaniotou, A. A.; Stavropoulos, G., Pyrolysis of used automobile tires and residual char utilization. *J. Anal. Appl. Pyrol.* **2003**, 70, 711-722.
118. Lucchesi, A.; Maschio, G., Semi-active carbon and aromatics produced by pyrolysis of scrap tires. *Conserv. Recycling* **1983**, 8, 85-90.
119. Jie, Z.; Jingdai, W.; Xiaohong, R.; Yongrong, Y.; Binbo, J., Surface Modification of Pyrolytic Carbon Black from Waste Tires and Its Use as Pigment for Offset Printing Ink. *Chin. J. Chem. Eng.* **2006**, 14, 654-659.
120. Rodriguez, I. d. M.; Laresgoiti, M. F.; Cabrero, M. A.; Torres, A.; Chomòn, M. J.; Caballero, B., Pyrolysis of scrap tyres. *Fuel Process. Technol.* **2001**, 72, 9-22.
121. Piskorz, J.; Majerski, P.; Radlein, D.; Wik, T.; Scott, D. S., Recovery of Carbon Black from Scrap Rubber. *Energy Fuels* **1999**, 13, 544-551.
122. Murena, F., Kinetics of sulphur compounds in waste tyres pyrolysis. *J. Anal. Appl. Pyrol.* **2000**, 56, 195-205.
123. Miranda, M.; Pinto, F.; Gulyurtlu, I.; Cabrita, I., Pyrolysis of rubber tyre wastes: A kinetic study. *Fuel* **2013**, 103, 542–552.
124. Berrueco, C.; Esperanza, E.; Mastral, F. J.; Ceamanos, J.; Garcìa-Bacaicoa, P., Pyrolysis of waste tyres in an atmospheric static-bed batch reactor: Analysis of the gases obtained. *J. Anal. Appl. Pyrol.* **2005**, 74, 245-253.
125. Barbooti, M. M.; Mohamed, T. J.; Hussain, A. A.; Abas, F. O., Optimization of pyrolysis conditions of scrap tires under inert gas atmosphere. *J. Anal. Appl. Pyrol.* **2004**, 72, 165-170.
126. Kyari, M.; Cunliffe, A.; Williams, P. T., Characterization of Oils, Gases, and Char in Relation to the Pyrolysis of Different Brands of Scrap Automotive Tires. *Energy Fuels* **2005**, 19, 1165-1173.
127. Banar, M.; Akyıldız, V.; Özkan, A.; Çokaygil, Z.; Onay, Ö., Characterization of pyrolytic oil obtained from pyrolysis of TDF (Tire Derived Fuel). *Energ. Convers. Manage*. **2012**, 62, 22-30.
128. Juma, M.; Koreňová, Z.; Markoš, J.; Annus, J.; Jelemenský, L., Pyrolysis and combustion of scrap tire. *Petroleum & Coal* **2006**, 48, 15-26.
129. Dìez, C.; Sànchez, M. E.; Haxaire, P.; Martìnez, O.; Moran, A., Pyrolysis of tyres: A comparison of the results from a fixed-bed laboratory reactor and a pilot plant (rotatory reactor). *J. Anal. Appl. Pyrol.* **2005**, 74, 254-258.
130. Aylòn, E.; Fernàndez-Colino, A.; Murillo, R.; Murillo, R.; Garcìa, T.; Mastral, A. M., Valorisation of waste tyre by pyrolysis in a moving bed reactor. *Waste Manage.* **2010**, 30, 1220-1224.
131. Kaminsky, W.; Mennerich, C., Pyrolysis of synthetic tire rubber in a fluidised-

bed reactor to yield 1,3-butadiene, styrene and carbon black. *J. Anal. Appl. Pyrol.* **2001**, 58-59, 803-811.
132. Dai, X.; Yin, X.; Wu, C.; Zhang, W.; Chen, Y., Pyrolysis of waste tires in a circulating fluidized-bed reactor. *Energy* **2001**, 26, 385-399.
133. Conesa, J. A.; Font, R.; Marcilla, A., Gas from the Pyrolysis of Scrap Tires in a Fluidized Bed Reactor. *Energy Fuels* **1996**, 10, 134-140.
134. Quek, A.; Balasubramanian, R., Liquefaction of waste tires by pyrolysis for oil and chemicals—A review. *J. Anal. Appl. Pyrol.* **2013**, 101, 1-16.
135. William J. Hall; Norasalwa Zakaria; Williams, P. T., Pyrolysis of latex gloves in the presence of Y-zeolite. *Waste Manage.* **2009**, 29, 797–803.
136. Stanciulescu, M.; Ikura, M., Limonene ethers from tire pyrolysis oil Part 2: Continuous flow experiments. *J. Anal. Appl. Pyrol.* **2007**, 78, 76-84.
137. Stanciulescu, M.; Ikura, M., Limonene ethers from tire pyrolysis oil Part 1: Batch experiments. *J. Anal. Appl. Pyrol.* **2006**, 75, 217-225.
138. Pakdel, H.; Pantea, D. M.; Roy, C., Production of dl-limonene by vacuum pyrolysis of used tires. *J. Anal. Appl. Pyrol.* **2001**, 57, 91–107.
139. Williams, P. T.; Brindle, A. J., Aromatic chemicals from the catalytic pyrolysis of scrap tyres. *J. Anal. Appl. Pyrol.* **2003**, 67, 143-164.
140. Williams, P. T.; Brindle, A. J., Catalytic pyrolysis of tyres: influence of catalyst temperature. *Fuel* **2002**, 81, 2425-2434.
141. Boxiong, S.; Chunfei, W.; Cai, L.; Binbin, G.; Rui, W., Pyrolysis of waste tyres: The influence of USY catalyst/tyre ratio on products. *J. Anal. Appl. Pyrol.* **2007**, 78, 243-249.
142. Boxiong, S.; Chunfei, W.; Binbin, G.; Rui, W.; Cai, L., Pyrolysis of waste tyres with zeolite USY and ZSM-5 catalysts. *Appl. Catal., B* **2007**, 73, 150-157.
143. Qu, W.; Zhou, Q.; Wang, Y.-Z.; Zhang, J.; Lan, W.-W.; Wu, Y.-H.; Yang, J.-W.; Wang, D.-Z., Pyrolysis of waste tire on ZSM-5 zeolite with enhanced catalytic activities. *Polym. Degrad. Stabil.* **2006**, 91, 2389-2395.
144. Olazar, M.; Aguado, R.; Arabiourrutia, M.; Lopez, G.; Barona, A.; Bilbao, J., Catalyst Effect on the Composition of Tire Pyrolysis Products. *Energy Fuels* **2008**, 22, 2909-2916.
145. Elbaba, I. F.; Wu, C.; Williams, P. T., Hydrogen production from the pyrolysise gasification of waste tyres with a nickel/cerium catalyst. Int. *J. Hydrogen Energy* **2011**, 36, 6628-6637.
146. Haydary, J.; Susa, D.; Dudáš, J., Pyrolysis of aseptic packages (tetrapak) in a laboratory screw type reactor and secondary thermal/catalytic tar decomposition. *Waste Manage.* **2013**, 33, 1136-1141.
147. Chao-Hsiung, W.; Ching-Yuan, C.; Yu-Fen, L.; Yeou-Lih, Y., Effects of Oxygen on Pyrolysis Kinetics of Tetra Pack. *J. Environ. Eng.* **2003**, 129, 382-286.
148. Wu, C.-H.; Liu, Y.-F., Pyrolysis Products of Tetra Pack in Different Oxygen Concentrations. *Energy Fuels* **2001**, 15, 841-847.
149. Korkmaz, A.; Yanik, J.; Brebu, M.; Vasile, C., Pyrolysis of the tetra pak. *Waste Manage.* **2009**, 29, 2836-2841.
150. Wu, C.-H.; Chang, H.-S., Pyrolysis of tetra pack in municipal solid waste. *J. Chem. Technol. Biot.* **2001**, 76, 779-792.
151. Grammelis, P.; Basinas, P.; Malliopoulou, A.; Sakellaropoulos, G., Pyrolysis kinetics and combustion characteristics of waste recovered fuels. *Fuel* **2009**, 88, 195-205.
152. Reyes, J. A.; Conesa, J. A.; Marcilla, A., Pyrolysis and combustion of polycoated cartons: kinetic model and MS-analysis. *J. Anal. Appl. Pyrol.* **2001**,

58–59, 747-763.
153. 152. Shen, D. K.; Gu, S., The mechanism for thermal decomposition of cellulose and its main products. *Bioresour.Technol.* **2009**, 100, 6496-6504.
154. Lin, Y.-C.; Cho, J.; Tompsett, G. A.; Westmoreland, P. R.; Huber, G. W., Kinetics and Mechanism of Cellulose Pyrolysis. *J. Phys. Chem. C* **2009**, 113, 20097-20107.
155. Sánchez-Jiménez, P.; Pérez-Maqueda, L.; Perejón, A.; Pascual-Cosp, J.; Benítez-Guerrero, M.; Criado, J., An improved model for the kinetic description of the thermal degradation of cellulose. *Cellulose* **2011**, 18, 1487-1498.
156. Mettler, M. S.; Mushrif, S. H.; Paulsen, A. D.; Javadekar, A. D.; Vlachos, D. G.; Dauenhauer, P. J., Revealing pyrolysis chemistry for biofuels production: Conversion of cellulose to furans and small oxygenates. *Energ. Environ. Sci.* **2012**, 5, 5414-5424.
157. Zhang, X.; Yang, W.; Blasiak, W., Kinetics of levoglucosan and formaldehyde formation during cellulose pyrolysis process. *Fuel* **2012**, 96, 383-391.
158. Grieco, E. M.; Baldi, G., Pyrolysis of polyethylene mixed with paper and wood: Interaction effects on tar, char and gas yields. *Waste Manage.* **2012**, 32, 833-839.
159. Sharypov, V. I.; Marin, N.; Beregovtsova, N. G.; Baryshnikov, S. V.; Kuznetsov, B. N.; Cebolla, V. L.; Weber, J. V., Co-pyrolysis of wood biomass and synthetic polymer mixtures. Part I: influence of experimental conditions on the evolution of solids, liquids and gases. *J. Anal. Appl. Pyrol.* **2002**, 64, 15-28.
160. Marin, N.; Collura, S.; Sharypov, V. I.; Beregovtsova, N. G.; Baryshnikov, S. V.; Kutnetzov, B. N.; Cebolla, V.; Weber, J. V., Copyrolysis of wood biomass and synthetic polymers mixtures. Part II: characterisation of the liquid phases. J*. Anal. Appl. Pyrol.* **2002**, 65, 41-55.
161. Sharypov, V. I.; Beregovtsova, N. G.; Kuznetsov, B. N.; Membrado, L.; Cebolla, V. L.; Marin, N.; Weber, J. V., Co-pyrolysis of wood biomass and synthetic polymers mixtures. Part III: Characterisation of heavy products. *J. Anal. Appl. Pyrol.* **2003**, 67, 325-340.
162. Jakab, E.; Várhegyi, G.; Faix, O., Thermal decomposition of polypropylene in the presence of wood-derived materials. *J. Anal. Appl. Pyrol.* **2000**, 56, 273-285.
163. Rutkowski, P.; Kubacki, A., Influence of polystyrene addition to cellulose on chemical structure and properties of bio-oil obtained during pyrolysis. *Energ. Convers. Manage.* **2006**, 47, 716-731.
164. Rausa, R.; Pollesel, P., Pyrolysis of automotive shredder residue (ASR) influence of temperature on the distribution of products. *J. Anal. Appl. Pyrol.***1997**, 40–41, 383-401.
165. Zolezzi, M.; Nicolella, C.; Ferrara, S.; Iacobucci, C.; Rovatti, M., Conventional and fast pyrolysis of automobile shredder residues (ASR). *Waste Manage.* **2004**, 24, 691-699.
166. de Marco, I.; Caballero, B. M.; Cabrero, M. A.; Laresgoiti, M. F.; Torres, A.; Chomón, M. J., Recycling of automobile shredder residues by means of pyrolysis. *J. Anal. Appl. Pyrol.* **2007**, 79, 403-408.
167. Joung, H.; Seo, Y.; Kim, K.; Hong, J.; Yoo, T., Distribution and characteristics of pyrolysis products from automobile shredder residue using an experimental semi-batch reactor. *Korean J. Chem. Eng.* **2007**, 24, 996-1002.
168. Santini, A.; Passarini, F.; Vassura, I.; Serrano, D.; Dufour, J.; Morselli, L., Auto shredder residue recycling: Mechanical separation and pyrolysis. *Waste Manage.* **2012**, 32, 852-858.

169. Hwang, I. H.; Yokono, S.; Matsuto, T., Pretreatment of automobile shredder residue (ASR) for fuel utilization. *Chemosphere* **2008**, 71, 879-885.
170. Lin, K.-S.; Chowdhury, S.; Wang, Z.-P., Catalytic gasification of automotive shredder residues with hydrogen generation. *J. Power Sources* **2010**, 195, 6016–6023.

2. Microwave and Materials

Radiation in the microwave (MW) region was initially used during the Second World War as a key technology in radar applications. During these first applications the ability of MW to heat foodstuff was discovered.

Nowadays MW is widely exploited in our daily-life in MW oven, chemist work as heating technology, and industrial applications from polymer curing to ceramic sintering.

The MW region of the electromagnetic spectrum corresponds to wavelengths from 1 cm to 1 m (30 GHz to 300 MHz). The wavelengths of 1–25 cm are used for radar and telecommunication issues, and by international agreement only the frequencies at 2.45 GHz (12.2 cm) and 900 MHz (33.3 cm) are available for heating purpose. Only if the leakage of stray microwave radiation is prevented other frequency may be used.

Today it is well known, that MW are able to heat a wide range of materials.

In conventional heating energy is transferred by three ways: convection, conduction, and radiation from the source to the surfaces of the material. A thermal gradient is always required to achieve heat transfer. MW delivers their energy content at molecular level that is thorough the conversion of the electromagnetic energy of the MW to thermal energy rather than heat transfer.[1] So far MW shows several physical differences compared to conventional heating, that is:[2]

- Volumetric heating of materials
- Selective heating
- High heating rates
- Reduction of processing time
- Increased product quality
- Processing of new materials
- Savings of energy consumption
- Green technology.

Indeed the transfer of energy does not rely on diffusion of heat from the surfaces, and it is possible to achieve rapid and uniform heating of thick materials (especially carbon, metals, and ceramics which are materials with low thermal

conductivities).

The first wide spreading measurement of MW interaction with materials was performed by von Hippel et al. providing the actual basic dielectric parameters governing the extent of interaction between microwaves and solid/solution samples.[3]

MW interaction with materials is not a quantum mechanical phenomenon localized on a single molecule but it is a collective property. In Figure 2.1 is reported the energy associated to a MW photon at 2.45 GHz and the energies relative to carbon-carbon and carbon-hydrogen covalent bond and the bond energy in an average ionic solid.

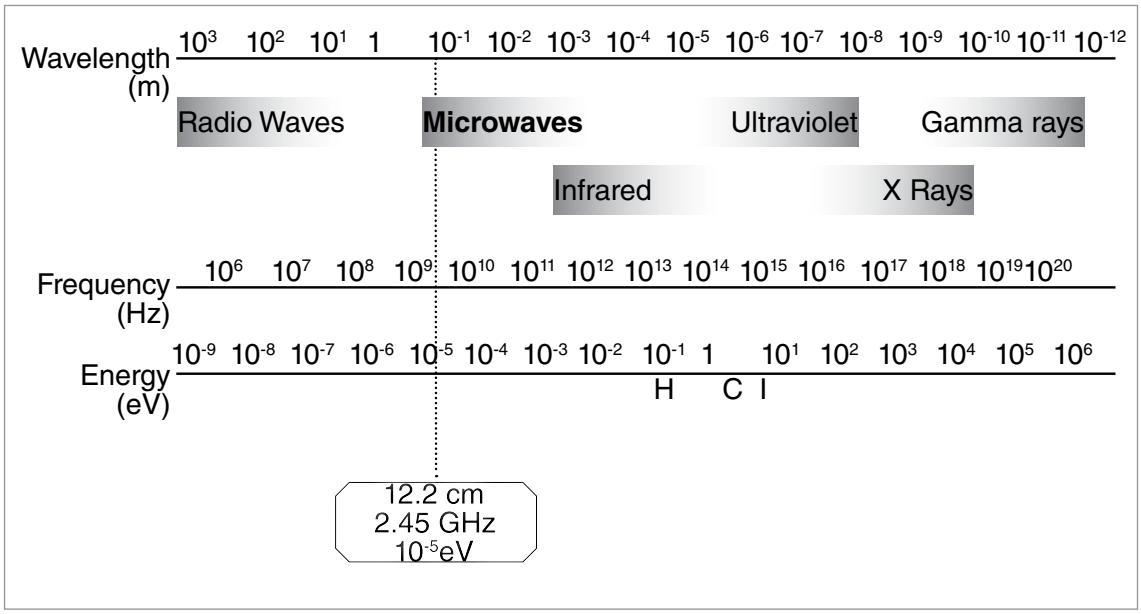

Figure 2.1. MW frequency and relative energy. C: carbon-carbon covalent bond energy; H: carbon-hydrogen covalent bond energy; I: ionic solid average bond energy.

In the following sections an introduction of MW equipment and MW interaction with material for heating purpose are briefly reviewed.

2.1. Microwave equipment

Any MW system comprises a MW source, a transmission line, and an applicator. The MW source is a device where the MW at a fixed frequency is produced. The transmission line transfers the MW from the source to the applicator. The applicator is the cavity where the sample is placed and heated, also known as the oven.

MW is generated by accelerating charges, and high power and frequencies are achieved inside vacuum tubes. The most used MW generator for heating application are magnetrons, traveling wave tubes, and klystrons. Magnetrons are used in domestic oven so they are mass produced and available on the market at very low price. They use resonant structures to generate the electromagnetic

field, and, therefore, they are capable of generating a fixed frequency of an electromagnetic field. For variable frequency applications traveling wave tubes are employed.

Magnetrons are constituted by an anode at a high potential compared to a cathode. Therefore the potential difference produces a strong electric field, then the cathode is heated to produce electron that are accelerated toward the anode by the electric field (Figure 2.2). An external magnet creates an orthogonal magnetic field that creates a circumferential force on the electron as it is accelerated to the anode. So far as electrons pass the resonant cavities, the cavities starts with oscillations in an electron cloud, and the frequency of the oscillations depends on the size of the cavities. At this point the electromagnetic energy is transferred to the applicator through a coaxial transmission line.

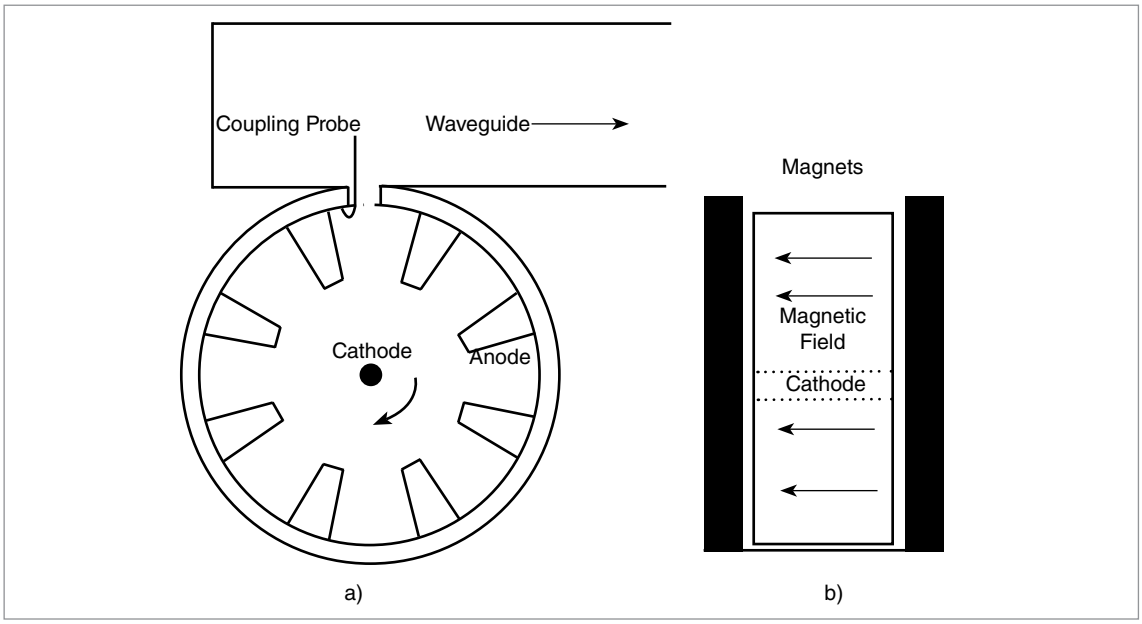

Figure 2.2. Schematic diagram of a magnetron. a) top view; b) side view.[1]

The output power can be adjusted in three ways. In the first one the magnetron works at full power but alternate on-off cycle. In the second the current amplitude of the cathode is varied. In the third the intensity of magnetic field is varied.[1]

The transmission line transfers energy from the source to the applicator. In low power systems, the transmission lines are often coaxial cables, which are similar to those used on televisions. At high frequencies and output power, the losses that occur in coaxial cables are significant, and hollow rectangular tubes are used. These devices are called waveguides and the electromagnetic waves propagate with low loss.

The applicator is a cavity where the MW energy is transferred to the sample. There are two main kind of applicator: single mode and multi-mode.

Single mode applicators are based on strict geometry and their size is close to wavelength used, and in order to maintain the resonant mode, they require

a microwave source that has little variation in the frequency output. In general, single mode cavities have one “hot spot” where the microwave field strength is high.

Multi-mode applicators have several high order mode at the same time in their cavity. They do not need fixed size at given frequency, and as the cavity size increases the number of mode increases as well. Usually the size of an applicator is larger than one wavelength. The rule of thumb to achieve uniformity within an applicator is to have the longest dimension 100 times greater than the wavelength of the operating frequency (for 2.45 GHz should be larger than 12 m).[1]

2.2. Microwave interaction with materials and microwave heating

MW interacts with materials following several mechanisms and an exhaustive review could become a huge work but far from the aim of this work.

Usually materials that are heated through MW are dielectrics. A dielectric material contains permanent or induced dipoles, which when placed between two electrodes acts as a capacitor (charge are stored and no direct current conductivity is observed if the electrodes are connected by a circuit). In this situation dielectrics show polarization from the finite displacement of charges or rotation of dipoles. This is different from conduction where a translational motion of electric charges is realized when a field is applied.

Also conducting materials are heated by the electric field due to the motion of its electric charges which cause Joule heating. It can be observed in metals but also in carbon-based materials where a graphitic texture is present (Figure 2.3).[4]

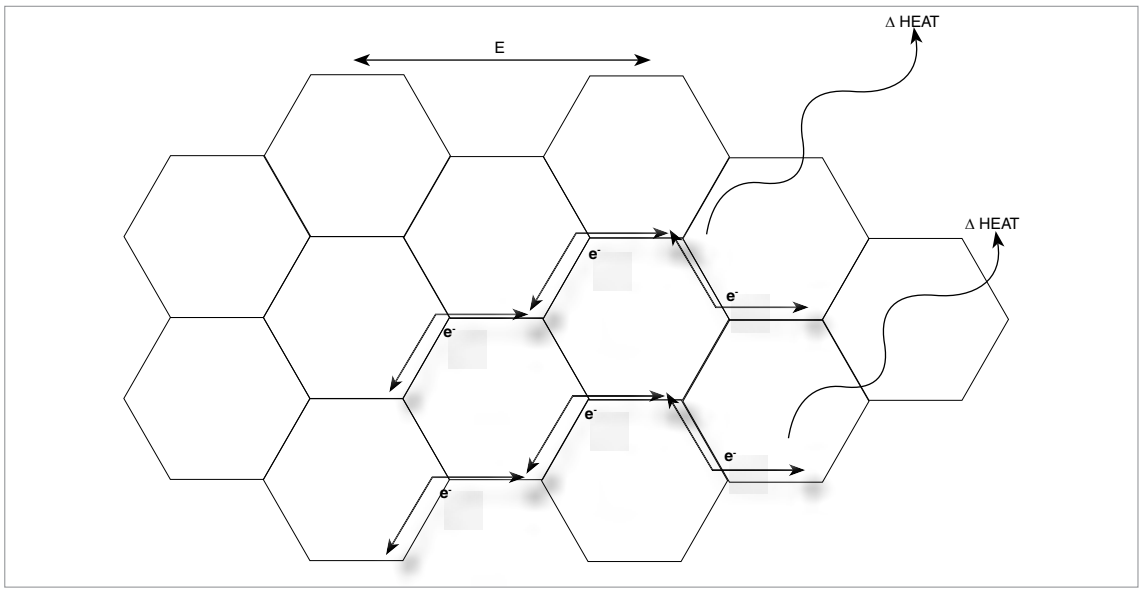

Figure 2.3. Schematic representation of MW heating of carbon material.

At molecular level dielectrics show two main effects when exposed to MW: a distortion of the distribution of the electronic cloud of the molecule or the physical

rotation of dipoles. The latter effect is predominant in dielectric heating because the rotational relaxation time occurs in the microwave region for many polar organic molecules.[5] In general terms if the external electric field is alternating, the dielectric response follows it, generally with some lag behind the field changes.

A measure of such response of a material to an external electric field is the dielectric permittivity, ε.[6] To quantify this phenomenon in an alternating field a complex dielectric permittivity that depends on the field frequency, ω, is formally introduced in 2.1:

$$\varepsilon(\omega) = \varepsilon'(\omega) + i\varepsilon''(\omega) \qquad \textbf{2.1}$$

The imaginary part of the 2.1 is greater when the lag in dielectric response is larger. The change of polarization is coupled by the motion of electric charges which generates heat inside the material. The effective high-frequency conductivity, σ, can be introduced in order to characterize the power of heating (P). The power of heating per volume is equal to the absorbed microwave power and it is reported in 2.2:

$$P = \sigma E^2 \qquad \textbf{2.2}$$

E is the strength of the electric field inside the material. σ is linked to the imaginary part of the dielectric permittivity as reported in 2.3:

$$\sigma = \omega \varepsilon_0 \varepsilon \qquad \textbf{2.3}$$

ε_0 is the permittivity of free space. While the MW pass through the material E decreases. This electromagnetic energy dissipation is characterized by the loss factor (2.4):

$$\tan\delta = \frac{\varepsilon''}{\varepsilon'} \qquad \textbf{2.4}$$

The penetration depth (L) of MW, that is the space in which the field strength is reduced by a factor "e", is described by 2.5:

$$L = \frac{c}{\omega}\sqrt{\frac{2[1+\sqrt{1+\tan^2\delta}\,]}{\varepsilon'\tan^2\delta}} \qquad \textbf{2.5}$$

Where c is the speed of light.

The incident electromagnetic wave can be also partially reflected by the surface of a material, the fraction of reflected power (R) is reported in 2.6:

$$R = \frac{1-\sqrt{2\varepsilon'(1+\sqrt{1+\tan^2\delta})}+\varepsilon'\sqrt{1+\tan^2\delta}}{1+\sqrt{2\varepsilon'(1+\sqrt{1+\tan^2\delta})}+\varepsilon'\sqrt{1+\tan^2\delta}} \qquad \textbf{2.6}$$

So far any process involving MW heating can be described by L and R. Furthermore the dependence of ε from ω determines the feature of MW heating at different frequencies.

In classical heating the energy is transferred by thermal radiation (usually in the infrared range). Its L is small (1 10^{-4} m) and the energy is localized in a thin layer over the material surface. Heating in this case depends only on heat transfer from

the hot surface to the cold bulk by thermal conductivity. Worthy of note is that polymers have a poor thermal conductivity.

The absorption of MW may vary strongly because tan δ values vary from 10^{-4} to 1 together with R and L. In Table 2.1 are reported some tanδ values of selected materials.

Table 2.1. Some tanδ values of selected materials at 298 K. [4, 5]

material	tanδ
Coal	0.02–0.08
Carbon foam	0.05–0.20
Charcoal	0.11–0.29
Carbon black	0.35–0.83
Activated carbon	0.57–0.80
Activated carbon	0.22–2.95
Carbon nanotube	0.25–1.14
CSi nanofibres	0.58–1.00
ZnO	0.0529
TiO	0.0322
H_2O	0.123
MeOH	0.659
EtOH	0.941
1-Propanol	0.757
Me_2SO	0.825
$HCONMe_2$	0.161
$MeNO_2$	0.064
THF	0.047
CH_2Cl_2	0.042
$CHCl_3$	0.091
MeCOMe	0.054
$MeCO_2Et$	0.059
HCO_2H	0.722
$MeCO_2H$	0.174
MeCN	0.062
PhCN	0.459
CH_2OHCH_2OH	1.35

A material that show a low tanδ ($<10^{-3}$) shows almost no heating when irradiated at 2.45 GHz and the MW pass through without any strong effects (Figure 2.4a). Anyway the not absorbed MW, if the oven is well designed, could be summed in phase enhancing E so the absorbed power. A possibility to heat low tanδ materials is to mix them with high tanδ materials such or metals.

Materials with high tanδ ($> 10^{-1}$) quickly interact with MW and they are heated at any MW frequency. Anyway the effective conductivity is typically so large that a strong reflection of radiation from the surface inhibits further heating (Figure 2.4b). The absorbed fraction of the incident MW power can be estimated approximately

as reported in 2.7:

$$1 - R \approx 2\sqrt{\frac{2}{\varepsilon' \tan^2 \delta}} \quad \textbf{2.7}$$

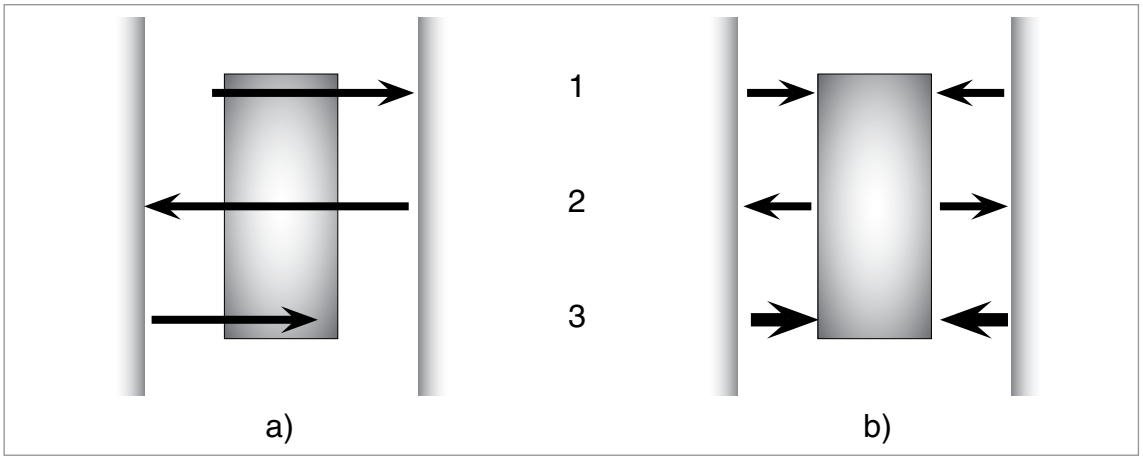

Figure 2.4. Schematic representation of a MW cavity. a) the MW are not absorbed, the sample has a low tanδ value, 1, incident radiation; 2 and 3, radiation returned to the sample after reflection from oven walls.; b) the MW are absorbed, the sample has a high tanδ value, 1, incident radiation; 2, radiation reflected from the sample; 3, radiation returned to the sample after reflection from oven walls.

Therefore the knowledge of dielectric properties, chemical composition, micro and macro structure are fundamental to apply worthwhile a MW heating. However a theoretical approach to a MW heating issue can give only qualitative information because these mechanisms are strongly dependent on the structure of materials, type and strength of chemical bonds among atoms.

Further consideration can be done when materials are heated at high temperature because changes in their structure affect tanδ and the other parameter described above. Indeed at elevated temperatures, microwave absorption grows sharply. This feature is found in ionic and covalent solids. In these solid the increase in MW absorption starts at temperatures about 40 – 50% of the melting temperature. In this temperature range the bonds between ions start to break, and the electrons in covalent materials begin to populate the conduction bands. The increase in microwave absorption with temperature can cause a thermal instability, which is known as a temperature runaway. Thus an increase in the local temperature is followed by an enhancement of MW absorption, which ensues in the local acceleration of heating and further growth of temperature.[6]

Reference

1. Thostenson, E. T.; Chou, T. W., Microwave processing: fundamentals and applications. *Compos. Part. A: Appl. S.* **1999**, 30, 1055-1071.
2. Feher, L. E., Energy Efficient Microwave Systems. Springer: 2009; p 124.
3. Von Hippel, A. R., *Dielectric materials and applications*. MIT Press, Cambridge, MA, 1954.
4. Menéndez, J. A.; Arenillas, A.; Fidalgo, B.; Fernández, Y.; Zubizarreta, L.; Calvo, E. G.; Bermúdez, J. M., Microwave heating processes involving carbon materials. *Fuel Process. Technol.* **2010**, 91, 1-8.
5. Tierney, J. P.; Lidstrom, P., *Microwave Assisted Organic Synthesis*. 1 ed.; Blackwell Publishing Ltd: Oxford, UK, 2005; p 289.
6. Bykov, Y. V.; Rybakov, K. I.; Semenov, V. E., High-temperature microwave processing of materials. *J Phys. D Appl. Phys* **2001**, 34, R55.

3. Microwave Processing of Materials

MW heating shows a sound and worthwhile application in several fields due to the benefits of this heating technology. It has been developed and used in food (for baking, vacuum drying, tempering and thawing, pasteurization, and sterilization),[1] polymer industries (for rubber vulcanization, polymerization or curing of resins and polymers by elimination of polar solvents),[2] chemical reactions and so on. In recent years there is a growing interest toward developing microwave assisted pyrolysis (MAP) processes. MW heating, as outlined in Section 2, may overwhelm all the heat transfer and diffusion problems by localizing the energy directly on compounds able to interact with MW. Furthermore may allow a careful control of pyrolysis parameters to maximize one of the products. Must be taken into account that operating parameters can induce and/or alter particular chemical reactions, resulting in different chemical profiles of the products themself.[3] As a consequence, feedstock for MAP requires few pretreatment and conditioning steps (such as grinding or chopping) with respect to conventional pyrolysis. These benefits may reduce time and energy, and they may allow a cleaner conversion to valuable products than gasification and conventional pyrolysis.

MW heating shows further difference and unique feature with respect to conventional and other heating methods. These effects are observed on materials which possess electrons able to move freely in its structure such as carbon or metals. These moving charges may cause the formation of arcing or microplasmas on the surface.[2, 4-8]

Anyway switching to a MW heated system may present some new problematic issue. Homogeneity of MW radiation and heating can be challenging on large sample and a mixing system may solve the problem. However the mixing system should be transparent to MW otherwise it may change the behavior of the pyrolysis itself. The formation of char into the oven may cover the quartz windows from which the MW are delivered into the oven. So the char may absorb the MW preventing them to enter inside the oven and this deposit may damage the windows themselves or the generator if the MW is sent back.

3.1. Biomasses

Pyrolysis of biomasses to obtain liquid, also known as bio-fuel, requires rapid heating at moderate temperature followed by a rapid quenching of the intermediate volatile products.[9, 10] In MAP this requirement is achieved without finely milling the feedstock because MW allows the volumetric heating of sample, furthermore the presence of water may enhance the heating rate and mitigate the temperature reached during pyrolysis. MAP has been employed to convert wood block to tar (up to 30 wt%), oil, and charcoal.[11] However, MAP sometimes may need other kind of pretreatments of biomasses because they are characterized by low tanδ values and shows poor MW absorption. Thus MW absorbers are added and homogeneously blended with biomass before MAP.

The rapid volumetric heating promote the rapid release of moisture from the feedstock, increasing the surface area and improving the pore structure, which favors a quick release of volatiles during pyrolysis. This account and the lower surface temperature (the heat is focused on the core of the feed) reduces the residence time (the time at which substances are heated at pyrolysis condition). So far char-catalyzed secondary cracking are minimized. Furthermore MW power may be easily controlled and the reaction behavior may be tuned to achieve mild pyrolysis conditions. The vapors coming out from the reactor must be fast cooled to avoid other char-catalyze reactions because char can be transported by the gas flow.

In Table 3.1 are listed the biomasses pyrolyzed and the MAP technology employed.

Table 3.1. Summary of MAP of biomass, compiled drawn by Yin.[9]

Biomass and pretreatments	MAP conditions	Products main features	Ref.
Aerobically digested sewage sludge, from an urban waste water treatment plant	15 g plus 1g of a MW absorber (graphite or char). 1 kW for 6 min. Temperature detected above 1270 K. He flow (15 mL/min).	Fast heating and preservation of some of initial functional groups. Secondary reactions to form polycyclic aromatic hydrocarbons (PAHs) are avoided. Products with high heating values.	12-14
Coffee hulls, rich in cellulose; 3 mm x 2 cm pellets	15 g plus 3 g of char from a previous experiment (as MW absorber). N_2 flow (60 mL/min). Temperature 773, 1073, and 1273 K. 20 min runs.	MAP produce large amount of gas and few liquids. The gas is rich in CO and H_2. Calorific values evaluated for the three products; energy recovery close to 100%.	15

(continue)

Larch, cylindrical blocks; 60-300 mm diameter, 80-12000g weight. No other pretreatments.	MW power up to 3 kW. Time from few to 90 minutes. N_2 flow (5 mL/min). Tar adheres to reactor walls.	Blocks of 80 mm releases moisture in 3 min. Linear decreasing of char yield with time. Tar max (25%) after 12 min. Tar comprises carboxylic acids, furfural, cresol, guaiacol, eugenol, arabinoses, xylitol, and levuglucosan.	[11]
Larch, used papers, and filter papers. Wood in cylindrical blocks.	MW power 0.1-1.5 kW. 3-14 min pyrolysis time. No gas flow.	Levuglucosan as major product, isolated as triacetate. Xylosan, galactosan, and mannosan are also found in minor amount.	[16]
Pine wood sawdust (dry basis), impregnated with additive in water solution.	15 untreated or 16.5 treated samples plus 25 g of SiC as MW absorber. Reactor prepared with layer of samples and SiC. Power adjusted to fixed temperature (623 K). No gas flow. Inner temperature 120 K higher than the measured outside. 12 min runs.	Additives increase char formation and changes the composition of gas and tar. No levuglucosan or trace of it is observed. Long residence time and low heating rate are the main reasons for low tar/liquid yields.	[17]
Pine wood sawdust, peanut shell, and maize stalk. Dried at MW for 6 min at 600 W.	Quick moisture release induced by MW increases surface area and modifies surface/pore structure, leading to quick release of volatiles during biomass pyrolysis, reducing secondary cracking, yielding more liquid and solid char. Water content is reduced due to weakened secondary pyrolysis	Main liquid compounds: alcohols, ketones, furfural, phenol, alkylated phenols, and furan derivatives.	[18]
Rice straw; as received without any treatments.	3-5 g per sample. No MW absorber added. N_2 flow (50 mL/min). Single-mode oven, power 100–500 W adjusted with temperature.	High H_2 production. 60% of input energy can be recovered. The liquid is highly alkylated and rich in oxygenated compounds; PAHs content is low.	[19, 20]
Wheat straw pellets; impregnated with additive in water.	150-200 g of samples, max power 1.2 kW. Temperature controlled at 453 K.	No PAHs detected. Liquid close to a fuel for transport applications.	[21]

(continue)

Fibrous cellulose, as received.	300 mg of sample. Oxygen free environment. 100–300 W, 373–573 K. Optimal temperature 453 K.	MW has a dramatic effect on the rate of decomposition when cellulose softens; yielding products which would require much higher temperatures (100 K higher) to be produced with conventional heating.	[22]
Chlorella sp. (a wide-type algae strain); naturally-dried.	30 g of sample and 6 g of char from previous pyrolysis as MW absorber. N2 flow (500 mL/min). Max power 1.25 kW. 20 min reaction time.	750 W is the optimum MW power which allows the maximum bio-oil yield of 28.6%. Better quality than lignocellulosic bio-oils in terms of physical and chemical properties; low oxygen content with aliphatic and aromatic hydrocarbons constituting 22.18%.	[23]
Corn stover; air dried then pulverized	700 W of power. Reaction temperature 788–958 K, reaction time 4–22 min.	The liquid mainly includes phenols (28–40 area%), aliphatic hydrocarbons (11–24 area%), aromatic hydrocarbons, furan derivatives, and some acids.	[24]
Distillers dried grain with solubles; no pretreatments.	100 g of sample. Reaction temperature 789–957 K, reaction time 4–22 min, and power 0.6-1.0 kW. No flow gas. Pyrolysis under N_2.	Reaction temperature and time are the main factors affecting yields. Highest heating value of liquid is obtained at 920 K for 8 min, which is 66.7% of the heating value of gasoline. Liquids contain a series of useful chemical compounds which are related to the pyrolysis conditions and can be blended with gasoline without phase separation.	[25]
Douglas fir; no pretreatments	Activated carbon is used as MW absorber and mixed in various ratios with samples to a total of 120 g. Different additive tested, temperature measured with infrared thermometer. 3-15 min reaction time	Increase in phenol and phenol derivatives. High concentration of long chain fatty acid esters was obtained in the presence of Zn powder.	[26]
Sewage sludge; from urban wastewater treatment plant	100 g of sample plus 25 g of graphite as MW absorber blended together. Power 0.2-1.2 kW. Max temperature 1473 K. N_2 flow (100 mL/min).	At 400 W yields 49.79% of liquid. Negligible PAHs presence.	[27]

(continue)

Anaerobic sewage sludge; from urban wastewater treatment plant	20 g of sample. Char residue from previous pyrolysis as MW absorber. Power 1 kW, 5 min pyrolysis time. N_2 flow (100 mL/min).	MW makes possible to achieve a volume reduction of more than 80%, obtaining a porous carbonaceous residue of basic nature and providing a source of fuel gases and liquids.	[28]
Four sewage sludges: three from urban waste water treatment plants and one from a milk-derivative factory.	15 of sample plus 0.5-3 g of strips of graphoil as MW absorber. He flow (10 mL/min). Power 1 kW. Pyrolysis time 4-14 min. Max temperature detected 1473 K.	Rapidly and efficiently dried and pyrolyzed. CaO, may play an important role in the catalytic reactions that enhance H_2 production. The gases are potential fuels and it makes them a valuable pyrolysis product.	[29]
Empty fruit bunch; 4 x 40 mm. No pretreatment.	100 g of sample mixed with activated carbon (as MW absorber) in different ratios. N_2 flow (4 mL/min). Pyrolysis time 25 min. Power 300 and 450 W.	5–21 wt.% liquid, 48–80 wt.% char and 14–31 wt.% gas. Pyrolysis in absence of MW absorber, but intensive ball lightning (plasma arc) phenomenon are observed. Liquid comprise high amount of phenolic compounds. Char has a calorific value of 25 MJ/kg and it has the potential to be used as fuel.	[30]
Oil palm shell; milled.	150 g of sample plus activated carbon (as MW absorber) in various ratios. N_2 flow (10 mL/min). Pyrolysis time 25 min. Power 300 and 450 W.	A metal stirrer can be successfully employed to pyrolyze solid biomass materials. The biomass to carbon ratio affects the temperature as well as the product yield. Carbonaceous material let to have an increase of temperature, and allows controlling it. 50 wt% carbon provided a temperature of 773 K, and the optimum yield and highest phenol content in the liquid. (oleic acid and phenol).	[31]
Wheat straw, no pretreatment	Power of 18 kW. N_2 flow (1000 mL/min). Reaction time 85 min when 0.334 kW/kg-straw MW power used; 46 min when 0.668 kW/kgstraw used. Final temperature about 873 K.	Pyrolysis products: close to 1:1:1 for gas, liquid and char. The gas: 18 vol.% CO, 36 vol.% H_2, 22 vol.% CH_4, 19 vol.% CO_2; LHV 15 MJ/Nm^3. Electricity consumption: 0.58–0.65 kWh/kgstraw.	[32]

(continue)

Wheat straw; air dried under sun irradiation.	5-30 g of sample plus residual char from residual experiment as MW absorber (in ratio 2:1). 10 min pyrolysis time. Temperature between 673-873 K. N_2 flow (3000 mL/min)	Temperature is the key parameter affecting MAP. High temperature increases the production of gas. Gas contains a higher concentration of syngas and lower concentrations of CO_2 and CH_4 with the increase in temperature. The high amounts of H_2 are attributed to the partial decomposition of CH_4.	[33]
Microalgae; dried at 378 K for 24h then milled.	30 g of sample mixed with MW absorber (activated carbon, CaO, SiC and solid residue). Power 0.75-2.25 kW. Pyrolysis time 20 min.	Power of 1.5 and 2.25 kW are optimal for maximum liquid yield of 35.83% and the maximum fuel yield of 74.93%, respectively. Pyrolysis reaction is enhanced in the most prominent way by mixing activated carbon.	[34]

The data reported in Table 3.1 show how many possibility are offered by a MAP process which may be tuned to yield products ranging from char to gas with desired properties according to biomass characteristics.

3.2. Polymers

The scientific literature for MAP of synthetic polymers is less abundant than related to biomass. The leading efforts are exploited in finding commercial application than sole scientific research so it is possible to find several patents on MAP of polymers, see Section 3.2.1. Anyway some of these papers are reviewed as follow.

Even simple hydrocarbons can undergo MAP over carbon as MW absorber to yield a large variety of molecular compounds from cyclic to linear alkanes and alkenes together with H_2 and gaseous hydrocarbons.[35]

PE as single polymer in a multi-layer system is pyrolyzed to a gas and a liquid/wax in the presence of carbon as MW absorber.[36] However in the same operating conditions but using activated carbon as MW absorber, the pyrolysis efficiency is improved. Activated carbon show an higher efficiency in transforming MW into heat, because they show higher tanδ values, than not-activated carbon (Table 2.1),[2] “microplasma” discharges are widely observed, and higher spot-point temperature has been claimed.

MAP of PS has been investigated in the presence of a MW absorber such as iron mesh,[37] or aluminum as coil or mesh.[38, 39] Iron can reach temperature up to 1470 K, and the main products collected were styrene, ethylbenzene, and condensed ring aromatics, but data about their relative abundance were not reported.[37] Using aluminum in various shapes and arrangements high temperatures were also achieved (aluminum melting point is 993 K); the best performance were obtained

by Hussain et al. with a coil which allows to convert PS in 88 wt% of a liquid, but also these authors did not report any information concerning qualitative and quantitative composition of products. [39]

MAP of PVC was exploited for dehydrochlorination of pure polymer or commercial resins. The elimination of HCl from PVC was active already at relative low temperature (below 550 K) and it was achieved with promising results over the Tg of PVC and with low (below 15%) decomposition of the residual polymeric matrix.[40, 41]

More efforts are spent in MAP of complex matrix such as ASR, waste electric and electronic equipment, or tire. Usually ASR does not show any MW absorption enough to pyrolyze ASR and a MW absorber is required. ASR was pyrolyzed into a liquid, a gas, and a solid with characteristic related to the distribution of material in the initial feed.[42, 43]

Meanwhile tire comprises carbon and metal wire in their structure which provide an already blended MW absorber.[44] The only reported paper on MAP of tire shows that the gas are rich in H_2 and the process can be performed in a very short time (4.5 min for 11.5 g of sample).[45]

MAP of waste electric and electronic equipment (WEEE) converts the polymeric matrix into hydrocarbons and left the inorganic in char. The degradation is already active at very low temperature (373 K).[46]

3.2.1. Patent Literature

Patent literature reports several apparatus which are claimed to recover worthwhile products from various polymeric wastes and coal in extremely different conditions. In Table 3.2 are summarized the main features of selected patents.

Table 3.2. Main features of patented MAP processes.

Feed material	MAP conditions	Products main features	Ref.
Coal	First heated at 600 K by hot gas then pyrolyzed at 700 K through MW. The gas is absorbed in an oil bath.	Products with commercial interest.	[47, 48]
Organic compounds recovered from organic industrial and household waste, organic fractions separated from inorganic.	MW heating in a vacuum zone (10 mmHg).	Works with carbohydrates. Liquid is used as fuel, gas comprise O_2, N_2, H_2, H_2O, CO_2, CO, and CH_4.	[49]

(continue)

Any polymeric waste mixed with carbonaceous materials as MW absorber.	Pre-heated from 523 to 773 K then pyrolyzed. Pyrolysis time 15-60 min.	A solid and a gas.	50-55
PAHs	Covered with inert and a MW absorber (granulated charcoal)	Condensation carbonaceous products.	56
Tire	MW system designed to work below 623K.	No information about products characteristics and distribution.	57
Tire	Tower-type reactor, N_2 flow.	No information about products characteristics and distribution.	58
Aluminum/polymer laminates	Two reactors filled with carbon as MW absorber.	Aluminum is recovered unscratched while polymers (PE) give their typical degradation product. Wax formation is avoided.	59
Any kind of waste	Circulating of feed from once to several times through the process, enabling the control of different processes of materials to yield desired end-products.	Reclaim of matter and energy through the production of solid and liquid products	60-64
Tire and petroleum derived polymeric materials.	Preheated, then moved in a second chamber to pyrolyze.	Liquid, gas, and char, no details are given.	65, 66
Organic materials	Reductive pyrolysis in the presence of an inert gas and MW	Pyrolysis products are recovered as fuel gases (C1-C6 alkanes) and distillates, such as a synthetic crude oil, heavy gas oil, lubricating base oils, naphtha, and middle distillates.	67
Biomass material, particularly plant-derived biomass material.	Biomass is agitated during the MAP. The pyrolysis temperature is between about 340 K and 450 K (torrefaction).	Char solid product use as feedstock coal and for fired power station. Also used as compressed char product, which can be prepared by further processing the char by mixing with a binding agent, such as starch, and the mixture is compressed.	68

(continue)

Carbon-containing feedstock such as: biomass, manure, plant-based cellulose, landfill material, and municipal solid waste.	A reaction chamber (for various kind of reactions) comprising at least one microwave-transparent chamber wall and a reaction cavity configured to hold the carbon-containing feedstock	Fuel like products.	[69]

The information provided in patents is much more limited than the one available in scientific publications. Thus little information can be obtained on product properties and distribution.

3.3. Other processed materials

MAP and other high temperature treatments by the means of MW are not limited to biomasses and synthetic polymers, but also other classes of waste or other materials are processed.

Waste engine oil is widely investigated through MAP to recover light hydrocarbons or even H_2 in the presence of carbon as MW absorber.[70-74] Light hydrocarbons show fuel like feature as density and calorific values.

Other syngas source by MAP is glycerol which is pyrolyzed in the presence of carbonaceous materials.[75]

Ceramic materials are heated through MW for sintering application for two main reason: the faster heating than conventional methods and the volumetric distribution of heat that avoid tension in the heated materials and more homogeneous characteristics.[76, 77]

MW heating of coal is performed and high temperature is reached in short time, and tar is collected and analyzed in comparable but faster way than conventional technologies.[78] MW heating for sulfur removal from coals are realized by long irradiation time and HCl addition to avoid sulfur fixation.[79] This MW based approach is extended also for sulfur removal from refinery streams[80] and in general for petroleum upgrading.[81]

Reference

1. Meredith, R., *Engineers' Handbook of Industrial Microwave Heating*. The Institution of Electrical Engineers: London, United Kindom, 1998; Vol. 25, p 377.
2. Menéndez, J. A.; Arenillas, A.; Fidalgo, B.; Fernández, Y.; Zubizarreta, L.; Calvo, E. G.; Bermúdez, J. M., Microwave heating processes involving carbon materials. *Fuel Process.Technol.* **2010**, 91, 1-8.
3. Luque, R.; Menendez, J. A.; Arenillas, A.; Cot, J., Microwave-assisted pyrolysis of biomass feedstocks: the way forward? *Energ. Environ. Sci.* **2012**, 5, 5481-5488.
4. Russell, A. D.; Antreou, E. I.; Lam, S. S.; Ludlow-Palafox, C.; Chase, H. A., Microwave-assisted pyrolysis of HDPE using an activated carbon bed. *RSC Advances* **2012**, 2, 6756-6760.
5. Menéndez, J. A.; Juàrez-Pérez, E. J.; Ruisànchez, E.; Bermùdez, J. M.; Arenillas, A., Ball lightning plasma and plasma arc formation during the microwave heating of carbons. *Carbon* **2011**, 49, 339-342.
6. Horikoshi, S.; Osawa, A.; Abe, M.; Serpone, N., On the Generation of Hot-Spots by Microwave Electric and Magnetic Fields and Their Impact on a Microwave-Assisted Heterogeneous Reaction in the Presence of Metallic Pd Nanoparticles on an Activated Carbon Support. *J. Phys. Chem. C* **2011**, 115, 23030-23035.
7. Dawson, E. A.; Parkes, G. M. B.; Barnes, P. A.; Bond, G.; Mao, R., The generation of microwave-induced plasma in granular active carbons under fluidised bed conditions. *Carbon* **2008**, 46, 220-228.
8. Tsukahara, Y.; Higashi, A.; Yamauchi, T.; Nakamura, T.; Yasuda, M.; Baba, A.; Wada, Y., In Situ Observation of Nonequilibrium Local Heating as an Origin of Special Effect of Microwave on Chemistry. *J. Phys. Chem. C* **2010**, 114, 8965-8970.
9. Yin, C., Microwave-assisted pyrolysis of biomass for liquid biofuels production. *Bioresour.Technol.* **2012**, 120, 273-284.
10. Bridgwater, A. V.; Peacocke, G. V. C., Fast pyrolysis processes for biomass. Renewable and Sustainable *Energy Reviews* **2000**, 4, 1-73.
11. Miura, M.; Kaga, H.; Sakurai, A.; Kakuchi, T.; Takahashi, K., Rapid pyrolysis of wood block by microwave heating. *J. Anal. Appl. Pyrol.* **2004**, 71, 187–199.
12. Domìnguez, A.; Menéndez, J. A.; Inguanzo, M.; Pis, J. J., Investigations into the characteristics of oils produced from microwave pyrolysis of sewage sludge. *Fuel Process.Technol.* **2005**, 86, 1007-1030.
13. Domínguez, A.; Menéndez, J. A.; Inguanzo, M.; Bernad, P. L.; Pis, J. J., Gas chromatographic–mass spectrometric study of the oil fractions produced by microwave-assisted pyrolysis of different sewage sludges. *J. Chromatogr. A* **2003**, 1012, 193-206.
14. Domìnguez, A.; Menéndez, J. A.; Inguanzo, M.; Pis, J. J., Production of bio-fuels by high temperature pyrolysis of sewage sludge using conventional and microwave heating. *Bioresour.Technol.* **2006**, 97, 1185-1193.
15. Domìnguez, A.; Menéndez, J. A.; Fernàndez, Y.; Pis, J. J.; Valente Nabais, J. M.; Carrott, P. J. M.; Ribeiro Carrott, M. M. L., Conventional and microwave induced pyrolysis of coffee hulls for the production of a hydrogen rich fuel gas. *J. Anal. Appl. Pyrol.* **2007**, 79, 128-135.
16. Yoshida, M. M. H. K. T.; Ando, K., Microwave pyrolysis of cellulosic materials for the production of anhydrosugars. *J. Wood Sci.* **2001**, 47, 5.
17. Chen, M.-q.; Wang, J.; Zhang, M.-x.; Chen, M.-g.; Zhu, X.-f.; Min, F.-f.; Tan, Z.-c., Catalytic effects of eight inorganic additives on pyrolysis of pine wood

sawdust by microwave heating. *J. Anal. Appl. Pyrol.* **2008**, 82, 145-150.
18. Wang, X.; Chen, H.; Luo, K.; Shao, J.; Yang, H., The Influence of Microwave Drying on Biomass Pyrolysis†. *Energy Fuels* **2007**, 22, 67-74.
19. Huang, Y. F.; Kuan, W. H.; Lo, S. L.; Lin, C. F., Hydrogen-rich fuel gas from rice straw via microwave-induced pyrolysis. *Bioresour. Technol.* **2010**, 101, 1968-1973.
20. Huang, Y. F.; Kuan, W. H.; Lo, S. L.; Lin, C. F., Total recovery of resources and energy from rice straw using microwave-induced pyrolysis. *Bioresour. Technol.* **2008**, 99, 8252-8258.
21. Budarin, V. L.; Clark, J. H.; Lanigan, B. A.; Shuttleworth, P.; Breeden, S. W.; Wilson, A. J.; Macquarrie, D. J.; Milkowski, K.; Jones, J.; Bridgeman, T.; Ross, A., The preparation of high-grade bio-oils through the controlled, low temperature microwave activation of wheat straw. *Bioresour. Technol.* **2009**, 100, 6064-6068.
22. Budarin, V. L.; Clark, J. H.; Lanigan, B. A.; Shuttleworth, P.; Macquarrie, D. J., Microwave assisted decomposition of cellulose: A new thermochemical route for biomass exploitation. *Bioresour. Technol.* **2010**, 101, 3776-3779.
23. Du, Z.; Li, Y.; Wang, X.; Wan, Y.; Chen, Q.; Wang, C.; Lin, X.; Liu, Y.; Chen, P.; Ruan, R., Microwave-assisted pyrolysis of microalgae for biofuel production. *Bioresour. Technol.* **2011**, 102, 4890-4896.
24. Lei, H.; Ren, S.; Julson, J., The Effects of Reaction Temperature and Time and Particle Size of Corn Stover on Microwave Pyrolysis. *Energy Fuels* **2009**, 23, 3254-3261.
25. Lei, H.; Ren, S.; Wang, L.; Bu, Q.; Julson, J.; Holladay, J.; Ruan, R., Microwave pyrolysis of distillers dried grain with solubles (DDGS) for biofuel production. *Bioresour. Technol.* **2011**, 102, 6208-6213.
26. Bu, Q.; Lei, H.; Ren, S.; Wanga, L.; Zhang, Q.; Tang, J.; Ruan, R., Production of phenols and biofuels by catalytic microwave pyrolysis of lignocellulosic biomass. *Bioresour. Technol.* **2012**, 108, 274-279.
27. Tian, Y.; Zuo, W.; Ren, Z.; Chen, D., Estimation of a novel method to produce bio-oil from sewage sludge by microwave pyrolysis with the consideration of efficiency and safety. *Bioresour. Technol.* **2011**, 102, 2053-2061.
28. Menéndez, J. A.; Inguanzo, M.; Pis, J. J., Microwave-induced pyrolysis of sewage sludge. *Water Res.* **2002**, 36, 3261-3264.
29. Menéndez, J. A.; Domìnguez, A.; Inguanzo, M.; Pis, J. J., Microwave pyrolysis of sewage sludge: analysis of the gas fraction. *J. Anal. Appl. Pyrol.* **2004**, 71, 657-667.
30. Salema, A. A.; Ani, F. N., Pyrolysis of oil palm empty fruit bunch biomass pellets using multimode microwave irradiation. *Bioresour. Technol.* **2012**, 125, 102-107.
31. Salema, A. A.; Ani, F. N., Microwave-assisted pyrolysis of oil palm shell biomass using an overhead stirrer. *J. Anal. Appl. Pyrol.* **2012**, 96, 162-172.
32. Zhao, X.; Zhang, J.; Song, Z.; Liu, H.; Li, L.; Ma, C., Microwave pyrolysis of straw bale and energy balance analysis. *J. Anal. Appl. Pyrol.* **2011**, 92, 43-49.
33. Zhao, X.; Wang, M.; Liu, H.; Li, L.; Ma, C.; Song, Z., A microwave reactor for characterization of pyrolyzed biomass. *Bioresour. Technol.* **2012**, 104, 673-678.
34. Hu, Z.; Ma, X.; Chen, C., A study on experimental characteristic of microwave-assisted pyrolysis of microalgae. *Bioresour. Technol.* **2012**, 107, 487-493.
35. Tanner, D. D.; Kandanarachchi, P.; Ding, Q.; Shao, H.; Vizitiu, D.; Franz, J. A., The Catalytic Conversion of C1-Cn Hydrocarbons to Olefins and Hydrogen: Microwave-Assisted C-C and C-H Bond Activation. *Energy Fuels* **2001**, 15, 197-

204.
36. Ludlow-Palafox, C.; Chase, H. A., Microwave-Induced Pyrolysis of Plastic Wastes. *Ind. Eng. Chem. Res.* **2001**, 40, 4749-4756.
37. Hussain, Z.; Khan, K. M.; Hussain, K., Microwave–metal interaction pyrolysis of polystyrene. *J. Anal. Appl. Pyrol.* **2010**, 89, 39-43.
38. Hussain, Z.; Khan, K. M.; Basheer, N.; Hussain, K., Co-liquefaction of Makarwal coal and waste polystyrene by microwave–metal interaction pyrolysis in copper coil reactor. *J. Anal. Appl. Pyrol.* **2011**, 90, 53-55.
39. Hussain, Z.; Khan, K. M.; Perveen, S.; Hussain, K.; Voelter, W., The conversion of waste polystyrene into useful hydrocarbons by microwave-metal interaction pyrolysis. *Fuel Process. Technol.* **2012**, 94, 145-150.
40. Moriwaki, S.; Machida, M.; Tatsumoto, H.; Otsubo, Y.; Aikawa, M.; Ogura, T., Dehydrochlorination of poly(vinyl chloride) by microwave irradiation. *Appl. Therm. Eng.* **2006**, 26, 745-750.
41. Ito, M.; Ushida, K.; Nakao, N.; Kikuchi, N.; Nozaki, R.; Asai, K.; Washio, M., Dechlorination of poly(vinyl chloride) by microwave irradiation I: A simple examination using a commercial microwave oven. *Polym. Degrad. Stabil.* **2006**, 91, 1694-1700.
42. Donaj, P.; Yang, W.; Błasiak, W.; Forsgren, C., Recycling of automobile shredder residue with a microwave pyrolysis combined with high temperature steam gasification. *J. Hazard. Mater.* **2010**, 182, 80-89.
43. Donaj, P.; Blasiak, W.; Yang, W.; Forsgren, C., Conversion of microwave pyrolysed ASR's char using high temperature agents. *J. Hazard. Mater.* **2011**, 185, 472-481.
44. Sharma, V. K.; Mincarini, M.; Fortuna, F.; Cognini, F.; Cornacchia, G., Disposal of waste tyres for energy recovery and safe environment—Review. *Energ. Convers. Manage.* **1998**, 39, 511-528.
45. Yatsun, A. V.; Konovalov, P. N.; Konovalov, N. P., Gaseous Products of Microwave Pyrolysis of Scrap Tires. *Solid Fuel Chem.* **2008**, 42, 187-191.
46. Andersson, M.; Knutson Wedel, M.; Forsgren, C.; Christéen, J., Microwave assisted pyrolysis of residual fractions of waste electrical and electronics equipment. *Miner. Eng.* **2012**, 29, 105-111.
47. Knapp, E. M.; Ellis, W. T. Recovery of gaseous hydrocarbons from pyrolysis of coal with microwave energy. US3523405A, 1970.
48. Knapp, E. M.; Ellis, W. T., Jr. Pyrolysis of coal with microwave energy. US3449213A, 1969.
49. Grannen, E. A.; Robinson, L. Microwave pyrolysis of wastes. US3843457A, 1974.
50. Holland, K. M. A. Pyrolysis and apparatus of organic materials using microwaves. EP780457A2, 1997.
51. Holland, K. M. Pyrolysis of macromolecular wastes by microwave heating. US5084140A, 1992.
52. Holland, K. M. Destruction of waste solids by pyrolysis. WO9202598A1, 1992.
53. Holland, K. M. Process of destructive distillation of organic material. 1992.
54. Holland, K. M. Pyrolysis of organic material such as scrap tires. WO8904355A1, 1989.
55. Holland, K. M. Destruction of plastics waste. WO8808871A1, 1988.
56. Dauennan, L. Microwave-Assisted Pyrolysis Of Waste Polyaromatic Hydrocarbons. US 5,698,762, 1997.

57. Bell, J. R.; Skeels, P. R. Apparatus and processes suitable for tire degradation. US6693265B1, 2004.
58. Kim, T., Jin The Waste rubber or waste tire resolution method and system by avail of microwave. WO2005073344A1, 2005.
59. Ludlow-Palafox, C.; Chase, H. A. Microwave induced pyrolysis reactor and method for recycling of laminates. WO2005061098A1, 2005.
60. Kasin, K. I. Microwave assisted flash pyrolysis system and method using the same. US20130032464A1, 2013.
61. Kasin, K. I. Novel microwave assisted flash pyrolysis system and method thereof. WO2013016866A1, 2013.
62. Kasin, K. I. Microwave gasification, pyrolysis and recycling of waste and other organic materials. US20090000938 A1. 2009.
63. Kasin, K. I. Screw conveyor with microwave generator for pyrolysis and recycling of organic waste. GB2420542A, 2006.
64. Kasin, K. I. Microwave gasification, pyrolysis and recycling of waste and other organic materials. WO2006083168A1, 2006.
65. Pringle, F. G. Microwave-Based Recovery Of Hydrocarbons And Fossil Fuels. US20070131591A1, 2007.
66. Pringle, J. A. Microwave Pyrolysis Apparatus For Waste Tires. US7101464B1, 2006.
67. Farneman, J. O.; Welch, K. L. Material recovery from reductive pyrolysis of organic feedstocks in inert gas in presence of electromagnetic radiation. US20080141589A1, 2008.
68. Taylor, R.; McMahon, L.; Way, G. P.W. Pyrolysis of biomass. WO2011107789A2, 2011.
69. Van, T. D.; Catto, M.; Aaron, S. System and method for production of fuel from a carbon-containing feedstock using a microwave-transparent reaction chamber. WO2011019931A1, 2011.
70. Lam, S. S.; Russell, A. D.; Lee, C. L.; Lam, S. K.; Chase, H. A., Production of hydrogen and light hydrocarbons as a potential gaseous fuel from microwave-heated pyrolysis of waste automotive engine oil. *Int. J. Hydrogen Energy* **2012**, 37, 5011-5021.
71. Lam, S. S.; Russell, A. D.; Lee, C. L.; Chase, H. A., Microwave-heated pyrolysis of waste automotive engine oil: Influence of operation parameters on the yield, composition, and fuel properties of pyrolysis oil. *Fuel* **2012**, 92, 327-339.
72. Lam, S. S.; Chase, H. A., A Review on Waste to Energy Processes Using Microwave Pyrolysis. *Energies* **2012**, 5, 4209-4232.
73. Lam, S. S.; Russell, A. D.; Chase, H. A., Pyrolysis Using Microwave Heating: A Sustainable Process for Recycling Used Car Engine Oil. *Ind. Eng. Chem. Res.* **2010**, 49, 10845–10851.
74. Lam, S. S.; Russell, A. D.; Chase, H. A., Microwave pyrolysis, a novel process for recycling waste automotive engine oil. *Energy* **2010**, 35, 2985-2991.
75. Fernández, Y.; Arenillas, A.; Bermúdez, J. M.; Menéndez, J. A., Comparative study of conventional and microwave-assisted pyrolysis, steam and dry reforming of glycerol for syngas production, using a carbonaceous catalyst. J*. Anal. Appl. Pyrol.* **2010**, 83, 155-159.
76. Bykov, Y. V.; Rybakov, K. I.; Semenov, V. E., High-temperature microwave processing of materials. *J Phys. D Appl. Phys* **2001**, 34, R55.
77. Charmond, S.; Carry, C. P.; Bouvard, D., Densification and microstructure evolution of Y-Tetragonal Zirconia Polycrystal powder during direct and hybrid

microwave sintering in a single-mode cavity. *J. Eur. Ceram. Soc.* **2010**, 30, 1211-1221.
78. Monsef-Mirzai, P.; Ravindran, M.; McWhinnie, W. R.; Burchill, P., Rapid microwave pyrolysis of coal Methodology and examination of the residual and volatile phases. *Fuel* **1995**, 74, 20-27.
79. Jie, W.; Jiankang, Y., Behaviour of coal pyrolysis desulfurization with microwave energy. *Fuel* **1993**, 73, 155-159.
80. Ito, E.; Veen, J. A. R. v., On novel processes for removing sulphur from refinery streams. *Catal.Today* **2006**, 116, 446-460.
81. Mutyala, S.; Fairbridge, C.; Paré, J. R. J.; Bélanger, J. M. R.; Ng, S.; Hawkins, R., Microwave applications to oil sands and petroleum: A review. *Fuel Process. Technol.* **2010**, 91, 127-135.

4. Microwave Pyrolysis System

The equipment used in this work was developed after several pyrolysis experiments and then patented.[1, 2] This equipment allows controlling the products properties by tuning the residence time inside the oven of selected compounds. By varying the MW power and inserting a fractionating system online with the gas flow. In the next sections the set-ups are described together with the sample preparation and products collection.

4.1. Oven and apparatus set-up

Two set-ups are used in this work. Both of them employ a MW oven (1, Figure 4.1 and Figure 4.2) with four external MW generators each having an absorption of electric power of 2 KW capable of delivering up to 6 KW of microwave power inside the oven. It was designed and supplied by Bi.Elle s.r.l. (Via Ho Chi Min, 6, Modena, Italy). Samples were placed in a 1000 cm^3 borosilicate Erlenmeyer flask (2), the container was placed inside the oven and connected with two condensing systems cooled at 298 K (5) and 263 K (6), respectively. Liquids were collected in the flask (7) and gas in the gasometer (8). The set-up indicate as "A" has an empty pipe in (4) (Figure 4.1); while the set-up indicate as "B" has a fractionating column in (4) (Figure 4.2). The column has a length of 0.2 m, internal diameter of 0.03 m and it was filled with glass spheres having a diameter of 4 mm.

Experiments were carried out in anoxic atmosphere without any carrier gas thus avoiding the dilution of gas products with carrier gas, and preventing the formation of oxygen and nitrogen containing compounds. The flow of pyrolysis products from the oven to the condensing system was achieved by the gas formed during pyrolysis, the pressure fall provided by the condensing system and the gasometer.

4.2. Variables

The choice of operative and descriptive parameters for any experiment is crucial because their evaluation and tuning may allow controlling the experimental behavior obtaining products with tailor made characteristics.

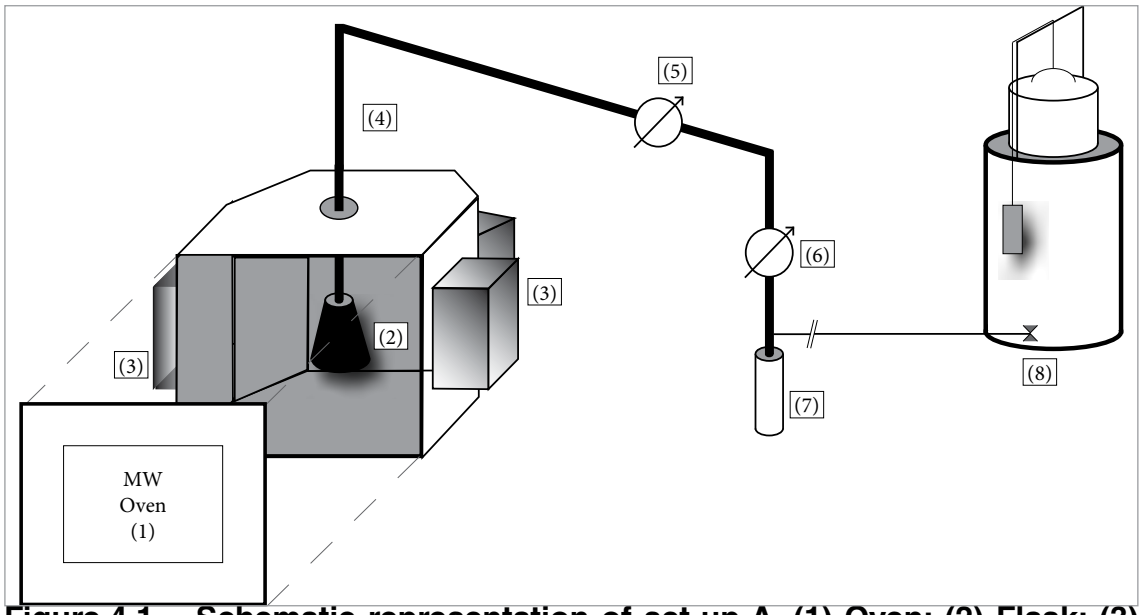

Figure 4.1. Schematic representation of set-up A. (1) Oven; (2) Flask; (3) MW suppliers; (4) Flat pipe; (5) Cooler at 298 K; (6) Cooler at 263 K; (7) Liquid collecting flask; (8) Gas collecting system.

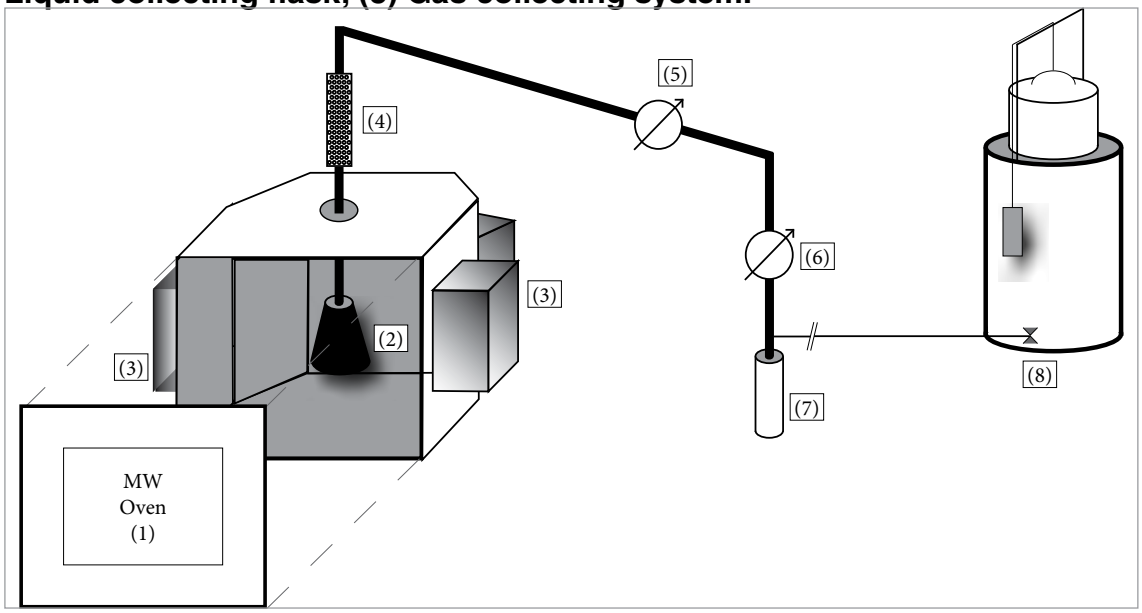

Figure 4.2. Schematic representation of set-up B. (1) Oven; (2) Flask; (3) MW suppliers; (4) Flat pipe (5) Cooler at 298 K; (6) Cooler at 263 K; (7) Liquid collecting flask; (8) Gas collecting system.

In a classical experiment temperature is the key parameter. Also in a MW heated system it remains a key parameter but it is hardly detected because mercury in glass and metal thermocouples interact with MW, infrared thermometers give only information about surface temperature, fiber optic thermometers give the temperature of material in strict contact with them and they are very fragile. Furthermore the temperature is strictly connected to the MW absorber.[3] A more detailed discussion is reported in Section 5.5 in light of the experimental findings. Thus temperature has not been chosen as descriptive parameter.

In a MAP experiment only the input MW power can be measured with high

precision. So MW power (P) may be a good descriptive parameter. Also feed mass (M) is easily determined so the ratio P/M may be a good parameter which represents the energy supplied to the feed. Anyway if both MW power and feed mass are varied together during the test, especially in a batch system, also this parameter may give misunderstanding informations.

A new parameter is introduced to overcome this difficulty, the ratio between MW power and square feed mass: P/M^2. The introduction of this parameter may allow evaluating the influence of reflection and penetration depth of MW inside the sample by working at fixed MW power and varying the feed mass.

4.3. Sample preparation and products collection

All samples were chopped to flakes of 2 × 2 cm and then dried at least for 24 h before pyrolysis. No further preparations or pretreatments were made.

Liquids were collected in a flask, centrifuged at 2000 rpm for 10 min and then filtered to evaluated and eliminate any particulate before any analysis. They were stored at 277 K.

Chars were recovered from the reactor as brittle pieces, milled to a homogeneous powder, separated from metal wires, if present, with a magnet, and stored in a desiccator.

Gas were collected in a gasometer and analyzed straight after the end of each experiment.

Reference

1. Frediani, P.; Rosi, L.; Frediani, M.; Undri, A.; Occhialini, S. Production of Hydrocarbons from Copyrolysis of Plastic and Tyre Material with Microwave Heating. WO2012110990, 2012.
2. Frediani, P.; Rosi, L.; Frediani, M.; Undri, A.; Occhialini, S.; Meini, S. Production of hydrocarbons from pyrolysis of tyres. WO2012110991, 2012.
3. Farag, S.; Sobhy, A.; Akyel, C.; Doucet, J.; Chaouki, J., Temperature profile prediction within selected materials heated by microwaves at 2.45 GHz. *Appl. Therm. Eng.* **2012**, 36, 360-369.

5. Waste Tire

MAP of tires was exploited and our main experimental findings have been already published.[1-3] In the next sections the data already reported are further discussed and enhanced with new experimental findings.

MAP of tires was performed without the addition of any MW absorbing material because carbon black is present in tire together with metal wires and they were MW absorbing materials and they allow a fast heating of tire chips.

The progressive destructive effect of MW radiation on tire chips was reported in Figure 5.1. After 40 s from MW irradiation the polymeric matrix in close contact with the absorbing material was heated and quickly melted, then pyrolyzed. Gas was formed inside the material, in close contact to the MW absorber, and shattered tire chips. During pyrolysis carbon particles were suspended in the melted polymeric matrix which was continuously pyrolyzed.

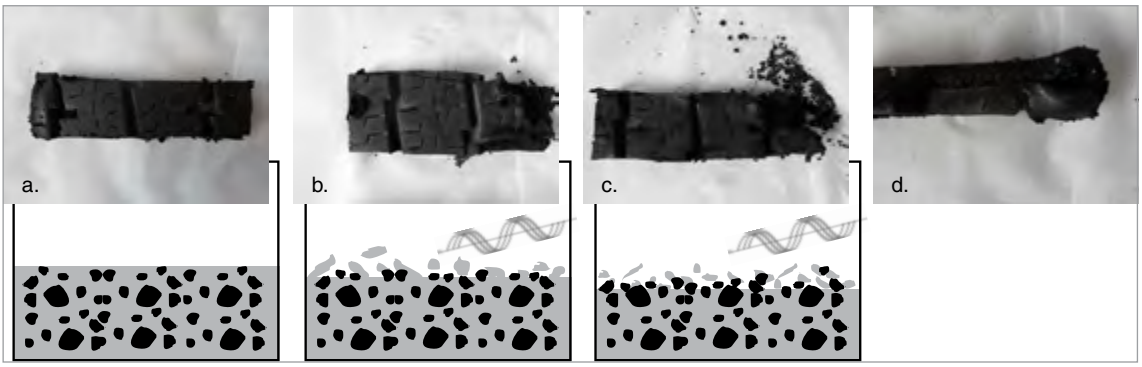

Figure 5.1. A tire chip after different irradiation time. (a) Tire chip not irradiated; (b) tire chip irradiated for 40 s; (c) tire chip irradiated for 90 s, it flakes if handled; (d) bulge effect of an irradiated tire chip, side view.

This pictorial representations show the progressive decomposition of tires to carbon particles partially coated with polymeric matrix and finally carbon particles alone, when all surrounding organic molecules were pyrolyzed. The presence of residual polymer from not fully pyrolyzed matrix was evidenced by CHN and FTIR (see Section 5.3). These results showed the possibility to pyrolyze whole tire without any previous treatments.

5.1. Operating Parameters and Yields

Pyrolysis were investigated by varying four parameters: apparatus set-up, tire brand, MW power (P) and tire chip mass (M). The experimental details together with the yield of solid, liquid, and gas are reported in Table 5.1. The ratio between microwave power (P) and tire mass square (M^2) was chosen as a descriptive parameter (Section 4.2).

In each experiment MW power was always kept constant and pyrolysis was stopped when gas evolution was not further detectable. Pyrolysis was assumed to be complete if organic materials were not detected in the residue analyzed via FT-IR (Section 5.3.3), and hydrogen detected by ultimate analyses was lower than 1 % (Section 5.3.1).

Pyrolysis entries are named “Tn” where “n” is an arbitrary ascending number for each experiment.

Table 5.1. MAP of tire: influence of tire brand, and reaction parameters on the yields of products formed (metal wires not include in yield calculations).

Entry	Set-up	Tire Brand	Power	Tire	P/M²	Time	Solid	Liquid	Gas
(kW)			*(kW)*		*(kW/kg²)*	*(min)*	*(wt%)*	*(wt%)*	*(wt%)*
T1	A	Tire M	6.0	208.8	137.6	14	41.1	31.5	27.4
T2	A	Tire G	6.0	250.4	95.7	17	42.4	42.8	14.8
T3	A	Tire M	4.8	212.8	106.0	15	40.6	43.1	16.3
T4	A	Tire M	3.0	233.3	55.1	35	43.2	42.6	14.1
T5	A	Tire G	3.0	250.9	47.7	38	44.6	38.8	16.6
T6	A	Tire M	3.0	1501.1	1.3	70	50.7	39.3	9.0
T7	A	Tire M	3.0	502.8	11.9	59	40.6	44.0	13.4
T8	A	Tire M	3.0	64.1	730.1	47	47.5	30.1	22.4
T9	A	Tire M	1.5	252.1	23.6	100	65.0	20.7	14.3
T10	B	Tire M	6.0	242.6	101.9	22	46.2	27.8	26.0
T11	B	Tire G	6.0	252.9	93.8	23	45.4	35.7	18.9
T13	B	Tire M	3.0	243.0	50.8	36	46.6	27.6	25.8
T14	B	Tire G	3.0	250.3	47.9	43	53.3	26.3	20.4
T15	B	Tire G	6.0	500.5	24.0	35	49.7	37.0	13.3
T16	B	Tire G	3.0	500.4	12.0	80	54.5	31.9	13.6

Entries T5 and T9 were the only two pyrolyses which showed noteworthy presence of residual organic compounds into solid, thus they were accounted as not-complete pyrolysis (see Section 5.3.1 and Section 5.3.3). Reducing P/M^2 ratio below 10×10^{-3} W/g^2 or using a MW power of 1.5 kW the pyrolysis was not completed and some residual compounds remained into the solid. In entry T5, a large mass of tire was used, the external part of the material was pyrolyzed and the residual carbon might shield the deeper material from the MW radiation,

according to Bykov et al.[4] Due to its low thermal conductivity, the inner part might be partially heated and they were not-fully decomposed. In entry T9 a MW power of 1.5 KW was high enough to keep the matrix molten but heat dispersion was too high to provide the temperature required for completing pyrolysis. However a complete pyrolysis could be achieved in these two experiments using a longer time.

Decreasing P/M^2 ratio a longer reaction time was necessary to pyrolyze tire chips. Also using a fractionating system (set-up B) the pyrolysis time was increased, because heavy substances were constrained for a longer time inside the reactor (Section 5.3). Different tire brands gave only negligible differences in pyrolysis time. This outcome suggested a close interaction between MW and absorbing material present in different tires. However Russell et al. reported different interaction between MW absorbing material and polymeric matrix by varying the structure of MW absorber especially its surface area.[5]

Experiments using set-up A were initially ran to analyze the behavior of different tire brands. A fast cracking of the polymeric matrix of *tire M* was performed (T1, Table 5.1), and a high yield of gas was obtained. Pyrolysis performed with *tire G* using the same P/M^2 ratio of T1 gave a larger amount of liquid and a reduced fraction of gas, while the amount of solid was almost the same. These results suggested that *tire M* had a composition able to form more stable radicals than those formed in the pyrolysis of *tire G*. These radical intermediates gave further reactions giving higher amount of low molecular weight compounds. Furthermore the two brands of tire contained the same amount of inorganic fillers because showed almost the same solid yield.

Variation in P/M^2 ratio deeply affected the yield of all the three products solid, liquid, and gas. Its effects might be clarified by taking into account two parallel phenomena: bond cleavage by pyrolysis or cross reaction between two radicals or a radical and another compound. Bond cleavage gave low molecular weight compounds through radical intermediates. These radicals may react with other compounds through several ways: transfer of a hydrogen atom, functional group migration (radical was transferred to other molecules), or coupling between radicals to form condensation product. Several condensation reactions might form large structure or even carbon network, so cocking occurred. Increasing radical formation the pyrolysis was more effective. An efficient pyrolysis could trigger other non-chemical effects such as transportation phenomena of inorganics and high boiling compounds which could be found mixed with the liquid fraction (no gas flow was employed). So far, aside from chemical composition of pyrolyzed tire, the increase of P/M^2 ratio promoted one or both of these effects.

Working with set-up A and reducing P/M^2 (from 730.1 to 11.9×10^{-3} W/g^2) the liquid yield rose from 30.1 to 44.0 % for *tire M*; while changing P/M^2 ratio (from

95.7 to 47.7 × 10^{-3} W/g^2) the yield decreased from 42.8 to 38.8 % for *tire G*. At the same time solid and gas yields showed an opposite trend. The only exception was for entry T1 which showed the highest gas yield. Probably the balance of the condition employed was particularly favorable to gas formation. Using *tire M* and high P/M^2 values both gas formation and cocking were promoted. The same behavior was evidenced for *tire G* at low P/M^2. Degradation products were easily formed from *tire M*, but they did not further react, meanwhile large amount of degradation products were formed from *tire G* but they further reacted. The pyrolysis time was increased by lowering P/M^2 ratio as well as for cocking reaction especially over 35 minutes.

Working with set-up B the following effects were noticed and attributed to the presence of a fractionating system:

- Transport phenomena were strongly limited or completely avoided;
- Low boiling compounds were almost the only present in the liquid collected, meanwhile high boiling compounds were separated inside the fractionating system and sent back into the reactor so they were further pyrolyzed (Figure 5.2).
- The residence time of high boiling compounds was increased (the threshold between low and high boiling compounds was still function of the P/M2 ratio and it was hardly predictable);
- Unsaturated substances remained for a long time at high temperature, gave Diels-Alder condensation followed by further pyrolysis reactions as proposed by Cunliffe and Williams.[6]

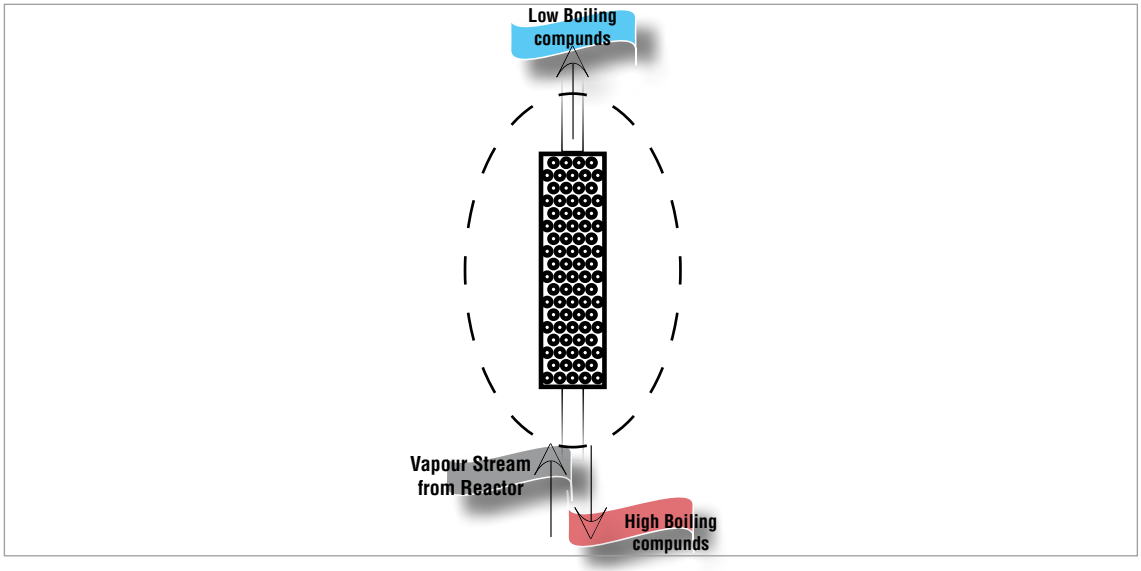

Figure 5.2. The fractionating system.

These hypotheses were supported by the findings reported in Table 5.1, especially the yields data. A lower yield of liquid was obtained using set-up B than set-up A. At the same time the yield of solid was increased while the amount of gas was almost the same. Furthermore transportation phenomena were avoided

and clear and transparent liquids were collected. Solid microparticles were not evidenced nor separated even after centrifugation at high speed for long time. Set-up B reduced the influence of P/M^2 ratio when *tire M* was used; the yields of solid, liquid and gas in pyrolysis T10 and T12 were almost the same as well as the properties of liquid products even if the P/M^2 ratio was 101.9 and 50.8×10^{-3} W/g^2 respectively. *Tire G* was more stable than *tire M* in the pyrolysis conditions and a lower amount of gas was obtained. This behavior might be attributed to the different composition of tire as above discussed and suggested by the different pyrolysis behavior of different classes of polymers.[7, 8]

5.2. Gas Product

The gas was analyzed by GC-FID and GC-TCD: small organic molecules were present such as methane, ethane, ethene, propene, C4 hydrocarbons and in low amount isoprene. Also inorganic molecules, such as: hydrogen, hydrogen sulfide, CO and CO_2 were identified. Under our GC conditions it was not possible to separate the mixture of C1 and C2 hydrocarbons; but we had no interest to do it because it was not relevant for our purpose.

The hydrocarbons identified in gas are reported in Table 5.2 (coded "TnG" where "n" is the pyrolysis entry).

Table 5.2. Main substances identified in gases.

	Substances											
Entry	C1 + C2	Propene	1-Butene	2-Butene-trans	2-Butene-cis	2-Methyl-1-butene	n-Pentane	Isoprene	2-Hexene (cis+trans)	TOTAL reported	HHV[a] (MJ/Kg)	LHV[a] (MJ/Kg)
T1G	46.54	9.27	22.06	1.99	1.24	-	1.20	10.23	-	92.53	47	43
T2G	46.63	14.76	23.70	0.60	0.31	2.62	0.00	2.29	0.00	90.91	46	43
T3G	64.7	8.05	15.21	-	0.27	0.79	-	5.13	2.05	96.20	49	46
T4G	76.79	3.70	10.10	0.94	0.56	-	0.75	3.60	-	96.44	50	46
T5G	46.58	13.90	17.14	2.22	1.40	3.06	-	2.70	-	86.99	44	41
T6G	26.28	11.71	39.80	2.74	1.10	-	3.45	3.41	-	88.49	44	41
T7G	51.18	10.91	14.16	1.68	0.96	1.64	-	1.99	-	82.52	42	39
T8G	38.13	13.42	21.78	2.19	1.34	-	7.67	3.78	-	88.31	44	41
T9G	70.29	3.27	14.56	1.19	0.61	0.94	-	5.18	-	96.04	49	46
T10G	42.03	13.73	23.58	2.31	1.38	3.22	-	2.05	-	88.30	44	41
T11G	0.15	4.98	64.24	6.41	3.33	4.77	-	3.25	-	87.13	42	39
T12G	26.71	7.60	15.82	1.69	1.10	4.81	-	2.86	-	60.58	30	28
T13G	39.03	16.27	23.81	2.15	1.21	3.33	-	2.36	-	88.15	44	41
T14G	52.19	15.64	11.59	1.93	1.33	1.98	-	1.37	-	86.04	44	41
T15G	51.12	17.16	11.31	1.69	1.22	1.47	-	1.13	-	85.09	43	40

[a]HHV and LHV were calculated from gas composition and tabulated calorific value.[9]

Working with set-up A and *tire M* (T4G and T9G) the highest value for C1 + C2 and 1-butene together with the lowest amount for other hydrocarbons was achieved. T9 was performed with the lowest MW power which promoted a slow heating ensuing a feeble gas flow. C1 + C2 hydrocarbons were the main products. In entry T4 working variables were balanced to promote an efficient pyrolysis, indeed C1 + C2 hydrocarbons were the main compounds collected but the gas yield was one of the lowest together with a high liquid yield. *Tire G* showed a different behavior because the C1 + C2 amount was low and the other hydrocarbons were increased. Probably it contained a large amount of polyisoprene which pyrolyzed giving a wider number of low molecular weight compounds than other rubber such as styrene-butadiene copolymers probably present in *tire M*.

Working with set-up B the gas yield increased with both tires. Surprisingly the C1 + C2 mixture was reduced with respect to the one collected with set-up A even if the residence time was improved. Probably C1 + C2 hydrocarbons were not formed by further pyrolysis of high boiling compounds kept in the oven.

T9G was also analyzed with a GC-TCD for H_2 quantification and a concentration of 35.7% (vol %) was found. It was lower than the value reported by other authors[10] for the gas mixture obtained by MW pyrolysis of tires but slightly higher than the amount present in the thermal pyrolysis.[11] Other inorganic substances were identified in an amount lower than 1%, such as H_2S, CO and CO_2, but they were not quantified.

5.3. Solid

The solid were odorless black powders, if fully pyrolyzed material was present. Incompletely pyrolyzed residue was a sticky, hard to handle solid. Solids were thoroughly characterized with several techniques and a detailed description is reported in the following sections. These characterization were run because new commercial applications for tire-derived char are of great interest[12] and several authors indicate the economic viability of tire pyrolysis on an industrial scale depends on finding uses for this solid waste.[13, 14] One of the most investigated applications for tire-derived char is the production of activated carbons through demineralization followed by physical or chemical activation,[6. 14-16] however this application need further research to reduce treatments costs.

5.3.1. Physical properties

The main physical properties of solids are reported in Table 5.3 (coded “TnS” where “n” is the pyrolysis entry).

Table 5.3. Properties of chars obtained by MAP of tires.

Entry	Tire M	Tire G	T1S	T2S	T3S	T4S	T5S	T6S	T7S	T8S	T9S	T10S	T11S	T12S	T13S	T14S	T15S
Set-up	-	-	A	A	A	A	A	A	A	A	A	B	B	B	B	B	B
Brand	-	-	*Tire M*	*Tire G*	*Tire M*	*Tire M*	*Tire G*	*Tire M*	*Tire M*	*Tire M*	*Tire M*	*Tire M*	*Tire G*	*Tire M*	*Tire G*	*Tire G*	*Tire G*
P/M^2 (10^3W/g^2)	-	-	137.6	95.7	106.0	55.1	47.7	1.3	11.9	730.1	23.6	101.9	93.8	50.8	47.9	24.0	12.0
Char yield (wt %)	-	-	41.1	42.4	40.6	43.2	44.6	50.7	40.6	47.5	65.0	46.2	45.4	46.6	53.3	49.7	54.5
Char yield[a] (wt %)	-	-	40.4	41.07	46.8	41.5	42.8	47.7	n.d.	43.4	53.4	43.1	43.9	45.6	51.6	48.4	52.7
GCV (MJ/Kg)	32±3	32±3	35±4	29±3	36±4	33±3	33±3	34±3	n.d.	n.d.	31±3	33±3	31±3	29±3	30±3	30±3	26±3
LCV (MJ/Kg)	30±3	30±3	35±4	29±3	36±4	33±3	33±3	34±3	n.d.	n.d.	30±3	33±3	31±3	28±3	30±3	29±3	26±3
C[b] (wt %)	88.19	87.48	89.33	91.44	89.99	89.01	91.77	89.70	89.25	92.03	88.71	88.09	91.33	90.51	92.77	91.16	92.75
H[b] (wt %)	7.23	7.52	0.35	0.38	0.58	0.83	0.86	1.61	0.33	0.53	3.21	1.00	0.87	2.55	0.55	1.38	1.09
N[b] (wt %)	0.23	0.35	0.15	0.01	0.01	0.48	0.01	0.42	0.80	0.01	0.33	0.21	0.01	0.01	0.01	0.01	0.41
S[b] (wt %)	1.8	1.7	2.3	1.6	1.8	2.0	1.6	1.6	1.6	1.6	1.3	1.5	1.5	2.4	1.7	0.7	2.0
O[c] (wt %)	2.55	2.97	7.87	6.57	7.63	7.68	5.76	6.67	8.02	5.83	6.45	9.20	6.29	4.53	4.97	6.78	3.75
S solid/S feed (%)	-	-	52.5	39.9	40.6	48.0	42.0	45.1	36.1	42.2	46.9	38.5	40.1	62.1	53.3	20.5	64.1
Ash (wt %)	2.18	2.67	7.93	6.14	7.72	7.57	4.74	6.29	7.40	9.50	5.88	8.57	5.96	7.37	4.65	6.93	4.12
Volatiles (wt %)	-	-	1.77	3.18	2.95	3.90	3.93	5.98	n.d.	4.60	17.90	6.70	3.19	2.25	3.14	2.79	3.32
Fixed carbon (wt %)	-	-	89.30	90.69	89.34	88.53	91.33	87.72	n.d.	85.90	76.23	84.73	90.86	90.38	92.21	90.28	92.56
Apparent Density (g/mL)	1.26[d]	1.14	0.401	0.424	0.420	0.492	0.407	0.560	n.d.	0.526	n.d.e	0.486	0448	0.453	0.499	0.489	0.519

[a] volatiles free basis; [b] performed on sample as collected; [c] by difference; [d] bulk density; [e] sticky char, not analyzed.

Only T6S and T9S were obtained from not-complete pyrolysis.

The calorific values were slightly higher than virgin tires, commercial pet coke, and coal (except for anthracite coal which usually shows similar values).[17] GCV and LCV were very close among each char and they were in the same range if standard deviations were taken into account. The GCV were higher than those reported by other authors.[9, 10]

Residual hydrocarbons were always present in char but they slightly affected LCV. They might be due to two different sources: absorbed compounds in the pore structure of char which were not able to leave the reactor at the end of the pyrolysis or residual polymeric matrix which was not fully-pyrolyzed. The presence of residual volatiles in the char was a peculiarity of the experimental methodology adopted because it was carried out in a batch process without a carrier gas. As a consequence a slight amount of liquid remained always in the reactor, about 2 - 5 wt% for complete experiments for both tire brand performed with set-up A.

T9S could be regarded as the only char with a relevant amount of volatiles (17.9 wt %). However this amount was close to that one reported for a typical petroleum coke, and lower than several coals.[17]

Working with set-up B the liquid returned back into the reactor and it was further pyrolyzed increasing the amount of volatiles at the end of the pyrolysis, as shown by T10S.

The ultimate analyses showed a sharp difference among pyrolysis run with different conditions especially with different P/M^2 ratio. Low hydrogen content (below 1 wt%) was shown using a P/M^2 higher than 47.7×10^{-3} W/g^2 and even for lower P/M^2 ratio if a MW power over 3 kW was employed. Using these conditions the amount of not pyrolyzed or absorbed compounds in the residue was reduced independently of set-ups and tire brands. Carbon content was always in the range of 89.33-92.03 wt % and it decreased if hydrogen increased.

The ultimate analysis of char reported by many authors seemed to be directly correlated to different initial tire composition[18, 19] especially for what concern the carbon amount. It is worthy to be noted that the hydrogen content varied always in the 1-3% range. Helleur et al.[20] and Zabaniotou and Stavropoulos[21] reported a hydrogen content, respectively of 1.3% and 3.3% for standard heating pyrolysis. I. de Marco Rodriguez et al.[22] also reported, for standard heating pyrolysis using an autoclave as a reactor, hydrogen content higher than 1% if pyrolysis was ran below 673 K. Aylon et al.[23] reported, for classical heating in a moving bed or in a fixed bed reactor, a hydrogen content slightly lower than 1%. Hydrogen higher than 1% in the char could be an indication of a not-fully pyrolyzed residue.

Sulfur seemed to be involved in various reactions, but only 50% of the initial sulfur present in tires remained in the char in agreement with the data reported by other authors for conventional heating pyrolysis.[22, 24] Anyway the amount of sulfur

was lower than those present in several petroleum cokes and always into the range of regular calcined feed (even if hydrogen content was not in the range of regular green coke).[17] Furthermore ultimate analyses suggested an intermediate composition between bitumen and anthracite coal,[17] however the sulfur content hinder the direct use of these materials as energy source if the plant is not equipped with a purification of the combustion gas.

Apparent density showed extremely low values but similar among each char even from different tire brands. These values were even lower than any commercial petroleum coke (around 0.8 g/cm^3)[17] and native or synthetic graphite (around 2.5 g/cm^3).[25, 26] These low values were probably connected with grinding method, pore size and their distribution.

Ash content was lower, in some case even half, than that one reported by several authors[22, 23, 27-29] and it is attributed to lower amount of inorganic additives present in tire.[18] Char from the two tire brands showed almost the same ash content suggesting a close amount of inorganic filler in tire. Anyway all carbons obtained did not meet the requirements of a carbon black for tire manufacturing due to its ash content, which should be below 0.5 wt%.[30]

5.3.2. ICP-MS

The ICP-MS of *tire M*, metal wires before and after pyrolysis (from *tire M*), and selected chars are reported in Table 5.4; Iron wires were eliminated from tires and chars before analyses.

Table 5.4. ICP-MS analyses of char, reported as mg/Kg (ppm).

Metal	Tire	Wire before MAP	Wire after MAP	T1A	T4S	T6S	T9S
^{51}V	3.2	1359	1400	3.8	0.9	23.8	0.3
^{52}Cr	4.4	197.1	1805	25.3	7.6	4.4	1.3
^{55}Mn	10.8	4504	5517	164	110	27	7.4
^{56}Fe	453	983442[a]	977680[a]	23370	15080	3622	937
^{59}Co	0.9	45.5	1754	144.4	13.1	239	6.3
^{60}Ni	4.3	163.6	1740	27	13.1	0.7	6.3
^{63}Cu	6.1	2947	2221	144	360	39.4	116
^{66}Zn	1299	1570	2176	58280	45130	13575	30660
^{75}As	0.5	1428	1330	1.5	1.4	4.4	0.3
^{114}Cd	0.3	1388	1440	6.2	5.5	1.1	4.1
^{123}Sb	4.4	2.3	< 0.1	14.1	14.4	2.3	13.4
^{138}Ba	34.2	1408	1457	4.7	4.6	1.7	3.5
^{208}Pb	130.4	1546	1480	76.7	113	28.1	71.5

[a] calculated by difference.

The distribution of each metal inside samples was not homogenous (see Section 5.3.5) and the results reported here coming from the most representative

samples analyzed for each char. Fe and Zn were the most abundant metals in any char. Fe was probably due to residue of metal wires present in virgin tires and it was present in char as very small particles pasted with carbon and not attracted by the magnet or they were non-ferromagnetic particles or included in some crystalline phases of ZnS (Section 5.3.6). Zn compounds derived from ZnO used as additive in tires formulation, and from brass coating of metal wires (see also Section 5.3.5). Cu was leaked from brass coating of metal wire. Other metallic elements were probably present in the carbon black or other additives used for tire production, indeed their abundance was below the restrictive European limits for commercial carbon blacks.[17]

5.3.3. FTIR

Infrared spectra were collected using two techniques: an attenuated total reflectance (ATR) to evaluate the surface composition and a transmission sampling technique (using KBr disk) to evaluate the presence of organic functional groups in the bulk of char.

IR spectra of degassed samples did not showed any peaks distinguishable from background. Therefore IR absorptions could be attributed to volatiles remained in the reactor, as previously hypothesized (Section 5.3.1) or to volatiles that were fully pyrolyzed in the course of heating at 623 K under a reduced pressure of 80 Pa for 5 h (degassing procedure).

Spectra from KBr disk showed very weak absorptions in each sample (Figure 5.3), with a maximum transmittance of 2.0 % and even if they were attributed with uncertainty, suggested the presence of low amount of hydrocarbons.

ATR spectra were extremely noisy due to scattering phenomena and the absence of absorbing substance on the surface except for T6S and T9S. These latter chars showed significant peaks. Aliphatic and aromatic hydrocarbons were present (Figure 5.3).

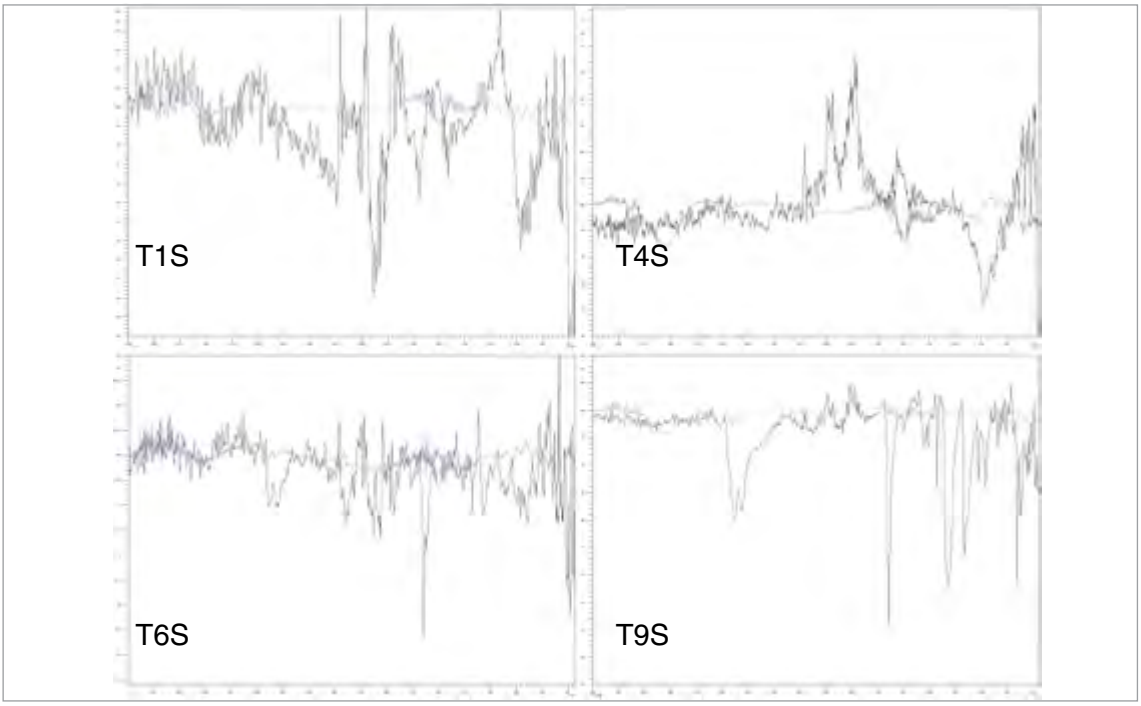

Figure 5.3. FTIR of T1S, T4S, T6S, and T9S.

Main frequencies identified in ATR spectra of T6S and T9S are listed as follow. Frequencies of alkanes were found at: 2950 (s) (H_2C-H asymmetric stretching), 2910 (s) (HC-H asymmetric stretching and C-H stretching), 1446 (m) and 1409 (w) (HC-H asymmetric bending), and 723 (m) (-(CH_2)n- rocking) cm^{-1}. Absorptions of aromatic groups were present at: 1720 (s) (aromatic combination bands), 1343 (m), 1254 (m), 1246 (m), 1231 (m), 1128 (m), 1023 (m), 967 (m) (aromatic C-H in-plane bending), 871 (w) (aromatic C-H out-of plane bending) cm^{-1}.

5.3.4. BET Surface area

The surface area and pore volume of collected and degassed samples are reported in Table 5.5.

Table 5.5. BET surface areas their pore volume and its distribution of collected and degassed char samples.

Entry	T1S	T4S	T6S	T9S
$P/M^2(10^3W/g^2)$	137.6	55.1	1.3	23.6
BET surface area, collected sample (m^2/g)	49	46.9	26.8	10.9
BET surface area, degassed sample (m^2/g)	65.3	65.0	45.0	32.6
Δ BET (m^2/g)	16.3	18.1	18.2	21.7
V_T (cm^3/g)	0.82	1.67	0.38	0.35
BJH PVD Macropore (%)	n.d.	n.d.	17.85	39.59
BJH PVD Mesopore (%)	n.d.	n.d.	82.15	60.41
BJH PSD Macropore (%)	n.d.	n.d.	9.33	25.02
BJH PSD Mesopore (%)	n.d.	n.d.	90.67	74.98

BET surface area of degassed char from complete pyrolysis was 65 m^2/g and

it seemed to be independent from P/M^2 ratio (see entry T1S and T4S). However if the sample contained volatiles, the surface area was reduced as expected. T6S showed lower values than T1S and T4S but higher than T9S, probably due to the presence of lower amount of volatiles. The lower values of BET area for degassed T6S and T9S could be a hint for the presence of heavy compounds which were not removed during the degassing procedure at 623 K and reduced pressure. They remained in the pore structure.

The presence of volatiles or high molecular weight compounds influenced also the porous structure of samples. T6S and T9S showed similar total pore volume (V_T), 0.35 and 0.38 cm^3/g respectively; meanwhile T1S and T4S showed higher values (0.82-1.67 cm^3/g), surprisingly higher than those reported by López et al. (among 0.3-0.5 cm^3/g).[12] Probably the carbon black employed in the two tire productions was different.

Microporosity BJH measurements were not detected due to limit of our instrument. However T1S and T4S probably showed a micropore structure with strongly trapped compounds preventing the evaluation. On the contrary T6S and T9S showed a mesopore structure (between 2 and 50 nm) which included the most pore volume and area.

5.3.5. Scanning electron microscopy

In Figure 5.4 SEM image of a tire M before pyrolysis and three images of char T1S and T9S, are reported.

No significant morphological variation was evidenced among each char obtained at different P/M^2 in a complete pyrolysis. Apparently MW neither modified the carbon black used as filler in tire nor noticeably affected the morphology of char (Figure 5.4c). The less magnified image (Figure 5.4b) show a macropore structure of T1S which was left after pyrolysis of the polymeric matrix. Meanwhile in T6S the macropore structure could not be observed (Figure 5.4d) because residual polymeric matrix and other organic substance filled it. Visual structure seemed to be similar to the one observe for not pyrolyzed tire (Figure 5.4a).

Back scattering images of char S1 showed a granular structure, with grain diameters in the range 2-50 mm. Bright spots and large dark areas were present. Different color areas and spots were investigated by X-EDS microanalysis. In Figure 5.5 a spread view of T1S back scattering image and X-EDS spectra of bright, gray and dark spots are reported. All bright spots showed close composition as well as for spots of different colors.

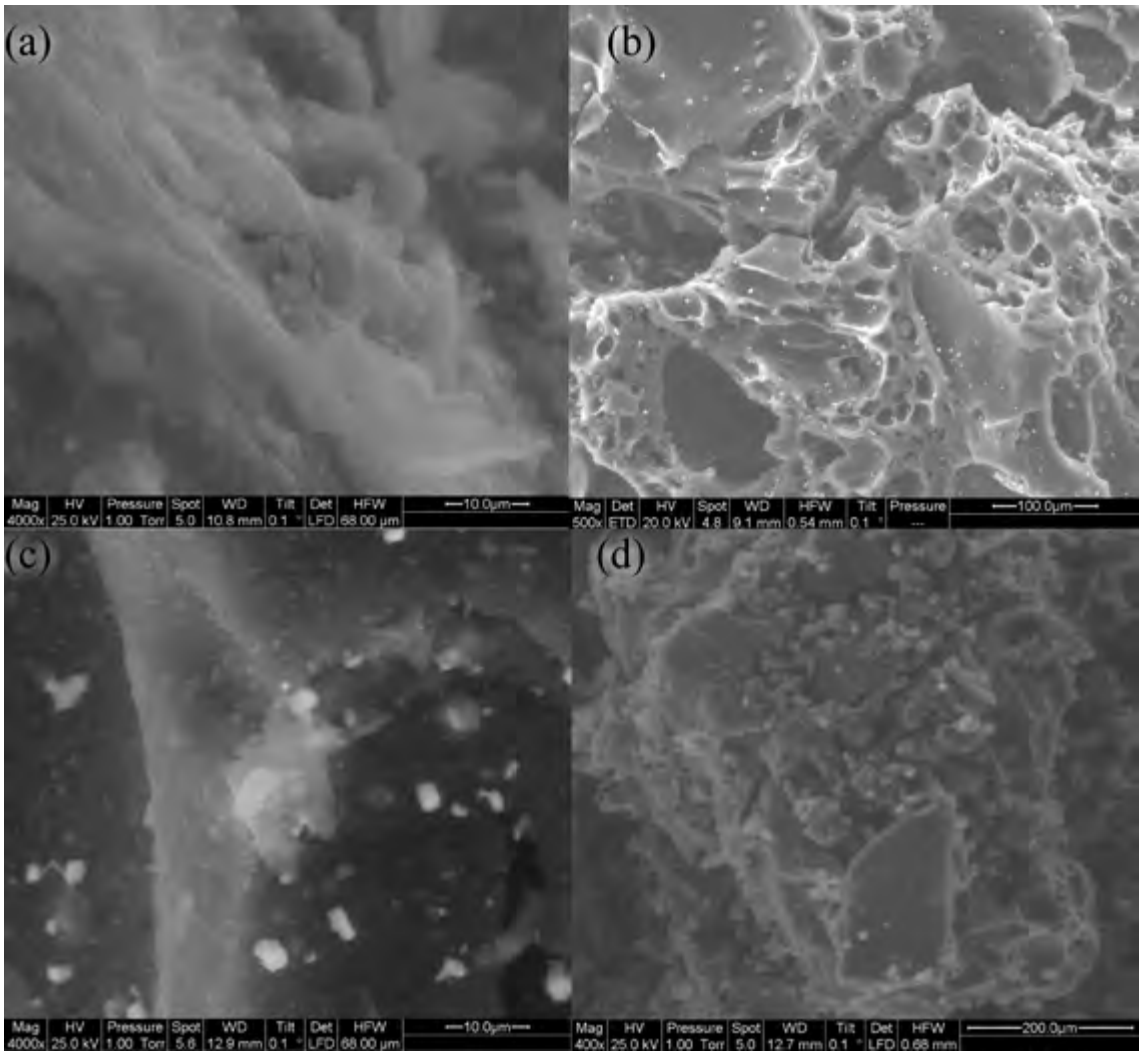

Figure 5.4. SEM images of: (a) tire M: magnification 4000 times; (b) T1S: magnification 500 times; (c) T1S: magnification 4000 times; (d) T9S: magnification 400 times.

Elements identified by microanalysis were those present in large amount in Table 5.4, together with Mg, Si, O, S and C. Sulfur was the main element, after C. Few differences between SEM X-EDS and ICP analyses are due to C, S and Si that were not examined by ICP and to Mg which was present only in low amount in the bright spot. These differences might be attributed to different sampling of the two analytical method, ICP was performed on the bulk of the char while X-EDS on spots of the micro-samples. Areas with different brightness were correlated to a different distribution of metals inside each sample (images with back scattered electrons, showed brighter areas in the presence of heavier elements): indeed the microanalysis reported for bright spots showed higher amounts of metals (Fe, Zn, Co, Cr, Cu, Si and Mg) than dark spots. The oxygen was probably due to inorganic compounds such as ZnO or silicates.

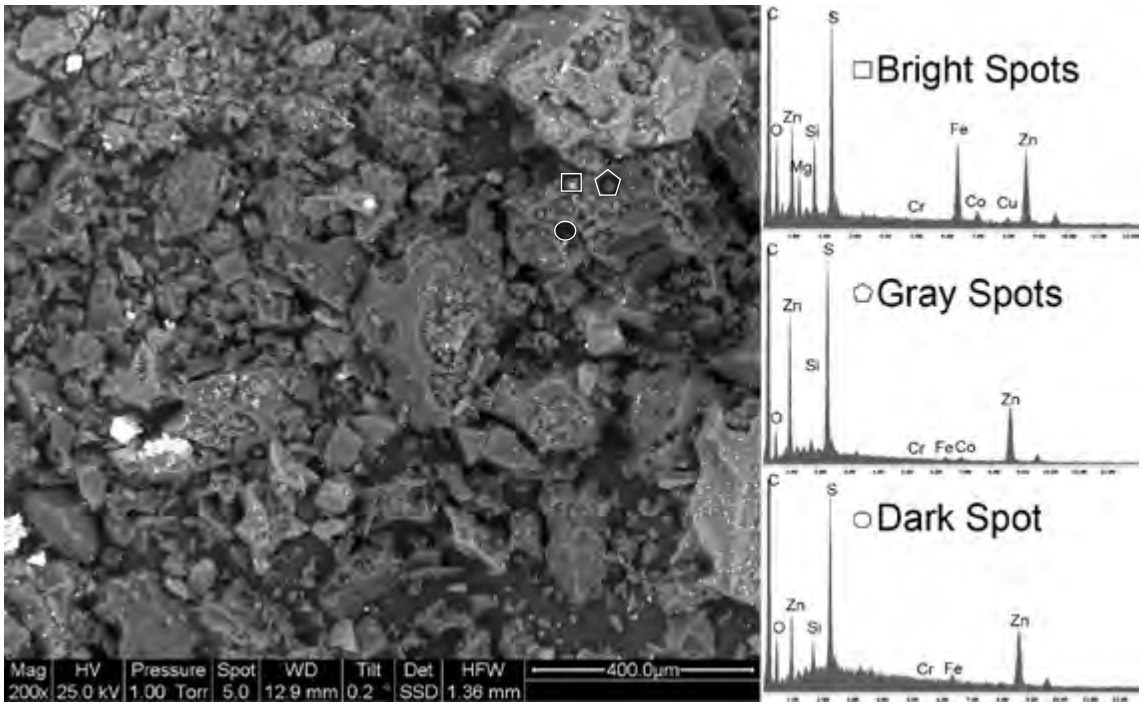

Figure 5.5. SEM back scattering image of S1. The microanalyses are referred to spots identified with the same shape in the SEM image.

On the contrary Ucar et al.[28] reported a homogenous distribution of particles over the sample surface and difference may be attributable to a different pyrolysis procedure and conditions.

Further consideration could be done on metal wires in consideration of their SEM images before and after pyrolysis together with the corresponding microanalyses (Figure 5.6).

The metal wire before pyrolysis showed a compact coating (Figure 5.6a) where the polymeric matrix was tight linked (Figure 5.6a black area in the low part of the wire). The microanalysis showed the presence of Cu and Zn (Figure 5.6c), suggesting the presence of a brass alloy. This presence was not surprising because brass is often employed to promote polymer adhesion on metal surface. The coating after pyrolysis (Figure 5.6b) showed a cracked surface while compact materials were present in the deep layers. The cracked surface was easily removed (Figure 5.6b) by a mild bending of the wire. On the cracked surface were present sulfur, Fe, Zn, and Cu (Figure 5.6d). The relative amount of Cu on the wire after pyrolysis was reduced, suggesting that Cu found in the char by ICP-MS analysis came from brass coating. Furthermore the sulfur compounds of tire probably reacted with Fe and Cu to give amorphous compounds not evidenced by XRD together with crystalline ZnS. The compact surface below the cracked layer showed iron as the sole metal (Figure 5.6d).

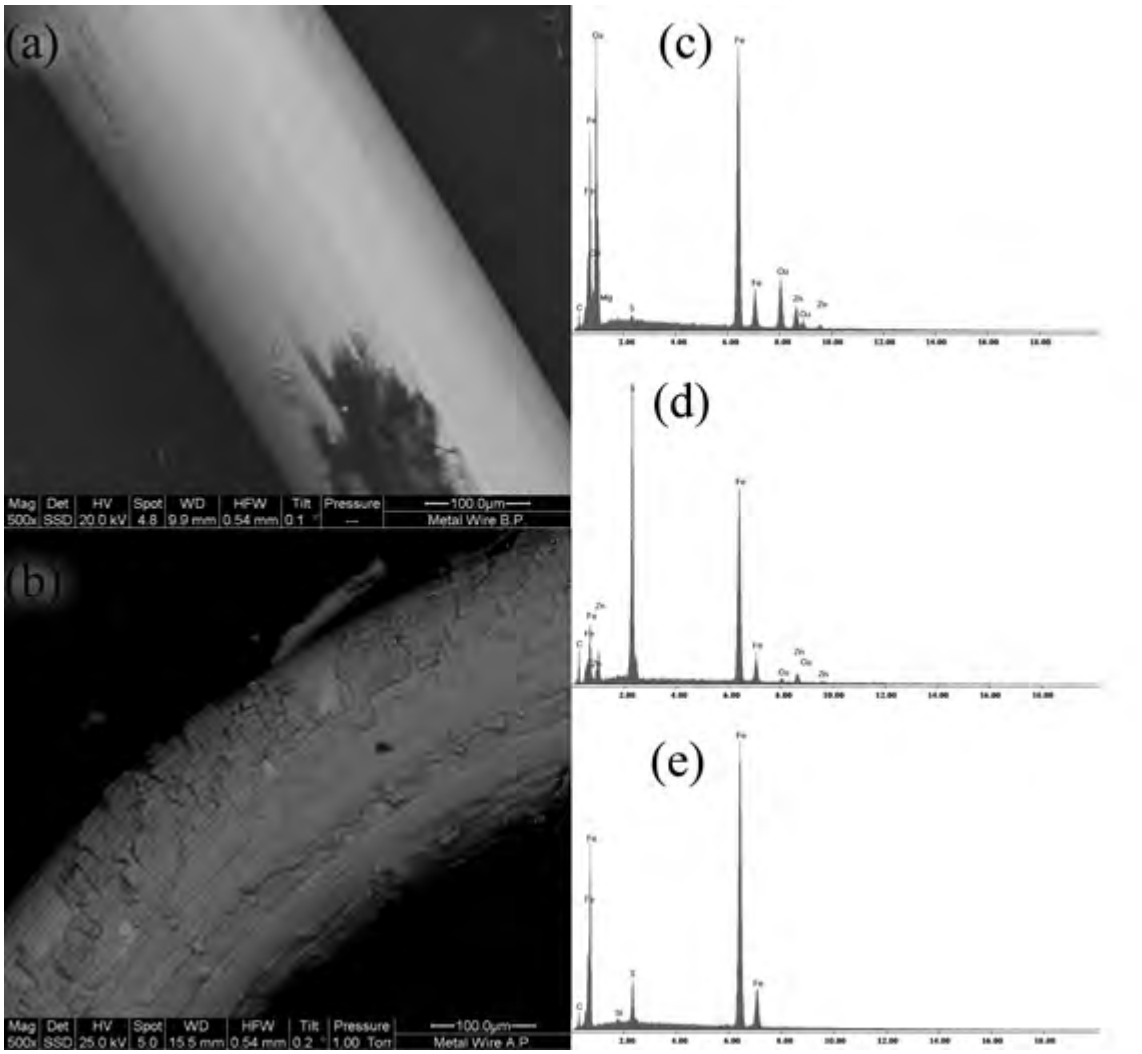

Figure 5.6. SEM images and microanalysis of metal wires. (a) metal wire before pyrolysis; (b) metal wire after pyrolysis; (c) microanalysis of metal wire before pyrolysis; (d) microanalysis of metal wire after pyrolysis, cracked coating; (e) microanalysis of metal wire after pyrolysis, inner surface.

Other metals were not detected except for Fe, that is the inner part of steel wires. Sulfur was also found in this layer but in minor amount with respect to the external surface, suggesting its migration from the rubber, through the brass, to wire during pyrolysis. These finding suggested that also metal wires were modified during MAP, brass coating was transformed and Cu was partially leaked. Furthermore the sulfur compounds partially reacted with the brass coating and ZnO filler forming ZnS which was present in char.

5.3.6. X-ray diffraction

X ray patterns of sample T1S, T4S and T9S were very close and they can be fully overlapped except for the different intensity of the broad peak centered at 25° (Figure 5.7). This peak was attributed to amorphous carbon in agreement with SEM morphological analyses (Section 5.3.5). T9S showed the highest intensity due to the high amount of residual not-pyrolyzed matrix and absorbed compounds

as previously reported for BET and ultimate analysis (Section 5.3.4).

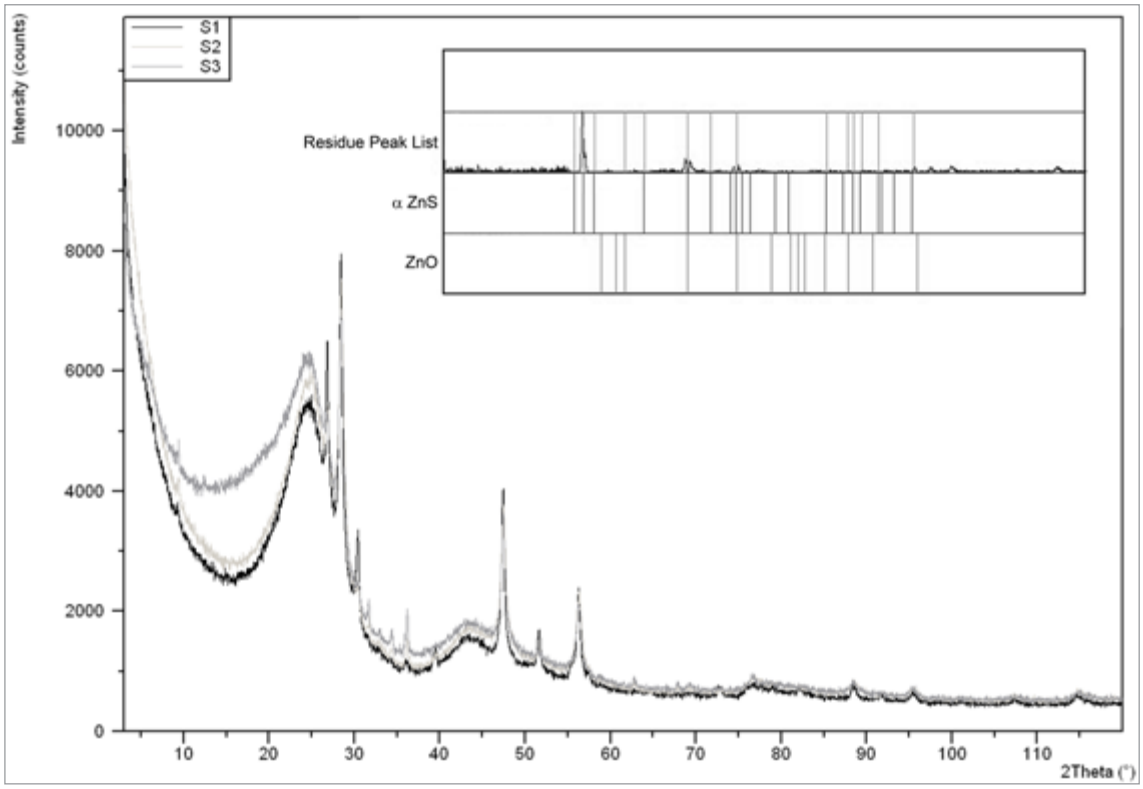

Figure 5.7. XRD patterns of samples T1S, T4S and T9S.

The crystalline phases were similar and peaks were attributed only to zinc compounds. The main compound was zinc sulfide crystallized in the cubic system (wurtzite, α ZnS) and only trace of zinc oxide was shown (zincite, ZnO). The reference peaks of zincite are at 2θ: 31.85, 34.55, 36.36, 47.70, 56.75, 63.09, 68.17, those of wurtzite at: 26.81, 28.41, 30.42, 39.47, 47.36, 51.58, 56.16, 57.33.[31]

The X ray patterns of T6S (Figure 5.8) showed some differences with respect to other samples.

The broad peak centered at 25° was also present as expected. Large amount of sphalerite (β ZnS), and only trace of wurtzite (α ZnS), and zincite (ZnO) were present in the spectrum of S4. The reference peaks of spharelite are at 2θ: 28.56, 33.09, 47.52, 56.29.[31]

In all samples any crystalline form of iron oxides were not detected. Crystalline forms of Fe might be present only, as inclusion compounds, in sphalerite and wurtzite crystal phases. Other elements identified via ICP-MS (Section 5.3.2), and SEM microanalysis (Section 5.3.5) were present in trace amount and they were not distinguishable from background noise or present as amorphous compounds.

Zinc silicate (Zn_2SiO_4) was not evidenced by X-ray analyses even if silicon was present in SEM microanalysis. Therefore silica compound identified by SEM X-EDS could be present in amorphous arrangements and not evidenced by X-ray analysis. In agreement with this hypothesis, Darmstadt et al.[32] reported the absence of peaks attributable to silicate, even if they were present in tire composition. On

the contrary silicates in the carbon from tire pyrolysis were evidenced by López et al.[27]

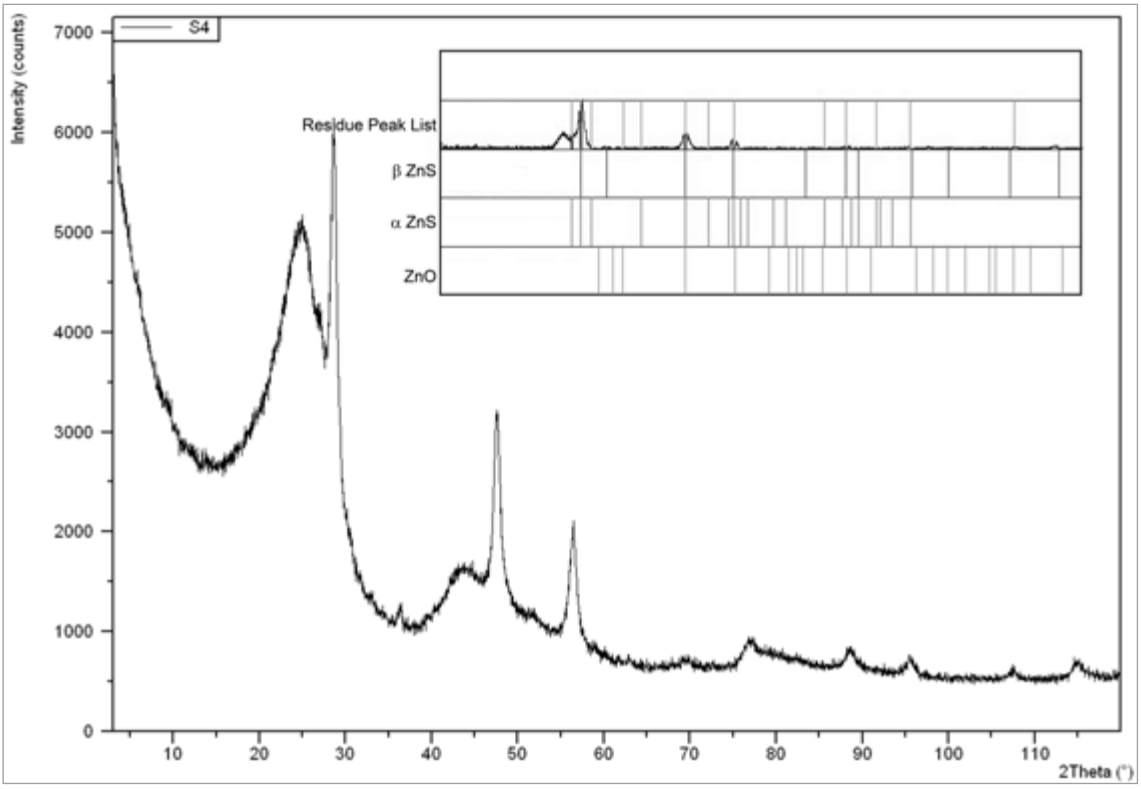

Figure 5.8. XRD patterns of sample T6S.

The temperature was not used as a descriptive parameter in MAP because it is hardly detected in a MW oven as above reported, thus crystalline form of ZnS might be a witness of the temperature reached in the course of an experiment. ZnO was present in tire formulation as an additive and it is stable below 973 K[33] while at higher temperature it reacted with sulfur compounds present in the pyrolysis reactor giving zinc sulfide in the crystalline form of sphalerite (β ZnS). Sphalerite is stable up to 1273 K, while at higher temperature it is converted into another crystalline form of zinc sulfide: wurtzite as reported by Darmstadt et al.[32] In our samples sphalerite was identified in sample T6S only while in the other samples wurtzite was almost exclusively present. These results are a strong indication that char T6S was heated at a pyrolysis temperature among 973 and 1273 K while the other samples T1S, T4S, and T9S containing almost exclusively wurtzite, must be heated at a pyrolysis temperature over 1273 K at least as spot-points temperature.

The presence of wurtzite and sphalerite in the char was a strong indication that high spots temperature were obtained during pyrolysis as hypothesized by many researchers in MAP of several organic materials.[5, 34-36]

5.3.7. Main achievements

Char obtained from MAP of waste tires showed chemical and physical characteristics slightly influenced by pyrolysis parameters and, mainly, by residual substances present.

BET surface areas, pore dimensions and distribution were influenced by the amount of absorbed compounds. Surface areas were increased by degassing the samples analyzed.

Metals were identified via ICP-MS and X-EDS analysis and they were presumably present in carbon black or other fillers employed for tire manufacturing and due to metal leaching from metal wires (especially for Cu and Zn compounds). In fact metal wires coating were almost completely destroyed and Fe, Cu and Zn compounds were released in char. These metals reacted with sulfur compounds present in tires giving sulfides and reducing the amount of sulfur compounds in liquid and gas.

XRD spectra of char gave relevant informations concerning crystalline ZnS phases sphalerite (β ZnS), and wurtzite (α ZnS). The presence of the crystalline wurtzite phase, stable over 1273 K, confirms that a high temperature was reached in MAP of tires when a P/M^2 ratio of 25.0×10^{-3} W/g^2 or higher was used. Char obtained using a lower P/M^2 ratio (1.3×10^{-3} W/g^2) showed sphalerite as the alone crystalline form of ZnS present and it was a witness of a lower pyrolysis temperature (700-1273 K).

Characteristics of carbon obtained from MAP were intermediate between anthracite and bitumen. The sulfur content was almost 50 % of that one present in waste tire. Anyway char showed relatively high content of sulfur and ash which hindered some direct uses. These characteristics allowed them to be employed as starting material for active carbon synthesis if a low expensive demineralization process is realized. Carbon characteristics precluded also its direct use in tire manufacturing because a preliminary process to reduce undesired component is required, or it might be usesed if different grades of carbon black were accepted.

5.4. Liquid

The liquid from pyrolysis of tire was always considered the most interesting product. First of all it may be an energy source due to its high GCV but moreover as source of products. Characteristics of liquids are influenced by working conditions and these parameters can be tuned to obtain tailor made products in function of their final use. Herein is reported a detailed chemo-physical characterization of liquid obtained from MAP of waste tire.

5.4.1. Physical properties

Physical properties of liquids are reported in Table 5.6 (coded "TnL" where "n" is the pyrolysis entry).

Ultimate analysis showed slight differences among liquids from pyrolysis experiments run in different conditions. The C/H molar ratio suggested the presence of both aliphatic and aromatic moieties as further confirmed by GC-MS (section 5.4.2) and ^{1}H-NMR (section 5.4.3). Oxygenated compounds were not present as also confirmed by spectroscopic analyses (section 5.4.5). The oxygen evaluated by difference was probably overestimated. Sulfur was in the range 0.5 -1.1% and sulfur compounds initially present were transformed in the same compounds using different operating parameters.

Remarkable influences of P/M^2 ratio were shown using set-up A on physical properties such as color, density, viscosity, HHV and LHV. When the P/M^2 ratio was decreased a pale-yellow, low density and low viscosity liquid was obtained instead of a dark-brown one. The different colors were connected with a different composition and to the presence of carbonaceous micro-particles (which do not precipitate even after spinning at 2000 rpm for 20 minutes). These particles were carried away from the reactor by the strong flow of the vapor formed when high P/M^2 ratio was used. Pictures of some liquid products, obtained at different P/M^2, are reported in Figure 5.9.

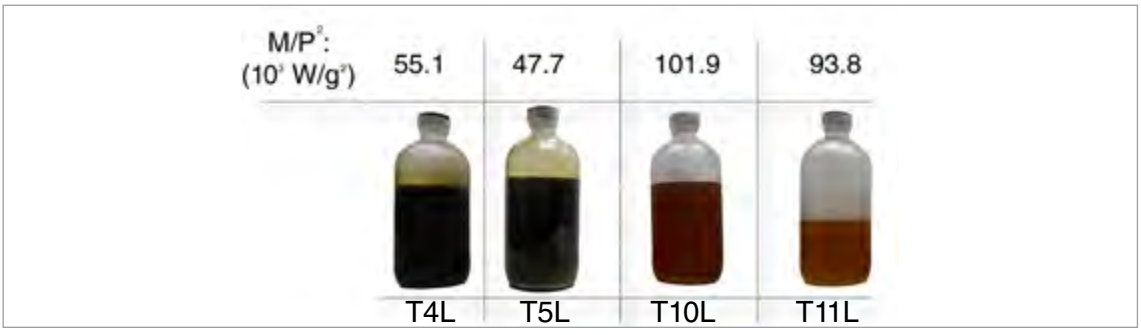

Figure 5.9. Aspect of some liquid products: T4L, T5L, T10L, and T11L.

Decreasing the mass of tire pyrolyzed at a constant MW power of 3kW (entries T6 – T8) the density and viscosity decreased as well, even if a dark-brown liquid was obtained. If a large amount of tires was pyrolyzed a higher quantity

of vapors was produced ensuing a fast stripping of products from the oven, that is a reduction of the residence time of the gas in the reactor. As a consequence the vapor was heated for a short time and the overall cracking effectiveness was partially reduced giving a liquid with a high density and viscosity (for comparison see T4L and T7L).

Table 5.6. Characteristic of liquid obtained by MAP of tire.

Entry	T1L	T2L	T3L	T4L	T5L	T6L	T7L	T8L	T9L	T10L	T11L	T12L	T13L	T14L	T15L
Set-up	A	A	A	A	A	A	A	A	A	B	B	B	B	B	B
Brand	Tire	Tire	Tire	Tire	Tire	Tire	Tire	Tire	Tire	Tire	Tire	Tire	Tire	Tire	Tire
	M	G	M	M	G	M	M	M	M	M	G	M	G	G	G
P/M^2 ($10^3W/g^2$)	137.6	95.7	106.0	55.1	47.7	1.3	11.9	730.1	23.6	101.9	93.8	50.8	47.9	24.0	12.0
Liquid yield (wt %)	31.5	42.8	43.1	42.6	38.8	39.3	44.0	30.1	20.7	27.8	35.7	27.6	26.3	37	31.9
HHV(MJ/Kg)	47±5	37±4	48±5	44±4	36±4	43±4	43±4	n.d.	43±4	45±5	n.d.	42±4	41±4	40±4	40±4
LHV(MJ/Kg)	45±4	35±4	46±5	42±4	34±4	41±4	40±4	n.d.	40±4	43±4	n.d.	40±4	39±4	38±4	38±4
C (wt %)	87.72	87.43	85.78	86.87	86.84	87.41	87.68	84.77	87.35	86.27	84.98	87.14	86.20	86.56	85.76
H (wt %)	11.31	9.85	11.01	10.12	10.97	10.77	10.84	10.78	11.83	8.53	9.30	9.33	9.27	10.72	10.17
N (wt %)	0.23	0.49	0.29	0.66	0.76	0.39	0.15	0.34	0.02	0.28	0.64	0.33	0.51	0.40	0.47
S (wt %)	0.7	1.1	1.0	0.9	0.8	0.8	0.8	n.d.	0.8	0.70	n.d.	0.80	0.50	0.70	0.80
O[a] (wt %)	0.04	1.13	1.92	1.45	0.63	0.63	0.53	4.11	0.00	4.22	5.08	2.40	3.52	1.62	2.80
C/H molar ratio	0.65	0.74	0.65	0.72	0.66	0.68	0.68	0.66	0.62	0.84	0.76	0.78	0.77	0.67	0.7
Viscosity (cP)	2.58	3.92	2.44	1.73	2.56	2.36	2.88	n.d.	0.73	0.90	1.25	1.00	0.73	1.34	0.89
Density (g/cm^3)	0.900	0.921	0.889	0.874	0.907	0.890	0.900	0.907	0.816	0.864	0.877	0.858	0.838	0.866	0.844

[a] by difference.

Furthermore the volume of the reactor played a role: If a 1000 mL vessel was used (T7L) instead of a large vessel of 5000 mL (T6L) the vapors remained in the oven for a shorter time and their cracking was partially reduced. In fact the liquid T7L has the highest viscosity among those obtained from *tire M*.

Moreover high P/M^2 ratio and strong flow of gases from the reactor were linked with two others outcomes that influenced the physical properties: a) deep cracking to volatile substances and b) pushing some molecules with relatively high molecular weight outside the oven.

Otherwise, if set-up B was used the influence of the P/M^2 ratio was negligible, liquids showed almost the same pale-yellow color, viscosity, density, and no remarkable physical differences were highlighted. The fractionating system prevented that high boiling substances, and particles to be pushed away. This set-up deeply affected the physical properties of liquid.

However it must keep in mind that all the liquid showed a viscosity lower than any crude oil and almost any commercial fuel oil.[9]

Using set-up A a direct correlation between P/M^2 ratio and calorific data (HHV and LHV) were found for liquid from *tire M* and lower values of HHV were found with *tire G*. If set-up B was used closer values of HHV were found independently of tire brand and P/M^2 ratio.

5.4.2. GC/MS

All liquids contained more than 300 different compounds (Table 5.8 and Figure 5.11) and an almost complete identification via GC/MS analysis was performed and reported in Table 5.7. Composition of liquid was evaluated by their chromatographic area without any response factors correction. They were identified using the NIST mass spectral library and reference compounds. Most of these compounds were present in amount lower than 1%. Toluene and limonene were the main compounds identified in each liquid even from different tire brands. The 15 main substances identified in liquid are reported in Table 5.8., they represent up to 46.08 % for T8L.

Several factors play a role on the formation of compounds: a) the P/M^2 ratio affected both the rate of heating and consequently the temperature reached by the sample, the rate of cracking, and the amount of vapor formed; b) the free volume of the reactor alongside the apparatus set-up influenced the residence time of products inside the reactor; c) the temperature reached by the absorber affected the qualitative and quantitative composition of liquids; d) the polymeric composition of tire. As a consequence a correlation between P/M^2, and other variables, with the amount of each compounds was not easily predictable.

Oxygenated compounds were not incontrovertible identified.

Table 5.7. Compounds identified in liquids.

		Set-up		A	A	A	A	A	A	A	A	B	B	B	B	B	B
		Brand		Tire M	Tire G	Tire M	Tire G	Tire M	Tire M	Tire M	Tire M	Tire M	Tire G	Tire M	Tire G	Tire G	Tire G
		P/M2 (103W/g2)		137.6	95.7	55.1	47.7	1.3	11.9	730.1	23.6	101.9	93.8	50.8	47.9	24.0	12.0
n°	Time	Substance	a.c.*														
1	12.0	2-butene-trans	C	1.7	0.3	1.5	0.4	1.2	1.2	1.1	1.1	0.8	2.1	1.1	0.2	0.7	1.7
2	12.2	butane	C	0.4	0.1	0.2	0.0	0.1	0.1	0.2	0.2	0.1	0.2	0.0			0.1
3	12.6	1-butene	C	0.3	0.1	0.2	0.1	0.1	0.1	0.2	0.2	0.1	0.2	0.1			0.1
4	13.5	2-methyl-1-butene	C	0.2	0.1	0.2	0.1	0.1	0.1	0.2	0.2		0.2	0.1			0.1
5	14.1	2-methylbutane	C	0.1	0.1	0.2	0.1	0.1	0.2	0.1	0.2	0.0	0.2	0.1	0.1		0.1
6	14.8	1-pentene	C	0.2	0.1	0.3	0.1	0.1	0.1	0.1	0.4	0.1	0.4	0.1	0.1	0.1	0.2
7	15.0	2-pentene-trans	C	0.8	0.1	0.6	0.1	0.3	0.4	0.5	0.7	0.2	0.6	0.3	0.2	0.1	0.3
8	15.3	pentane	C	0.1	0.1	0.3	0.1	0.2	0.1	0.1	0.4	0.1	0.3	0.1	0.1	0.1	0.3
9	15.5	2-methyl-1,3-butadiene	C	3.2	0.4	1.7	0.4	0.9	1.3	3.6	1.5	0.5	2.2	0.6	0.4	0.5	0.9
10	15.6	2-pentene-cis	C	0.2	0.1	0.2	0.1	0.1	0.1	0.2	0.3	0.1	0.4	0.2	0.1	0.1	0.3
11	16.3	3-methyl-1-hexene	C	2.1	0.3	1.6	0.4	1.0	1.1	1.8	1.4	0.5	1.9	0.7	0.5	0.4	1.0
12	16.4	1.4-pentadiene	P	0.4	0.1	0.2	0.1	0.1	0.1	0.3	0.3	0.1	0.4	0.2	0.1		0.1
13	17.1	cyclopentadiene	P	0.5	0.1	0.3	0.1	0.1	0.1	0.5	0.3	0.1	0.6	0.3	0.1		0.2
14	18.5	4-methyl-1-pentene	P	0.3	0.1	0.2	0.1	0.1	0.1	0.2	0.3	0.1	0.3	0.1	0.1		0.1
15	18.6	3-methyl-1-pentene	P	0.1		0.1	0.1	0.1	0.1		0.1	0.0		0.1			0.1
16	19.6	2-methylpentane	P	0.2		0.4		0.3	0.2	0.2	0.6			0.1	0.1		0.2
17	21.1	2-methyl-1-pentene	P	0.1	0.1	0.1	0.2	0.1	0.1	0.4	0.7		0.6	0.2	0.3		0.3
18	21.2	1-hexene	C	0.3		0.4		0.2	0.2			0.2	0.2				0.0
19	22.1	hexane	C	0.0		0.0	0.1	0.2	0.1	0.1	0.4	0.1		0.1	0.1		0.2
20	22.3	3-hexene-cis	P			0.0	0.1	0.6	0.0		0.1						
21	22.6	3-hexene-trans	P	0.1		0.0			0.1	0.1	0.1			0.0			
22	22.8	2.3-dimethyl-1-butene	P	0.2		0.3	0.1	0.2	0.2	0.2	0.5	0.1		0.1	0.1		0.1

(continue)

23	23.1	3-methyl-2-pentene	P	0.3		0.4	0.1	0.2	0.2	0.2	0.6	0.1		0.1	0.1		0.0
24	24.0	2-methyl-2-pentene	P	0.4		0.5	0.1	0.3	0.3	0.3	0.7	0.1			0.1		0.1
25	24.7	methylcyclopentane	P	0.1		0.2	0.0	0.2	0.1	0.6	0.3	0.1					0.1
26	25.0	2,4-dimethylpentane	P	0.1		0.2		0.2	0.1		0.3	0.0		0.0			0.0
27	25.2	2-methyl-1.3-pentadiene	P	0.3		0.2		0.1	0.1	0.3	0.4	0.1		0.1			0.0
28	25.3	1,3-cyclohexadiene	P	0.4		0.4		0.2	0.2	0.7	0.6	0.2	0.2	0.1	0.1		0.1
29	25.5	1,3-hexadiene	P	0.3		0.3		0.1	0.2	0.3	0.4	0.1					0.0
30	25.7	1,4-cyclohexadiene	P	0.3		0.3		0.1	0.2	0.6	0.5	0.2	0.2	0.1			0.0
31	26.1	1,4-hexadiene	P	0.2		0.1		0.1	0.1	0.2	0.2	0.0		0.0			
32	26.7	2-methyl-1-hexene	P	0.4		0.1		0.1	0.2	0.4	0.0	0.1		0.0			
33	26.9	3-methylcyclopentene	P			0.6	0.0	0.4	0.3	0.3	0.6	0.2	0.2	0.1		0.1	0.2
34	27.0	benzene	C	4.0	0.1	1.8	0.1	0.9	1.2	5.7	2.8	1.5	0.7	0.8	0.1	0.3	0.2
35	27.4	3,4-dimethyl-2-pentene	P	0.3		0.4		0.3	0.3	0.2	0.7	0.2		0.1			0.1
36	28.1	2,4-dymethyl-2-pentene	P	0.4		0.2		0.1	0.1	0.4	0.3	0.1		0.0			
37	28.4	4-methyl-1-hexene	P	0.1		0.1			0.1		0.2						
38	29.5	cyclohexene	P	0.3		0.3		0.3	0.2	0.2	0.5	0.1		0.1			
39	30.9	1-heptene	C	0.2		0.3		0.2	0.2	0.3	0.7	0.2	0.2	0.1	0.1	0.1	0.2
40	31.0	2,2,4-trimethylpentane	P	0.1		0.2		0.2	0.1	0.1	0.3	0.1		0.1			0.1
41	32.0	2,4-dimethyl-1,3-pentadiene	P	0.6		0.6	0.0	0.4	0.4	0.4	1.8	0.2	0.2	0.2	0.1	0.1	0.1
42	32.1	Heptane	C	0.1		0.3		0.2	0.1	0.1		0.1		0.1	0.1	0.1	0.2
43	32.3	2-methyl-2-hexene	P	0.1		0.1		0.1	0.1	0.1	0.3	0.1		0.0			0.0
44	33.2	5,5-dimethyl-2-hexene	P	0.5		0.7	0.0	0.6	0.5	0.4	1.2	0.3	0.2	0.2	0.1	0.1	0.2
45	33.9	3-ethylcyclopentene	P	0.1		0.1			0.1		0.2	0.1		0.0			
46	34.3	4-methyl-2-pentanone	P	0.3		0.5	0.0	0.5	0.4	0.1	1.0	0.1		0.1		0.1	0.2
47	34.9	2,3,4-trimethyl-2-pentene	P	0.3		0.3		0.3	0.2	0.2	0.6	0.0		0.1	0.1		0.1
48	35.4	ethylcyclopentane	P	0.1		0.1		0.1	0.1	0.1	0.2	0.2		0.0			0.0
49	35.6	1-methyl-1,3-cycloesadiene	P	0.4		0.6	0.0	0.3	0.4	0.6	1.1	0.1	0.2	0.2	0.1		0.1
50	35.9	1-methyl-1,4-cycloesadiene	P	0.1		0.1			0.1	0.1	0.3	0.1		0.0			0.0

(continue)

51	36.5	5,5-dimethylcyclopentadiene	P	0.1		0.2		0.1	0.1	0.2	0.4	0.4		0.1	0.1		0.0
52	37.3	2-methyl-2,4-hexediene	P	0.4	0.1	0.7	0.1		0.6	0.6	1.3	0.1	0.4	0.4	0.3	0.3	0.5
53	37.5	1-ethylcyclopentene	P	0.1		0.2		0.8	0.1		0.3	4.6		0.1			0.1
54	37.8	toluene	C	4.5	0.8	3.0	1.4	0.1	2.2	8.5	3.5	0.1	6.3	4.1	2.1	2.5	3.4
55	37.9	2-methylthiophene	P	0.2		0.2		2.2	0.1	0.2	0.3	0.1		0.1			0.0
56	38.1	5,5-dimethyl-1,3-cyclopentadiene	P	0.2	0.1	0.2		0.1	0.1		0.2			0.1	0.1		0.0
57	38.2	2-methyl-2,4-hexadiene	P	0.0		0.1	0.1		0.0	0.3		0.1		0.0	0.2	0.3	0.3
58	38.4	3,3-dimethyl-1-hexene	P	0.1		0.1		0.1	0.1	0.4	0.2	0.2	0.4	0.0			0.0
59	38.8	1-octyne	U	0.3	0.1	0.5	0.1	0.4	0.3	0.4	1.0	0.5	0.3	0.2	0.2	0.2	0.3
60	39.5	2,2,4,4-tetramethylpentane	P	0.4		0.7	0.1	0.7	0.5	0.6	1.1	0.1	0.4	0.4	0.3	0.3	0.5
61	39.9	1,2-dimethylcycloesane	P	0.1		0.1		0.1	0.1	0.1	0.3	0.1		0.0			0.1
62	40.6	2-methyl-1-heptene	P	0.1		0.1		0.1	0.1	0.1	0.2	0.2					0.1
63	41.0	1-octene	C	0.2		0.2	0.1	0.1	0.1	0.3	0.6	0.1	0.4		0.2	0.2	0.4
64	41.3	1-methyl-2-ehtyl-cyclopenatne	P	0.1		0.1		0.1	0.1	0.2	0.3	0.1		0.1	0.1		0.0
65	42.0	octane	C	0.1		0.2	0.1	0.2	0.2	0.2	0.8		0.3	0.2	0.2		0.0
66	42.2	1-ehtylcyclohexene	P	0.0		0.0			0.0			0.0					0.4
67	42.3	2-octene	P	0.1		0.1			0.1		0.2			0.0			0.0
68	42.5	1,3-dimethylcycloesane	P	0.2		0.2		0.1	0.1	0.2	0.2	0.0		0.0			0.0
69	42.8	1.3-dimetil-1-cicloesene	P	0.1		0.2	0.1	0.2	0.1		0.6			0.0	0.1		0.1
70	43.6	3-propylcyclopentene	P	0.1		0.1	0.0		0.1	0.1	0.2			0.0			0.0
71	44.1	5,5-dimethyl-1,3-hexadiene	P	0.2		0.3	0.1	0.3	0.1	0.1	0.6	0.1		0.2	0.2	0.1	0.1
72	44.2	1,4-dimethyl-1-cyclohexene	P	0.1		0.2	0.0	0.2	0.1	0.3	0.1	0.1		0.1	0.1		0.1
73	44.7	4-vinylcyclohexene	P	0.9	0.1	0.6	0.2	0.5	0.6	1.1	0.9	0.4	0.5	0.4	0.3	0.2	0.3
74	44.9	2,5,5-trimethyl-1-hexen-3-yne	U	0.2		0.2	0.1	0.2	0.2	0.2	0.4	0.1		0.1	0.1		0.0
75	45.3	1,2-dimethylcyclohexene	P	0.2		0.3	0.1	0.2	0.2	0.2	0.8	0.1		0.1	0.2		0.1
76	45.7	1-methyl-2-methylenecyclohexane	P	0.2		0.2	0.1	0.1	0.1	0.2	0.3	0.1		0.1	0.1		0.0

(continue)

77	46.4	etenhylcyclohexane	P	0.2		0.2	0.1	0.2	0.2	0.2	0.4	0.1		0.1	0.1		0.1
78	46.8	ethylbenzene	C	2.2	1.1	2.2	1.5	1.8	1.6	2.3	2.7	2.6	4.7	2.8	2.4	2.2	3.7
79	47.5	1,4-dimethylbenzene	C	3.8	0.6	2.4	0.9	1.5	1.6	5.1	3.5	2.3	3.5	2.4	1.5	0.9	1.9
80	47.8	2-methyl-2-octene	P	0.0	0.1	0.1	0.0	0.1	0.3	0.2	0.4	0.1		0.6	0.1	0.1	0.1
81	48.1	octahydropentalene	P	0.2	0.1	0.1		0.3	0.1	0.2	0.7	0.3	0.2	0.2	0.2	0.2	0.2
82	49.0	styrene	C	3.1	1.3	1.4	1.2	0.9	1.1	2.8	1.5	2.7	4.5	1.9	1.8	1.4	1.8
83	49.5	1.2-dimethylbenzene	C	1.0	0.3	0.8	0.4	0.5	0.6	1.5	1.3	0.7	1.0	0.8	0.8	0.4	0.6
84	50.0	1-nonene	C	0.3	0.1	0.4	0.2	0.3	0.0	0.4	0.7	0.4	0.6	0.5	0.6	0.3	0.7
85	50.5	1,4-bis(methylene)cyclohexane	U	0.1		0.2	0.0	0.2	0.1		0.5	0.1		0.1	0.2		0.1
86	50.7	7,7-dimethyl-2-methylene-bicyclo[2.2.1]heptane	U	0.2	0.1	0.2	0.1	0.1	0.2	0.2	0.3	0.1	0.4	0.1	0.1		0.1
87	50.9	nonane	C	0.1	0.1	0.2	0.1	0.2	0.1	0.2	0.4	0.2		0.2	0.4	0.2	0.5
88	51.2	1,2,3-trimethylcyclohexane	P	0.1		0.1	0.1	0.1	0.1	0.3	0.3	0.1		0.1	0.1		0.1
89	51.7	3,5,5-trimethylcyclohexene	P	0.2	0.1	0.3	0.1	0.3	0.2	0.1	0.6	0.1		0.2	0.2	0.1	0.2
90	52.2	cumene	C	0.3	0.2	0.5	0.3	0.4	0.3	0.3	1.0	0.3	0.5	0.5	0.6	0.3	0.5
91	52.8	1,2-dimethylcyclohexene	P	0.1		0.1	0.1	0.1	0.1		0.4	0.0		0.1	0.2		0.1
92	53.3	1-butylcicloesene	P	0.2		0.2	0.1	0.2	0.2	0.2	0.3	0.1		0.1	0.2		0.1
93	53.7	2-methylstirene	P	0.2	0.1	0.2	0.1	0.2	0.1	0.2	0.2	0.2	0.2	0.2	0.3	0.1	0.2
94	54.0	4-methyl-1-(1-methylethyl)-cyclohexene	P	0.1		0.1	0.0	0.1	0.1	0.1	0.3	0.3		0.1	0.1		0.0
95	54.5	2,5-dimethyl-3-vinyl-1,4-hexadiene	P	0.2	0.1	0.3	0.1	0.3	0.2	0.3		0.2	0.2	0.3		0.2	0.2
96	54.6	propylbenzene	C	0.4	0.2	0.5	0.3	0.5	0.4	0.3	1.2	0.3	0.6	0.5	0.7	0.3	0.7
97	54.8	4-methyl-1-(1-methylethyl) cyclohexene	P	0.2	0.1	0.2	0.1	0.3	0.2	0.2	0.4	0.5		0.2	0.2	0.1	0.1
98	55.0	5-ethyl-1-methylthiophene	P	0.3	0.1	0.4	0.2	0.8	0.3	0.4		0.2	0.5	0.2	0.3	0.2	0.4
99	55.2	1,2,3-trimethylbenzene	C	1.3	0.4	1.2	0.6	0.2	1.0	1.6	2.1	1.1	1.0	1.6	1.1	0.5	0.8
100	55.4	1,2,4 trimethylbenzene	P	0.6	0.3	0.8	0.5	0.6	0.6	0.8	1.1	0.8	0.9	1.1	1.0	0.4	0.7

(continue)

101	55.6	isolimonene	P	0.4	0.2	0.4	0.3	0.4	0.4	0.7	0.6	0.3	0.5	0.4	0.5	0.3	0.4
102	55.8	1,3,4 trimethylbenzene	P	0.3	0.1	0.2	0.1	0.1	0.2	0.3	0.3	0.2	0.2	0.2	0.3		0.1
103	55.9	4-methyl-1-decene	P	0.1	0.1	0.2	0.1	0.2	0.2	0.2	0.3	0.1		0.2	0.3		0.2
104	56.3	2,6,6-trimethylbicyclo[3.1.1] heptane	U	0.1	0.1	0.2	0.1	0.1	0.2	0.2	0.5	0.2	0.2	0.3	0.3	0.1	0.2
105	56.5	-methylstyrene	C	0.6	0.3	0.4	0.4	0.2	0.3	0.5	0.9	0.6	0.9	0.5	0.6	0.3	0.4
106	56.6	1-ethyl-4-methylbenzene	P	0.3	0.2	0.3	0.2	0.1	0.2	0.4		0.2	0.3	0.3	0.4	0.2	0.3
107	56.7	1,3,5-trimethylcyclohexane	P	0.1	0.1	0.1	0.1	0.2	0.1		0.2	0.1		0.2	0.2		0.1
108	57.0	1-methyl-4-(1-methylethyl) cyclohexene	P	0.1	0.1	0.2	0.1	0.1	0.2		0.4	0.2	0.2	0.3	0.4	0.1	0.2
109	57.5	2-propenylbenzene	P	0.7	0.2	0.6	0.2	0.2	0.3	1.1	0.6	0.5	0.4	0.3	0.6	0.2	0.4
110	57.7	1,3,5-trimethylbenzene	P	1.4	0.4	1.1	0.6	0.5	0.5	0.9	1.4	1.1	1.5	1.3	1.0	0.4	0.7
111	58.0	1-decene	C	0.1	0.2	0.1	0.2	0.3	0.1	0.8	0.3	0.1	0.6	0.3	0.9	0.3	0.9
112	58.5	3,5-dimethyl-1,6-octadiene	P	0.2	0.2	0.3	0.2	0.3	0.3	0.4	0.6	0.3	0.3	0.3	0.4	0.2	0.4
113	58.8	decane	C	0.2	0.2	0.3	0.3	0.4	0.2	0.2	0.4	0.3	0.5	0.3	0.6	0.3	0.7
114	58.9	7,7-dimethyl-2-methylenebicyclo[2.2.1]heptane	U	0.3	0.2	0.4	0.3	0.1	0.4	0.5	0.5	0.4	0.4	0.4	0.6	0.2	0.4
115	59.1	(1-methylpropyl)-benzene	P	0.1	0.1	0.1	0.1	0.2	0.1	0.3	0.2	0.1		0.2	0.2		0.2
116	59.3	1,5-cyclodecadiene	U	0.2	0.2	0.2	0.2	0.1	0.2		0.2	0.2	0.2	0.2	0.3	0.1	0.2
117	59.5	3-(1,1-dimethylethyl)-thiophene	P	0.1	0.1	0.2	0.1	0.3	0.1	0.1	0.2	0.1	1.3	0.2	0.2		0.1
118	59.9	1-ethyl-3-methylbenzene	P	1.0	0.6	1.0	0.9	0.7	0.2	0.8	1.3	1.0		1.2	1.6	0.5	1.0
119	60.1	1,2,4,5-tetramethylbenzene	C	0.8	0.7	1.4	1.0	1.5	0.6	0.9	2.1	1.5	1.6	2.2	1.9	0.7	1.4
120	60.6	1-methyl-4-(1-methylethyl) cyclohexne	P	0.2	0.3	0.4	0.3	0.5	1.2	0.4	0.6	0.3	0.5	0.4	0.6	0.3	0.5
121	60.9	limonene	C	3.8	4.3	3.4	2.8	3.6	3.4	9.0	2.5	3.3	9.8	4.3	3.5	5.4	8.8
122	61.3	indene	C	0.9	0.4	0.4	0.5	0.1	0.2	0.2	0.3	0.6	0.8	0.7	0.6	0.2	0.2
123	61.7	1-methyl-2-pentylcyclohexane	P	0.5	0.5	0.7	0.5	0.6	0.5	1.2	0.8	0.7	0.9	0.8	0.9	0.6	1.1
124	61.8	1,4-diehtylbenzene	P	0.2	0.1	0.2	0.2	0.2	0.2	0.2		0.2		0.3	0.3		0.1

(continue)

125	61.9	1-methyl-3-propylbenzene	P	0.1		0.2	0.1	0.1	0.1	0.5	0.2	0.2		0.2	0.3		0.1
126	62.4	butylbenzene	P	0.3	0.3	0.4	0.4	0.3	0.3	0.3	0.6	0.5	0.6	0.6	0.8	0.3	0.6
127	63.1	1-methyl-2-propylbenzene	P	0.1	0.2	0.2	0.2	0.2	0.2		0.2	0.1	0.2	0.2	0.4	0.1	0.3
128	63.4	2,2-dimethyl-4-decene	P	0.2	0.2	0.3	0.2	0.4	0.3		0.3	0.3	0.4	0.4	0.4	0.3	0.5
129	64.0	1,2-dimethyl-4-ethylbenzene	P	0.1	0.3	0.3	0.3	0.3	0.3	0.1	0.4	0.4	0.4	0.5	0.7	0.2	0.4
130	64.5	1-methyl-4-(1-methylethenyl) benzene	P	0.8	0.5	0.6	0.4	0.4	0.5	0.7	0.7	0.5	0.6	0.6	0.5	0.2	0.4
131	64.6	2,3-dihydro-1-methylindene	P		0.2	0.2	0.3	0.2	0.2	0.1		0.2	0.2	0.3	0.7	0.2	0.3
132	64.9	1-methyl-4-(1-methylethylidene) cyclohexene	P	0.3		0.3	0.3	0.4	0.3	0.2	0.3	0.4	0.4	0.4	0.4	0.3	0.4
133	65.1	1-undecene	C	0.2	0.3	0.2	0.4	0.2	0.2	0.2	0.2	0.4	0.7	0.4	0.9	0.3	0.8
134	65.6	1,1-cycloexylphenylethane	P	0.1	0.3	0.2	0.2	0.2	0.2		0.2	0.2	0.2	0.2	0.4	0.1	0.2
135	65.8	undecane	C	0.2	0.5	0.2	0.5	0.2	0.2	0.1	0.3	0.3	0.9	0.4	1.0	0.5	1.0
136	66.2	(1,1-dimethylpropyl)benzene	P	0.3	0.3	0.3	0.3	0.3	0.3		0.4	0.3	0.2	0.3	0.5	0.2	0.3
137	66.9	1,2,4,5-tetramethyil-benzene	P	0.4	0.4	0.2	0.5	0.4	0.3		0.3	0.5	0.4	0.5	0.7	0.2	0.4
138	67.8	1-ethyl-3-(1-methylethyl) benzene	P	0.1	0.2	0.2	0.2	0.2	0.2		0.2	0.1		0.2	0.5		0.1
139	68.2	4-metil-2,3-diidro-1H-indene	P	0.5	0.3	0.7	0.5	0.4	0.4	0.1	0.4	0.5	0.2	0.6	0.8	0.2	0.3
140	68.4	1,3-diethyl-5-methylbenzene	P	0.3	0.1	0.5	0.1	0.3	0.3	0.2	0.1	0.2		0.2	0.3		0.1
141	68.6	4-pentenylbenzene	P	0.2	0.3	0.2	0.3	0.2	0.5	0.1	0.1	0.7	0.2	0.5	0.5	0.2	0.3
142	68.8	1-methyl-1H-indene	P	0.9	0.6	0.5	0.7	0.3	0.4	0.7	0.2	1.2	0.9	0.9	1.1	0.3	0.4
143	68.9	5-methyl-2,3-dihydro-1H-indene	P	0.3	0.4	0.4	0.5	0.3	0.3	0.2	0.3	0.8	0.4	0.6	1.0	0.3	0.6
144	69.1	3-methyl-1H-indene	P	0.5	0.5	0.3	0.5	0.2	0.3	0.5	0.2	1.0	0.7	0.7	0.9	0.3	0.4
145	69.3	pentylbenzene	P	0.3	0.4	0.4	0.5	0.3	0.3	0.2	0.2	0.6	0.5	0.6	0.9	0.3	0.6
146	71.1	naphthalene	C	1.0	0.9	0.4	0.8	0.1	0.4	1.1	0.2	1.0	1.0	1.0	1.3	0.5	0.4
147	71.4	1-methyl-4-(1-methyl-2-propenyl)benzene	P	0.4	0.5	0.4	0.5	0.2	0.3	0.1	0.3	0.5	0.3	0.6	1.1	0.3	0.4
148	71.7	1-dodecene	C	0.2	0.4	0.2	0.4	0.1	0.2	0.1	0.1	0.4	0.7		0.8	0.4	0.7

(continue)

149	72.0	(1-methyl-1,3-butadienyl) benzene	P	0.1	0.3	0.3	0.3	0.3	0.1		0.2	0.3	0.2	0.4	0.4	0.1	0.2
150	72.1	1,6-dimethyl-2,3-dihydro-1H-indene	P	0.1	0.3		0.4		0.3		0.2	0.4	0.4		0.9	0.2	0.4
151	72.3	dodecane	C	0.1	0.2	0.2	0.4	0.2	0.1		0.1	0.2	0.5	0.3	1.0	0.4	0.9
152	72.9	benzothiazole	C	0.6	0.6	0.6	0.5	0.5	46.0	0.3	0.3	0.6		0.7	0.8	0.4	0.5
153	73.2	1,2-dimethyl-2,3-dihydro-1H-indene	P	0.1	0.2	0.1	0.2	0.1	0.1	0.1		0.2		0.1	0.2	0.1	0.2
154	73.8	cyclopentylbenzene	P	0.1	0.4	0.2	0.4	0.3	0.2		0.0	0.3	0.2	0.3	0.9	0.3	0.4
155	74.2	3-phenil-2-pentene	P	0.0	0.2	0.1	0.2	0.2	0.1		0.1	0.1		0.2	0.4	0.1	0.1
156	74.4	3-ethyl-2,3-dihydro-1H-indene	P	0.1	0.2	0.1	0.2	0.2	0.1		0.1	0.2		0.2	0.5		0.2
157	74.8	(1-methyl-1,3-pentadienyl) benzene	P	0.1	0.3	0.2	0.3	0.2	0.2		0.2	0.2		0.2	0.3		0.1
158	75.4	(1,1-dimethyl-2-propenyl) benzene	P	0.1	0.4	0.2	0.4	0.2	0.1		0.1	0.2		0.3	0.7	0.1	0.2
159	75.6	1,2-dihydro-6-methylnaftalene	P	0.3	0.4	0.3	0.5	0.2	0.3	0.2	0.1	0.5	0.3	0.5	0.6	0.2	0.3
160	75.8	hexylbenzene	P	0.2	0.4	0.2	0.4	0.2	0.2	0.1	0.1	0.4	0.4	0.4	0.7	0.3	0.5
161	76.0	1,3-dimethyl-1H-indene	P	0.3	0.4	0.3	0.5	0.2	0.3	0.1	0.1	0.5	0.3	0.5	0.7	0.2	0.3
162	76.1	1-(2-methylene-3-butenyl)-1-(1-methylenepropyl)ciclopropane	P	0.5	0.4	0.3	0.4	0.2	0.2		0.2	0.4	0.3	0.3	0.4	0.3	0.3
163	76.2	1,2,3,4-tetrahydro-2-methyl-naftalene	P		0.2	0.2	0.3	0.3	0.2			0.2		0.4	0.7	0.2	0.2
164	76.5	(1-methyl-1,3-butadienyl) benzene	P	0.3	0.4	0.3	0.5	0.2	0.2	0.1	0.1	0.4	0.2	0.4	0.7	0.2	0.2
165	76.7	(1-methylene-2-pentenyl) benzene	P	0.1	0.3	0.2	0.4	0.2	0.2	0.1	0.1	0.3		0.2	0.5	0.2	0.2
166	77.1	1-phenylcyclohexane	P	0.1	0.3	0.2	0.5	0.3	0.2		0.1	0.4		0.4	0.7	0.2	0.3

(continue)

167	77.4	4,7-dimethyl-2,3-dihydro-1H-indene	P	0.2	0.4	0.3	0.5	0.2	0.3		0.1	0.4	0.2	0.1	0.7	0.3	0.3
168	77.6	2-ethyl-1,2,3,4-tetrahydronaftalene	P	0.0	0.1	0.2	0.1	0.3	0.1		0.0	0.1		0.1	0.3		0.1
169	77.7	1-tridecene	C	0.1	0.4	0.2	0.4	0.4	0.1		0.1	0.4	0.6	0.4	0.6	0.3	0.6
170	78.0	1-methylnaphtalene	C	0.9	1.1	0.6	1.2	0.2	0.5	0.6	0.2	1.3	1.3	1.3	1.6	0.8	1.1
171	78.3	tridecane	C	0.1	0.5	0.2	0.5	0.1	0.2	0.1	0.1	0.4	0.6	0.4	0.9	0.5	1.0
172	78.6	5-ethyl-1,2,3,4-tetrahydronaftalene	P	0.1	0.2	0.1	0.2	0.2	0.1		0.1	0.2		0.2	0.3	0.1	0.2
173	79.0	2-methylnaftalene	C	0.6	0.8	0.4	1.0	0.1	0.4	0.4	0.1	0.9	0.8	0.8	1.2	0.5	0.6
174	79.6	3-etil-3-metilexane	U	0.2	0.4	0.2	0.4	0.3	0.3		0.1	0.4	0.2	0.3	0.5	0.2	0.3
175	79.7	cyclohexylbenzene	P	0.1	0.3	0.2	0.3	0.2	0.2		0.1	0.2		0.2	0.4	0.2	0.3
176	80.0	1,2,3,4-tetrahydro-1,8-dimethylnaphtalene	P	0.1	0.3	0.1	0.2	0.2	0.1		0.1	0.6		0.2	0.5	0.1	0.2
177	80.5	(1,1-dimethyl-2-butinyl)benzene	P	0.2	0.2	0.2	0.4	0.1	0.2		0.1	0.4		0.2	0.2	0.2	0.2
178	81.2	1-(1-buten-3-yl)-2-vinylbenzene	P	0.1	0.4	0.1	0.5	0.3	0.2		0.1	0.4		0.2	0.5	0.3	0.3
179	81.3	1,2-dipropylcyclopentane	P	0.1	0.1	0.1	0.2	0.1	0.1		0.1	0.1		0.1	0.2	0.1	0.2
180	81.8	heptylbenzene	P	0.1	0.3	0.2	0.4	0.1	0.1		0.1	0.3	0.2	0.3	0.4	0.3	0.3
181	82.2	1,2,3,4-tetrahydro-2,7-dimethylnaftalene	P	0.1	0.3	0.2	0.3	0.2	0.2		0.1	0.3		0.2	0.3	0.2	0.2
182	82.4	1-tetradecene	C	0.3	0.5	0.4	0.5	0.5	0.4	0.2	0.2	0.4	0.4	0.4	0.2	0.6	0.7
183	82.5	biphenyl	C	0.6	0.8	0.4	0.8	0.3	0.3	0.3		0.9	0.7	0.8	0.6	0.5	0.5
184	82.7	1,2,3-trimethyl-1H-indene	P	0.3	0.6	0.4	0.6	0.4	0.3	0.1	0.1	0.6	0.3	0.5	0.4	0.4	0.4
185	83.1	1,1,3-trimethyl-1H-indene	P	0.2	0.3	0.1	0.3	0.2	0.2		0.1	0.4		0.2	0.3	0.1	0.2
186	83.4	tetradecane	C	0.3	0.6	0.4	0.6	0.4	0.3	0.1	0.1	0.6	0.7	0.5	0.5	0.5	0.8
187	83.7	1-ethylnaftalene	P	0.4	0.8	0.4	0.7	0.3	0.4	0.1	0.1	0.8	0.4	0.5	0.4	0.4	0.3
188	83.9	2,3-dimethylnaftalene	P	0.2	0.4	0.3	0.8	0.4	0.2	0.1	0.1	0.4	0.2	0.6	0.2	0.2	1.3
189	84.3	2,2,4,4,5,5,7,7-octamethyloctane	P	0.4	0.6	0.4	0.6	0.5	0.4	0.1	0.2	0.6	0.5	0.5		0.7	0.8

(continue)

190	84.5	1,7-dimethylnaftalene	P	0.2	0.3	0.3	0.4	0.3	0.3	0.1		0.4	0.2	0.4	0.2	0.2	0.2
191	84.7	2,5-dimetil-benzo[b]tiofene	P	0.1	0.2	0.1	0.3	0.3	0.1		0.0	0.2		0.2	0.2	0.2	0.2
192	85.2	2,6-dimethylnafatalene	P	0.4	0.9	0.4	0.7	0.3	0.3	0.2	0.1	0.9	0.4	0.6	0.3	0.4	0.3
193	85.4	1,5-dimethylnafatalene	P	0.4	0.7	0.5	0.8	0.5	0.5	0.3	0.2	0.8	0.6	0.8	0.3	0.6	0.7
194	85.9	2,4-dimethylquinoline	U	0.2	0.5	0.3	0.5	0.4	0.4		0.1	0.1	0.2		0.1	0.4	0.3
195	86.3	1,8-dimethylnaftalene	P	0.2	0.5	0.2	0.4	0.3	0.3		0.1	0.4	0.3	0.3	0.2	0.4	0.3
196	86.5	1,2,3,4-tetrahydro-1,4,6-trimethylnaftalene	P	0.2	0.4	0.2	0.4	0.3	0.3		0.1	0.3	0.2	0.3	0.1	0.3	0.4
197	86.7	(2-ethyl-4-methyl-1,3-pentadienyl)benzene	P	0.1	0.4	0.2	0.3	0.3	0.3		0.1	0.2	0.2	0.2	0.1	0.3	0.3
198	87.1	(3,3-dimethyl-1-methylene-butyl) benzene	P	0.3	0.8	0.3	0.7	0.6	0.5	0.1	0.1	0.6	0.4	0.4	0.2	0.5	0.4
199	87.5	(3-cyclopentylpropyl)benzene	P	0.1	0.4	0.1	0.4	0.2	0.2		0.1	0.3	0.3	0.2	0.1	0.4	0.4
200	88.2	3-methyl-1,1'-diphenil	P	0.3	0.7	0.3	0.7	0.3	0.3	0.1	0.1	0.7	0.4	0.4	0.2	0.5	0.2
201	88.7	1-pentadecene	C	0.6	1.4	0.7	1.3	0.3	0.3	0.1	0.1	1.2	1.1	0.8	0.3	1.0	0.8
202	89.1	2-etil-5-metil-benzo[b]tiofene	P	0.1	0.2	0.1	0.3		0.2			0.2		0.1	0.1	0.2	0.1
203	89.2	pentadecane	C	0.4	1.4	0.8	1.2	0.8	0.7	0.2	0.2	1.3	1.8	1.1	0.4	1.9	2.3
204	89.8	1,3,4,5,6,7-hexahydro-1,1,5,5-tetramethyl-2h-2,4a-methanonaphthalene	U	0.3	0.6	0.2	0.8	0.3	0.2		0.1	0.7	0.3	0.3		0.5	0.2
205	90.1	dibenzyl	P	0.1	0.3	0.1	0.2	0.1	0.1	0.1	0.0	0.1		0.1		0.1	0.0
206	90.4	7,11-dimethyl-3-methylene-1,6,10-dodecatriene	U	0.1	0.5	0.2	0.4	0.4	0.3		0.0	0.3	0.3	0.2		0.5	0.3
207	90.6	2-(1-methylethyl)-naphthalene	P	0.1	0.4	0.2	0.4	0.2	0.2		0.0	0.3		0.1			0.1
208	90.8	trimethylnaphtalene	P	0.1	0.3	0.1	0.3	0.2	0.2		0.0	0.2		0.1		0.3	0.1
209	91.2	trimethylnaphtalene	P	0.3	0.6	0.4	0.7	0.6	0.5		0.1	0.7	0.4	0.6	0.1	0.2	0.2
210	91.5	1,2-dihydro-2,5,8-trimethyl-naphthalene	P	0.0	0.3	0.0	0.2	0.1	0.1			0.1		0.0		0.2	0.1

(continue)

211	91.9	trimethylnaphtalene	P	0.1	0.4	0.2	0.4	0.2	0.2		0.0	0.3	0.2	0.2		0.3	0.1
212	92.1	trimethylnaphtalene	P	0.1	0.6	0.2	0.4	0.3	0.2		0.0	0.3	0.2	0.2		0.4	0.1
213	92.8	2,2'-dimethylbiphenyl	P	0.3	0.9	0.3	0.6	0.4	0.3	0.1	0.1	0.6	0.3	0.3		0.7	0.1
214	93.7	1-hexadecene	C	0.3	0.7	0.3	0.6	0.3	0.4		0.1	0.6	0.7	0.4		0.8	0.2
215	93.8	1,1'-ethylidenebisbenzene	P	0.1	0.3	0.1	0.3	0.2	0.2	0.3		0.2		0.1		0.3	0.0
216	94.1	3,4'-dimethyl- 1,1'-diphenyl	P	0.2	0.3	0.2	0.3		0.3			0.2	0.7	0.1		0.2	
217	94.1	hexadecane	C		0.5	0.2	0.4	0.4			0.1	0.4		0.3	0.1	0.9	0.6
218	94.3	diphenylamine	U	0.1	0.5	0.1	0.2	0.2	0.2	0.3		0.1	0.2	0.1		0.5	
219	94.7	3-methyl-1,1'-diphenyl	P	0.1	0.4	0.2	0.4	0.3	0.2			0.2		0.2		0.4	0.0
220	95.1	1-(2-propenyl)-naphthalene	P	0.1	0.3	0.1	0.2	0.3	0.3		0.0	0.1		0.1		0.3	0.0
221	95.3	1-methyl-2-pentyl-cyclohexane	P	0.2	0.4	0.2	0.3	0.3	0.3		0.1	0.2	0.2	0.1		0.4	0.1
222	95.4	1-methyl-4-(phenylmethyl)-benzene	P	0.2	0.5	0.2	0.5	0.3	0.3		0.0	0.3	0.2	0.2		0.6	
223	95.8	1,4,5,8,9,10-hexahydroanthracene	P	0.2	0.6	0.1	0.4	0.1	0.3	0.1	0.0	0.2		0.0		0.2	
224	96.3	1,3,5-tris(1-methylethyl)-benzene	P	0.1	0.3	0.1	0.3	0.3	0.3		0.0	0.1		0.1		0.2	
225	96.6	1,1'-(1,3-propanediyl)bis-benzene	P	0.2	0.8	0.2	0.6	0.5	0.4		0.1	0.3	0.6	0.2		0.9	0.1
226	97.0	4,9-dipropyldodecane	P	0.1	0.3	0.1	0.3	0.3	0.4		0.0	0.2		0.1		0.5	0.1
227	97.7	decylbenzene	P	0.1	0.3	0.1	0.3	0.1	0.1		0.0			0.1		0.4	
228	98.0	1-methyl-7-(1-methylethyl)-phenanthrene	P	0.2	0.4	0.1	0.4	0.6	0.3	0.2	0.0	0.1	0.3	0.1		0.6	0.1
229	98.4	1-heptadecene	C		0.5	0.2	0.4	0.3	0.3	0.1	0.1	0.2	0.5	0.2		0.9	0.1
230	98.9	heptadecane	C	0.6	1.5	0.9	1.0	0.9	0.8	0.5	0.2	0.9	2.4	1.2		3.1	0.7
231	99.4	2,6,10,14-tetramethylhexadecane	U	0.3	0.6	0.3	0.4	0.5	0.4	0.3	0.1	0.2	0.4	0.2		1.3	0.2
232	99.6	2-methyl-9H-fluorene	P		0.7	0.2	0.4	0.3	0.3	0.1	0.0	0.1	0.2	0.1		0.6	

(continue)

233	99.9	1-(1-methylehtyl)-9,10-dihydroanthracene	U	0.1	0.3	0.1	0.2	0.1	0.2		0.0	0.1		0.1		0.3	
234	100.6	1-methyl-4-(phenylmethyl)-benzene	P	0.1	0.4	0.2	0.2	0.1	0.1			0.0		0.0		0.3	
235	101.0	2,2-dimethylundecane	P		0.4	0.1	0.3	0.4	0.3	0.2	0.0	0.1	0.2	0.1		0.7	0.1
236	101.3	1,1'-(1,4-butanediyl)bis-benzene	P		0.4	0.2	0.2	0.2	0.3	0.3	0.0	0.1		0.1		0.7	
237	101.9	1,1'-(2-methyl-2-propenylidene) bis-benzene	P	0.0	0.4	0.1	0.2	0.1	0.3	0.2		0.1		0.0		0.5	
238	103.2	phenanthrene	P	0.2	0.4	0.1	0.3	0.1	0.3	0.2	0.0	0.1	0.2	0.1		0.4	
239	105.1	9,10-dihydro-9,10-dimethylanthracene	P	0.1	0.4	0.1	0.3	0.4	0.2	0.3	0.0			0.0		0.7	
240	106.9	1-nonadecene	C	0.1	0.4	0.1	0.3	0.2	0.2	0.1				0.0		0.2	0.0
241	107.2	nonadecane	C		0.3	0.1	0.3	0.3	0.2		0.0		0.5	0.0		1.1	0.0
242	109.3	1-methylanthracene	P	0.1	0.3	0.1	0.2	0.1	0.3	0.2	0.0			0.0		0.4	
243	110.0	2-methyl anthracene	P	0.1	0.3	0.1	0.2	0.6	0.3	0.1	0.0					0.3	
244	110.4	4-methylphenanthrene	P	0.2	0.3	0.0	0.2	0.1		0.1						0.2	
245	110.6	9-methylanthracene	P		0.3	0.0	0.3	0.1				0.0	0.2	0.0		0.3	
246	112.7	1-phenylnaphtalene	P	0.2	0.3	0.1	0.2	0.1	0.1					0.0		0.3	
		Aliphatic		**37.0**	**24.3**	**40.6**	**24.3**	**35.5**	**32.3**	**41.9**	**51.3**	**33.7**	**45.2**	**29.7**	**26.4**	**32.1**	**43.1**
		Hetero-aliphatic		**0.5**	**0.2**	**0.7**	**0.3**	**3.2**	**0.5**	**0.8**	**0.5**	**0.4**	**1.9**	**0.5**	**0.5**	**0.2**	**0.5**
		Aromatic single ring		**35.0**	**23.0**	**30.9**	**27.1**	**22.4**	**23.8**	**37.9**	**34.4**	**32.9**	**36.8**	**37.1**	**41.4**	**21.1**	**31.2**
		PAHs		**10.9**	**21.2**	**9.7**	**19.4**	**10.8**	**11.3**	**7.0**	**2.4**	**16.8**	**12.2**	**13.7**	**10.4**	**15.9**	**8.6**
		Hetero-aromatic		**1.1**	**2.0**	**1.2**	**1.9**	**1.3**	**1.3**	**0.5**	**0.4**	**1.1**	**0.4**	**1.0**	**1.2**	**1.7**	**1.1**
		TOTAL		**84.4**	**70.6**	**83.1**	**72.9**	**73.3**	**69.2**	**88.1**	**89.0**	**84.8**	**96.4**	**81.9**	**79.9**	**70.9**	**84.5**

*a.c.: attribution confidence; C, certain (>98%); P, probable (86-97%); U, uncertain (<85%).

Table 5.8.15 main compounds in liquids from MAP of tire.

		Entry	T1L	T2L	T4L	T5L	T6L	T7L	T8L	T9L	T10L	T11L	T12L	T13L	T14L	T15L
		Set-up	A	A	A	A	A	A	A	A	B	B	B	B	B	B
		Brand	Tire M	Tire G	Tire M	Tire G	Tire M	Tire M	Tire M	Tire M	Tire M	Tire G	Tire M	Tire G	Tire G	Tire G
		P/M^2 ($10^3W/g^2$)	137.6	95.7	55.1	47.7	1.3	11.9	730.1	23.6	101.9	93.8	50.8	47.9	24.0	12.0
n°	Time	Substance														
1	12.0	2-butene-trans	1.7	0.3	1.5	0.4	1.2	1.2	1.1	1.1	0.8	2.1	1.1	0.2	0.7	1.7
9	15.5	2-methyl-1,3-butadiene	3.2	0.4	1.7	0.4	0.9	1.3	3.6	1.5	0.5	2.2	0.6	0.4	0.5	0.9
11	16.3	3-methyl-1-hexene	2.1	0.3	1.6	0.4	1.0	1.1	1.8	1.4	0.5	1.9	0.7	0.5	0.4	1.0
34	27.0	benzene	4.0	0.1	1.8	0.1	0.9	1.2	5.7	2.8	1.5	0.7	0.8	0.1	0.3	0.2
54	37.8	toluene	4.5	0.8	3.0	1.4	0.1	2.2	8.5	3.5	0.1	6.3	4.1	2.1	2.5	3.4
78	46.8	ethylbenzene	2.2	1.1	2.2	1.5	1.8	1.6	2.3	2.7	2.6	4.7	2.8	2.4	2.2	3.7
79	47.5	1,4-dimethyl-benzene	3.8	0.6	2.4	0.9	1.5	1.6	5.1	3.5	2.3	3.5	2.4	1.5	0.9	1.9
82	49.0	styrene	3.1	1.3	1.4	1.2	0.9	1.1	2.8	1.5	2.7	4.5	1.9	1.8	1.4	1.8
83	49.5	1.2-dimethyl-benzene	1.0	0.3	0.8	0.4	0.5	0.6	1.5	1.3	0.7	1.0	0.8	0.8	0.4	0.6
90	52.2	cumene	0.3	0.2	0.5	0.3	0.4	0.3	0.3	1.0	0.3	0.5	0.5	0.6	0.3	0.5
99	55.2	1,2,3-trimethylbenzene	1.3	0.4	1.2	0.6	0.2	1.0	1.6	2.1	1.1	1.0	1.6	1.1	0.5	0.8
100	55.4	1,2,4 trimethylbenzene	0.6	0.3	0.8	0.5	0.6	0.6	0.8	1.1	0.8	0.9	1.1	1.0	0.4	0.7
110	57.7	1,3,5-trimethylbenzene	1.4	0.4	1.1	0.6	0.5	0.5	0.9	1.4	1.1	1.5	1.3	1.0	0.4	0.7
121	60.9	limonene	3.8	4.3	3.4	2.8	3.6	3.4	9.0	2.5	3.3	9.8	4.3	3.5	5.4	8.8
146	71.1	naphthalene	1.0	0.9	0.4	0.8	0.1	0.4	1.1	0.2	1.0	1.0	1.0	1.3	0.5	0.4
		Aliphatic	**10.8**	**5.4**	**8.2**	**4.0**	**6.6**	**7.0**	**15.5**	**6.4**	**5.1**	**15.9**	**6.8**	**4.6**	**6.9**	**12.4**
		Aromatic	**23.1**	**6.4**	**15.5**	**8.2**	**7.6**	**11.1**	**30.6**	**20.9**	**14.1**	**25.6**	**18.4**	**13.7**	**9.7**	**14.8**
		Total	**33.9**	**11.7**	**23.8**	**12.2**	**14.2**	**18.1**	**46.1**	**27.4**	**19.2**	**41.5**	**25.1**	**18.3**	**16.6**	**27.2**

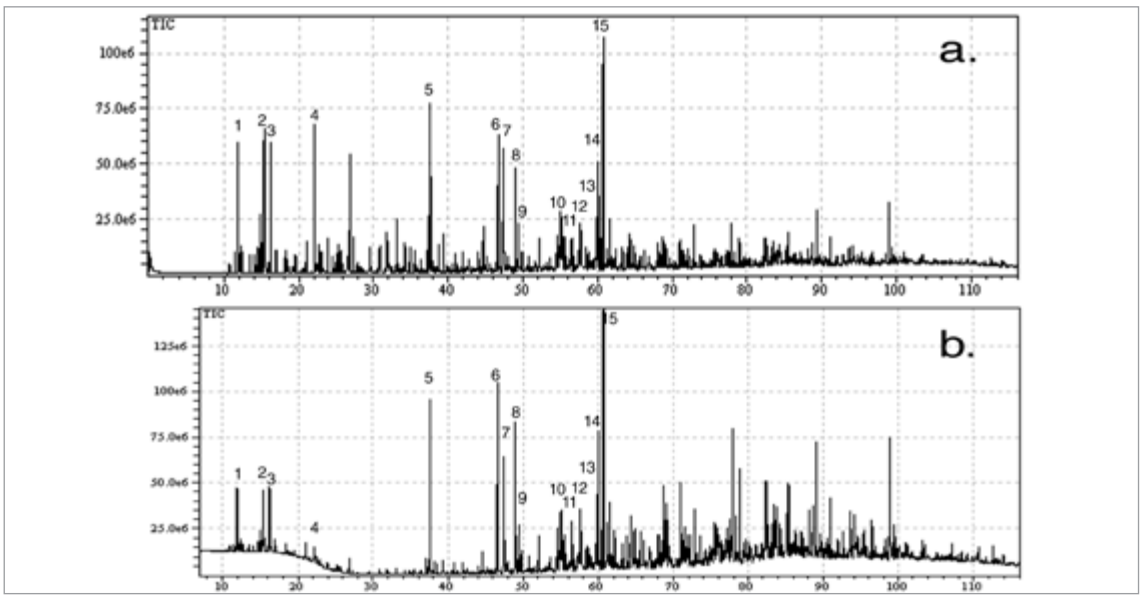

Figure 5.10. Total ion chromatography of samples: a. T4L; b. T5L. The numbers in the chromatogram correspond to those reported in Table 5.8.

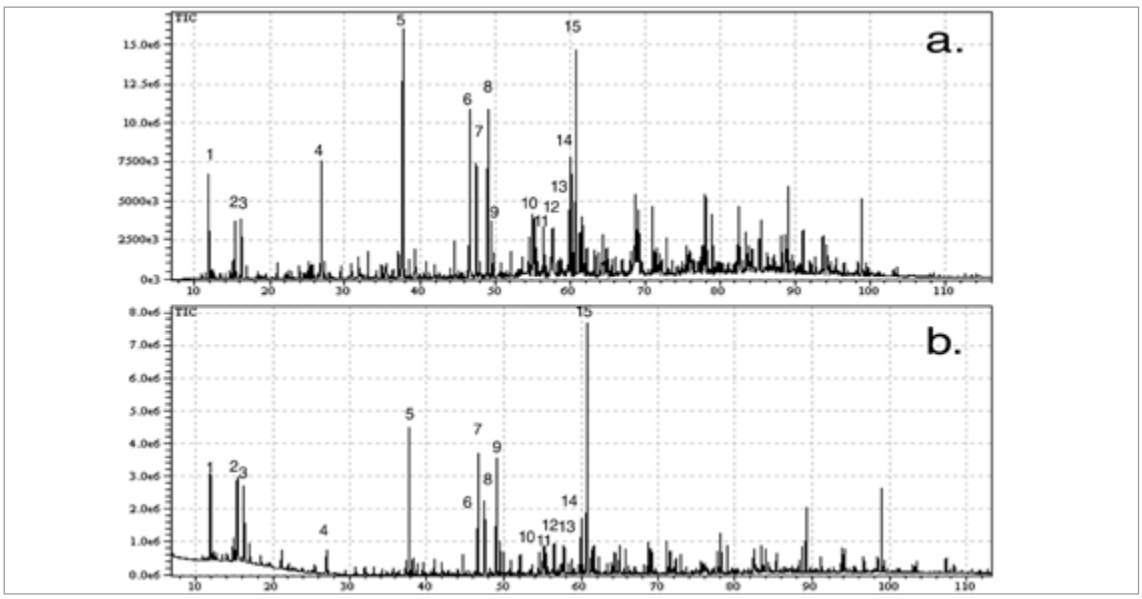

Figure 5.11. Total ion chromatography of samples: a. T10L; T11L The numbers in the chromatogram correspond to those reported in Table 5.8.

Working with set-up A aliphatic and single ring aromatic compounds were more abundant than PAH using *tire M* instead of *tire G*.

Working with set-up B the amount of aliphatic and aromatic compounds were higher for *tire G* than *M*; while the amount of PAH was reduced. Probably increasing the residence time, due to the fractionating system, prevented the formation or allowed the cracking of condensed ring structure. The latter hypothesis was supported by the increasing amount of char.

The most abundant aliphatic compounds were linear alkane and alkene from C4 to C19, 2-methyl-1,3-butadiene (isoprene), and limonene. A scheme showing the formation of limonene through radical pyrolysis of polyisoprene is reported in

Figure 1.20.

T11L and T15L, obtained with set-up B, using *tire G* and, respectively, the highest and lowest P/M^2 ratio, contained almost the same high amount of limonene due to initial tire composition and two opposite effects. The first one, for T11L, the pyrolysis with the highest P/M^2 ratio, promotes a fast cracking and a high volume of gas was produced, pushing the newly formed limonene outside the reactor. On the contrary, for T15L, the pyrolysis with the lowest P/M^2 ratio, caused a slow and less efficient cracking avoiding the pyrolysis of substances having a relatively low stability, like limonene.

Single ring aromatics were mainly benzene, toluene, xylenes, and trimethylbenzenes. Their amount was low in liquid obtained from *tire G* via set-up A, probably due to low amount or absence of styrene rubber in tire. In liquid obtained via set-up B the amount of aromatics was always increased because Diels-Alder condensations and dehydrogenation reactions might take place as suggested by Cunliffe et al.,[6] involving reactions reported in Figure 1.12.

In addition to single ring aromatic hydrocarbons, relevant amount of polyaromatic hydrocarbon were present such as 1H-indene, and naphthalene, anthracene, phenanthrene, and their mono- and poly-methyl substituted. Their formation might follow the steps reported in Figure 1.18.

Hetero-compounds contained sulfur, such as thiophene and its alkyl-derivatives, and they gave the typical strong smell of liquids. They might be formed by reaction between sulfur and radical intermediates. Also Williams and Bottrill found large amount of sulfur compounds in liquid from classical pyrolysis.[37] The most abundant hetero-aromatic was benzothiazole. Its derivatives are usually employed as additive in tire formulation,[38] but they were pyrolyzed and only benzothiazole was present in liquid. Further discussion on benzothiazole and hetero compounds is reported in Section 5.6.

As note before the use of set-up B, especially for *tire M*, minimized the influence of P/M^2 ratio. Similar amount of aromatics and non-aromatics were present in these liquid.

5.4.3. ^{1}H-NMR

The amount of different classes of organic products was also evaluated via ^{1}H-NMR. The nature of protons was assigned as follow: δ 8.0-6.6 (aromatic ring); 6.0-4.5 (C=CH olefins); 3.0-2.0 (Ar-CH), 2.0-1.5 (CH paraffins), 1.5-1.0 (CH_2 paraffins), and 1.0-0.6 (CH_3 paraffins) ppm (Figure 5.12). The amount of hydrocarbon types was calculated according to the Myer's formulas[39] and reported in Table 5.9.

Liquids obtained using set-up A from *tire M* showed lower amount of aromatics and olefins with respect to those obtained with set-up B due to a less efficient

cracking (T1L and T10L for instance). Enhancing the residence time olefins might react to form aromatic (Figure 1.12). *Tire G* showed the same amount of aromatics at fixed P/M^2 ratios independent by set-up used. Meanwhile the amount of paraffin was reduced and olefin was increased switching from set-up A to set-up B; paraffin compounds were pyrolyzed to form olefin but there was not a relevant transformation of olefin to aromatics. The low amount of olefin in T5L suggested the paraffinic nature of the polymer matrix which was first pyrolyzed to paraffin, while olefin were formed only if harsh conditions (high P/M^2 ratio) or long residence time (set-up B) was employed.

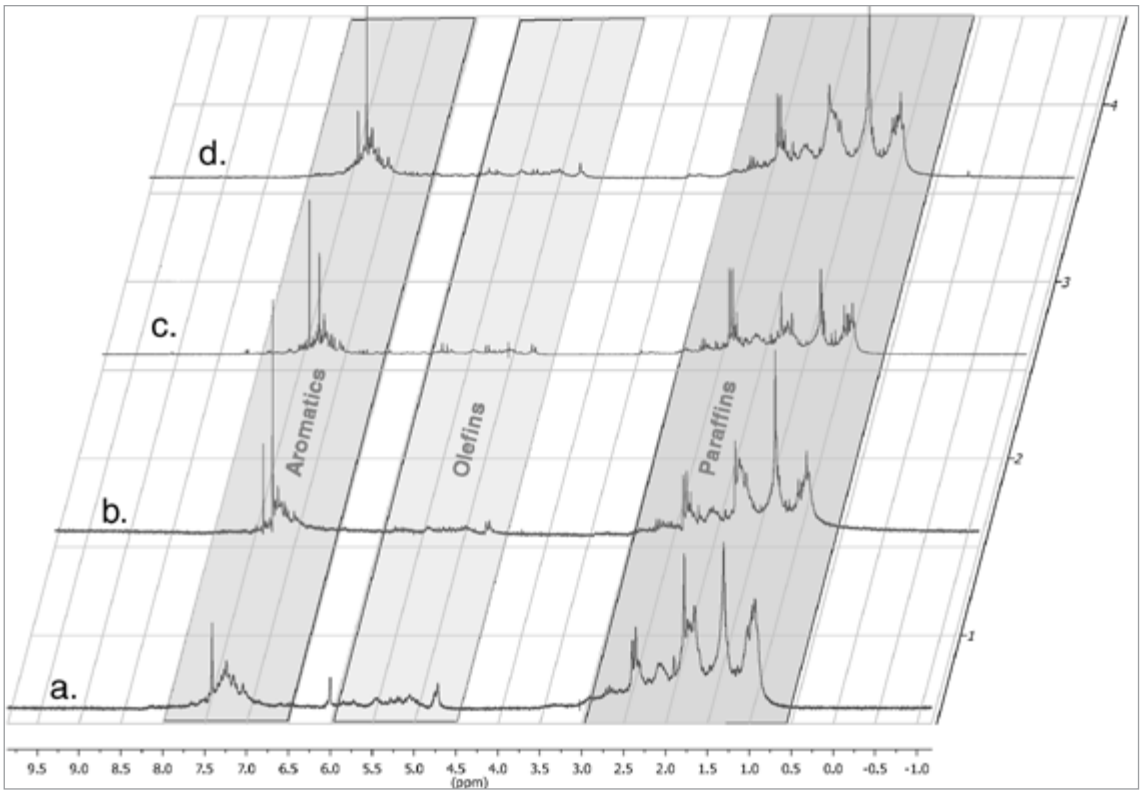

Figure 5.12. 1H-NMR spectra of samples: a. T4L; b. T5L; c. T10L; d. T11L. The range of aliphatic, olefinic and aromatic resonances are reported.

The high amount of paraffins was in agreement with the high LHV value of liquids, even if GC-MS analysis showed large amount of aromatic compounds up to 51.78 % for T13L. The contrast among NMR and GC-MS data is only apparent, since alkyl substituted aromatics are entirely attributed to aromatics, when GC analysis is employed, but splitted between aliphatic and aromatic groups, when NMR analysis is used.

No signals were found outside δ 8.0-0.6 ppm range, confirming the absence of carboxylic acid or aldehydic compounds. This evidence is in contrast with conventional wisdom on the analysis of liquid formed in the pyrolysis of tires reported in literature where oxygenated compounds were always found.[11, 40] Their absence was not surprising because our MAP was carried out in the absence of

oxygen, while in classical pyrolysis air was sometimes employed as combustive agent in the reactor.

Table 5.9. Abundance for each proton class in liquids from MAP of tires.

Entry	Set-up	Tire Brand	P/M² (10^3W/g²)	Aromatic (vol%)	Paraffin (vol%)	Olefin (vol%)
T1L	A	Tire M	137.6	24.0	35.1	40.9
T2L	A	Tire G	95.7	28.2	56.3	15.5
T3L	A	Tire M	106.0	22.3	37.7	40.0
T4L	A	Tire M	55.1	21.7	47.3	31.0
T5L	A	Tire G	47.7	25.8	66.7	7.6
T6L	A	Tire M	1.3	29.1	53.7	17.2
T7L	A	Tire M	11.9	16.9	74.9	8.1
T8L	A	Tire M	730	26.1	49.0	24.9
T9L	A	Tire M	23.6	20.0	39.8	40.3
T10L	B	Tire M	101.9	30.3	42.0	27.6
T11L	B	Tire G	93.8	27.1	48.1	24.8
T12L	B	Tire M	50.8	31.0	45.0	24.0
T13L	B	Tire G	47.9	24.8	46.6	28.6
T14L	B	Tire G	24	23.6	59.8	16.6
T15L	B	Tire G	12	21.1	53.5	25.3

5.4.4. Distillation curve

The amount of distillate collected below 473 K and the total distillable fraction together with the maximum distillation temperature are reported in Table 5.10.

Table 5.10. Distillation curve of liquids from MAP of tire.

Entry	Set-up	Tire Brand	P/M² (10^3W/g²)	Distilled below 473 K (%)	Distilled over 473 K (%)	T_{max} (K)	Total distilled (%)	Not Distilled (%)
T1L	A	Tire M	137.6	13.25	15.93	492	29.18	70.82
T2L	A	Tire G	95.7	25.82	25.12	582	50.94	49.06
T4L	A	Tire M	55.1	29.18	29.25	528	68.43	41.57
T5L	A	Tire G	47.7	27.70	27.65	583	55.43	44.57
T6L	A	Tire M	1.3	35.37	47.47	579	82.84	17.16
T7L	A	Tire M	11.9	35.48	25.24	595	60.72	39.28
T8L	A	Tire M	730	30.34	42.48	533	73.15	26.85
T9L	A	Tire M	23.6	74.61	-	473	74.61	25.39
T10L	B	Tire M	101.9	44.99	20.05	597	65.04	34.96
T11L	B	Tire G	93.8	32.77	44.34	595	77.11	22.89
T12L	B	Tire M	50.8	43.28	37.35	579	80.63	19.37
T13L	B	Tire G	47.9	65.51	25.73	548	91.24	8.76
T14L	B	Tire G	24	33.28	23.30	591	79.88	20.12
T15L	B	Tire G	12	64.40	19.04	543	83.44	16.56

A different distillation behavior was noticed for liquids from pyrolysis of different tire brands, but product distilled below 473 K, and total amount of distilled products was increased if the P/M^2 ratio decreased, and the set-up A was used.

As well as for other properties, when *tire M* was pyrolyzed with set-up B differences were reduced, the amount of distillable fraction below 473 K was almost the same, using different P/M^2 ratio (T10L, and T12L, Table 5.10), but higher than the one achieved with set-up A (T1L, and T4L). A sharp difference was noticed concerning the distillable fraction when the P/M^2 ratio was further reduced and more than 80% (T12L) of liquid was distilled instead of 65% (T10L). This behavior was attributed to a more efficient cracking and reduced transportation phenomena of pyrolyzed substances. This behavior was also observed for pyrolysis of *tire G*. The improvement of distillable fraction was higher when pyrolysis of *tire G* was run at low P/M^2. This fraction was higher in liquids from entries T13L than T12L (respectively 91.24 and 80.63 wt %) or T11L than T10L (respectively 77.11 and 65.04 wt %). However a further reduction of P/M^2 did not improve the amount of distillable fraction that remain in the range 79.9-91.2 %.

The residue contained oligomers formed in the course of the pyrolysis by coupling of radical intermediates as usually happen in the thermal cracking and as also reported by Kyari et al.[11] analyzing the liquid via size exclusion chromatography.

5.4.5. FTIR

IR analysis did not evidence any remarkable differences among liquids obtained by different pyrolysis: absorptions of alkane/alkyl, alkene and aryl groups were present (Table 5.11).

Table 5.11. IR absorptions of liquids from MAP of tires[a].

Frequency	Attribution	T1L	T2L	T3L	T4L	T5L	T6L	T7L	T8L	T9L	T10L	T11L	T12L	T13L	T14L	T15L
3104; 3060	Aromatic C-H stretching	w	w	w	w	w	w	w	w	w	w	w	w	w	w	w
3082; 3027	Terminal vinyl C-H stretching	w	w	w	w	w	w	w	w	w	w	w	w	w	w	w
3009	Internal alkene C-H stretching	n.d.	n.d.	n.d.	n.d.	n.d.	n.d.	n.d.	n.d.	n.d.	n.d.	n.d.	n.d.	n.d.	n.d.	n.d.
2961; 2870	Methyl C-H stretching	s	s	s	s	s	s	s	s	s	s	s	s	s	s	s
2920; 2860	Methylene C-H stretching	s	s	s	s	s	s	s	s	s	s	s	s	s	s	s
1691; 1752; 1804; 1877; 1944	Aromatic combination band	n.d.	n.d.	n.d.	n.d.	n.d.	n.d.	n.d.	n.d.	n.d.	n.d.	n.d.	n.d.	n.d.	n.d.	n.d.
1630	Alkenyl C=C stretching	w	w	w	w	w	w	w	w	w	w	w	w	w	w	w
1601; 1576; 1495; 1450	C=C-C aryl ring stretching	m	m	m	m	m	m	m	m	m	m	m	m	m	m	m
1452	HC-H bending	s	s	s	s	s	s	s	s	s	s	s	s	s	s	s
1202; 1083; 1028; 1020	Aromatic C-H in-plane bending	w	w	w	w	w	w	w	w	w	w	w	w	w	w	w
840: 774; 755; 748;	Aromatic C-H out-of-plane bending	m	m	m	m	m	m	m	m	w	w	m	w	m	m	m
729	-(CH_2)n- rocking	s	s	s	s	s	s	s	s	s	s	s	s	s	s	s

[a] Intensity reported as follow: s, strong; m, medium; w, weak; n.d. not detected

There were not relevant differences among spectra.The FT-IR spectra of some liquids, collected in ATR mode, are reported in Figure 5.13.

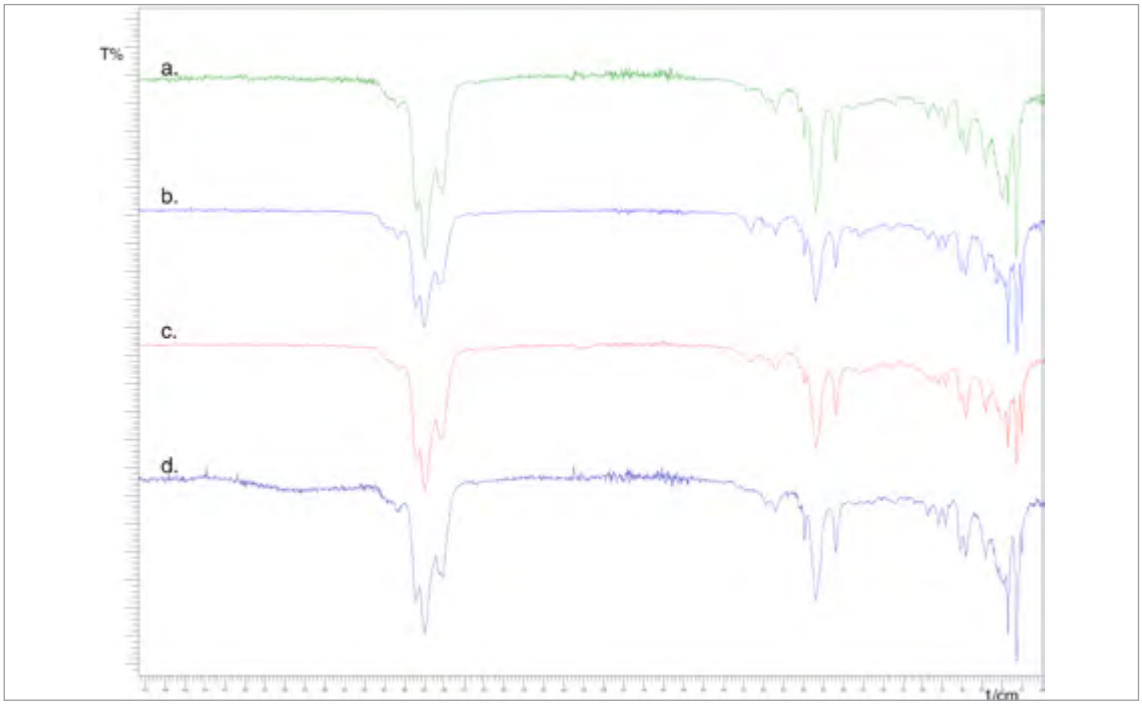

Figure 5.13. FT-IR spectra of liquids : a. T4L; b. T5L; c. T10L; d. T11L.

Peaks attributable to carbonyl or carboxyl groups, between 1725÷1700 cm^{-1}, were not distinguishable from background noise.

5.4.6. Main achievements

MAP of two different brands of tire was achieved obtaining liquids having physical and chemical properties very close to commercial fuels even if a hydrodesulfurization process is required. Reactions were run using different amounts of tire in a batch laboratory scale using different apparatus set-up. Pyrolysis were performed in an anoxic atmosphere without any carrier gas, avoiding mass transportation phenomena and increasing the residence time of the gas inside the oven. Furthermore the gas fraction was not diluted by the carrier. An on-line fractionating system (a packed column filled with glass spheres) was sometimes inserted between the oven and the condensing system (set-up B). Results, obtained using different apparatus set-up, were compared especially with regard to the liquid product. The use of a fractionating system increased the residence time of the high boiling substances avoiding their stripping from the reactor. A correlation between pyrolysis and liquid characteristics was obtained using the ratio between the microwave power (P) and square mass (M^2), the P/M^2 parameter. This ratio was used as descriptive parameter because it gave a bright and concise correlation among different experimental conditions and results of pyrolysis test.

Lowering the P/M^2 ratio, or more generally the microwave power, liquid showed a progressive reduction of viscosity, density, and calorific values together with an increasing amount of liquid distilled below 473 K. This behavior was independent on brand of tires employed. *Tire M* pyrolyzed with set-up A gave the highest liquid yield (42.6 wt%) using a P/M^2 ratio of 55×10^{-3} W/g^2. This liquid showed a low density (0.874 g/cm^3), viscosity (1.73 cPs), and the distillable fraction below 473 K was 30 wt%. *Tire G* gave the highest liquid yield (42.8 wt%) using a P/M^2 ratio of 96×10^{-3} W/g^2 with a density of 0.921 g/cm^3, viscosity of 3.92 cPs, and a distillable fraction below 473 K of 26 wt%.

Remarkable differences were evidenced when set-up B was employed, namely using a fractionating system inserted between the oven and the condensing system. A pale-yellow transparent liquid was obtained instead of a dark-brown opaque one, with lower density and viscosity, and containing a large amount of aromatics and olefins.

Pyrolysis of *tire M* with set-up B minimize any effect of P/M^2 ratio even if the liquid product was obtained with a lower yield 28 wt%, but having a density of 0.86 g/cm^3 viscosity of 1 cPs, and the distillable fraction below 473 K was 44 wt%. So far in these conditions liquids showed the same physical properties of that one obtained with set-up A, but in a shorter time.

Also pyrolysis of *tire G* using set-up B gave liquids with lower values of physical properties; even if the influence of different set-up is less evident for *tire G* than *tire M*, the density was reduced from 0.92 to 0.88 g/cm^3, and viscosity from 3.92 to 1.25 cPs. In the same time the distillable fraction was increased up to 91.2 % of the liquid collected.

The chemical composition of liquids were also affected by the use of different set-up and high amount of aromatics and olefins were present than in the liquid obtained with set-up A, even if lower changes were shown for *tire G*. The lower influence of different set-up was attributed to a different composition of tire. T*ire G* might have a prevailing aliphatic composition (polyisoprene moiety was higher than in *tire M*) which gave less stable radical intermediates during pyrolysis.

As a conclusion the set-up B gave a more efficient pyrolysis, giving a liquid product with more affordable properties very close to those of a commercial fuel even if a hydrodesulfurization treatment must be undergone, before its use.

5.5. Temperature detection problem

Temperature is a key parameter to describe almost any chemical reaction and pyrolysis experiment. However in a MW heated system the detection of temperature shows some hard challenges. Several devices are available for temperature detection in classical heated system, such as alcohol, mercury-in-glass, infrared thermometer, or thermocouple. Alcohol and mercury-in-glass thermometer cannot

be used in a MW pyrolysis system because their temperature limit is below the common operating temperature and mercury absorbs MW.

Thermocouple are made in metals. They are widely used to detect temperature in classical heating system. However in a MW system metal absorb MW and it is heated so they cannot be employed in any MW system.

Infrared thermometer does not have any temperature limitations but it provides the surface temperature. A schematic representation of temperature detection with an infrared thermometer is reported in Figure 5.14a. This thermometer gave the medium temperature of the oven reported in Figure 5.14a, furthermore the ability to measure only the surface temperature is a limitation of this thermometer. In a pyrolysis experiment, where a lot of vapors are produced, the temperature measured is that of vapor (Figure 5.14b). Furthermore in a MW system radiation is turned into heat inside the absorber which is usually covered by vapors during pyrolysis so the temperature measure by an infrared thermometer is that one of the gases present in the reactor.

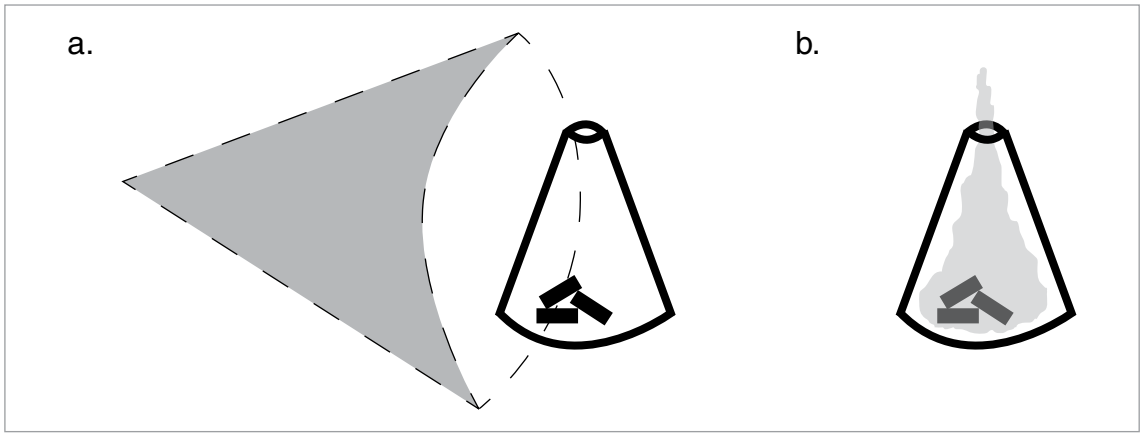

Figure 5.14. Infrared thermometer. a. cone of temperature detection; b. the vapor covered the feed and only the vapor temperature is detected.

Other systems are available on the market, where the metal is replaced with monolithic single-crystal which does not interact with MW: fiber optic thermometers. They can provide information on the working temperature , but also this thermometer shows some limitation because they detected the temperature of object in thigh contact with it.

In the reported MAP several efforts were devoted to understand the pyrolysis temperature.

The MW oven is equipped with an infrared thermometer, it provided the vapor temperature. As a matter of fact the temperature measured by the infrared thermometer was in agreement with the temperature of the gas flow measured at the exit of the oven. It was calibrated correlating the temperature of a silicon oil bath measured by the infrared and a mercury-in-glass thermometer. A linear relationship was obtained (R^2 = 0.9910, Equation 5.1):

$$T^{EXT} = \frac{(T^{IR} - 18.861)}{0.469} \quad \textbf{5.1}$$

Where T^{IR} was the temperature of the infrared thermometer and T^{EXT} the temperature extrapolated. The temperature of pyrolysis T6, T7, and T8 was detected also using a fiber optic thermometer. In Table 5.12 are summarized the temperature detected and extrapolated.

Table 5.12. Temperature detected and extrapolated in MAP.

Entry	Temperature detected (K)	Temperature extrapolated (K)
T1	573	872
T2	553	830
T3	546	814
T4	523	765
T5	503	723
T6	533	787
T7	513	745
T8	453	617
T9	523	765
T10	563	851
T11	563	851
T12	523	765
T13	533	787
T14	573	872
T15	483	681

Temperatures measured by the infrared thermometer (T^{IR}) and extrapolated (T^{EXT}) were different from those measured with the fiber optic thermometer because the heat of the sample, having a poor thermal conductivity, is not uniformly distributed. The heterogeneous distribution of the MW absorber results in a spot point temperature profile. An experiment (entry T8) was arranged with fiber optic thermometer in close contact with the tire chips to measure the temperature of the heated tire surface. Tire chips were piled around the fiber optic thermometer to avoid the problem of contact losing during the experiment especially when the tire chips collapsed; the tire chips remained in strict contact with the fiber optic thermometer and the temperature was correctly detected. It was higher (719 K) than the one extrapolated (617 K) because a lower amount of tire was used, a lower amount of gases was produced and rapidly distilled away and the overall measurable temperature by the infrared thermometer inside the oven was consequently lower.

Further consideration has been extrapolated from XRD analysis of char. Two crystalline forms of ZnS (sphalerite, β ZnS; wurtzite α ZnS) was found due to ZnO transformation during pyrolysis. Wurtzite phase is stable over 1273 K,

confirming that a high temperature was reached in MAP. When sphalerite is the sole or predominant phase a pyrolysis temperature between 700 and 1273 K was achieved because this is the range of stability of sphalerite. These values are higher than those measured and extrapolated using the previusly reported methods.

As a conclusion of temperature detection, our evidence shows that the MW radiation is transformed into heat inside the absorber and initially only the polymeric matrix in close contact with the surface of the absorber is heated to the pyrolysis temperature. As a consequence temperature is not a good parameter to characterize a MAP experiment.

5.6. Hydrodesulfurization

All liquid collected contained variable amount of sulfur, as evidenced in Section 5.4.1, which limited any further use.[41, 42] Furthermore the presence of unsaturated compounds reduced the stability of liquids if they were stored. These two problematic issues might be eliminated by a hydrodesulfurization process (HDS) which could reduce the amount of sulfur and hydrogenate the unsaturated bonds. Moreover an HDS process might reduce corrosive effects.

Typical HDS processes work with pressure of hydrogen in the range 68 – 138 atm and temperature around 570 – 710 K. The feed stream is mixed with hydrogen and heated before it is passed through the catalyst bed in the reactor. The outgoing gas/liquid mixture is separated and the hydrogen in the gas is purified and recycled. The H_2S separated from hydrogen is transformed in elemental sulfur through the Claus process.[43] The most employed are molybdenum/cobalt based catalysts because they are active to HDS but do not hydrogenate aromatic rings and they are not deactivated by sulfur compounds [43]

A commercial HDS catalyst was tested on reference compounds and on liquids obtained in MAP of tires to check sulfur removal and double bonds hydrogenation. It was a molybdenum/cobalt supported catalyst which was activated through reaction with dimethyldisulfide at room temperature for 24 h prior HDS experiments. Reactions were carried out in a stainless steel autoclave without stirring. The detailed experimental procedure can be found in "Appendix II: Analytical Methods".

Benzo[b]thiophene (BT) and benzothiazole (BTZ) were chosen as reference compounds and they were HDS using anhydrous toluene or the fraction distilled below 579 K of liquid T6L as solvent. In Table 5.13 are summarized the results.

BT is particularly challenging to hydrogenate[44-50] and for this reason was chosen as main referring compound. BTZ was present as main hetero-compound in liquids thus its hydrogenation was also investigated.

HDS is usually run in a continuous process while the tests were carried out in a batch process in toluene as solvent to allow the tuning of the reaction condition.

Low conversion of BT was achieved working at 553 K and 10 atm of H_2 (6%, HDS_01); however raising temperature of 30 K the reaction was about 5 time faster (HDS_02). HDS efficiency was improved also increasing the H_2 pressure from 10 to 50 atm (HDS_03); this latter pressure is closer to the one used in continuous processes and it was chosen for further investigation. 2,3-dihydrobenzo[b] thiophene and ethylbenzene were the products identified through GC-MS as expected from the data reported by Frediani et al.[44]

Table 5.13. HDS parameters and yields.

Entry	Sulfur compound	Solvent (10 mL)	Catalyst (wt %)[a]	T (K)	H_2 (Atm)	Time (h)	Sulfur compound conv (%)
HDS_01	BT	Toluene	10.4	553	10	4	6
HDS_02	BT	Toluene	9.0	583	10	4	33
HDS_03	BT	Toluene	12.2	553	50	4	88
HDS_04	BT	Toluene	10.5	553	50	2	43
HDS_05	BT	Toluene	12.6	553	50	1	19
HDS_06	BT	Toluene	20.6	553	50	1	41
HDS_07 (6 run)	BT	Toluene	20.4	553	50	2	mean 89
HDS_08	BT	T6L	23.6	553	50	4	8
HDS_09	BT	T6L	15.9	553	50	2	6
HDS_10	BT	T6L	11.6	553	50	24	11
HDS_11	BT	T6L	18.0	583	50	2	19
HDS_12	BT	T6L	13.1	583	50	24	>99
HDS_13 (6 run)	BT	T6L	58.5	583	50	4	mean 63
HDS_14 (6 run)	BTZ	Toluene	9.7	553	50	2	75
HDS_15	BTZ	Toluene	26.4	583	50	2	83
HDS_16	BTZ	T6L	31.1	583	50	2	80

[a] The catalyst Albemarle KF752 is a supported catalyst of unknown composition and the reported percentage was referred on the whole weight.

A linear conversion of BT as a function of time was shown (HDS_04, HDS_05, and HDS_07). Moreover the catalyst might be used for 6 run, using every time a fresh solution, without losing its activity (HDS_07).

Switching from toluene to T6L as solvent the conversion of BT dramatically dropped (HDS_08 – HDS_10) and the conversion never overcame 11 % even after 24 h. Increasing temperature (HDS_11) and the catalyst amount (HDS_12) the conversion increased as expected. Probably compounds present in T6L interacted with the catalyst reducing its activity.

The catalyst might be reused for 6 run with comparable results (HDS_12), but the conversion of BT did not overcome 63 %; a nonlinear correlation between time or catalyst amount with conversion was obtained. Indeed the catalyst was also active toward double bonds hydrogenation and low conversion of BT was achieved when working at 553 K. At this temperature alkenes had a very low reactivity but

a strong interaction with the catalyst and lower the overall hydrogenation (Figure 5.15).

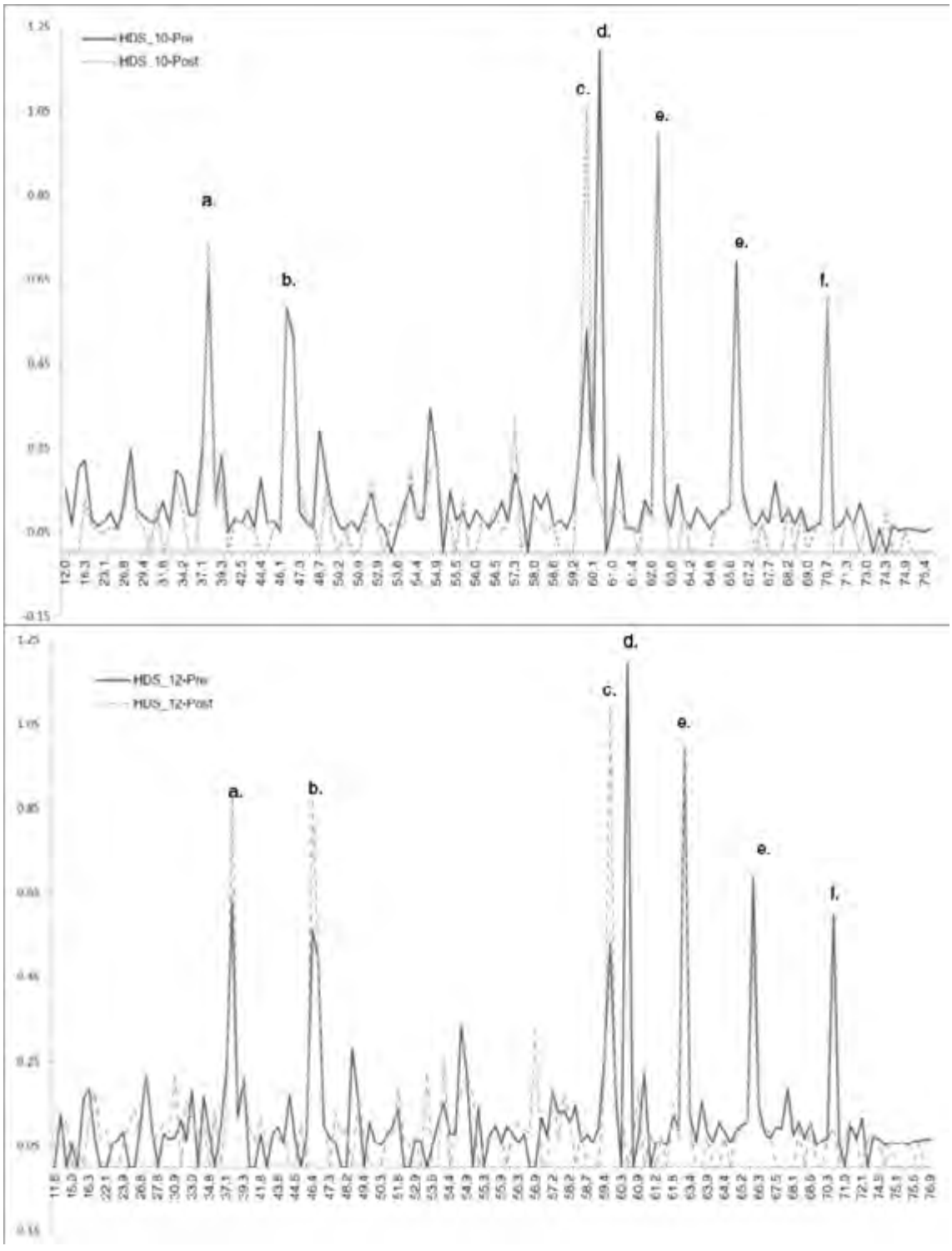

Figure 5.15. TIC of HDS 10 and HDS_12 before (dotted lines) and after (solid lines) normalized to internal standard. In both TIC: a. toluene; b: ethylbenzene; c. limonene; d. tetrahydrolimonene; e. internal standard; f. BT.

The evident reduction of the peak of limonene and the appearance of a new peak attribute to the tetrahydrolimonene is shown in Figure 5.15; while in TIC of HDS_10 there was not noticeable reduction of BT. Meanwhile in HDS_12, BT

disappeared and ethylbenzene was increased. All the reaction involved in the HDS process of liquid derived from tire pyrolysis mixed with BT are reported in Figure 5.16.

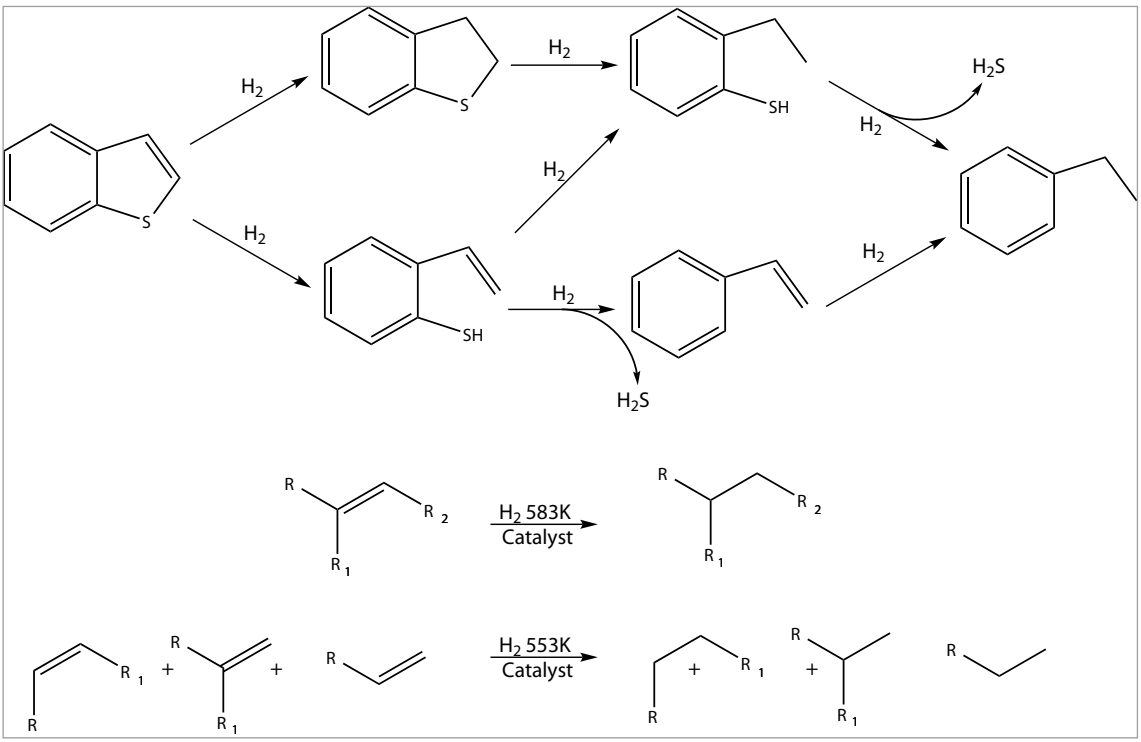

Figure 5.16. HDS of BT in liquid from MAP of tires.

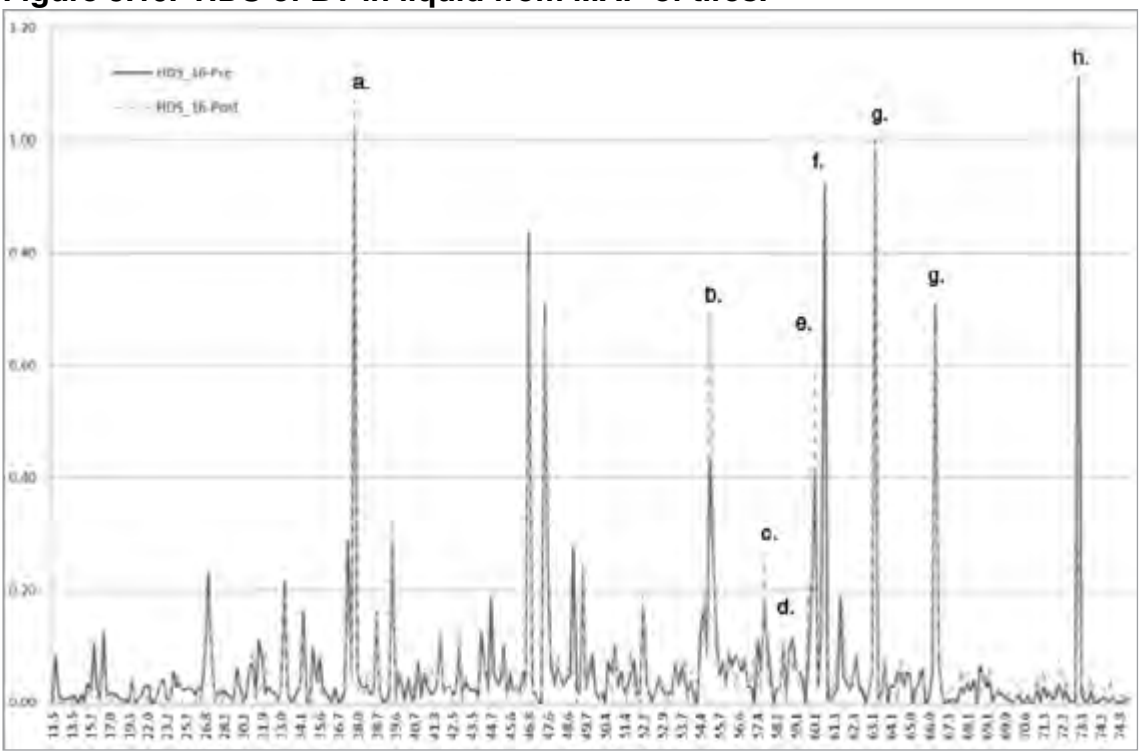

Figure 5.17. TIC of HDS_16 before (dotted lines) and after (solid lines) normalized to internal standard. In both TIC: a. toluene; b: aniline; c. N-methylaniline; d. N,N-dimethylaniline; e. limonene; f. tetrahydrolimonene; g. internal standard; h. BTZ.

BTZ was converted easily than BT and already at 553 K and 50 atm (HDS_14 and HDS_15) it is converted to: aniline, N-methylaniline, and N,N-dimethylaniline. A comparable conversion of BTZ was achieved also using T6L as solvent (HDS_16).

In Figure 5.17 is reported the TIC of HDS_16 before and after HDS.

The reduction of BTZ was evident but also the hydrogenation of some alkene moieties such as styrene and limonene.

Liquids obtained from MAP of tire can be efficiently treated with conventional and well-established technologies to reduce their sulfur and reactive double bonds.

Reference

1. Undri, A.; Sacchi, B.; Cantisani, E.; Toccafondi, N.; Rosi, L.; Frediani, M.; Frediani, P., Characterization of Carbon from Microwave Assisted Pyrolysis of Tires. *J. Anal. Appl. Pyrol.* **2013**, 104, 396-404.
2. Undri, A.; Rosi, L.; Frediani, M.; Frediani, P., Upgraded Fuel from Microwave Assisted Pyrolysis of Waste Tire. *Fuel* **2014**, 115, 600-608.
3. Undri, A.; Meini, S.; Rosi, L.; Frediani, M.; Frediani, P., Microwave Pyrolysis of Polymeric Materials: Waste Tires Treatment and Characterization of the Value-Added Products. *J. Anal. Appl. Pyrol.* **2013**, 103, 149-158.
4. Bykov, Y. V.; Rybakov, K. I.; Semenov, V. E., High-temperature microwave processing of materials. *J. Phys. D Appl. Phys.* **2001**, 34, R55.
5. Russell, A. D.; Antreou, E. I.; Lam, S. S.; Ludlow-Palafox, C.; Chase, H. A., Microwave-assisted pyrolysis of HDPE using an activated carbon bed. *RSC Advances* **2012**, 2, 6756-6760.
6. Cunliffe, A. M.; Williams, P. T., Composition of oils derived from the batch pyrolysis of tyres. *J. Anal. Appl. Pyrol.* **1998**, 44, 131-152.
7. Aguado, R.; Olazar, M.; José, M. J. S.; Gaisàn, B.; Bilbao, J., Wax Formation in the Pyrolysis of Polyolefins in a Conical Spouted Bed Reactor. *Energy Fuels* **2002**, 16, 1429-1437.
8. Kaminsky, W.; Mennerich, C.; Zhang, Z., Feedstock recycling of synthetic and natural rubber by pyrolysis in a fluidized bed. *J. Anal. Appl. Pyrol.* **2009**, 85, 334-337.
9. Parkash, S., Petroleum Fuels Manufacturing Handbook. The McGraw-Hill Companies, Inc.: **2010**; p 463.
10. Yatsun, A. V.; Konovalov, P. N.; Konovalov, N. P., Gaseous Products of Microwave Pyrolysis of Scrap Tires. *Solid Fuel Chem.* **2008**, 42, 187-191.
11. Kyari, M.; Cunliffe, A.; Williams, P. T., Characterization of Oils, Gases, and Char in Relation to the Pyrolysis of Different Brands of Scrap Automotive Tires. *Energy Fuels* **2005**, 19, 1165-1173.
12. López, F. A.; Centeno, T. A.; Alguacil, F. J.; Lobato, B.; Urien, A., The GRAUTHERMIC-Tyres process for the recycling of granulated scrap tyres. J. *Anal. Appl. Pyrol.* **2013**, 103, 207–215.
13. Piskorz, J.; Majerski, P.; Radlein, D.; Wik, T.; Scott, D. S., Recovery of Carbon Black from Scrap Rubber. *Energy Fuels* **1999**, 13, 544-551.
14. Chan, O. S.; Cheung, W. H.; McKay, G., Preparation and characterisation of demineralised tyre derived activated carbon. *Carbon* **2011**, 49, 4674-4687.
15. Teng, H.; Lin, Y.-C.; Hsu, L.-Y., Production of Activated Carbons from Pyrolysis of Waste Tires Impregnated with Potassium Hydroxide. *J. Air Waste Manag.* **2000**, 50, 1940-1946.
16. Lin, Y.-R.; Teng, H., Mesoporous carbons from waste tire char and their application in wastewater discoloration. *Microporous Mesoporous Mater.* **2002**, 54, 167–174.
17. Crelling, J. C.; Hagemann, H. W.; Sauter, D. H.; Ramani, R. V.; Vogt, W.; Leininger, D.; Krzack, S.; Meyer, B.; Orywal, F.; Reimert, R.; Bonn, B.; Bertmann, U.; Klose, W.; Dach, G., Coal. In Ullmann's Encyclopedia of Industrial Chemistry, Wiley-VCH Verlag GmbH & Co. KGaA: 2000.
18. Murillo, R.; Aylón, E.; Navarro, M. V.; Callén, M. S.; Aranda, A.; Mastral, A. M., The application of thermal processes to valorise waste tyre. *Fuel Process. Technol.* **2006**, 87, 143-147.

19. Juma, M.; Korenová, Z.; Markoš, J.; Annus, J.; Jelemenský, L., Pyrolysis and combustion of scrap tire. *Petroleum & Coal* **2006**, 48, 15-26.
20. R., H.; Popovic, N.; Ikura, M.; Stanciulescu, M.; Liu, D., Characterization and potential applications of pyrolytic char from ablative pyrolysis of used tires. *J. Anal. Appl. Pyrol.* **2001**, 58-59, 813-824.
21. Zabaniotou, A. A.; Stavropoulos, G., Pyrolysis of used automobile tires and residual char utilization. *J. Anal. Appl. Pyrol.* **2003**, 70, 711-722.
22. Rodriguez, I. d. M.; Laresgoiti, M. F.; Cabrero, M. A.; Torres, A.; Chomòn, M. J.; Caballero, B., Pyrolysis of scrap tyres. *Fuel Process. Technol.* **2001**, 72, 9-22.
23. Aylòn, E.; Fernàndez-Colino, A.; Navarro, M. V.; Murillo, R.; Garcìa, T.; Mastral, A. M., Waste Tire Pyrolysis: Comparison between Fixed Bed Reactor and Moving Bed Reactor. *Ind. Eng. Chem. Res.* **2008**, 47, 4029-4033.
24. Kaminsky, W.; Mennerich, C., Pyrolysis of synthetic tire rubber in a fluidised-bed reactor to yield 1,3-butadiene, styrene and carbon black. *J. Anal. Appl. Pyrol.* **2001**, 58-59, 803-811.
25. Chen, G.; Wu, D.; Weng, W.; Wu, C., Exfoliation of graphite flake and its nanocomposites. *Carbon* **2003**, 41, 579-581.
26. Vohler, O.; Nutsch, G.; Collin, G.; von Sturm, F.; Wege, E.; Frohs, W.; Henning, K.-D.; von Kienle, H.; Voll, M.; Kleinschmit, P.; Vostrowsky, O.; Hirsch, A., Carbon. In Ullmann's Encyclopedia of Industrial Chemistry, Wiley-VCH Verlag GmbH & Co. KGaA: 2000.
27. López, F. A.; Centeno, T. A.; Alguacil, F. J.; Lobato, B.; López-Delgado, A.; Fermoso, J., Gasification of the char derived from distillation of granulated scrap tyres. *Waste Manage.* **2012**, 32, 743-752.
28. Ucar, S.; Karagoz, S.; Ozkan, A. R.; Yanik, J., Evaluation of two different scrap tires as hydrocarbon source by pyrolysis. *Fuel* **2005**, 84, 1884–1892.
29. Napoli, A.; Soudais, Y.; Lecomte, D.; Castillo, S., Scap Tyre pyrolysis: Are the effluents valuable products? *J. Anal. Appl. Pyrol.* **1997**, 40-41, 373-382.
30. Sahouli, B.; Blacher, S.; Brouers, F.; Sobry, R.; Van den Bossche, G.; Diez, D.; Darmstadt, H.; Roy, C.; Kaliaguine, S., Surface morphology of commercial carbon blacks and carbon blacks from pyrolysis of used tyres by small-angle X-ray scattering. *Carbon* **1996**, 34, 633-637.
31. The International Centre for Diffraction Data. http://www.icdd.com/ (Accessed: 15.03.2013),
32. Darmstadt, H.; Roy, C.; Kaliaguine, S., Characterization of pyrolytic carbon blacks from commercial tire pyrolysis plants. *Carbon* **1995**, 33, 1449-1455.
33. Darmstadt, H.; Roy, C.; Kaliaguine, S., ESCA characterization of commercial carbon blacks and of carbon blacks from vacuum pyrolysis of used tires. *Carbon* **1994**, 32, 1399-1406.
34. Horikoshi, S.; Matsubara, A.; Takayama, S.; Sato, M.; Sakai, F.; Kajitani, M.; Abe, M.; Serpone, N., Characterization of microwave effects on metal-oxide materials: Zinc oxide and titanium dioxide. *Appl. Catal., B* **2009**, 91, 362-367.
35. Lam, S. S.; Chase, H. A., A Review on Waste to Energy Processes Using Microwave Pyrolysis. *Energies* **2012**, 5, 4209-4232.
36. Menéndez, J. A.; Arenillas, A.; Fidalgo, B.; Fernández, Y.; Zubizarreta, L.; Calvo, E. G.; Bermúdez, J. M., Microwave heating processes involving carbon materials. *Fuel Process. Technol.* **2010**, 91, 1-8.
37. Williams, P. T.; Bottrill, R. P., Sulfur-polycyclic aromatic hydrocarbons in tyre pyrolysis oil. *Fuel* **1995**, 74, 736-742.
38. Mark, J. E.; Erman, B.; Eirich, F. R., Science and Technology of Rubber. 3

ed.; Elsevier Academic Press: Burlington, 2005.
39. Myers, M. E.; Stollstelmer, J.; Wims, A. M., Determination of Hydrocarbon-Type Distribution' and Hydrogen/Carbon Ratio of Gasolines by Nuclear Magnetic Resonance Spectrometry. *Anal. Chem.* **1975**, 47, 2010-2015.
40. Laresgoiti, M. F.; Caballero, B. M.; de Marco, I.; Torres, A.; Cabrero, M. A.; Chomón, M. J., Characterization of the liquid products obtained in tyre pyrolysis. *J. Anal. Appl. Pyrol.* **2004**, 71, 917-934.
41. Quek, A.; Balasubramanian, R., Liquefaction of waste tires by pyrolysis for oil and chemicals—A review. *J. Anal. Appl. Pyrol.* **2013**, 101, 1-16.
42. Frigo, S.; Seggiani, M.; Puccini, M.; Vitolo, S. Liquid fuel production from waste tyre pyrolysis and its utilisation in a Diesel engine. *Fuel* **2014**, 116, 399-408
43. Speight, J. G., The Chemistry and Technology of Petroleum. CRC Press: Laramie, Wyoming, 2006.
44. Frediani, P.; Salvini, A.; Finocchiaro, S., Ruthenium carbonyls as benzo[b] thiophene hydrodesulfurization catalysts in homogeneous phase. *J. Organomet. Chem.* **1999**, 584, 265-273.
45. Bianchini, C.; Casares, J. A.; Meli, A.; Sernau, V.; Vizza, F.; Sànchez-Delgado, R. A., Efficient rhodium catalysts for the hydrogenolysis of thiophenic molecules in homogeneous phase. *Polyhedron* **1997**, 16, 3099-3114.
46. Vanrysselberghe, V.; Froment, G. F., Hydrodesulfurization of Dibenzothiophene on a $CoMo/Al_2O_3$ Catalyst: Reaction Network and Kinetics. *Ind. Eng. Chem. Res.* **1996**, 35, 3311-3318.
47. Sánchez-Delgado, R. A., Breaking C---S bonds with transition metal complexes. A review of molecular approaches to the study of the mechanisms of the hydrodesulfurization reaction. *J. Mol. Catal.* **1994**, 86, 287-297.
48. Froment, G. F.; Depauw, G. A.; Vanrysselberghe, V., Kinetic Modeling and Reactor Simulation in Hydrodesulfurization of Oil Fractions. *Ind. Eng. Chem. Res.* **1994**, 33, 2975-2988.
49. Bianchini, C.; Meli, A.; Vizza, F., Role of single-site catalysts in the hydrogenation of thiophenes: from models systems to effective HDS catalysts. *J. Organomet. Chem.* **2004**, 689, 4277-4290.
50. Chehata, A.; Oviedo, A.; Arévalo, A.; Bernès, S.; Garcìa, J. J., Reactivity of $[Ru_3(CO)_{12}]$ with Dibenzothiophene, Methylbenzothiophene, and Methyldibenzothiophene. *Organometallics* **2003**, 22, 1585-1587.

6. Microwave Assisted Pyrolysis of Waste Polymers

Most of the polymers are not able to convert microwave (MW) radiation into heat so the addition of a MW absorber was mandatory to perform MAP. Synthetic polymers (HDPE, PP, and PS) were pyrolyzed using binary mixture of chopped polymers and a MW absorber.

MAP of HDPE, PP, and PS were investigated by evaluating three parameters: MW power, microwave absorber, and apparatus set-up. Chips of polymer were mechanically mixed with the absorber (Figure 6.1a), and then introduced into the oven. Initially polymers were heated and melted by the MW absorber, then they incorporated the absorber (Figure 6.1b) and pyrolysis took place (Figure 6.1c).

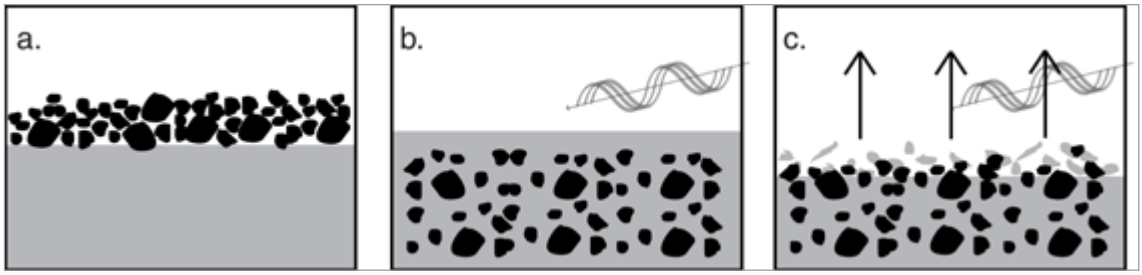

Figure 6.1. Degradation of polyolefins during MW irradiation: a. polyolefin and MW absorber; b. Melted polymer swallowed the MW absorber; c. pyrolysis take place.

Tire, char from MAP of tire, and iron power were chosen as MW absorbers. The solid obtained from MAP of polymers comprised mainly or exclusively the MW absorber and its characterization is not reported. Furthermore no particular modification was highlighted on absorber from preliminary studies.

6.1. Polyethylene

MAP of HDPE was investigated with the aim to obtain liquid with tunable properties from a wax to a low viscosity liquid. The results reported herein were already partially published.[1]

6.1.1. Operating conditions and yields

the operating parameters employed (entries are named “PEn” where “n” is an arbitrary ascending order for each experiment) are reported in Table 6.1.

Table 6.1. MAP of HDPE, operating parameters.

Entry	Set-up	MW Absorber	Power *(kW)*[a]	Polymer *(g)*	MW Absorber *(g)*	Time *(min)*	Solid *(wt%)*	Liquid *(wt%)*	Gas *(wt%)*
T4	A	Tire M	3	-	233.3	35	43.2	42.6	14.1
PE1	A	Tire M	1.8(13); 2.7(4); 3.0(16)	144.6	302.7	33	31.3	47.9	20.7
PE2	A	Tire M	1.2(55); 1.5(125); 2.7(65); 3.0(10); 6.0(5)	106.7	255.3	260	30.1	49.7 [b]	20.2
PE3	A	Carbon	3.0(61); 6.0(14)	150.5	70.2	75	0.4	83.9	15.7
PE4	A	Fe	3.0	139.3	59.9	136	10.6	81.8	7.6
T12	B	Tire M	3.0	-	243.0	36	46.6	27.6	25.8
PE5	B	Tire M	1.8(13); 3(47); 6.0(60)	139.5	285.0	120	33.2	43.9 [c]	22.9
PE6	B	Carbon	3.0(27); 6.0(73)	115.6	60.0	100	0.6	80.2	19.2
PE7	B	Fe	3	133.3	64.1	142	5.9	71.9	22.2

a) within brackets the time for which each MW power was employed. b) two liquid fractions were collected, the first working between 1.2-2.7 kW (yield 12.7 wt%) and the second between 2.7-6.0 kW (yield 37.0 wt%); c) two liquid fractions were collected, the first working between 1.8-3.0 kW (yield 17.8 wt%) and the second between 3.0-6.0 kW (yield 26.1 wt%).

MAP of tire alone (entries T4 and T12) were reported as referring pyrolysis to help results interpretation when tire was used as MW absorber. Indeed products

from MAP of tire were mixed with those from HDPE.

MAP of HDPE in the presence of tire as MW absorber (PE1, and the second fraction of entry PE2_II, Table 6.1) gave a waxy product (from HDPE pyrolysis), mixed with the liquid formed from tire pyrolysis, when a high MW power was used. These waxy products were solid at room temperature. Using carbon as MW absorber, liquid solidified already in cooling systems and in order to collect it the temperature of the cooling system was set at 300 K (PE3, Table 6.1).

Working with a low MW power (among 1.2-2.7 kW, the first fraction of entry PE2, Table 6.1) a more efficient degradation of HDPE to low molecular weight compounds was obtained, and a semi-fluid liquid was collected (yield 12.7 wt%). However at this level of MW power pyrolysis could not be completed and a fully degradation of HDPE was only achieved by increasing MW power up to 6 kW (yield of liquid 37.0 wt%, PE2L_II). Anyway this latter fraction was a wax/liquid mixture with an appearance close to that one of entry PE1 as already outlined.

On the contrary set-up B allowed obtaining always a low viscosity liquid, fluid at room temperature, in a short time using a high MW power in the presence of carbon as MW absorber. This set-up allowed only distilling low boiling compounds as outlined in Chapter 5. The heavy fraction, carried away by the gas and vapors formed, was separated in the fractionating system and sent back to the oven as expected (Entries PE5 – PE7, Table 6.1). Higher amount of gas was formed, together with a low viscosity liquid, due to the increased efficiency of the pyrolysis.

A completely different behavior was observed when iron was the absorber and a low viscosity liquid was always collected even if the MW power was kept at 3.0 kW for the entire pyrolysis (entry PE4). Iron showed an efficient interaction with MW and it was heated in shorter time than tire and carbon. This effect led to a fast pyrolysis of HDPE and short residence time. First of all working with set-up A, a comparable yield in liquid was observed between entries PE4 and PE3 but for PE4 a lower gas yield was formed. Higher solid yield was observed in entry PE4 than PE3 because cocking phenomena were improved. Working with set-up B the cocking phenomenon was less effective but the gas formation was improved as expected (entry PE7, Table 6.1).

The solid in MAP of HDPE in the presence of tire was accountable only to tire residue, as confirmed by pyrolysis in the presence of carbon as MW absorber (entries PE3 and PE6). The residue was 0.4 and 0.6 wt% respectively because cocking, or formation of carbon structure from HDPE, was negligible. So far if tire was the MW absorber the solid collected was attributable only to not-pyrolyzable products present in tire.

Finally the MAP of HDPE in the presence of tire as MW absorber suggested the possibility to perform MAP of any inorganic and/or organic pollutant containing HDPE. In fact tire or carbon, other than MW absorber, could be seen as an

inorganic/polymeric pollutant mixed with waste HDPE which did not affect the pyrolyses.

6.1.2. Liquid product

6.1.2.1. Physical properties

Physical properties of liquids, coded as "PEnL" where "n" is an arbitrary ascending number for each experiment were strongly affected by reaction conditions (Table 6.2).

Table 6.2. Characteristic of liquid obtained by MAP of HDPE.

Entry	Density	Viscosity	HHV	LHV	Ultimate analyses				C/H molar ratio
					C	H	N	S	
	(g/cm³)	*(cP)*	*(MJ/kg)*	*(MJ/kg)*	*(wt%)*	*(wt%)*	*(wt%)*	*(wt%)*	
T4L	0.874	1.73	44±4	42±4	86.87	10.12	0.66	0.9	0.72
PE1L	n.d.	n.d.	42±4	40±4	83.01	12.86	1.03	0.8	0.54
PE2L_I	0.780	0.57	39±4	36±4	85.31	12.81	1.21	0.7	0.55
PE2L_II	n.d.	n.d.	43±4	41±4	86.05	7.06	2.11	0.5	1.02
PE3L	n.d.	n.d.	47±5	44±4	84.82	14.66	0.49	0.03	0.48
PE4L	0.777	n.d.	41±4	38±4	85.51	14.36	0.00	0.0	0.50
T12L	0.858	1.00	42±4	40±4	87.14	9.33	0.33	0.8	0.78
PE5L_I	0.763	0.49	41±4	39±4	83.53	12.32	1.00	0.4	0.57
PE5L_II	0.910	1.31	45±4	42±4	85.89	11.94	0.97	0.3	0.60
PE6L	0.762	1.04	48±5	44±4	84.58	15.37	0.00	0.0	0.46
PE7L	0.784	n.d.	42±4	39±4	84.83	14.53	0.00	0.0	0.49

PE1L, PE2L_II, and PE3L were waxy liquids, solid at room temperature; therefore density and viscosity were not evaluated. Using low MW power the residence time of the polymer in the oven was increased because volatiles were slower produced and the residence time was increased (no gas flow employed), thus polymers degradation was considerably improved. As a result of this experimental condition PE5L_I showed the lowest density and viscosity among every experiment because it was collected in the first step of the process, when very low MW power and set-up B were employed. Anyway this fraction was only 1/3 of the liquid collected. On the contrary PE5L_II had a higher viscosity and density, even if it was partially diluted with the liquid from MAP of tire. However it must be considered that the viscosity was only 1.31 cP while PE2L_II and PE3L were solid at room temperature.

The C/H molar ratios of all liquids from MAP of HDPE were close and as expected these values were lower than liquid from MAP of tire alone, confirming a predominant aliphatic composition of these liquids.

All liquids showed very high calorific values and together with their extremely

low heteroatoms content were suited for direct energy production or source of chemicals.

6.1.2.2. GC/MS

All liquids contained a large number of compounds especially when tire pyrolysis products were present. In Table 6.3 are listed only the most representative compounds identified only from MAP of HDPE. Abundances were evaluated by the TIC without any response factor correction. In Figure 6.2 and Figure 6.3are reported TICs of PE2L_II and PE6L for visual comparative purposes.

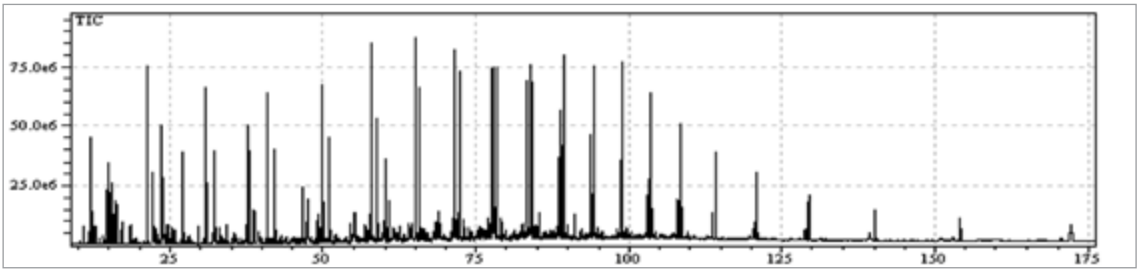

Figure 6.2. TIC of samples obtained from MAP of HDPE with set-up A: PE2L_II.

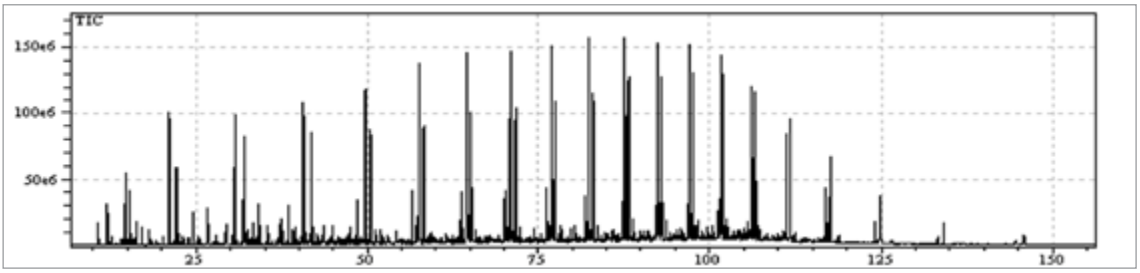

Figure 6.3. TIC of samples obtained from MAP of HDPE with set-up B: PE6L.

MAP of HDPE gave mainly aliphatic hydrocarbons through the reaction schemes reported in Figure 1.12a,b. Low amount of aromatic were present and they might be formed through an aromatization process during the cracking of HDPE followed by a radical rearrangement (Figure 1.12b) or a Diels Alder condensation (Figure 1.12d).[2] Large amount of aromatics were formed through pyrolysis of tire due to polyisoprene cracking (Figure 1.19), or decomposition of other polymers containing an aromatic moiety and present in tire (for instance styrene rubber, Figure 1.14).

As a witness of this assumption PE4L, PE6L, and PE7L (obtained using Fe or carbon as MW absorber) showed a low presence of aromatics, while T4L and T12L, where only tire was pyrolyzed, showed the highest amount of aromatics.

Table 6.3. Compounds in liquids from MAP of HDPE.

Furthermore collecting the liquid in two fractions, higher amount of aromatics were present in the first fraction collected when low MW power was used (PE1L_I

and PE5L_I). These fractions were richer in aromatics than PE1L_II and PE5L_II respectively. The aromatic compounds were the same

		Entry		**T4L**	**PE2L_I**	**PE2L_II**	**PE4L**	**T12S**	**PE5L_I**	**PE5L_II**	**PE6L**	**PE7L**
		Set-up		A	A	A	A	B	B	B	B	B
		Absorber		-	Tire M	Tire M	Fe	-	Tire M	Tire M	Carbon	Fe
n°	Time	Substance	a.c.									
1	12.0	2-butene-trans	C	1.5	1.2	0.8	0.3	1.1	1.7	0.6	0.3	0.2
2	12.2	butane	C	0.2	0.3	0.2	0.2	0.0	0.4	0.1	0.2	0.2
3	12.6	1-butene	C	0.2	0.1	0.1	0.1	0.1	0.2	0.1	0.1	0.0
4	14.8	1-pentene	C	0.3	0.7	0.6	0.5	0.1	0.9	0.8	0.5	0.5
5	15.0	2-pentene-trans	C	0.6	0.5	0.1	0.0	0.3	0.4		0.0	0.0
6	15.3	pentane	C	0.3	0.7	0.4	0.4	0.1	0.9	0.3	0.4	0.4
7	15.5	2-methyl-1,3-butadiene	C	1.7	1.0	0.2	0.0	0.6	1.4	0.1	0.1	0.0
8	15.6	2-pentene-cis	C	0.2	0.3	0.2	0.1	0.2	0.3	0.2	0.1	0.0
9	16.3	3-methyl-1-hexene	C	1.6	1.2	0.3	0.0	0.7	1.5	0.1	0.1	0.0
10	16.4	1.4-pentadiene	P	0.2	0.2	0.2	0.1	0.2	0.3	0.2	0.2	0.1
11	17.1	cyclopentadiene	P	0.3	0.2	0.2	0.1	0.3	0.3	0.3	0.1	0.1
12	21.2	1-hexene	C	0.4	1.9	1.6	1.5	0.2	3.2	2.7	1.4	1.6
13	22.1	hexane	C	0.0	1.0	0.6	0.7	0.1	1.2	0.5	0.6	0.5
14	22.5	2-hexene	P	0.1	0.0	0.2	0.1	0.0	0.0	0.1	0.1	0.0
15	24.7	methylcyclopentane	P	0.2	0.3	0.2	0.3		0.4	0.1	0.2	0.2
16	26.9	3-methylcyclopentene	P	0.6	0.7	0.3	0.2	0.1	0.6	0.2	0.4	0.1
17	27.0	benzene	C	1.8	1.6	0.9	0.1	0.8	1.1	1.3	0.1	0.1
18	29.5	cyclohexene	P	0.3	0.4	0.2	0.1	0.1	0.3	0.2	0.2	0.1
19	30.9	1-heptene	C	0.3	1.7	1.5	1.4	0.1	2.7	2.2	1.5	1.4
20	32.1	heptane	C	0.3	1.4	0.8	1.1	0.1	1.9	0.7	1.1	1.0
21	32.5	2-heptene	P	0.1	0.2	0.1	0.1	0.0	0.2	0.1	0.1	0.1
22	34.2	methylcyclohexane	P		0.2	0.1	0.3		0.1	0.1	0.3	0.2

(continue)

23	35.4	ethylcyclopentane	P	0.1	0.9	0.1	0.1	0.0	0.2		0.1	0.1
24	35.6	1-methyl-1,3-cycloesadiene	P	0.6	0.7	0.2	0.1	0.2	0.6		0.2	0.1
25	35.9	1-methyl-1,4-cycloesadiene	P	0.1	0.2	0.1	0.1	0.0	0.2		0.1	0.0
26	37.3	2-methyl-2,4-hexediene	P	0.7	1.1	0.2	0.0	0.4	0.7		0.2	0.1
27	37.5	1-ethylcyclopentene	P	0.2	0.3	0.1	0.1	0.1	0.2		0.2	0.1
28	37.8	toluene	C	3.0	2.4	1.2	0.1	4.1	3.5	1.5	0.1	0.2
29	40.6	2-methyl-1-heptene	P	0.1	0.2	0.1	0.0	0.0	0.2		0.0	0.0
30	41.0	1-octene	C	0.2	1.6	1.2	1.4	0.2	2.4	2.1	1.5	1.4
31	41.3	1-methyl-2-ehtylcyclopentane	P	0.1	0.2	0.1	0.1	0.1	0.2		0.1	0.1
32	42.0	octane	C	0.2	1.4	0.8	1.1	0.2	2.1	0.8	1.1	1.0
33	42.3	2-octene	P	0.1	0.1	0.1	0.1	0.0	0.3		0.1	0.1
34	43.1	3-octene	P	0.0	0.1	0.1	0.1		0.2		0.1	0.0
35	43.6	3-propylcyclopentene	P	0.1	0.1	0.1	0.1	0.0	0.2		0.1	0.1
36	45.3	1,2-dimethylcyclohexene	P	0.3	0.4	0.1	0.1	0.1	0.3		0.0	0.1
37	47.5	1,4-dimethylbenzene	C	2.4	2.0	0.4	0.1	2.4	2.8		0.0	0.0
38	48.0	1-ethylcyclohexene	P	0.3	0.1	0.1	0.1	0.0	0.3		0.1	0.1
39	48.9	1,3-nonadiene	P		0.1	0.4	0.4				0.4	0.3
40	50.0	1-nonene	C	0.4	1.9	1.3	1.6	0.5	3.0	2.3	1.8	1.7
41	50.9	nonane	C	0.2	1.4	0.9	1.0	0.2	2.2	1.1	1.1	1.0
42	51.1	2-nonene	P	0.1	0.2	0.1	0.1	0.1	0.2	0.1	0.1	0.1
43	53.4	butylcyclohexane	P	0.2	0.1	0.1	0.1		0.2		0.1	0.1
44	56.9	1,3-decadiene	P		0.2	0.2	0.4		0.6	0.2	0.4	0.3
45	58.0	1-decene	C	0.1	2.0	1.7	2.4	0.3	4.2	3.4	2.4	2.7
46	58.8	decane	C	0.3	1.4	1.0	1.1	0.3	2.0	1.6	1.2	1.2
47	58.9	2-decene	P	0.2	0.5	0.2	0.1		0.5	0.2	0.2	0.1
48	64.3	1,3-undecadiene	U		0.2	0.1	0.4		0.6	0.1	0.5	0.4

(continue)

49	65.1	1-undecene	C	0.2	1.1	1.8	2.4	0.4	1.9	4.1	2.4	2.6
50	65.8	undecane	C	0.2	1.2	1.5	1.4	0.4	1.5	2.7	1.4	1.5
51	66.6	2-undecene	P	0.1	0.2	0.2	0.1		0.2	0.1	0.1	0.1
52	68.5	pentylcyclohexane	P		0.1		0.1		0.2	0.3	0.1	0.1
53	68.6	pentylcyclopentane	P		0.0	0.2	0.0		0.2	0.2	0.1	0.0
54	71.0	1,3-dodecadiene	P		0.1	0.3	0.4		0.1	0.1	0.4	0.4
55	71.7	1-dodecene	C	0.2	0.5	1.6	2.1		0.9	4.4	2.3	2.4
56	71.8	3-dodecene	P		0.1	0.3	0.1		0.1	0.2	0.2	0.1
57	72.3	dodecano	C	0.2	0.7	1.7	1.7	0.3	0.8	3.6	1.7	1.6
58	73.1	2-dodecene	P	0.0	0.0	0.1	0.1				0.1	0.1
59	77.0	1,3-tridecadiene	P		0.1	0.1	0.4			0.5	0.5	0.5
60	77.7	1-tridecene	C	0.2	0.3	1.4	2.2	0.4	0.4	4.6	2.2	2.5
61	78.3	tridecane	C	0.2	0.6	1.7	1.8	0.4	0.3	4.3	1.7	1.7
62	79.1	2-tridecene	P		0.0	0.4	0.1				0.2	0.1
63	82.4	1-tetradecene	C	0.4	0.1	1.3	2.5	0.4	0.1	4.8	2.4	2.9
64	82.9	1,3-tetradecadiene	P			0.1	0.5			0.2	0.3	0.5
65	83.4	tetradecane	C	0.4	0.2	1.7	1.5	0.5	0.1	4.9	1.8	1.8
66	84.1	2-tetradecene	P			0.1	0.1			0.1	0.2	0.1
67	86.9	3-tetradecene	U			0.1	0.1			0.1	0.1	0.1
68	88.1	1,3-pentadecadiene	P				0.5			0.4	0.4	0.5
69	88.7	1-pentadecene	C	0.7	0.2	1.1	2.6	0.8		4.3	2.4	3.0
70	89.2	pentadecane	C	0.8	0.4	2.0	1.7	1.1		5.5	1.8	2.1
71	89.5	2-pentadecene	P				0.1				0.1	0.1
72	90.0	3-pentadecene	U				0.2				0.1	0.2
73	93.3	1,3-hexadecadiene	P			0.1	0.5			0.1	0.3	0.4
74	93.7	1-hexadecene	C	0.3	0.2	1.1	2.3	0.4		2.5	2.1	2.5

(continue)

75	94.1	hexadecane	C	0.2	0.3	1.6	1.8	0.3	4.1	1.9	2.2
76	94.5	2-hexadecene	P			0.2	0.2			0.2	0.2
77	95.0	3-hexadecene	P			0.2	0.2			0.3	0.2
78	98.1	1,3-heptadecadiene	P		0.1	0.3	0.5			0.4	0.4
79	98.4	1-heptadecene	C	0.2	0.1	0.8	2.3	0.2	1.3	2.0	2.4
80	98.9	heptadecane	C	0.9	0.3	1.7	1.9	1.2	3.0	1.9	2.3
81	99.0	cyclohepatadecane	P				0.2			0.3	0.2
82	99.7	2-heptadecene	P			0.2	0.1			0.2	0.2
83	102.7	1,3-octadecadiene	P			0.1	0.5			0.4	0.3
84	103.3	1-octadecene	C		0.3	0.6	2.3		2.0	1.8	2.1
85	103.6	octadecane	C		0.3	1.4	2.2		0.3	1.9	2.5
86	104.4	2-octadecene	P			0.2	0.2			0.1	0.2
87	105.9	3-octadecene	U			0.1	0.2			0.2	0.2
88	107.6	1,3-nonadecadiene	P		0.1	0.1	0.4			0.3	0.3
89	108.2	1-nonadecene	C	0.1	0.1	0.6	2.1	0.0	1.3	1.7	1.8
90	108.7	nonadecane	C	0.1	0.2	1.3	2.1	0.0		2.0	2.6
91	109.5	2-nonadecene	U		0.0	0.2	0.2			0.3	0.2
92	112.9	decylcyclohexane	P			0.1	0.1			0.2	0.1
93	113.2	1,3-icosadiene	P		0.0	0.2	0.3			0.1	0.1
94	113.8	1-icosene	C		0.1	0.4	1.9		0.2	1.2	1.4
95	114.4	icosane	C		0.2	2.1	2.2		0.8	1.5	2.5
96	115.3	2-icosene	P			0.1	0.2			0.0	0.2
97	119.9	1,3-henicosdiene	P			0.3	0.4			0.2	0.1
98	120.6	1-henicosene	P		0.1	0.4	1.5		0.1	0.6	1.0
99	121.3	henicosane	P		0.1	2.1	2.3		0.5	1.2	2.2
100	122.5	2-henicosene	P			0.1	0.3			0.1	0.2

(continue)

101	128.9	1-docosene	P		0.1	0.3	1.3			0.3	0.3	0.8
102	129.8	docosane	P		0.1	1.0	2.3				1.0	1.9
103	139.6	1-tricosene	P			0.3	1.0				0.1	0.5
104	140.7	tricosane	P			0.7	1.9				0.5	1.5
105	142.8	2-tricosene	P			0.1	0.2				0.1	0.1
106	153.3	1-tetracosene	P			0.1	0.7				0.2	0.5
107	154.7	tetracosane	P			0.6	1.7					1.1
108	171.0	1-pentacosene	P			0.1	0.5					0.2
109	172.9	pentacosane	P			0.5	1.5					0.8
110	194.2	1-hexacosene	P				0.4					0.1
111	196.5	hexacosane	P				1.2					0.6
112	224.3	1-heptacosene	P				0.3					0.1
113	227.3	heptacosane	P				1.0					0.4
114	263.7	1-octacosene	P				0.2					0.1
115	267.6	octacosane	P				0.8					0.3
		Alkane		4.4	12.2	26.2	36.6	5.2	13.4	34.7	25.7	35.1
		Alkene		11.7	20.7	27.4	46.4	7.6	29.1	47.1	39.5	43.9
		Aliphatic cyclic		3.3	4.8	2.0	2.1	1.0	4.5	1.3	2.8	1.7
		Aromatic		7.1	6.0	2.5	0.2	7.4	7.4	2.8	0.2	0.3
		TOTAL		26.6	43.8	58.0	85.3	21.2	54.4	85.9	68.2	80.9

*a.c.: attribution confidence; C, certain (>98%); P, probable (86-97%); U, uncertain (<85%).

reported by Undri et al.[3, 4] in MAP of tires (see also Section 5) and Laresgoiti et al.[5] in conventional heating pyrolysis of tires. The formation of aromatics was not affect by the presence of HDPE ruling out reactions among tire and HDPE or their degradation products during pyrolysis.

The main compounds present in the aliphatic fractions from MAP of HDPE were linear alkanes, and the corresponding 1-alkene and 1,3-dialkene. These compounds were formed through the homolytic C-C bond cleavage of HDPE (Figure 1.12a). There was a broad distribution of these compounds, no more than 5 %, for each alkane/alkene couple. Polymeric matrix of tire contributed to the formation of linear hydrocarbons up to C12 (L1 and L8), while longer chain hydrocarbons were formed only by HDPE pyrolysis. Long chain alkane (>C12) were more abundant than the corresponding 1-alkene or in close amount with them.

Russell et al.[6] reported different amounts of alkane/alkene, and aromatics working with different MAP temperatures, when active carbons were used as MW absorber. Over 773 K they observed a rising abundance of cyclo-, and branched alkenes, while working at 873 K aromatics represented up to 45.3 % of the overall compounds. Aromatics and branched hydrocarbons were present in very low amount in the liquids analyzed. This disagreement might be attributed to a less efficient interaction between HDPE and the MW absorber or to the different operating system such as the very large amount of carbon used by Russel et al. Even if the residence time in the oven was improved by using set-up B the presence of large amount of branched aliphatic and aromatics compounds were not shown. Carbon, Fe, or tire employed as MW absorber interacted with MW but probably high spot temperature as reported by Russell et al. did not occur with the same frequency in our experimental conditions.

6.1.2.3. FTIR

In Figure 6.4 are reported the FTIR spectra of liquids collected from MAP of HDPE.

These FTIR spectra confirm the GC-MS data, and there were not well-defined differences among liquids obtained from MAP of HDPE. Frequencies of alkanes were found at: 2957 (s), and 2870 (m) (H_2C-H asymmetric/symmetric stretching) 2924 (s), and 2853 (s) (HC-H asymmetric/symmetric stretching), 1452 (m), and 1377 (m) (HC-H bending) and 722 (w) (-$(CH_2)_n$- rocking) cm-1. Absorptions of alkene group were present at: 3080 (w) (CH_2=C-H stretching), 3026 (w) (cis- or trans- CH=C-H) and 1641 (w) (alkenyl C=C stretching) cm^{-1}. Absorptions of aromatic groups were shown at: over 3000 (w) (aromatic C-H stretching, mixed with other signals), 1720 (w) (aromatic combination bands), 1605 (w) (aromatic ring stretching), 991 (w) and 964 (w) (Aromatic C-H in-plane bending), 889 (w),

813 (w), 696 (m) and 677 (m) (Aromatic C-H out-of plane bending) cm^{-1}. Aromatic absorptions were not present, as expected, in PE3L, PE4L, PE6L, and PE7L (Figure 6.4a,b,c,d) because these liquids were exclusively formed through MAP of HDPE in the presence of carbon or Fe as MW absorber and they did not contain any compounds from tire pyrolysis.

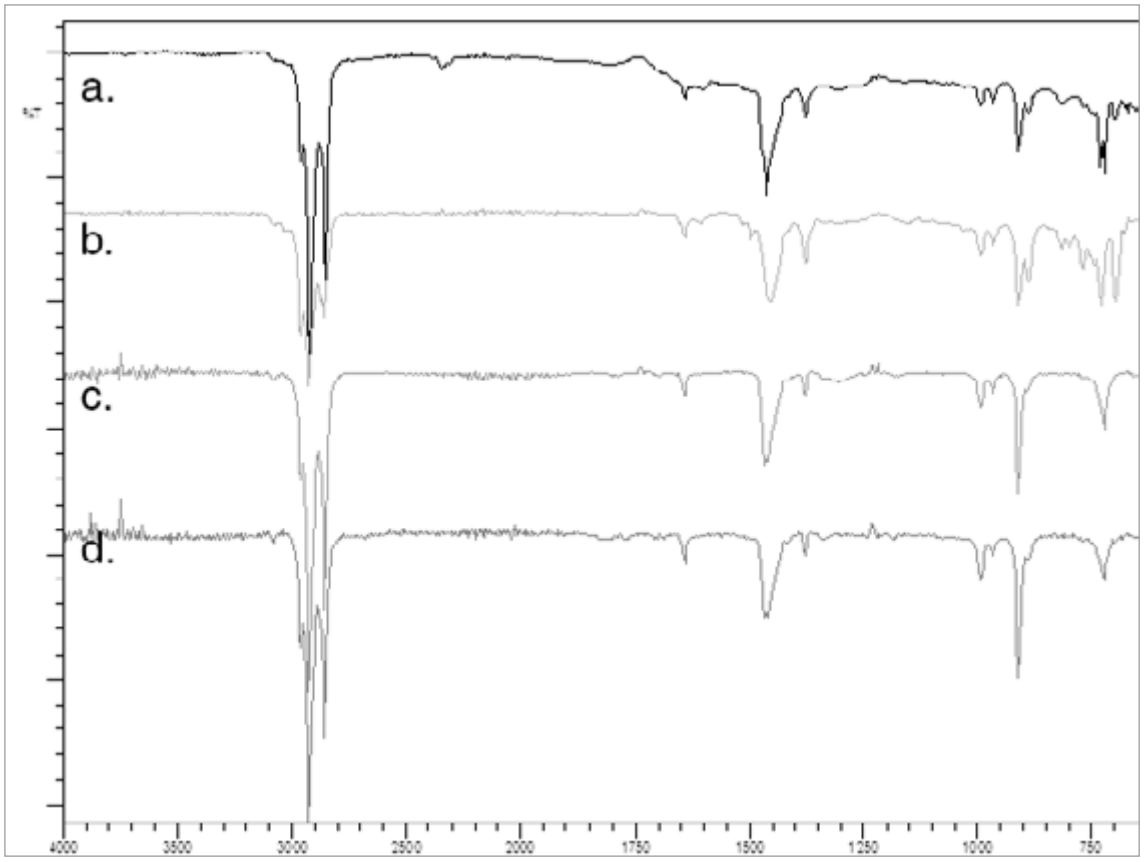

Figure 6.4. FT-IR spectra of liquids: a) PE1L; b) PE5L_I; c) PE3L; d) PE6L.

Very close FTIR spectra were collected from liquids obtained in different MAP conditions; small differences were accountable only for the compounds formed in the degradation of the MW absorber.

6.1.2.4. Distillation curve

The amount of distillate collected below 473 K, the total distillable fraction, and the maximum distillation temperature are reported in Table 6.4.

PE1L and PE3L were solid at room temperature and they were not distillable in the condition reported.

Liquids collected from MAP of HDPE PE2L_I and PE5L_I, both obtained using low MW power, were distillable in large extent below 473 K. Amounts of these distillates were close and apparently there was no strong influence of set-up when low MW power was employed. However must be noted that PE5L_I was 17.8 wt%, which was significantly higher than the amount of PE2L_I (12.7 wt %).

Using Fe as absorber only 10.81 wt% of liquids were distilled below 473 K and

the remaining fraction was not distilled over 473 K, even for PE7L which was obtained through set-up B.

Table 6.4. Distillation of liquids from MAP of HDPE.

Entry	Set-up	MW Absorber	Distilled below 473 K	Distilled over 473 K	Tmax Distillation	Total distilled	Not distilled
			(%)	*(%)*	*(K)*	*(%)*	*(%)*
T4L	A	Tire M	29.18	29.25	528	58.43	41.57
PE2L_I	A	Tire M	72.53	0.00	468	72.53	27.47
PE2L_II	A	Tire M	11.54	35.15	518	46.68	53.32
PE4L	A	Fe	10.31	0.00	365	10.31	89.69
T12L	B	Tire M	43.28	37.35	579	80.63	19.37
PE5L_I	B	Tire M	81.93	0.00	474	81.93	18.87
PE5L_II	B	Tire M	31.69	5.18	511	36.87	63.13
PE6L	B	Carbon	30.35	45.45	519	75.80	24.20
PE7L	B	Fe	31.94	0.00	365	31.94	68.06

Working with set-up B the amount distilled below 473 K increased three times respectively from PE2L_II and PE5L_II, PE4L and PE7L.

Finally the distillation curve showed the possibility to employ these liquid as fuels especially those obtained when carbon or Fe were the MW absorber because they did not contain any sulfur compounds. On the contrary liquids from MAP of polyolefin using tire as MW absorber contained sulfur compounds due to the liquid formed through pyrolysis of tire.

6.2. Polypropylene

MAP of PP was investigated in order to obtain worthwhile liquids with tunable proprieties. The results reported herein were already partially published.[1]

6.2.1. Operating conditions and yields

In Table 6.5 are reported the operating parameters employed (entries are named "PPn" where "n" is an arbitrary ascending order for each experiment).

Table 6.5. MAP of PP, operating parameters.

Entry	Set-up	MW Absorber	Power *(kW)*[a]	Polymer *(g)*	MW Absorber *(g)*	Time *(min)*	Solid *(wt%)*	Liquid *(wt%)*	Gas *(wt%)*
T4	A	Tire M	3	-	233.3	35	43.2	42.6	14.1
PP1	A	Tire M	1.8(9); 2.7(5); 3.0(36)	126.7	258.7	50	29.4	58.9	11.7
PP2	A	Carbon	3.0(63); 6.0(5)	142.2	82.9	68	12.0	74.7	13.3
PP3	A	Carbon	1.2(120); 1.5(42); 2.7(12); 3.0(21); 6.0 (32)	124.0	57.6	215	11.9	60.6	27.5
PP4	A	Fe	3.0	117.2	62.6	60	11.1	56.7	32.2
PP5	B	Carbon	3.0	123.8	46.7	40	9.1	56.5	34.4
PP6	B	Fe	3.0	114.0	64.9	77	13.3	45.6	41.1

a) within brackets the time for which each MW power was employed.

MAP of tire alone (entry T4) was reported as referring pyrolysis to help results interpretation of entry when tire was used as MW absorber. Indeed products from MAP of tire were mixed with those from PP.

MAP of PP gave a low viscosity liquid in any pyrolysis condition due to its lower stability[7] than HDPE and using a reaction time to 50 min a complete degradation

was achieved (entry PP1, Table 6.5).

In MAP of PP an efficient cracking was achieved and a low viscosity liquid was formed.

There was always high formation of solid (roughly 10 wt%) when carbon and Fe were MW absorber (PP2 – PP6). Anyway the pyrolyzed PP contained large amount of ash (5.5 % as evaluated by proximate analysis, "Appendix I: Materials and Instruments"), and char amount could be partially attributable to coking reactions.

Formation of liquid was reduced and formation of gas was increased when working with set-up B instead of set-up A, and using Fe as MW absorber instead of carbon. Indeed the lowest liquid yield was achieved for PP6 (45.6 %; Fe as absorber and set-up B), while the highest liquid yield was obtained for PP2 (74.7 %; carbon as absorber and set-up A).

6.2.2. Liquid product

6.2.2.1. Physical properties

Physical properties of liquids, coded as "PPnL" where "n" is the pyrolysis entry, Table 6.6, were strongly affected by reaction conditions.

Table 6.6. Characteristic of liquid obtained by MAP of PP.

Entry	Density	Viscosity	HHV	LHV	Ultimate analyses				C/H molar ratio
					C	H	N	S	
	(g/cm³)	*(cP)*	*(MJ/kg)*	*(MJ/kg)*	*(wt%)*	*(wt%)*	*(wt%)*	*(wt%)*	
T4	0.874	1.73	44±4	42±4	86.87	10.12	0.66	0.9	0.72
PP1L	0.831	2.99	46±5	44±4	84.54	11.71	1.93	0.5	0.61
PP2L	0.746	>4	38±4	34±3	84.30	14.34	0.00	0.1	0.49
PP3L	0.746	0.63	38±4	35±4	85.53	14.48	0.00	0.0	0.50
PP4L	0.752	>4	38±4	35±4	85.12	14.03	0.00	0.0	0.50
PP5L	0.760	0.95	41±4	38±4	85.60	14.41	0.00	0.0	0.50
PP6L	0.746	0.57	39±4	37±4	85.34	14.38	0.00	0.0	0.50

MAP of PP gave always low viscosity liquid (0.63-4.0 cP) with almost the same low density when tire pyrolysis products were not present (0.746 – 0.760 g/cm³).

C/H molar ratios of all liquids from MAP of PP were close and as expected they were lower than liquid from MAP of tire alone, confirming the prevailing aliphatic composition of these liquids.

All liquids had a high calorific value (LHV about 35 MJ/Kg) and could be employed for energy production or as a source of chemicals.

6.2.2.2. GC/MS

All liquids contained a large number of compounds especially when tire pyrolysis products were present. In Table 6.7 are listed only the most representative compounds identified from MAP of PP. Abundances were evaluated by the TIC without any response factor correction. In Figure 6.5 and Figure 6.6 are reported TICs of PP1L and PP5L for visual comparative purposes.

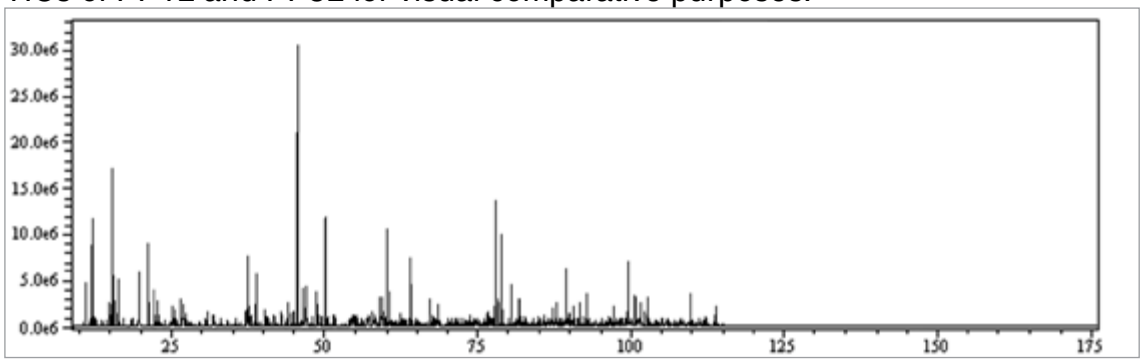

Figure 6.5. TIC of samples obtained from MAP of PP with set-up A: PP1L.

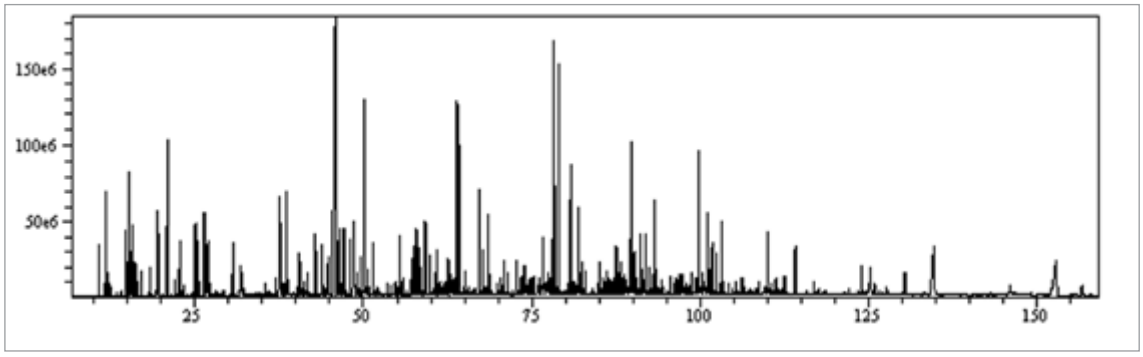

Figure 6.6. TIC of samples obtained from MAP of PP with set-up B:PP5L.

MAP of PP mainly formed methyl branched alkanes and alkenes, which were ascribable to C-C bond cleavage from PP backbone. C9-C12 hydrocarbons were prevalent over other compounds and among them 2,4-dimethyl-1-heptene was the major one (12.47 and 17.80 for PP2L and PP6L respectively). Their wide formation might be interpreted with the merging of two issues: the absence of a gas flow and their relatively low boiling point (range between 400 and 470 K).[7] The absence of a gas flow increased the residence time of compounds and only products having a relatively low boiling point were able to leave the reactor.

Cyclization and aromatization reactions were present and their influence were slightly enhanced by using set-up B. PP was more reactive in MAP condition than HDPE and single ring aromatics were always collected in the products in spite of the set-up and absorber employed.

Fe as MW absorber showed a high efficiency to transfer heat to the polymeric matrix. Indeed using set-up B (PP6L) more C9-C12 hydrocarbons were collected than using set-up A (PP4L). Meanwhile close pyrolysis efficiency to PP4L was achieved working with carbon as MW absorber in PP5L using set-up B.

Table 6.7. Compounds in liquids from MAP of PP.

		Entry		T4L	PP1L	PP2L	PP3L	PP4L	PP5L	PP6L
		Set-up		A	A	A	A	A	B	B
		Absorber		Tire M	Tire M	Carbon	Carbon	Fe	Carbon	Fe
n°	Time	Substance	a.c.							
1	10.9	Propene	C		0.89	0.02	0.47	0.28	0.38	0.37
2	12.0	2-Butene-trans	C	1.53	2.28	0.04	0.95	0.65	0.75	0.86
3	12.2	Butane	C	0.15	0.2		0.10	0.04	0.07	0.05
4	12.6	1-butene	C	0.24	0.16		0.05	0.04	0.06	0.07
5	14.8	1-pentene	C	0.26	0.51		0.61	0.22	0.43	0.36
6	14.9	2-methyl-1-butene	P		0.47		0.23	0.22	0.21	0.37
7	15.3	Pentane	C	0.29	3.8	0.11	1.50	1.13	1.1	1.51
8	15.5	2-methyl-1,3-butadiene	P	1.68	1.23		0.13	0.20	0.17	0.32
9	15.6	2-pentene-cis	C	0.23	0.57		0.67	0.25	0.48	0.4
10	16.2	2-methyl-2-butene	P		0.3		0.43	0.07	0.21	0.11
11	16.4	1,3-pentadiene	C	0.23	1.14		0.26	0.16	0.2	0.28
12	17.1	Cyclopentadiene	P	0.29	0.21		0.14	0.17	0.18	0.26
13	18.5	4-methyl-1-pentene	P	0.15	0.18		0.36	0.07	0.2	0.1
14	19.6	2-methyl-pentane	P	0.38	1.62	0.03	1.63	0.37	0.96	0.54
15	21.1	2-methyl-1-pentene	P	0.13	2.54	0.08	2.62	1.93	1.85	3.04
16	22.1	hexane	C	0.04	1.02		0.20	0.04	0.12	0.08
17	22.3	3-hexene-cis	P	0.04	1.02		0.28	0.25	0.05	
18	22.8	2,3-dimethyl-1-butene	P	0.32	0.63		0.74	0.09	0.42	0.18
19	24.0	2-methyl-2-pentene	P	0.45	0.12				0.03	
20	24.7	methylcyclopentane	P	0.20					0.04	
21	25.0	2,4-dimethylpentane	P	0.15			0.14		0.07	
22	25.2	2-methyl-1,3-pentadiene	P	0.24	0.46		0.74	0.38	0.56	0.75

(continue)

23	25.3	1,3-cyclohexadiene	P	0.36	0.22		0.10	0.06	0.11	0.13
24	25.5	1,3-hexadiene	P	0.25	0.41		0.52	0.23	0.42	0.48
25	25.7	1,4-cyclohexadiene	P	0.29	0.18		0.10		0.1	0.13
26	26.41	2,4-dimethyl-1-pentene	P		0.79	0.02	1.19	0.48	0.71	0.83
27	26.9	3-methyl-cyclopentene	P	0.58	0.23		0.14	0.04	0.09	0.08
28	27.0	benzene	C	1.76	0.64		0.38	0.46	0.50	0.81
29	27.4	3,4-dimethyl-2-pentene	P	0.42	0.12		0.59	0.35	0.42	0.66
30	28.4	4-methyl-1-hexene	P	0.09			0.06	0.02	0.03	0.05
31	29.5	Cyclohexene	P	0.33			0.05	0.10	0.05	0.06
32	30.9	1-heptene	C	0.33	0.36		0.49	0.25	0.48	0.46
33	32.0	2,4-dimethyl-1,3-pentadiene	P	0.60	0.23		0.44	0.12	0.24	0.19
34	32.1	Heptane	C	0.29	0.18		0.32	0.05	0.19	0.19
35	32.3	2-methyl-2-hexene	P	0.12	0.15		0.12	0.03	0.06	0.1
36	37.3	2-methyl-2,4-hexediene	P	0.74	0.44		0.25	0.12	0.17	0.22
37	37.8	toluene	C	2.95	2.30		1.27	0.84	1.13	1.52
38	37.70	4-methyl-3-heptene	P		0.47		0.83	0.43	0.57	0.79
39	38.4	3,3-dimethyl-1-hexene	P	0.10	0.3		0.21	0.78	0.92	
40	38.839	2,4-dimethylhexane	P		1.3	0.03	1.52			1.23
41	40.6	2-methyl-1-heptene	P	0.12	0.4		0.45	0.29	0.33	0.54
42	41.0	1-octene	C	0.23	0.24		0.39	0.24	0.26	0.4
43	42.84	2,4-dimethyl-2-heptene	P				0.16	0.55	0.64	0.89
44	44.01	2,4-dimethylheptane	P		0.49		0.05	0.18	0.49	0.3
45	46.004	2,4-dimethyl-1-heptene	P		12.47	0.5	7.65			17.80
46	46.8	ethylbenzene	C	2.19	1.06	0.02	0.96	0.24	0.63	
47	47.5	1,4-dimethylbenzene	C	2.41	1.22		0.62	0.45	0.57	0.42
48	49.0	styrene	C	1.43	0.9		0.61	0.81	0.65	1.02

(continue)

49	49.5	1,2-dimethylbenzene	C	0.78	0.48		0.20	0.22	0.33	
50	50.0	2,4,6-trimethyl-1-heptene	P		0.23	0.09	0.50	2.40	2.33	3.45
51	50.9	nonane	C	0.21	2.98		0.53	0.24	0.32	0.40
52	51.7	3,5,5-trimethylcyclohexene	P	0.25	0.27		0.08	0.52	0.37	0.86
53	55.2	1,2,3-trimethylbenzene	P	1.19	0.37		0.25		0.48	
54	55.4	1,2,4 trimethylbenzene	P	0.78	0.23		0.28	0.06	0.14	0.16
55	56.5	-methylstyrene	C	0.40	0.1		0.15		0.14	0.15
56	57.79	1-decene	C		0.31		0.18	0.44		0.62
57	58.0	1,9-decadiene	P	0.13	0.37		0.48	0.05	0.36	0.11
58	58.0	2,4,6-trimethyl-2-octene	P		0.29		0.08	0.48	0.48	
59	58.5	2,4,6-trimethyl-1-octene	P	0.34			0.60	0.33	0.32	0.78
60	58.8	Decane	C	0.28	0.23	0.02	0.61	0.31		0.45
61	59.0	4-methyldecane	P				0.35	0.42	0.53	0.18
62	59.46	2-methyldecane	P		0.74		0.13	0.46	0.63	0.61
63	64.1	2,4,6-trimethyl-1-nonene	P		1.79	0.09	0.32	2.58	1.88	3.59
64	64.3	2,4,6-trimethyl-2-nonene	P		0.96	0.06	2.23	1.33	1.12	1.86
65	67.27	2,4,6,8-tetramethyl-1-nonene	P		0.61	0.03	0.15	0.79	0.82	1.18
66	67.68	2,4,6,8-tetramethyl-2-nonene	P		0.28	0.02	0.11	0.26	0.35	0.40
67	68.67	2,4,6,8-tetramethyl-1,3-nonadiene	P		0.62	0.03	0.12	0.87	0.60	1.29
68	70.85	2,4,6,8-tetramethyl-2-nonene	P		0.07		0.06	0.32	0.29	0.27
69	71.7	1-dodecene	C	0.24	0.2		0.36	0.04	0.23	0.46
70	72.71	2,4,6,8-tetramethyl-1-decene	P				0.39	0.29	0.26	0.05
71	74.00	2,4,6,8-tetramethyldecane	P		0.16	0.02	0.11	0.25	0.34	0.21
72	76.78	2,4,6,8-tetramethyl-2-decene	P		0.19	0.02	0.13	0.60	0.48	0.12
73	78.2	2,4,6,8-Tetramethyl-1-undecene	P		3.4	0.77	0.22	4.37	2.58	0.27
74	78.58	2,4,6,8-tetramethyl-1-undecene	P		0.8	0.31	0.30	1.16	1.02	0.21

(continue)

75	79.1	2,4,6,8-Tetramethylundecane	P		2.24	0.74	2.21	3.13	2.03	5.03
76	80.68	2,4,6,8,10-pentamethyl-1-undecene	U		0.12	0.42	1.45	0.80	0.94	3.53
77	81.93	2,4,6,8,10-pentamethyl-2-undecene	U		0.98	0.33	0.74	0.35	0.55	0.91
78	87.5	4,6,8,10-Tetramethyltridecane	U		0.11	0.4	0.21	0.38	0.42	0.09
79	88.0	2,4,6,8,10-Pentamethyl-2-tridecene	U		0.5	0.27	0.25	0.25	0.34	0.11
80	89.7	2,4,6,8,10-Pentamethyl-3-tridecene	U		0.14	0.55	0.18	1.39	1.15	0.17
81	90.2	2,4,6,8,10-Pentamethyl-1-tridecene	U		1.34	2.47	0.10	0.37	0.38	0.12
82	91.0	2,4,6,8,10-Pentamethyl-4-tridecene	U		0.18	1.95	0.49	0.65	0.63	0.92
83	91.6	2,4,6,8,10-Pentamethyl-5-tridecene	U		0.18	0.74	0.24	0.18	0.25	
84	91.9	2,4,6,8,10-Pentamethyl-6-tridecene	U		0.14	1.33	0.07	0.45	0.47	
85	92.4	3,5,7,9,11-Pentamethyl-1-tetradecene	U		0.5	0.37	0.27	0.28	0.23	0.37
86	93.2	3,5,7,9,11-Pentamethyl-1,12-tetradecadiene	U		0.19	2.18	0.22	1.04	0.66	0.12
87	96.566	3,5,7,9,11-Pentamethyl-1,3-tetradecadiene	U		0.09	0.66	0.05	0.14	0.2	
88	98.4	1-heptadecene	C	0.17		0.53	0.06	0.10	0.16	0.07
89	98.9	heptadecane	C	0.86	0.13	0.96	0.06	0.28	0.22	
90	99.415	2,4,6,8,10,12-Hexamethyl-1,3-pentadecadiene	U			0.49	0.11	0.17	0.2	
91	99.8	2,4,6,8,10,12-Hexamethyl-1-pentadecene	U		0.15	2.81	0.09	1.24	1.06	
92	101.0	2,4,6,8,10,12,14-heptamethyl-1,3-pentadecadiene	U		1	0.31	0.09	0.98	0.89	0.06
93	101.4	2,4,6,8,10,12-Hexamethyl-2-pentadecene	U			3.1	0.33	0.37	0.31	0.45
94	101.8	3,5,7,9,11,13-Hexamethyl-2-hexadecene	U		0.21	0.95	0.08	0.47	0.46	0.07
95	102.5	2,4,6,8,10,12-Hexamethyl-3-pentadecene	U			1.46	0.25	0.40	0.34	0.32
96	103.1	3,5,7,9,11,13-Hexamethyl-1-hexadecene	U		0.33	2.13	0.04	0.97	0.56	0.09
97	106.0	3,5,7,9,11,13-Hexamethyl-1,3-hexadecadiene	U		0.21	0.33	0.05	0.30	0.21	
98	108.8	2,4,6,8,10,12,14-Heptamethylheptadeca-1,3-diene	U			0.45		0.28	0.2	
99	110.0	2,4,6,8,10,12,14-Heptamethylheptadec-1-ene	U		0.94	1.88	0.05	0.73	0.62	
100	112.5	2,4,6,8,10,12,14-Heptamethylheptadec-2-ene	U		0.14	0.78	0.15	0.24	0.25	

(continue)

101	114.2	3,5,7,9,11,13,15-Heptamethyloctadeca-1,3-diene	U		0.65	1.64	0.08	0.92	0.7	
102	125.2	3,5,7,9,11,13,15-Heptamethyloctadec-3-ene	U			0.32	0.04	0.55	0.64	
104	134.7	3,5,7,9,11,13,15,17-Octamethylicosa-1,3-diene	U			0.11		0.17	2.26	
		Alkane		2.65	15.20	2.31	9.67	7.28	7.49	10.87
		Alkene		9.38	46.99	30.64	33.60	38.80	39.03	52.59
		Cyclic alkane		0.20	0.00	0.00	0.00	0.00	0.04	0.00
		Cyclic Alkene		2.10	1.11	0.00	0.61	0.89	0.90	1.52
		Aromatic		13.89	7.30	0.02	4.72	3.08	4.57	4.08
		TOTAL		28.22	70.6	32.97	48.6	50.05	52.03	69.06

*a.c.: attribution confidence; C, certain (>98%); P, probable (86-97%); U, uncertain (<85%).

Fe was more efficient than carbon to convert and ransfer the MW radiation, as heat, to the polymeric matrix.

6.2.2.3. FTIR

The FTIR spectra of liquids collected from MAP of PP are reported in Figure 6.7.

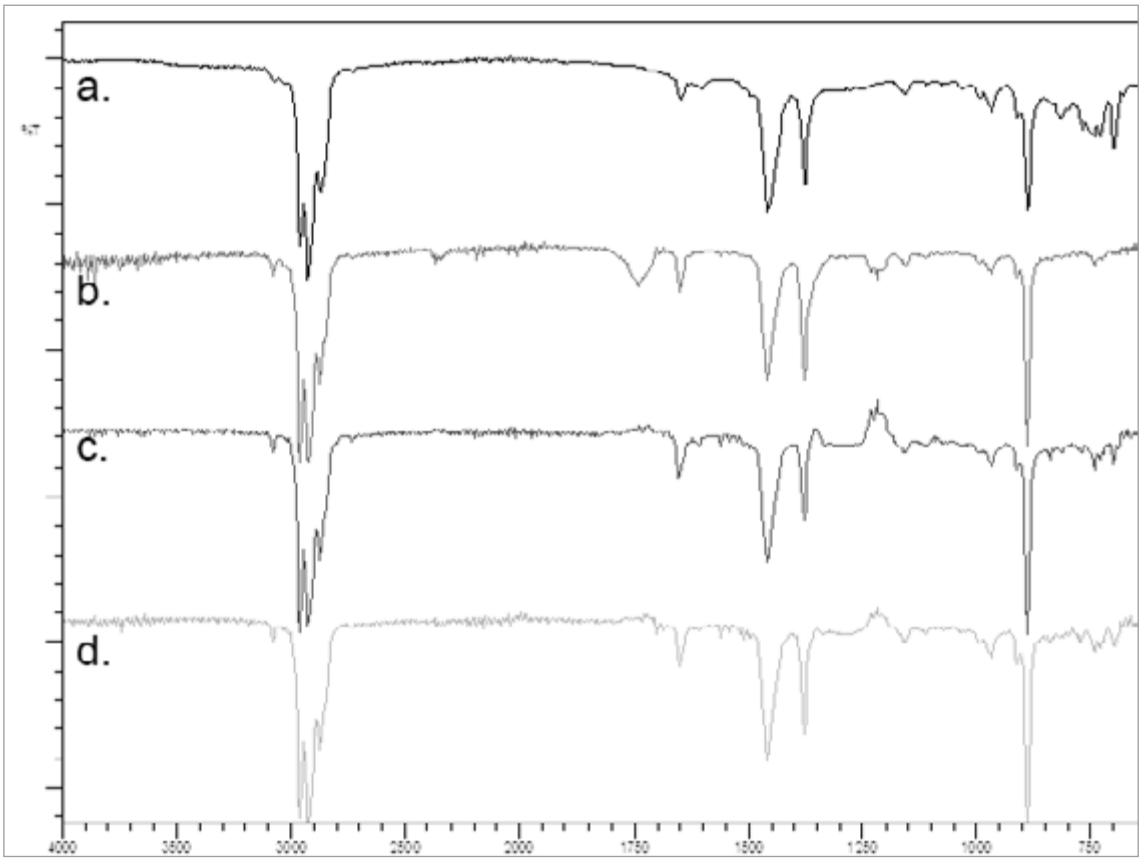

Figure 6.7. FTIR spectra of liquids from MAP of PP. a) PP1L; b) PP2L; c) PP3L; d) PP5L.

These FTIR spectra confirm the GC-MS data, and there were not well-defined differences among liquids obtained from MAP of HDPE or PP, except for weak absorptions due to aromatic moieties. Frequencies of alkanes were found at: 2957 (s), and 2870 (m) (H_2C-H asymmetric/symmetric stretching) 2924 (s), and 2853 (s) (HC-H asymmetric/symmetric stretching), 1452 (m), and 1377 (m) (HC-H bending) and 722 (w) (-$(CH_2)_n$- rocking) cm^{-1}. Absorptions of alkene group were present at: 3080 (w) (CH2=C-H stretching), 3026 (w) (cis- or trans- CH=C-H) and 1641 (w) (alkenyl C=C stretching) cm-1. Absorptions of aromatic groups were shown at: over 3000 (w) (aromatic C-H stretching, mixed with other signals), 1720 (w) (aromatic combination bands), 1605 (w) (aromatic ring stretching), 991 (w) and 964 (w) (aromatic C-H in-plane bending), 889 (w), 813 (w), 696 (m) and 677 (m) (aromatic C-H out-of plane bending) cm^{-1}.

Very close FTIR spectra were collected from liquids obtained in different MAP conditions; small differences were accountable only for compounds formed in the degradation of the MW absorber.

6.2.2.4. Distillation curve

The amount of distillate collected below 473 K, the total distillable fraction, and the maximum distillation temperature are reported in Table 6.8.

Table 6.8. Distillation of liquids.

Entry	Set-up	MW Absorber	Distilled below 473 K (%)	Distilled over 473 K (%)	Tmax Distillation (K)	Total distilled (%)	Not distilled (%)
T4L	A	Tire M	29.18	29.25	528	58.43	41.57
PP1L	A	Tire M	14.81	7.05	514	21.86	78.14
PP2L	A	Carbon	64.18	0.00	465	64.18	35.82
PP3L	A	Carbon	68.67	10.35	500	79.13	20.87
PP4L	A	Fe	51.72	22.87	588	74.58	25.42
PP5L	B	Carbon	71.35	0.00	473	71.35	28.65
PP6L	B	Fe	60.28	0.00	468	60.28	39.72

Using set-up A liquids, except those where tire was the MW absorber, were largely distillable below 473 K. These data confirmed that the amount of liquid distillable below 473 K was not affected by the pyrolysis condition.

Using set-up B large amount of liquids were distillable (71.35 and 60.28 % for PP5L and PP6L respectively). Only negligible differences were evidence in the distillation curve when set-up B was employed with respect to set-up A. Thus PP was efficiently pyrolyzed in any condition employed.

Finally the distillation curve showed the possibility to employ these liquids as fuels especially those obtained when carbon or Fe were the MW absorber because they did not contain any sulfur compounds. On the contrary liquids from MAP of PP using tire as MW absorber contained sulfur compounds due to the liquid formed through pyrolysis of tire.

6.3. Polystyrene

MAP of PS was performed to transform an aromatic polymer into a liquid with high amount of styrene and single ring aromatics. The results reported herein were already partially published.[8]

6.3.1. Operating conditions and yields

Microwave assisted pyrolysis (MAP) of PS was investigated by varying three parameters: microwave power, microwave absorber, and apparatus set-up (Table 6.9, entries are named "PPn" where "n" is an arbitrary ascending number for each experiment). Although temperature plays an important role, this parameter is detected with high uncertainty in MAP, as previously reported in Section 5.5 and by Bykov et al.,[10] but it was not used as a descriptive parameter.

During MAP polymers were initially melted then the absorber was incorporated into the melted PS and pyrolysis started.

Table 6.9. MAP of PS operating parameters

Entry	Set-up	MW Absorber	Power	Polymer	MW Absorber	Time	Solid	Liquid	Gas
			(kW)[a]	*(g)*	*(g)*	*(min)*	*(wt%)*	*(wt%)*	*(wt%)*
T4	A	Tire M	3	-	233.3	35	43.2	42.6	14.1
PS1	A	Tire M	3	141.1	298.4	43	31.8	57.4	10.8
PS2	A	Carbon	3(46); 6(13)	196.3	106.7	59	6.8	89.3	3.9
PS3	A	Carbon	1.2(82); 1.5(58); 3(45)	160.3	81.8	185	0.9	96.1	3.0
PS4	A	Carbon	3	100.4	47.3	22	9.8	86.5	3.7
PS5	A	Fe	3			29	1.9	88.3	9.8
PS6	B	Carbon	3	100.3	50.2	28	10.0	83.6	6.4
PS7	B	Fe	3(24); 6(47)	146.1	71.1	71	32.0	64.5	3.5

a) within brackets the time for which each MW power was employed.

PS in the presence of carbon as MW absorber was almost completely converted into a liquid fraction using MAP (PS2, Table 6.9). Reducing MW power the yield of liquid was further increased (PS3, Table 6.9). In this latter pyrolysis solids yield was lower than 1.0 wt%; while it was improved up to 6.8, 9.8 and 10.0 wt% (PS2, and PS3 respectively) increasing MW power. Gas was formed in small amount in PS2 – PS4 and its yield was improved (PS6) through the use of a fractionating system. Gas from MAP of PS alone contained C1-C4 hydrocarbons, and there was not noteworthy variation of their relative distribution among each experiment.

The high yield of gas in PS1 was largely attributable to tire degradation[3] while that one of solid was due to fillers and other inorganic compounds present in

tire that contribute to increase the yield of the residue present at the end of the experiment.

As well as for MAP of PE and PP (see Sections 6.1.1 and 6.2.1), Fe showed a completely different behaviour than carbon as MW absorber. Using set-up A (PS5) PS was pyrolyzed to a liquid fraction with close yield to PS4 (88.3% for PS5 and 86.5% for PS4) but with small amount of solid and high amount of gas. Iron was able to convert and fast transfer the energy to the polymeric matrix ensuing negligible cocking phenomena and strong gas formation. Meanwhile using set-up B the effect was completely opposite, cocking was enhanced while gas formation was avoided. Probably the presence of a fractionating system (set-up B) promoted the condensation of benzene ring by increasing the residence time of high boiling compounds.

All liquids obtained in the presence of carbon and Fe were clear pale-yellow solutions in contrast with the results reported by Onwudili et al.[11] They used a classical heating and a closed batch system obtaining a dark-coloured liquid at low temperature (623 K) and char from condensation of aromatics, using higher temperature (723 K). These different results might be attributed to the different heating system and the different apparatus employed.

Reactions involving char or gas formation were reduced by using low MW power (PS3). Anyway a MW power of 3 kW was enough to promote aromatic condensation (PS4, Table 6.9) as suggested for MAP of PS by Hussain et al.[12] Furthermore improving the residence time in the oven, achieved with the fractionating system (PS6), the condensation and gasification reactions were slightly enhanced. This issue were clearer when Fe was the MW absorber as previously highlighted.

Separate considerations might be done when tire was the MW absorber. The amount of tire was higher than carbon because it contains more of 50 % products unable to absorb MW. Liquids from MAP of PS obtained in the presence of tire contained the same compounds formed in all other PS pyrolysis together with those formed from MAP of tire alone. It is possible to evaluate the contribution of tire and PS to the liquid formed. The amount of liquid from PS was calculated assuming the same yields of experiment 5 for MPA of PS where carbon was the MW absorber (PS4) while the yields of tire were assumed to be analogous to that reported in T4. These results (Table 6.10) were compared with the results obtained in PS1.

Experimental yield for gas were the same than calculated while that one of solid was slightly higher and that one of liquid slightly lower than those calculated. Probably the degradation products of tire and PS reacted together to form a slight amount of solid through liquid cooking.

Solids formed by PS pyrolysis were mixed with large amount of MW absorber in all experiments and they were not characterized (see also Section 5.3).

Table 6.10. Yield calculation for entry 5, together with the experimental values.

	Solid		Liquid		Gas	
	Tire	PS	Tire	PS	Tire	PS
Relative amount calculated (g)[a]	104.6[b]	13.8[c]	103.2[b]	122.1[c]	34.2[b]	7.7[c]
Total amount calculated (g)	118.5		225.2		41.9	
Yield calculated (%)	30.9		58.8		10.9	
Experimental yield (%)	31.8		57.4		10.8	

a) Starting materials: tire 298.4 g, PS 141.1 g, b) amount calculated from MAP of tire, T4; c) amount calculated from PS4.

The MAP of PS in the presence of tire (PS1, Table 6.9) or carbon (PS2-PS4, and PS6 Table 6.9) suggested the possibility to perform a MAP process in the presence of an inorganic and/or organic material. In fact tire or carbon, other than MW absorber, could be seen as a pollutant mixed with waste PS which did not affect the pyrolyses results as evidenced in Table 6.10.

6.3.2. Liquid product

6.3.2.1. Physical properties

Physical characteristics of liquids from MAP of PS with carbon or tire as MW absorber were not affected by variation of MW power, or apparatus set-up, meanwhile Fe affected deeply them (Table 6.11).

Table 6.11. Physical characteristics of liquid obtained by MAP of PS.

Entry	Density	Viscosity	HHV	LHV	Ultimate analyses					C/H molar ratio
					C	H	N	S	O[a]	
	(g/cm³)	*(cP)*	*(MJ/kg)*	*(MJ/kg)*	*(wt%)*	*(wt%)*	*(wt%)*	*(wt%)*	*(wt%)*	
T4L	0.874	1.73	44±4	42±4	86.87	10.12	0.66	0.9	1.45	0.72
PS1L	0.896	0.79	40±4	39±4	88.48	8.52	1.67	0.4	0.93	0.87
PS2L	0.917	0.90	41±4	39±4	90.61	7.66	0.96	0.0	0.77	0.99
PS3L	0.891	0.79	41±4	40±4	90.76	9.01	0.23	0.0	0.00	0.85
PS4L	0.923	0.91	41±4	40±4	90.39	7.74	1.00	0.0	0.87	0.97
PS5L	0.930	1.07	42±4	40±4	91.92	8.08	0.00	0.0	0.00	0.95
PS6L	0.913	0.80	40±4	39±4	91.70	8.05	0.07	0.0	0.18	0.96
PS7L	0.903	0.78	42±4	40±4	90.67	8.58	0.00	0.0	0.75	0.88

a) by difference.

Density was in a narrow range among 0.891 - 0.930 g/cm^3 and viscosity was also in a very thin interval (0.79 – 1.07 cP). Furthermore close values of ultimate analyses and C/H molar ratios suggested that all liquids had similar composition even if different reaction condition were used. Some differences were shown for PS1L because this liquid contained products from MAP of PS and tire. These

differences were confirmed by the data of T4L, the liquid obtained by MAP of tire alone. The C/H molar ratio increased from PS3L to PS1L and PS2L confirming the prevailing presence of aryl moiety in liquids from PS pyrolysis. Worthy of note were the date reported for PS5L and PS7L. Density and C/H molar ratio of PS5L was the highest while the one of PS7L the lowest of all pyrolysis. Working without a fractionating system (set-up A) preserve most of the aromatic fraction of liquid while working with a fractionating system reduce the aromatic content of liquids.

Also the high heating value (HHV) of liquids from MAP of PS shown the same tendency of C/H molar ratio, they were close to styrene, benzene, and ethyl benzene HHV (42.20, 41.83, and 43.00 MJ/kg respectively).[9]

The presence of compounds from MAP of tire did not affect significantly density, viscosity, HHV, and lower heating value (LHV) of PS1L with respect to PS2L – PS7L. Only T4L showed different values because this liquid was obtained from MAP of tires alone.

6.3.2.2. GC/MS

Liquids contained few compounds when PS was pyrolyzed in the presence of carbon or Fe as evidenced by GC-MS analysis, while a large number of components were present if tire was the MW absorber due to its simultaneous degradation. In Table 6.12 are listed the compounds identified in MAP of PS and only the main compounds from tire degradation (T4L). Their abundance was evaluated by the total ion chromatography (TIC) without any response factor correction. In Figure 6.8 are reported the TIC of PS1L, PS2L, and PS4L.

As expected from literature the main products of PS pyrolysis were aromatic hydrocarbons such as: benzene, toluene, ethylbenzene, styrene, and α-methylstyrene.[11-15]. They represented up to 91.26 % of products present in liquids, and single ring aromatic compounds reached up to 94.99 % in PS4L. Styrene was always the predominant compound in each liquid, also in L5 where the liquid was diluted by tire degradation products. The highest amount of styrene was present in PS4L and PS5L (65.98 and 63.27 %, respectively).

Also PS6L contained large amount of styrene (60.09%). This evidence for PS5L was surprising because the fractionating system, improved the residence time of products in the oven and styrene could be further degraded or condensed. In fact the yield of solid (10.0 wt%) and gas (6.4 wt%) products were enhanced. Probably styrene was not involved in these reactions because was rapidly distilled away.

On the contrary PS7L showed a low amount of styrene, in this case styrene was dramatically reduced by using Fe as MW absorber together with a fractionating system. However Fe showed similar features to carbon in producing styrene when a fractionating system was not employed.

Table 6.12. Compounds identified in liquids from MAP of PS, by GC-MS.

		Entry		T4L	PS1L	PS2L	PS3L	PS4L	PS5L	PS6L	PS7L
		Set-up		A	A	A	A	A	A	B	B
		Absorber		Tire M	Tire M	Carbon	Carbon	Carbon	Fe	Carbon	Fe
No.	R.t.	Substance	a.c.*								
1	12.0	2-Butene-trans	C	1.5	1.9						
2	16.4	1,3-Pentadiene	C	1.6	0.9						
3	19.6	3-Methyl-1-hexene	C	1.6	0.7						
4	27.0	Benzene	C	1.7	1.1	1.6	0.8	2.1	1.4	1.2	0.7
5	37.8	Toluene	C	2.9	7.6	9.0	11.0	8.0	5.2	9.3	9.2
6	46.8	Ethylbenzene	C	2.1	16.3	8.7	10.1	4.8	1.4	5.6	18.0
7	47.5	1,4-Dimethylbenzene	C	2.3	1.0						0.0
8	49.0	Styrene	C	1.4	24.9	47.7	50.1	66.0	63.3	60.1	34.4
9	49.5	1,2-Dimethylbenzene	C	0.8	0.3						0.0
10	52.2	Cumene	C	0.4	3.5	0.7	1.4	0.3		0.5	4.5
11	55.2	1,2,3-Trimethylbenzene	P	1.2	0.4						0.0
12	55.4	1,2,4-Trimethylbenzene	P	0.8	0.3						
13	56.5	-Methylstyrene	C	0.4	8.7	13.4	14.1	10.4	4.7	13.3	12.7
14	57.7	1,3,5-Trimethylbenzene	P	1.1	0.4						
15	59.9	1-Ethyl-3-methylbenzene	P	1.0	1.1				0.5		
16	60.1	1,2,4,5-Tetramethylbenzene	P	1.4	0.5						
17	60.9	Limonene	C	3.4	1.6						
18	96.8	1,3-Diphenylpropane	P	0.2	3.9	2.8	3.4	0.9	1.7	1.9	5.0
19	98.6	3-Butenylbenzene	P		0.5	5.1	1.3	2.4		2.9	2.2
20	98.8	Cyclopropane-1,1-diyldibenzene	P		0.6	2.5	0.6	1.1		0.9	
21	99.8	3-butene-1,3-diyldibenzene	P		0.5				11.6		

(continue)

22	110.7	2-Phenylnaphtalene	P		0.6	1.6	0.2	0.5	0.4	0.2	
		Total Aromatic		17.7	72.4	93.1	92.9	96.4	90.0	95.8	86.7
		Total Aliphatic		8.1	5.1	0.0	0.0	0.0	0.0	0.0	0.0

*a.c.: attribution confidence; C, certain (>98%); P, probable (86-97%); U, uncertain (<85%).

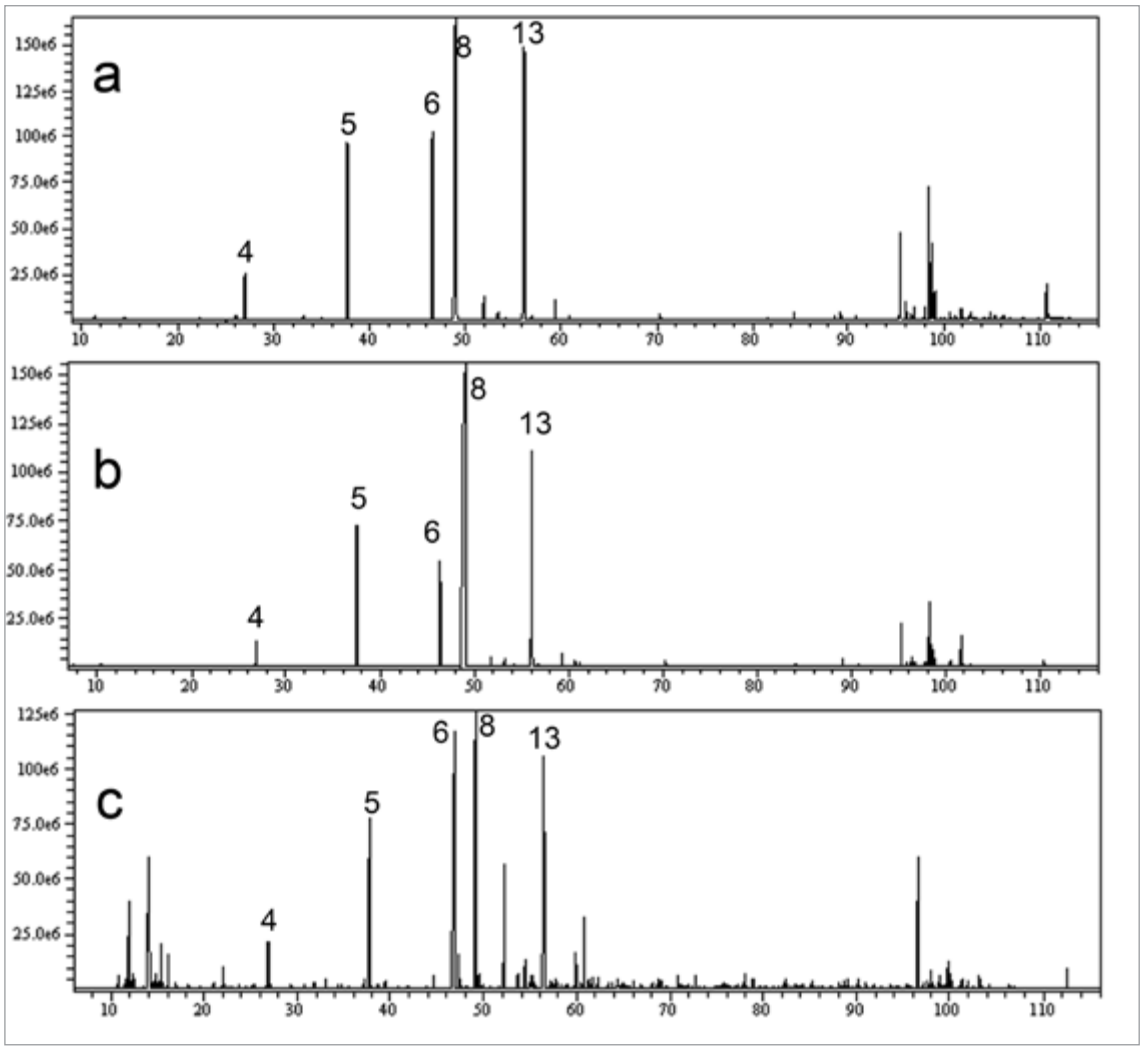

Figure 6.8. TIC of a) PS2L; b) PS4L; c) PS1L. The numbers in the chromatogram correspond to those reported in Table 6.12**.**

Styrene formation increased from PS2L, to PS3L, to PS6L and PS4L even if the MW power did not remain constant. In PS1L the styrene amount was close to that shown in PS2L (42.15 and 47.69 % respectively) if the dilution effect caused by liquids from tire pyrolysis were taken in account.

The formation of α-methylstyrene was not influenced by MW power or apparatus set-up, and it was almost steady in the 11 - 15% range. Other single ring aromatic compounds (toluene and ethylbenzene) were also detected in a narrow distribution range which did not suggest any clear influence of pyrolysis variables tested. Otherwise switching MW absorber from carbon to Fe brought several changes in distribution of compounds other than styrene. P5L contained less α-methylstyrene but a compounds in large amount (11.56%) which was hardly found in other liquid, 3-butene-1,3-diyldibenzene, a possible dimer of styrene. However P7L, always obtained with Fe but using a fractionating system, showed the same amount of α-methylstyrene than any other liquid.

Without a fractionating system styrene was quickly produced and it stayed for a

shorter time at the pyrolysis condition because, as previously reported, Fe rapidly transfers heat to the polymeric feed as heat (see Section 6.1.2)

Additional aromatic compounds were detected such as 1,3-diphenylpropane, and apparently their amount increased by improving the residence time, that is the fractionating system reduces the amount of styrene while increase the amount of 1,3-diphenylpropane. Other aromatics were present in minor amount but an incontrovertible attribution was not possible due to their low amount and similar mass spectra.

An increase of ethylbenzene, cumene and 1,4-dimethylbenzene were shown in PS1L that is in pyrolysis run with tire as MW absorber. These improvements might be attributed to a reaction between intermediates from MAP of PS and tire.

Limonene was present only in liquid when tire was the MW absorber confirming its formation through polyisoprene pyrolysis of rubber present in tires.[2] This hypothesis was supported by the composition of the liquids from PS pyrolysis in the presence of carbon as MW absorber: limonene was never present. Its amount was close in PS1L and T4L if the dilution effect of products from MAP of PS was taken into account. The yield of the main compounds was calculated with the formula: Yield compound (%) = TICarea (%) × Liquid yield (%) and the results are reported in Figure 6.9.

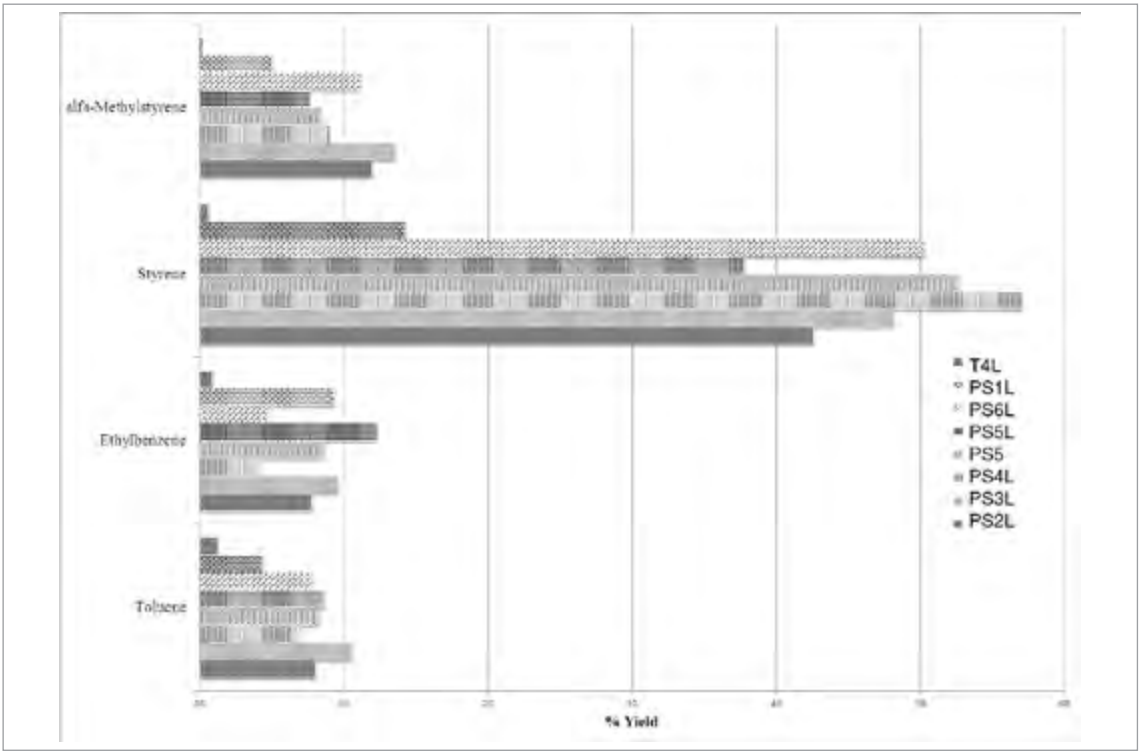

Figure 6.9. Yields calculated for the main aromatic compounds.

This figure gives a clear indication of the efficiency of the reverse polymerization of waste polystyrene.

The GC/MS analyses showed strong differences from the data reported by

Onwudili[11] and Hussain[12, 16, 17] due to different heating technology, in the first case, and to the very high temperature employed by the second author. Furthermore the latter study was obtained working in a flux of N_2 which was not used in this work.

6.3.2.3. FTIR

FTIR spectra of liquids confirmed the GC/MS data, indeed absorptions of aromatic hydrocarbons were the only detected (Table 6.13) in PS2L-PS7L while aliphatic and aromatics hydrocarbons were present in PS1L and T4L.

Table 6.13. IR absorptions of liquid samples[a].

Frequencies	Attribution	T4L	PS1L	PS2L	PS3L	PS4L	PS5L	PS6L	PS7L
3104; 3060	Aromatic C-H stretching	n.d.	m	m	m	m	m	m	m
3082; 3027	Terminal vinyl C-H stretching	w	m	m	m	m	m	m	m
3009	Internal alkene C-H stretching	n.d.	m	w	w	w	w	w	w
2961; 2870	Methyl C-H stretching	s	m	n.d.	w	n.d.	n.d.	n.d.	n.d.
2920; 2860	Methylene C-H stretching	s	m	n.d.	w	n.d.	n.d.	n.d.	n.d.
1691; 1752; 1804; 1877; 1944	Aromatic combination band	w	n.d.	w	w	w	w	w	w
1630	Alkenyl C=C stretching	w	w	s	m	m	m	m	m
1601; 1576; 1495; 1450	C=C-C aryl ring stretching	w	m	s	m	m	m	m	m
1412	Vinyl C-H in-plane bending	n.d.	w	m	w	m	w	w	w
1290	Vinylidene C-H in-plane bending	n.d.	w	w	n.d.	w	w	w	w
1202; 1083; 1028; 1020	Aromatic C-H in-plane bending	w	m	m	m	m	m	m	m
990; 907	Vinyl C-H out-of-plane bending	n.p.	s	s	s	s	s	s	s
840: 774; 755; 748; 731	Aromatic C-H out-of-plane bending	w	s	s	s	s	s	s	s
694	C-C ring bending	w	s	s	s	s	s	s	s

IR analysis showed similar absorptions among liquids obtained in different MAP conditions as shown in Figure 3; strong differences were shown only in spectra

from PS1L and T4L (Figure 6.10d,e), because these spectra were obtained from oil containing the product of tire degradation. These spectra were substantially different in 3200 – 2900 cm^{-1} region from L1, L2 and L4 (Figure 6.10a,b,c) even through a visual evaluation. The absorptions reported in Table 6.13 were in agreement with those reported by Mo et al. [13]

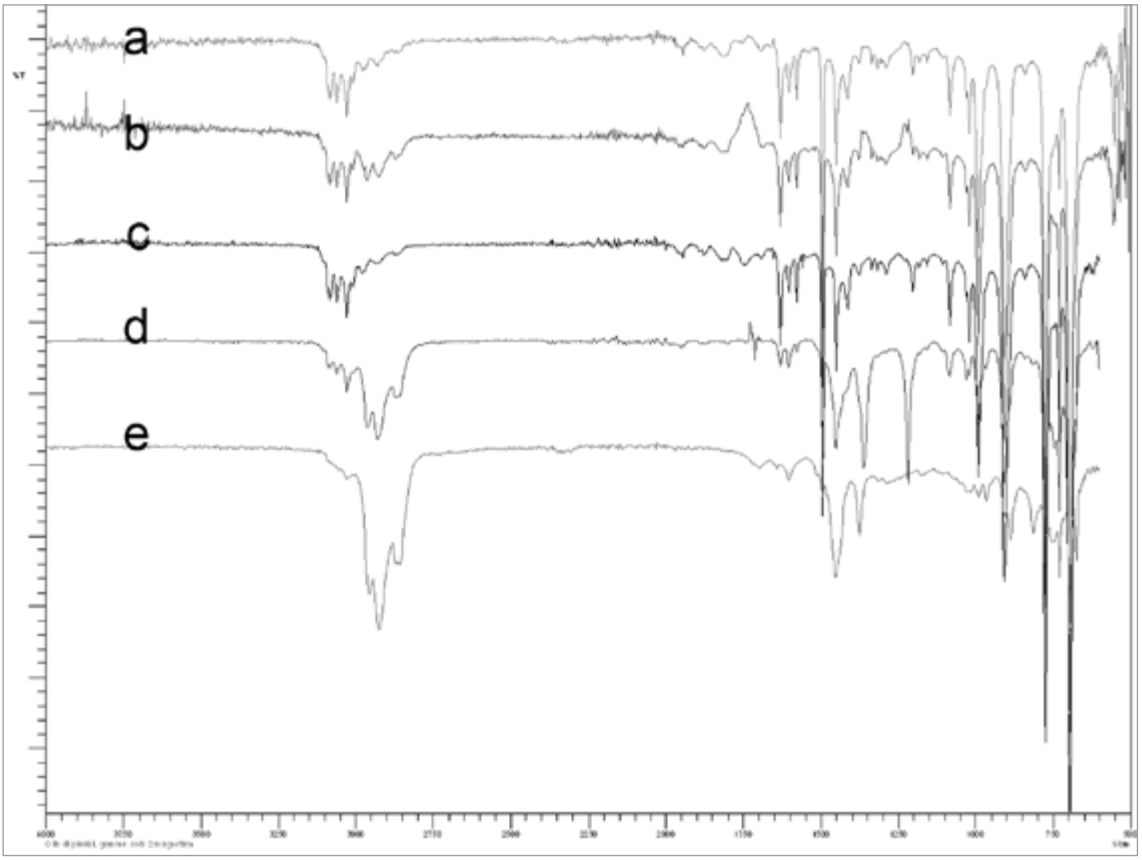

Figure 6.10. FTIR of: a) PS2L; b) PS4L; c) PS6L; d) PS1L; e) T4L.

6.4. Main achievements

Microwave assisted pyrolysis (MAP) of HDPE, PP, and PS was performed using different MW absorbers (tire, carbon, or Fe), apparatus set-up, and MW power, obtaining a high quality liquid fraction with tailoring properties. The main achievements might be summarized in the following key points.

MAP of polyolefins (HDPE and PP) might be carried out with a low MW power obtaining a liquid having a low viscosity, but HDPE was only partially decomposed while PP and PS were fully pyrolyzed. A low viscosity liquid was always formed when a fractionating system was placed on the oven, avoiding to waxy products to leave the reactor. Liquids from MAP of HDPE contained a mixture of linear alkanes, the corresponding 1-alkenes, and a very low amount of aromatics. On the contrary liquids from MAP of PP contained a mixture of methyl branched alkanes and alkenes, some aromatics and dienes. The relative amounts of these products were affected by pyrolysis conditions.

From MAP of PS a clear and low viscosity liquids were always collected together with low amount of gas (3.0 wt %) and solid (0.9 wt %). Styrene in the liquid was increased up to 65.98 % by using a MW power of 3 KW. The liquid shows lower density and viscosity if a fractionating system was inserted between the oven and the coolers due to lower presence of high molecular weight compounds and it contained up to 92.70% of single ring aromatic compounds such as styrene, toluene, ethylbenzene, and α-methylstyrene.

The gas from MAP of HDEP, PP, and PS did not contain neither nitrogen, usually employed as carrier, nor combustion gas present in classical pyrolysis and could be used for energy production without any treatments.

Tire and carbon could be assimilated to pollutant other than MW absorber, and they did not markedly affect the pyrolyses results, but almost only the products composition if some of these materials might be pyrolyzed. In fact some cross reactions between intermediates from PS and tire degradation products were observed. These results let us to affirm that MAP of HDPE, PP, and PS might be performed even when large amount of inorganic and polymeric compounds was present as contaminants.

Finally waste polyolefins may be disposed through MAP pyrolysis obtaining liquids that may be employed as a source of chemicals or fuel without any preliminary treatments.

The environmental burden caused by a polluted waste HDPE, PP, and PS, otherwise difficult to recycle, could be efficiently reduced together with its valorisation by MAP producing large amount of valuable chemicals such as styrene and other aromatics while gas and solid may be used as fuel.

This process is an efficient green chemical approach to waste polymers producing valuable chemicals and avoiding pollution due to some plastic waste.

Reference

1. Undri, A.; Rosi, L.; Frediani, M.; Frediani, P. Efficient Disposal of Waste Polyolefins through Microwave Assisted Pyrolysis. *Fuel* **2013**, 116, 662-671.
2. Cunliffe, A. M.; Williams, P. T. Composition of oils derived from the batch pyrolysis of tyres. *J. Anal. Appl. Pyrol.* **1998**, 44, 131-152.
3. Undri, A.; Meini, S.; Rosi, L.; Frediani, M.; Frediani, P. Microwave Pyrolysis of Polymeric Materials: Waste Tires Treatment and Characterization of the Value-Added Products. *J. Anal. Appl. Pyrol.* **2013**, 103, 149-158.
4. Undri, A.; Sacchi, B.; Cantisani, E.; Toccafondi, N.; Rosi, L.; Frediani, M.; Frediani, P. Characterization of Carbon from Microwave Assisted Pyrolysis of Tires. *J. Anal. Appl. Pyrol.* **2013**, 104, 396-404.
5. Laresgoiti, M. F.; Caballero, B. M.; de Marco, I.; Torres, A.; Cabrero, M. A.; Chomón, M. J. Characterization of the liquid products obtained in tyre pyrolysis. *J. Anal. Appl. Pyrol.* **2004**, 71, 917-934.
6. Russell, A. D.; Antreou, E. I.; Lam, S. S.; Ludlow-Palafox, C.; Chase, H. A. Microwave-assisted pyrolysis of HDPE using an activated carbon bed. *RSC Advances* **2012**, 2, 6756-6760.
7. Aguado, R.; Olazar, M.; José, M. J. S.; Gaisàn, B.; Bilbao, J. Wax Formation in the Pyrolysis of Polyolefins in a Conical Spouted Bed Reactor. *Energy Fuels* **2002**, 16, 1429-1437.
8. Undri, A.; Rosi, L.; Frediani, M.; Frediani, P. Reverse Polymerization of Waste Polystyrene through Microwave Assisted Pyrolysis. *J. Anal. Appl. Pyrol.* **2013**, http://dx.doi.org/doi:10.1016/j.jaap.2013.10.001.
9. Haynes, W. M.: CRC Handbook of Chemistry and Physics; CRC Pr Inc: Colorado, USA, **2011**.
10. Bykov, Y. V.; Rybakov, K. I.; Semenov, V. E. High-temperature microwave processing of materials. *J. Phys. D Appl. Phys* **2001**, 34, R55.
11. Onwudili, J. A.; Insura, N.; Williams, P. T. Composition of products from the pyrolysis of polyethylene and polystyrene in a closed batch reactor: Effects of temperature and residence time. *J. Anal. Appl. Pyrol.* **2009**, 86, 293-303.
12. Hussain, Z.; Khan, K. M.; Hussain, K. Microwave–metal interaction pyrolysis of polystyrene. *J. Anal. Appl. Pyrol.* **2010**, 89, 39-43.
13. Mo, Y.; Zhao, L.; Chen, C.-L.; Tan, G. Y. A.; Wang, J.-Y. Comparative pyrolysis upcycling of polystyrene waste: thermodynamics, kinetics, and product evolution profile. *J. Therm. Anal. Calorim.* **2013**, 111, 781-788.
14. Undri, A.; Rosi, L.; Frediani, M.; Frediani, P.: Microwave Pyrolysis of Polymeric Materials. In Microwave Heating; Chandra, U., Ed.; InTech: Janeza Trdine 9, 51000 Rijeka, Croatia, **2011**; pp 219.
15. Park, J. J.; Park, K.; Kim, J.-S.; Maken, S.; Song, H.; Shin, H.; Park, J.-W.; Choi, M.-J. Characterization of Styrene Recovery from the Pyrolysis of Waste Expandable Polystyrene. *Energy Fuels* **2003**, 17, 1576-1582.
16. Hussain, Z.; Khan, K. M.; Basheer, N.; Hussain, K. Co-liquefaction of Makarwal coal and waste polystyrene by microwave–metal interaction pyrolysis in copper coil reactor. *J. Anal. Appl. Pyrol.* **2011**, 90, 53-55.
17. Hussain, Z.; Khan, K. M.; Perveen, S.; Hussain, K.; Voelter, W. The conversion of waste polystyrene into useful hydrocarbons by microwave-metal interaction pyrolysis. *Fuel Process. Technol.* **2012**, 94, 145-150.

7. Composites, waste multi-layer packaging

Microwave assisted pyrolysis (MAP) waste and/or polluted multi-layer beverage packaging (WMP) is reported in this section. WMP interacted with microwave radiation (MW) and they could be heated to pyrolysis temperature. However heating rate was much lower than using any other MW absorber tested in Section 6 and their mixing with the composite material was necessary to perform MAP in a short time.

7.1. Operating parameters and yields

MAP of WMP was investigated at constant MW power of 3 kW varying two parameters: microwave absorber, and apparatus set-up (Table 7.1).

Table 7.1. Microwave assisted pyrolysis of WMP*.

Entry	Set-up	MW Absorber		WMP	Time	Al		Solid	Liquid Upper phase	Liquid Bottom phase	Gas
		type	*(g)*	*(g)*	*(min)*	*(g)*	*(%)*	*(wt%)*	*(wt%)*	*(wt%)*	*(wt%)*
WMP1	A	-	-	165.4	52	12.0	7.3	31.6	7.8	35.9	24.7
T4	A	Tire	233.3	-	35	-		43.2	42.6	-	14.1
WMP2	A	Tire	61.5	123.0	41	7.4	6.0	34.3	24.3	18.6	22.8
WMP3	A	Carbon	20.1	149.4	40	11.7	7.8	24.9	8.5	24.1	42.5
WMP4	A	Fe	76.8	158.1	27	17.9	11.3	32.4	9.8	33.0	24.8
WMP5	B	Carbon	64.3	154.2	62	12.9	8.4	59.9	6.0	25.0	9.0
WMP6	B	Fe	76.8	155.2	40	14.9	9.6	28.7	8.1	28.5	34.7

* Al residual foils were separated and excluded from yields calculation.

In spite of the use of different pyrolysis conditions the liquid collected formed two phases. The bottom phase was always a clear low viscosity fluid with a color from pale yellow to dark-orange. The upper phase, except for entry 6, was a waxy liquid, solid at room temperature; it was formed by organic products from PE pyrolysis accordingly to data reported in the literature.[1-4]

MAP of WMP has been performed without the addition of a MW absorber, WMP1 (Table 7.1). The absence of an added MW absorber did not affect the pyrolysis behavior and yields were close to those obtained using iron as MW absorber (WMP4). Al of WMP was initially heated by the MW and contributed to heat paper and PE. Furthermore the formation of sparks was observed and nearby paper or PE was pyrolyzed to char which, in turn, was able to absorb MW improving the MW absorbing capacity of the material. Pyrolysis in the presence of an added MW absorber allowed to reduce the reaction time of 30% Using tire as microwave absorber allowed also to verify if MAP could be achieved in the presence of any inorganic and/or organic pollutant. The liquid formed from tire degradation was enclosed in the upper phase, and a higher amount of this organic phase was collected with respect to any other pyrolysis of WMP (WMP2).

Fe as MW absorber reduced considerably the pyrolysis time with respect to carbon or tire (WMP4 and WMP5), confirming its high ability to convert MW into heat ensuing a faster pyrolysis.

Al was always recovered as unscratched material at the end of each experiment (Figure 7.1), suggesting that pyrolysis temperature never exceeded 993 K (Al melting point), not even in spot points close to Al foil.

Figure 7.1. Aluminum recovered after MAP.

Close yields were obtained independently on different MW absorber employed (none, tire, and Fe respectively, WMP1, WMP2, and WMP4). On the contrary in WMP3, performed with carbon, as MW absorber, the bottom liquid fraction and solid were strongly reduced while higher gas yields was obtained.

In WMP5 and WMP6 using set-up B, the fractionating system avoid to high boiling fractions to leave the oven, and the residence time of only high boiling compounds was increased leading to an increase of gas and char formation and a decrease of liquid yield.[5-7] In fact in WMP6 the gas and solid were significantly higher than WMP4. Surprisingly using set-up B and carbon as MW absorber (WMP5) the lowest gas yield and the highest solid one were obtained. Probably pyrolysis intermediates reacted among them and further pyrolyzed yielding char.

Results from WMP6 was in agreement with reported data on cellulose pyrolysis[8-10]: fast heating minimized char formation while slow heating maximized it. So far Fe showed a faster heating and high rate of heat transfer to WMP than carbon.

The bottom liquid phase was the mostly reduced working with set-up B.

The upper liquid phase of WMP6 was a waxy product. It was unexpected, the pyrolysis in the presence of Fe as absorber was very fast (40 min instead of 62 min, WMP6 and WMP5 respectively) and the fractionating system did not prevent the distillation of products having a relatively high molecular weight.

7.2. Liquid products

7.2.1. Physical properties

Physical properties of liquids were reported in Table 7.2; entries are coded as "WMPnL" where "n" is the pyrolysis entry, followed by "-H" for upper phase fraction or "-W" for bottom phase fraction. In T4 where tire was the only pyrolyzed material a homogeneous liquid was obtained.

The physical properties showed that the upper light fractions (WMPnL-H) were composed of hydrocarbons with a water content below 0.1 wt% while the heavy liquid fractions (WMPnL-W) were mainly composed of water (up to 92.6 wt% Table 7.2). Different MW absorber did not considerably affect the physical properties of liquids.

Working with set-up B, the overall amount of water was increased in the bottom phase up to 77.6 wt% (WMP6L-W) and 92.6 wt% (WMP5L-W), because the improved residence time increased the pyrolysis efficiency thus oxygenated hydrocarbons had been further pyrolyzed to CO_x or alkene and water, in agreement to their oxygen content and data reported in the literature.[8,11,12]

Table 7.2. Physical characteristics of liquid obtained by MAP of WMP.

Entry	Set-up	Absorber	Density	Ultimate analyses					C/H molar ratio	Water content
			(g/cm^3)	C (*wt%*)	H (*wt%*)	N (*wt%*)	O (*wt%*)	S (*wt%*)		(*wt%*)
WPM1L-W	A	-	1.089	19.18	10.43	0.50	0.0	69.89	0.15	73.8
WPM1L-H	A	-	-	77.42	12.49	2.64	0.0	7.45	0.52	n.d.
T4L	A	Tire	0.874	86.87	10.12	0.66	0.9	1.45	0.71	n.d.
WPM2L-W	A	Tire	1.073	16.15	7.25	0.00	0.0	76.60	0.19	77.6
WPM2L-H	A	Tire	-	76.45	10.57	1.90	0.0	11.08	0.60	n.d.
WPM3L-W	A	Carbon	1.075	17.41	10.67	0.46	0.0	71.46	0.14	74.1
WPM3L-H	A	Carbon	-	73.13	10.18	0.75	0.0	15.94	0.60	n.d.
WPM4L-W	A	Fe	1.100	21.72	9.78	0.63	0.0	67.87	0.18	63.3
WPM4L-H	A	Fe	-	85.51	12.37	0.64	0.0	1.48	0.58	n.d.
WPM5L-W	B	Carbon	1.022	8.86	10.93	1.26	0.0	78.95	0.07	92.6
WPM5L-H	B	Carbon	0.804	83.13	10.18	0.75	0.0	5.94	0.68	n.d.
WPM6L-W	B	Fe	1.054	14.72	10.35	1.02	0.0	73.91	0.12	77.6
WPM6L-H	B	Fe	-	82.07	12.75	0.92	0.0	4.26	0.54	n.d.

* by difference. n.d.: not detected.

7.2.2. GC/MS analysis

Liquid fractions were analyzed through GC/MS. Compositions were evaluated by the total ion chromatography (TIC) without any response factor correction. WMPnL-H fractions were waxy liquid which solidified at room temperature except for WMP5L-H (Table 7.3). Waxy products were not analyzed by GC/MS because, as previously reported, it was not possible to introduce them in the chromatograph and probably they were not vaporized nor eluted. In Table 7.4 are reported the main organic products present in the heavy liquid fractions (WMPnL-W); water was excluded from the composition.

The main classes of products in WMP5L-H (Table 7.3) were linear alkanes and

1-alkenes due to PE pyrolysis according to data reported in the literature.[13-16] They were formed by direct cleavage of carbon-carbon bonds. It was not surprising that a C25 hydrocarbon was the longest one, because the use of a fractionating system improved the residence time of long chain compounds and promoted their pyrolysis.[5,7] Anyway the presence of cyclic and aromatic compounds was unexpected because Undri et al. (Section 6) did not found these compounds in MAP of high density polyethylene (HDPE) working in the same conditions, also if a fractionating system was used.[7] Their wide presence could be explained by low density polyethylene (LDPE) pyrolysis or interaction with cellulose products during pyrolysis. In fact branched PE such as LDPE are usually employed to prepare films used for WMP as confirmed by FTIR of the plastic layer of the WMP employed. Furthermore LDPE might pyrolyze in a way very close to PP where aromatic compounds are formed. In fact LDPE contains large amount of tertiary carbons with respect to HDPE and an intermediate behavior between HDPE and PP may be expected. On the other hand aromatics may be formed through an interaction between cellulose and PE intermediates inside the reactor. It is in fact reported that cellulose is extremely reactive and during pyrolysis produces large amount of radicals. These intermediates could be involved in reactions with other molecules such as PE to give cyclization and aromatization reactions.[11] These latter reactions are enhanced in MAP when an active carbon was used as MW absorber as a very efficient heat transfer agents.[13] Single ring aromatic compounds were the main products present in these fractions, however also indene, naphthalene, and their methyl derivates were formed. Also some products from cellulose pyrolysis were found in this fraction (2-methylfuran, 3-methylbut-3-en-2-one, 2,5-dimethylfuran, furfural, cyclohexanone, 5-methylfuran-2-carbaldehyde, and phenol). They showed higher affinity with the hydrocarbon fraction than to water.

Table 7.3. Compounds identified in WMP5L-H from MAP of WMP by GC/MS analyses.*

Entry	Compound	Area (%)	Entry	Compound	Area (%)
1	But-1-ene	0.3	40	Indene	0.7
2	Acetone	0.3	41	3-Methylphenol	0.7
3	Pent-1-ene	0.5	42	Undec-1-ene	3.6
4	Pentane	0.4	43	Undecane	2.7
5	Pent-2-ene	0.3	44	1-Methyl-1H-indene	0.6
6	Butan-2-one	0.4	45	Naphatalene	1.1
7	Hex-1-ene	2.3	46	Dodec-1-ene	2.3
8	2-Methylfuran	0.3	47	Dodecane	2.5
9	Hex-2-ene	0.4	48	Tridec-ene	1.5
10	Methylcyclopentane	0.3	49	1-Methylnaphtalene	0.7
11	3-Methylcyclopentene	0.4	50	Tridecane	1.7

(continue)

12	Benzene	1.9	51	2-Methylnaphtalene	0.8
13	3-Methylbut-3-en-2-one	0.3	52	Bipheyl	0.3
14	Cyclohexene	0.3	53	Tetradec-1-ene	1.1
15	2-Methylhex-ene	0.3	54	Tetradecane	1.3
16	Hept-1-ene	2.5	55	Pentadec-1-ene	1.0
17	2,5-Dimethylfuran	0.3	56	Pentadecane	1.1
18	Heptane	2.1	57	Hexadec-1-ene	0.8
19	Hept-2-ene	0.5	58	Hexadecane	0.8
20	Methylcyclohexane	0.4	59	Heptadec-1-ene	0.5
21	Toluene	3.6	60	Heptadecane	0.8
22	1-Methylcyclohexene	0.4	61	Octadec-1-ene	0.4
23	Oct-1-ene	3.0	62	Octadecane	0.6
24	Octane	2.5	63	Nonadec-1-ene	0.3
25	Furfural	0.3	64	Nonadecane	0.5
26	Oct-2-ene	0.5	65	Eicos-1-ene	0.3
27	Cyclohexanone	0.3	66	Eicosane	0.5
28	Ethylbenzene	2.6	67	Henicos-1-ene	0.4
29	1,4-Dimethylbenzene	1.0	68	Henicosane	0.3
30	Styrene	2.3	69	Docos-1-ene	0.4
31	1,2-Dimethylbenzene	1.7	70	Docosane	0.4
32	Non-1-ene	3.4	71	Tricos-1-ene	0.1
33	Nonane	2.5	72	Tricosane	0.3
34	5-Methylfuran-2-carbaldehyde	0.5	73	Tetracos-ene	0.1
35	Propylbenzene	0.7	74	Tetracosane	0.2
36	Phenol	0.3	75	Pentacos-1-ene	0.1
37	1-Ethyl-3-methylbenzene	1.2	76	Pentacosane	0.4
38	Dec-1-ene	4.1			
39	Decane	2.7		**Total identified**	79.6

* Compositions were reported by percent peak areas without any response factors correction; other peaks in concentration lower than 0.1 % were not reported.

On the other hand Russell et al.[13] reported in pyrolysis of HDPE different amounts of alkane/alkene and aromatics working with MAP at different temperatures, when active carbons were used as MW absorber. Over 773 K they reported a rising abundance of cyclo- and branched alkenes while working at 873 K aromatics were present up to 45.3 % of the overall compounds. The different results obtained may be attributed to an efficient interaction between PE and cellulose intermediates or to the different operating system.

The main component of the bottom phase was water (Table 7.2) and it was not detected by GC/MS nor considered in the composition reported in Table 7.4. Almost all listed substances were those usually identified and reported for classical pyrolysis of cellulose.[8,17-20]

Table 7.4. Compositions of heavy liquid phases by GC/MS analyses from MAP of WMP.*

Entry	Substance	WMP1L-W	WMP2L-W	WMP3L-W	WMP4L-W	WMP5L-W	WMP6L-W
1	Acetaldehyde	1.0	1.2	1.8	0.6	3.5	0.9
2	Acetone	1.8	2.0	3.8	1.3	7.1	2.6
3	2-Oxopropanal	1.3	0.5	1.3	0.2	0.6	0.0
4	Formic acid	3.1	1.9	2.0	2.3	0.0	4.0
5	2-Hydroxyacetaldehyde	0.8	0.3	0.0	0.0	0.0	0.0
6	Acetic acid	10.6	10.3	16.5	3.5	23.3	4.8
7	1-Hydroxypropan-2-one	9.6	9.4	13.7	10.4	15.1	25.9
8	1-Hydroxybutan-2-one	2.6	1.6	2.9	1.2	2.2	1.2
9	Furfural	1.6	1.4	2.0	1.1	4.1	2.3
10	2-Furanmethanol	2.5	3.2	3.1	1.3	3.9	3.4
11	2(5H)-Furanone	3.0	2.0	3.2	2.7	1.0	4.6
12	Cyclohexanone	3.8	2.3	4.2	4.0	0.7	4.6
13	3-Methylcyclopenta-1,2-dione	2.3	1.5	2.3	3.1	0.0	4.4
14	2-Methylphenol	1.4	0.9	2.0	0.5	0.3	1.9
15	2-Propenyl butanate	2.0	0.3	0.5	3.6	0.0	0.0
16	Unidentified alcohol	5.7	4.2	4.3	8.0	0.0	1.2
17	5-(Hydroxymethyl)-2-furancarboxaldehyde	1.1	0.8	1.0	0.9	0.0	0.0
18	1,6-Anhydro-β-D-glucopyranose (Levuglucosan)	4.9	1.9	2.3	0.0	0.0	0.0
	Total identified	59.1	45.4	67.1	44.7	61.7	61.8

* Compositions were reported by percent peak areas without any response factors correction; other peaks in concentration lower than 0.1 % were not reported.

Levuglucosan was collected in low amount with respect to other reported pyrolysis.[8,17,21,22] It might be further degraded after its formation in appropriate pyrolysis conditions[9,17] suggesting that samples were heated at higher temperature or for a prolonged time. As a confirm to this suggestions levuglucosan was not present in the liquid obtained from pyrolysis performed with set-up B. Furthermore 1,6-anhydro-β-glucofuranose and glyceraldehyde also are widely reported as cellulose pyrolysis products[17] but they were not identified among products formed. Probably these compounds were completely pyrolyzed or they were not formed in the conditions tested.

Several effects were accountable to the MW absorber. WMP2L-W contained water soluble products from tire degradation and pyrolysis of cellulose. Carbon as MW absorber with set-up A (WMP3L-W) was able to promote a more efficient

pyrolysis than the Al present in WMP as the sole MW absorber (WMP1L-W). Indeed lower amount of levuglucosan and other heavy compounds were found in low extent together with low molecular weight products such as acetaldehyde, acetone, and in higher amount acetic acid, and 1-hydroxypropan-2-one. WMP5L-W, obtained with set-up B and carbon as MW absorber, showed even lower amount of heavy pyrolyzable compounds and the highest amount of acetic acid.

Fe as MW absorber showed other effects. Levuglucosan, if formed, was always further pyrolyzed and it was not found even in trace (WMP4L-W), suggesting a very efficient heating or its Fe catalyzed decomposition. Also acetic acid was present in lower amounts (3.51 - 4.84 %, WMP4L-W and WMP6L-W respectively). Fe might work as a catalyst for pyrolysis or it reacted with organic acid present in the reaction medium. It contributed to reduce the amount of free acid and, somehow, to upgrade the quality of this fraction.

7.2.3. FT-IR analysis

FTIR spectra were recorded on heavy and light fractions. Spectra of upper phase of each liquid did not show remarkable water absorption (Table 7.5). Only WMP1L-H showed medium intensity water absorptions due to small amount of water swallowed by the wax present (Figure 7.2).

Table 7.5. FTIR absorption of upper liquid phases, WMPnL-H**.***

Frequency *(cm^{-1})*	**Attribution**	**WMP1L-H**	**T4L**	**WMP2L-H**	**WMP3L-H**	**WMP4L-H**	**WMP5L-H**	**WMP6L-H**
3475	Alcohol O-H stretching	m	n.d.	n.d.	m	m	n.d.	w
3078, 3020	Terminal vinyl C-H stretching	w	w	w	w	w	w	w
2957, 2872	Methyl C-H stretching	m	s	s	m	m	m	m
2924, 2854	Methylene C-H stretching	m	s	s	m	m	s	s
1710	Carboxylic/ketone C=O	s	n.d.	m	s	s	m	s
1668	Conjugated C=O	w	n.d.	w	w	w	w	w
1640	Alkenyl C=C stretching	w	w	w	w	w	w	w
1496, 1457	C=C-C aryl ring stretching	m	w	m	m	m	m	m
1407, 1366	Phenol or tertiary alcohol O-H bending	m	n.d.	m	m	m	w	m
1279	Primary or secondary O-H in-plane bending	m	n.d.	w	m	m	w	w
1238, 1193	Phenol C-O stretching	m	n.d.	w	m	m	w	w
1202; 1083, 1028, 1020	Aromatic C-H in-plane bending	m	w	w	m	m	w	w
1080	Secondary alcohol, C-O stretching	m	n.d.	w	m	m	n.d.	w
1050, 1039	Primary alcohol C-O stretching	s	n.d.	w	s	s	w	w

(continue)

840, 774, 755, 748, 731	Aromatic C-H out-of-plane bending	m	w	m	m	m	w	m
694	C-C ring bending	m	w	m	m	m	w	m
615 br	Alcohol O-H out-of-plane bending	w	n.d.	n.d.	w	w	n.d.	n.d.

* Absorption intensities: s: strong; m: medium; w: weak; br: broad; n.d.: not detected.

FTIR spectra confirmed the prevailing presence of alkane and alkene in WMPnL-H fractions. However noteworthy absorptions of alcohols and phenols groups were incontrovertibly evidenced. Probably some aromatic and alcoholic substances had higher affinity for this hydrocarbon phase than the aqueous one as confirmed also by GC/MS data.

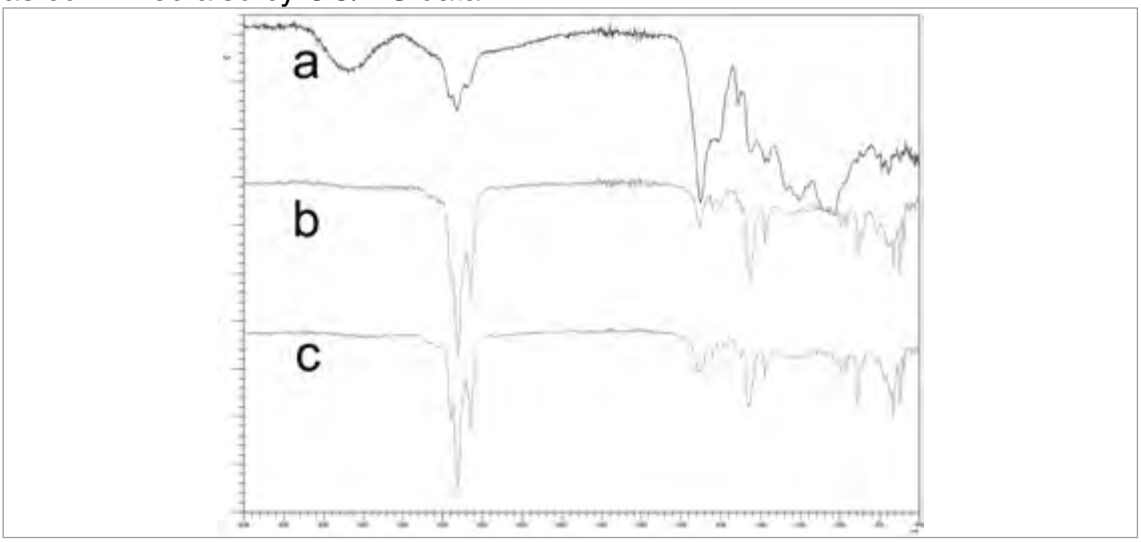

Figure 7.2. FTIR spectra of: a. WMP1L-H; b. WMP2L-H; c. WMP5L-H.

Bottom phase showed strong water absorption bands which overwhelm any other absorption. Thus FTIR spectrum of pure water was subtracted from spectra of WMPnL-W (Figure 7.3) to remove water absorptions; the residual absorptions and their relative attributions are reported in Table 7.6.

Table 7.6. FTIR absorptions of heavy liquid phases, WMPnL-W. *

Frequency *(cm^{-1})*	**Attribution**	**WMP1L-W**	**WMP2L-W**	**WMP3L-W**	**WMP4L-W**	**WMP5L-W**	**WMP6L-W**
3475	Alcohol O-H stretching	m	s	m	m	m	m
2954, 2886	Methyl C-H stretching	m	m	m	m	w	w
1712	Carboxylic/ketone C=O	s	s	s	s	s	s
1668	Conjugated C=O	m	m	m	w	m	m
1407, 1366	Phenol or tertiary alcohol O-H bending	w	m	m	m	m	m
1279	Primary or secondary O-H in-plane bending	w	m	m	m	s	m

(continue)

1238, 1193	Phenol C-O stretching	w	m	m	m	m	m
1080	Secondary alcohol, C-O stretching	s	s	s	m	s	s
1050, 1039	Primary alcohol C-O stretching	s	s	s	m	s	s
615 broad	Alcohol O-H out-of-plane bending	w	s	s	s	s	s

* Absorption intensities: s: strong; m: medium; w: weak.

WMPnL-W fraction contained large amount of water soluble compounds which included the following functional groups: alcohols, carbonyls, carboxyls, and phenols in agreement with by GC/MS analyses (Section 7.2.2). Medium/weak absorptions of methyl group were always present. They intensities were weaker in WMP5L-W and WMP6L-W; because these liquids were collected with set-up B and the methyl containing intermediates were further pyrolyzed.

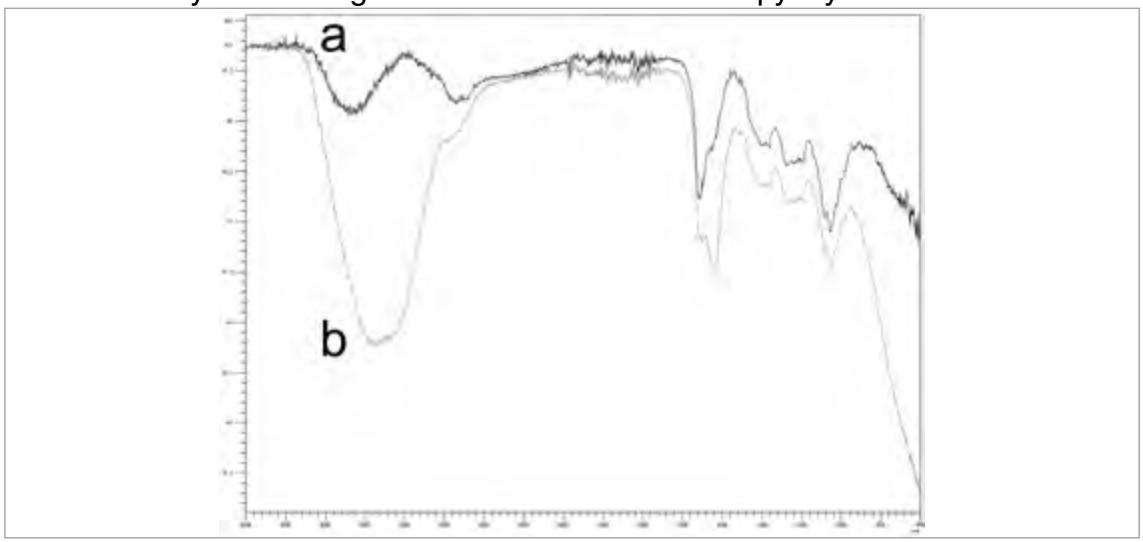

Figure 7.3. FTIR spectra of a: WMP4L-W, water spectrum subtracted; b: WMP4L-W.

7.2.4. ^{1}H NMR

WMPnL-H fractions were also analyzed via ^{1}H-NMR (Figure 7.4). Distribution of different proton classes (aromatics, paraffins, and olefins) were evaluated using Myers equation;[23] the chain length of linear alkanes from PE pyrolysis was evaluated through the following equation: Chain Length = $2 + 3(I_i/I_t)$.

Where I_i was the integral of the internal -CH_2- groups (δ: 1.10 - 1.45 ppm) and I_t was the integral of the terminal -CH_3 groups (δ: 0.60 - 1.00 ppm). These data are summarized in Table 7.7.

Table 7.7. Proton distribution and medium chain length of a linear alkane from ^{1}H-NMR.

	WMP1L-H	T4L	WMP2L-H	WMP3L-H	WMP4L-H	WMP5L-H	WMP6L-H
Aromatics *(vol%)*	16.0	21.7	17.4	9.3	5.7	20.2	10.9
Paraffins *(vol%)*	70.6	47.3	54.1	63.7	75.5	53.6	64.8
Olefins *(vol%)*	13.4	31.0	28.5	27.0	18.9	26.2	24.2
Chain Length *(n° of atoms)*	18.8	-	8.2	18.5	22.5	16.0	17.1

The presence of aromatics (5.7 - 32.7%) was in agreement with GC/MS data. As above hypothesized, pyrolysis of cellulose produced large amount of radicals intermediates which might reacted with PE degradation products to form aromatics.

The presence of olefins was in agreement with GC/MS data and results reported in the literature.[7,13] In fact the main pyrolysis products of PE are alkanes and 1-alkenes together with minor amount of aromatics and cyclic hydrocarbons.[7] Pyrolysis performed with Fe as MW absorber showed a lower amount of aromatics; probably the faster heating, already described, improved the gas formation and reduced the residence time (shortest pyrolysis time, Table 7.1). So far aromatization reaction occurred in minor extent.

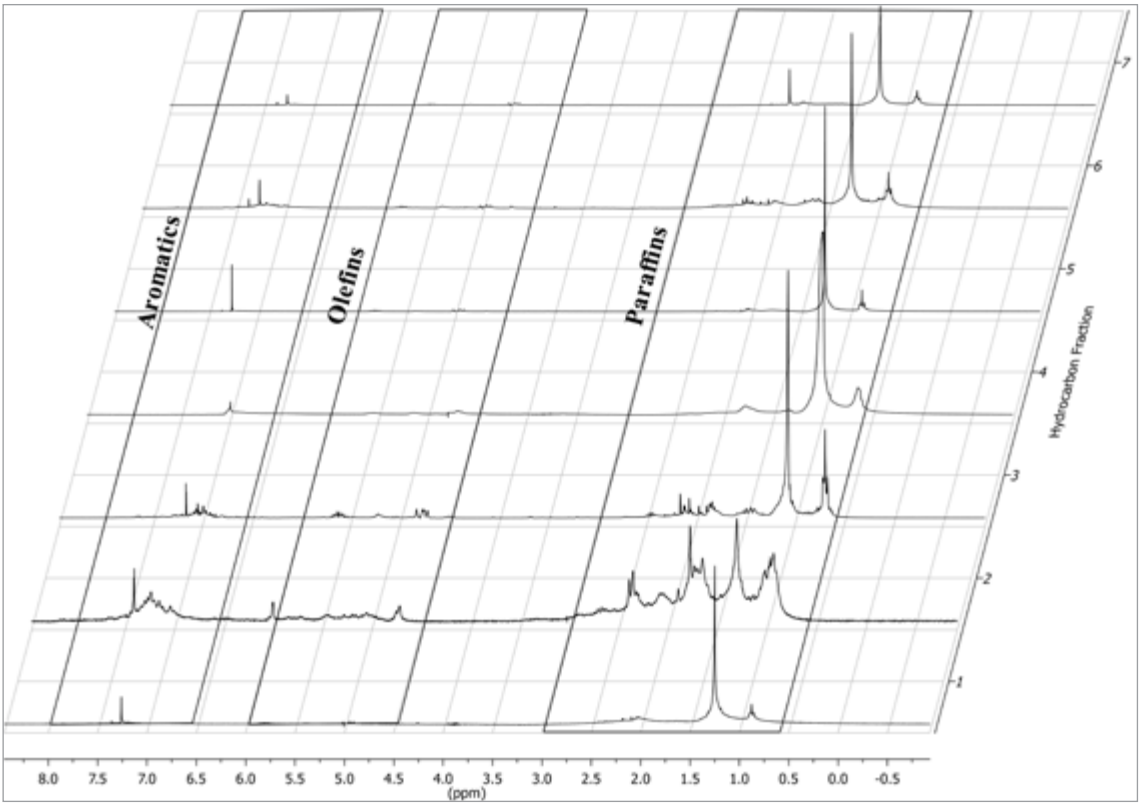

Figure 7.4. ^{1}H-NMR of LnH where n is the number reported in ordinates.

The chain length, evaluated through ^{1}H-NMR was reported in Table 7.7 even if it was an approximate value (alkene presence was not taken in account) but

it allowed a good assessment of pyrolysis efficiency. The presence of carbon as MW absorber did not show any difference with respect to pyrolysis run without MW absorber. A heating efficiency was achieved in both cases. Fe heated faster PE in WMP than carbon, but the fast heating is presumably the cause of the presence of products having longer chains and a waxy behavior. Compounds having up to 23 atoms per chain were evidenced for WMP5L-H in agreement with GC-MS analyses.

Liquid from MAP of WMP using tire as MW absorber showed the shortest chain length of hydrocarbons because products from tire degradation are mixed with those from PE pyrolysis already shown by GC-MS analysis.

Working with set-up B, as expected, improved the overall pyrolysis efficiency and the chain length of compounds was reduced.

WMPnL-W fractions were also analyzed via ^{1}H-NMR (Figure 7.5). Distribution of different proton classes were assigned as follow (partially using ranges reported by Özbay et al.[24]): δ 13.0-12.0 (mobile proton of carboxylic acid); 10.0-9-0 (aldehyde); 9.0-6.5 (aromatic, furan, and C=CH-OCC); 6.5-5.0 (phenolic "OH" or C=CH olefins); 5.0-3.3 (CH_2-O-C; or CH_2-OOC; or ring-join methylene, Ar-CH_2-Ar); 3.3-2.0 (CH_3, CH_2, and CH on aromatic ring); 2.0-1.6 (CH, CH_2 of alkyl gropus; CH_2 and CH in β position to an aromatic ring); 1.6-1.0 (CH_2, CH_3 of alkyl groups, CH_3 in β position and CH_2 and CH in γ position to an aromatic ring or ether oxygen); 1.0-0-5 (CH_3 of alkyl groups or in γ position or further of an alkyl chain linked to an aromatic ring).

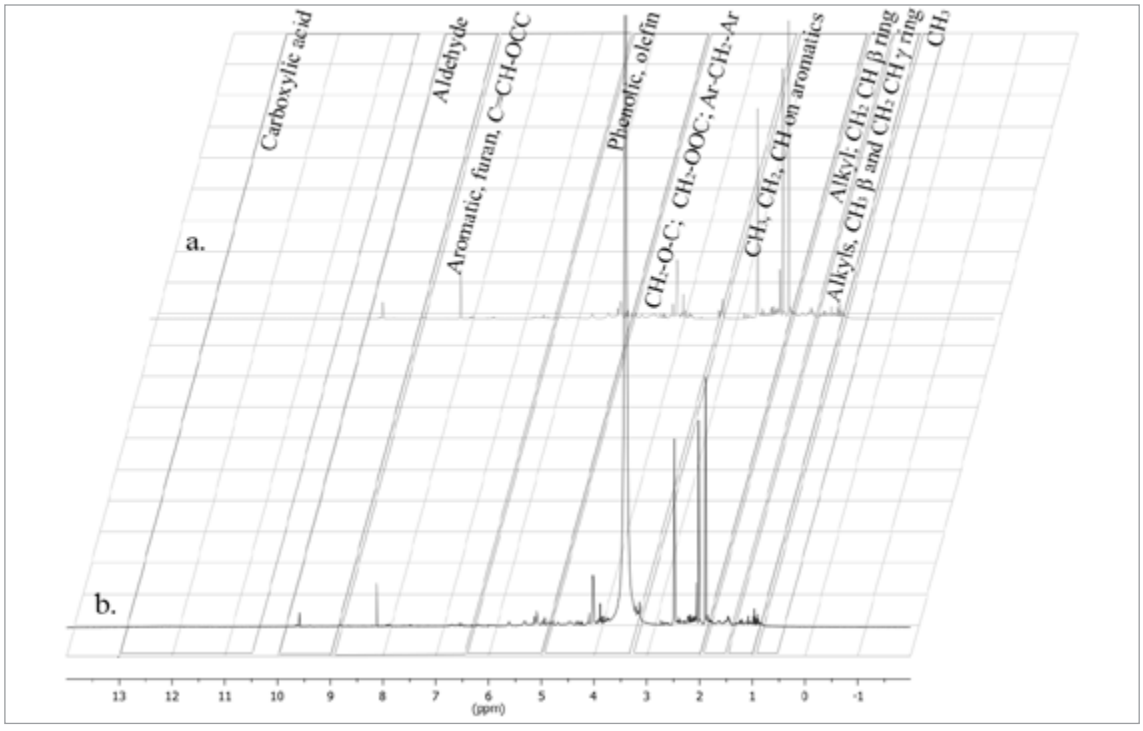

Figure 7.5. ^{1}H NMR spectrum of WMP2L-W (b) and its relative water subtract spectrum (a) together with the integral region.

Integrals of ^{1}H NMR spectra of WMPnL-W fractions are reported in Table 5, they were calculated after subtracting the water peak, and then integrals were normalized to 1000.0.

Table 7.8. Normalized areas of water fractions.

Hydrogen class	Mobile proton from carboxylic acids	Aldehydes	Aromatic, furan, and C=CH-OCC	Phenolic "OH" or C=CH olefins	CH_2-O-C; or CH_2-OOC; or ring-join methylene, Ar-CH_2-Ar	CH_3, CH_2, and CH on aromatic ring	CH, CH_2 alkyl gropus; CH_2, CH β to an aromatic ring	CH_2, CH_3 alkyl groups, CH_3 in β and CH_2, CH in γ to an aromatic ring or ether oxygen	CH_3 of alkyl groups or in γ or further of an alkyl chain linked to an aromatic ring
Chemical shift (ppm)	13.0-12.0	10.0-9.0	9.0-6.5	6.5-5.0	4.5-3.3	3.3-2.0	2.0-1.6	1.6-1.0	1.0-0.5
Entry									
WMP1L-W	0.1	11.8	35.5	98.5	217.7	328.9	143.7	115.9	47.9
WMP2L-W	0.2	9.3	41.9	120.9	239.9	260.3	162.8	115.2	49.4
WMP3L-W	0.1	9.7	26.0	43.2	297.2	340.2	146.2	98.0	39.3
WMP4L-W	12.2	58.7	188.1	187.4	196.1	226.6	61.6	49.0	20.3
WMP5L-W	0.1	7.9	18.4	7.3	112.1	435.6	224.2	107.7	86.8
WMP6L-W	0.0	13.0	40.3	54.5	260.4	350.7	154.2	74.7	52.1

The signal of acid protons was barely noticeable from background, if present they were in very low amount and hardly discriminated. Also aldehydes integrals were weakly present suggesting that the medium strength carbonyl band in FTIR was probably attributable to ketones. The strongest signals were those related to protons close to oxygen or aromatic moieties. These data were in agreement with GC/MS and FTIR analyses. All results reported in Table 7.8 were very close among them suggesting a weak influence of the reaction condition over products distribution. Only WMP4L-W showed some remarkable differences. Indeed aldehydes and furans were more abundant, probably the simultaneous use of set-up A and Fe as MW absorber promoted slightly different reaction path than in any other conditions.

7.3. Gas product

Gas was mainly constituted by C1 – C3 hydrocarbons and CO_x, while several C4 hydrocarbons were identified as minor products. Hydrocarbon was mainly formed from PE pyrolysis; while CO_x were due to cellulose degradation products accordingly to literature.[8,17,25] CO_2 amount was improved enhancing the residence time. Indeed total amount of CO_2 was 0.087 and 0.113 mol respectively for WMP4 and WMP6.

7.4. Solid product

Solid residues were mainly constituted by MW absorber, Al, and char formed by WMP residue (except for WMP1, where only Al and WMP residue were present). Solid from WMP1, did not had any MW absorber and it was composed of Al and residue of paper foils (Figure 7.1a). It contained high amount of ash (17% for solid, from WMP1, Al foil depleted) from paper manufacturing and an ultimate composition of C: 66.0%, H: 1.0%, and N: 0.5% suggesting a formulation $C_{11}H_2N_{0.08}O_4$.

7.5. Main achievements

Fuel has been obtained, even in relatively low amount by waste and/or polluted multi-layer beverage packaging (WMP) through microwave assisted pyrolysis (MAP). Two apparatus set-up and three MW absorbers (tire, powder of carbon or Fe) were tested. The main achievements of this research are:

Microwave assisted pyrolysis (MAP) of WMP might by run with or without a MW absorber, and five products were always collected: char, gas, unscratched Al, and two liquid fractions.

Fe promoted a faster pyrolysis than the others MW absorbers, and avoided the formation of large amount of cyclic and aromatic compounds from PE layers. Furthermore Fe let a better pyrolysis of anydrosugars and acids from paper pyrolysis.

Pyrolysis time with carbon as MW absorber was higher than using any other absorbers, and is allowed cross reaction between paper and PE degradation products enhancing aromatics formation.

An organic liquid fraction containing large amount of hydrocarbons, useful as fuel or the source of chemicals might be obtained, even in limited amount, using set-up B. Also a liquid containing large amount of water was recovered from the heavy liquid fraction. It contained large amounts of oxygenated organic compounds, such as acetic acid, and 2-hydroxypropan-2-one as the main components.

A fractionating system (set-up B), inserted between the oven and the condensing system increases the residence time of high M_w products in the oven. As a consequence char formation was enhanced together with the pyrolysis efficiency and large amount of compounds having a lower molecular weight were formed than pyrolysis ran without the fractionating system, that is liquid shows better performances as fuel.

Reference

1. Ludlow-Palafox, C.; Chase, H. A. Microwave-Induced Pyrolysis of Plastic Wastes. *Ind. Eng. Chem. Res*. **2001**, 40, 4749-4756.
2. Arabiourrutia, M.; Elordi, G.; Lopez, G.; Borsella, E.; Bilbao, J.; Olazar, M. Characterization of the waxes obtained by the pyrolysis of polyolefin plastics in a conical spouted bed reactor. *J. Anal. Appl. Pyrol.* **2012**, 94, 230-237.
3. Elordi, G.; Olazar, M.; Lopez, G.; Artetxe, M.; Bilbao, J. Product Yields and Compositions in the Continuous Pyrolysis of High-Density Polyethylene in a Conical Spouted Bed Reactor. *Ind. Eng. Chem. Res.* **2011**, 50, 6650-6659.
4. Elordi, G.; Olazar, M.; Lopez, G.; Amutio, M.; Artetxe, M.; Aguado, R.; Bilbao, J. Catalytic pyrolysis of HDPE in continuous mode over zeolite catalysts in a conical spouted bed reactor. *J. Anal. Appl. Pyrol.* **2009**, 85, 345-351.
5. Undri, A.; Rosi, L.; Frediani, M.; Frediani, P. Upgraded Fuel from Microwave Assisted Pyrolysis of Waste Tire. *Fuel* **2014**, 115, 600-608.
6. Undri, A.; Rosi, L.; Frediani, M.; Frediani, P. Reverse Polymerization of Waste Polystyrene through Microwave Assisted Pyrolysis. *J. Anal. Appl. Pyrol*. **2013**, http://dx.doi.org/doi:10.1016/j.jaap.2013.10.001.
7. Undri, A.; Rosi, L.; Frediani, M.; Frediani, P. Efficient Disposal of Waste Polyolefins through Microwave Assisted Pyrolysis. *Fuel* **2013**, 116, 662-671.
8. Lin, Y.-C.; Cho, J.; Tompsett, G. A.; Westmoreland, P. R.; Huber, G. W. Kinetics and Mechanism of Cellulose Pyrolysis. *J. Phys. Chem. C* **2009**, 113, 20097-20107.
9. Ronsse, F.; Bai, X.; Prins, W.; Brown, R. C. Secondary reactions of levoglucosan and char in the fast pyrolysis of cellulose. *Environ. Prog. Sustain. Energy* **2012**, 31, 256-260.
10. Wang, Y.; Li, X.; Mourant, D.; Gunawan, R.; Zhang, S.; Li, C.-Z. Formation of Aromatic Structures during the Pyrolysis of Bio-oil. *Energy Fuels* **2012**, 26, 241–247.
11. Korkmaz, A.; Yanik, J.; Brebu, M.; Vasile, C. Pyrolysis of the tetra pak. *Waste Manage.* **2009**, 29, 2836-2841.
12. Liu, C.; Huang, J.; Huang, X.; Li, H.; Zhang, Z. Theoretical studies on formation mechanisms of CO and CO_2 in cellulose pyrolysis. *Comp. Theor. Chem.* **2011**, 964, 207-212.
13. Russell, A. D.; Antreou, E. I.; Lam, S. S.; Ludlow-Palafox, C.; Chase, H. A. Microwave-assisted pyrolysis of HDPE using an activated carbon bed. *RSC Advances* **2012**, 2, 6756-6760.
14. Mastral, F. J.; Esperanza, E.; Garcìa, P.; Juste, M. Pyrolysis of high-density polyethylene in a fluidised bed reactor. Influence of the temperature and residence time. *J. Anal. Appl. Pyrol.* **2002**, 63, 1-15.
15. Kim, S.-S.; Kim, S. Pyrolysis characteristics of polystyrene and polypropylene in a stirred batch reactor. *Chem. Eng. J.* **2004**, 98, 53-60.
16. Kaminsky, W.; Zorriqueta, I.-J. N. Catalytical and thermal pyrolysis of polyolefins. *J. Anal. Appl. Pyrol.* **2007**, 79, 368-374.
17. Shen, D. K.; Gu, S. The mechanism for thermal decomposition of cellulose and its main products. *Bioresour. Technol.* **2009**, 100, 6496-6504.
18. Zhang, X.; Yang, W.; Blasiak, W. Kinetics of levoglucosan and formaldehyde formation during cellulose pyrolysis process. *Fuel* **2012**, 96, 383-391.
19. Mettler, M. S.; Mushrif, S. H.; Paulsen, A. D.; Javadekar, A. D.; Vlachos, D. G.; Dauenhauer, P. J. Revealing pyrolysis chemistry for biofuels production: Conversion of cellulose to furans and small oxygenates. *Energ. Environ. Sci.* **2012**,

5, 5414-5424.
20. Sánchez-Jiménez, P.; Pérez-Maqueda, L.; Perejón, A.; Pascual-Cosp, J.; Benítez-Guerrero, M.; Criado, J. An improved model for the kinetic description of the thermal degradation of cellulose. *Cellulose* **2011**, 18, 1487-1498.
21. Choi, S.-S.; Kim, M.-C.; Kim, Y.-K. Influence of silica on formation of levoglucosan from carbohydrates by pyrolysis. *J. Anal. Appl. Pyrol.* **2011**, 90, 56-62.
22. Patwardhan, P. R.; Satrio, J. A.; Brown, R. C.; Shanks, B. H. Product distribution from fast pyrolysis of glucose-based carbohydrates. *J. Anal. Appl. Pyrol.* **2009**, 86, 323-330.
23. Myers, M. E.; Stollstelmer, J.; Wims, A. M. Determination of Hydrocarbon-Type Distribution' and Hydrogen/Carbon Ratio of Gasolines by Nuclear Magnetic Resonance Spectrometry. *Anal. Chem.* **1975**, 47, 2010-2015.
24. Özbay, N.; Pütün, A. E.; Pütün, E. Structural analysis of bio-oils from pyrolysis and steam pyrolysis of cottonseed cake. *J. Anal. Appl. Pyrol.* **2001**, 60, 89-101.
25. Paulsen, A. D.; Mettler, M. S.; Vlachos, D. G.; Dauenhauer, P. J. The Role of Sample Dimension and Temperature in Cellulose Pyrolysis. *Energy Fuels* **2013**, 27, 2126–2134.

8. Biomasses, wood pellets

Microwave assisted pyrolysis (MAP) of wood pellets (WP). MAP of WP was exploited by varying four parameters: set-up, MW power, MW absorber, and mixing protocol between WP and MW absorber.

8.1. Operating conditions and yields

WP were able to interact with MW radiation even without a MW absorber, and they were transformed into three products: liquid (also known as bio-oil), gas, and char.

When MAP was carried out in the presence of a MW absorber (carbon or Fe) and MW were turned on, WP did not melt and they did not amalgamate with MW absorber because WP contained non-thermoplastic polymer.[1,2] MW absorber remained on the outer surface of pellets and at the end of pyrolysis WP kept their former shape and they could be quantitatively separated from the MW absorber. Manual separation was achieved by splitting up the residual WP, when carbon was the MW absorber, or with the aid of a magnet, when Fe was the MW absorber (Figure 8.1b).

Figure 8.1. WP after pyrolysis: a) from WP2, no MW absorber; b) from WP6, carbon was the MW absorber; c) from WP12, Fe was the MW absorber.

The mixing protocol between WP and MW absorber might be of crucial importance to control the final products characteristics because a different distribution of the MW absorber on the surface of WP might influence final properties of products. Indeed three way of mixing the MW absorber with WP was tested: none, the MW absorber were simply transferred in the reaction flask; mild agitation, MW absorber and WP were manually shaken for 15 seconds prior pyrolysis; strong agitation, MW absorber and WP were shaken for at least 90

seconds prior pyrolysis.

Carbon did not show any remarkable difference in yield and physical characteristics of products among different mixing protocol. Meanwhile Fe showed sound differences switching from a protocol to another one. Three pyrolyses were run with different agitation: WP3, none; WP4, mild; and WP5, strong (Table 8.1) to report any effects and difference.

The operating parameters employed, set-up, MW absorber, and MW power are reported in Table 8.1 (entries are named "WPn" where "n" is an arbitrary ascending number for each experiment).

Table 8.1. MAP of WP, operating parameters.

Entry	Set-up	Absorber	Absorber	WP	MW power	WP/ Absorber	Time	Solid	Liquid	Gas
			(g)	*(g)*	*(kW)*		*(min)*	*(wt%)*	*(wt%)*	*(wt%)*
WP1	A	-	150.5	-	3	-	10	95.75	0.00	4.25
WP2	A	-	150.1	-	3	-	36	61.16	27.98	10.86
WP3	A	-	151.0	-	3	-	45	68.08	23.25	8.68
WP4	A	Fe	150.4	78.6	3	1.9	26	46.28	35.44	18.28
WP5	A	Fe	150.5	78.9	3	1.9	26	38.01	39.27	22.72
WP6	A	Fe	151.1	81.3	3	1.9	26	32.50	41.50	26.01
WP7	A	Carbon	300.2	63.5	3	4.7	25	22.95	47.70	29.35
WP8	A	Carbon	150.5	78.8	3	1.9	23	23.26	41.86	34.88
WP9	A	Carbon	211.7	75.0	1.2-3.0	2.8	67	24.89	46.10	29.00
WP10	B	Fe	149.0	77.6	3	1.9	29	32.75	34.56	32.68
WP11	B	Fe	150.5	78.6	3	1.9	26	35.35	37.41	27.24
WP12	B	Carbon	150.6	78.6	3	1.9	24	25.90	40.77	33.33
WP13	B	Carbon	301.0	100.0	3	3.0	35	23.62	42.92	33.46
WP14	B	Carbon	212.0	75.3	1.2-3.0	2.8	67	26.32	41.89	31.79

Entries WP1, WP2, and WP3, were performed without any MW absorber. Only in these pyrolyses WP did not preserve their former shape and partially bulged or burst. The internal part of WP were initially heated in agreement with Miura et al.,[3,4] Farag et al.[5], and Vongpradubchai and. Rattanadecho.[6] Even WP1, which was interrupted after 10 min as soon as vapor evolution was stopped, showed this bulge/burst effect. WP1 clearly displayed that a simple drying of WP without losing their former shape was impracticable in this condition (Figure 8.1a). Most of WPs were converted into gas and liquid was not recovered although few drops of it were recovered from the glass joint and some analysis were performed (liquid yield below 0.005 wt%).

WP2 and WP3 were performed in the same conditions but substantial

differences in yield were highlighted. The oven always showed a homogeneous magnetic field in spite of feeding materials employed (see Section 5 and 6) so far this different behavior might be explained only through non-homogeneity of samples.[1,2,7,8] 150 g of WP were not a representative sample. The distribution of wood pellets inside the reactor was crucial for reproducibility of MAP. Furthermore formation of randomly distributed carbon and/or char during pyrolysis might vary stochastically the absorbing ability of WP. A critical issue was represented by the moisture content. As a matter of fact only water was able to absorb MW radiation and cause pyrolysis while heating up.[9] However only strong MW radiation is able to pyrolyze WP without a MW absorber as reported by Robinson et al. who impregnated WP to increase the moisture content.[9]

These accounts were true only for MAP without MW absorber. Indeed if a MW absorber was present and the same mixing protocol was employed pyrolysis were reproducible. The energy was transferred in a completely different way; MW absorber was in contact with the outer surface of WP so heat was transferred from the outside to the inside part of pellets while without a MW absorber the heat was produced into the center of WP.

WP3, WP4, and WP5 were performed under the same operating conditions but different mixing protocol. The solid yield decreased as the mixing strength and time were improved (46.3, 38.0, and 32.5 wt% respectively). The solid yield was greater because the pyrolysis was not complete, in agreement with ultimate analyses which showed a rising carbon content as the mixing was stronger (see Section 8.2.2). Therefore a strong mixing protocol was adopted for the other pyrolysis. However this protocol was not enough to achieve a good reproducibility of tests (difference in yield higher than 1 wt%) when Fe was the absorber, WP10 and WP11.

Effects from mixing protocol were not evidenced in pyrolyses where carbon was the MW absorber. The yield reproducibility was within the range of 1 wt% and herein were reported only the most relevant pyrolysis. The carbon employed had a density of 0.5 g/cm^3 while Fe had a density of 7.86 g/cm^3 (see Section 5.3.1).[10] So far carbon took up a volume 16 times higher than Fe(0) for the same amount of absorber. Its distribution, even after the mild mixing protocol, was enough to envelop homogenously WP. Furthermore carbon was more finely grinded than Fe and could adhere more efficiently to the rough surface of WP. Furthermore the surface tension of carbon was very close to WP with respect to Fe.

Nevertheless Fe as MW absorber increased the formation of solid compared to carbon (about 32 wt% for Fe and about 23 wt% for carbon). Simultaneously higher yield of liquid and gas were observed when carbon was the MW absorber instead of Fe. Fe seemed to promote condensation reactions to yield non-volatiles compounds (solid or products remained trapped in the solid structure).

Indeed Fe salts (such as: $FeCl_3$ or $Fe(acac)_3$) are employed as catalyst in several coupling reactions for instance with Grignard reagents.[11] So far the Fe(0), used as MW absorber, or its oxidate forms which might be formed by reaction with oxygenated molecules present in the oven, could be involved in catalytic cycles involving radicals as proposed for classical Grignard reactions.[12,13] This behavior is not surprisingly because homolitic bonds cleavage led to radical formation in pyrolysis reactors. However in a MW system the cleavage took place near the MW absorber which was Fe in this case. Fe in the presence of macromolecules probably promoted their pyrolysis and in the same time it might promote radical coupling. As further support of this hypothesis the amount of volatiles (from proximate analysis) present in all solid/char obtained in the presence of Fe(0) had values ranging between 35-60 wt% while in the same operating conditions char obtained in the presence of carbon had values between 13-16 wt% (Table 8.1).

Using set-up B instead of set-up A the solid yield increased slightly with detriment of liquid yield due to cocking reactions. Variations on gas yield were minimal between the two set-ups. Probably pyrolysis condition promoted coupling and/or cocking reaction among pyrolysis products also in the fractionating system or the increased residence time, especially for high boiling compounds, promoted cocking.

8.2. Solid Product

Solid product were a mixture of MW absorber (if present) and residual WP. They were always quantitatively separated at the end of each pyrolysis. The MW absorber were not analyzed because a detailed characterization of carbon from MAP of tire is reported in Section 5.3.[10]

Herein is reported a characterization of solids/char due to WP.

8.2.1. Physical properties

The main physical properties of char are reported in Table 8.2 (coded “WPnS” where “n” is the pyrolysis entry).

Complete conversion of WP yielded pellets with variable carbon content between 77 and 89 wt% and hydrogen content between 0.3 and 3 wt%. This variation was connected manly to moisture content, and low boiling compounds which remained absorbed into solids. Indeed relatively high quantity of moisture were present even over 11 wt% for WP4S. Furthermore in all char was observed a very high amount of volatiles which dropped below 16 wt% if carbon was the MW absorber. Chars obtained from classical and MW assisted pyrolysis, of almost any feed retained variable amount of compounds partially pyrolyzed in relation to their chemical, morphological, pore, and surface area structure (See Section 5.3).[10,14,15] Indeed in MAP of wood blocks Miura et al.[3] observed formation of char having

a high surface area (up to 500 m^2/g). However the BET surface area developed in the solid investigated was minimal compared to reported values and it did not exceed 3 m^2/g. Probably the pore structure of pellets were filled due to the claimed coupling/cooking reactions.

Table 8.2. Solids from MAP of WP.

Entry	Absorber	C (wt%)	H (wt%)	N (wt%)	O[a] (wt%)	Moisture (wt%)	Volatiles (wt%)	Ash (wt%)	Fixed carbon (wt%)	BET area (m^2/g)	HHV (MJ/kg)	LHV (MJ/kg)
WP	-	44.81	5.87	0.59	48.73	8.68	80.93	1.38	9.01	-	17.7	16.4
WP1S	-	46.37	5.64	0.15	47.84	5.96	83.52	1.04	9.48	n.d.	18.3	17.0
WP2S	-	88.58	4.81	1.94	4.67	2.22	48.41	2.41	46.96	n.d.	n.d.	n.d.
WP3S	-	56.21	5.61	0.26	37.92	2.59	75.05	1.18	21.18	n.d.	21.3	20.0
WP4S	Fe	42.28	2.93	0.20	54.58	11.83	59.43	8.02	20.73	n.d.	26.1	25.5
WP5S	Fe	74.86	3.54	0.33	21.26	1.79	45.11	3.08	50.03	0.0274	31.4	30.6
WP6S	Fe	65.47	4.37	0.00	30.16	14.41	14.41	5.13	66.04	n.d.	n.d.	n.d.
WP7S	Carbon	83.32	0.32	0.82	15.54	5.06	3.35	9.34	82.25	n.d.	35.9	35.9
WP8S	Carbon	77.90	2.34	0.31	19.45	2.34	13.00	4.80	79.86	2.7955	31.5	31.0
WP9S	Carbon	86.48	1.48	0.65	11.03	6.49	9.57	5.09	78.86	n.d.	31.3	31.0
WP10S	Fe	66.03	3.35	0.00	30.62	5.58	25.88	10.63	57.91	n.d.	n.d.	n.d.
WP11S	Fe	77.53	3.23	0.34	18.89	1.21	35.44	3.63	59.73	0.1716	29.9	29.1
WP12S	Carbon	77.34	3.02	0.37	19.26	3.17	15.72	3.92	77.19	0.9938	31.2	31.0
WP13S	Carbon	86.51	1.67	0.35	11.47	n.d.	n.d.	7.40	n.d.	n.d.	31.5	31.1
WP14S	Carbon	88.87	0.00	0.00	11.13	1.96	0.93	3.09	94.03	n.d.	33.4	33.3

a) by difference; n.d.: not detected.

Similar achievements were also reported for char from classical pyrolysis and low surface areas were observed;[16] these characteristics are indication of a good ability of char to absorb small molecules.

When Fe(0) was the MW absorber the percentage of fixed carbon calculated over the solid was lower than in MAP using carbon as MW absorber. However the amount of fixed carbon calculated over the initial amount of WP in these pyrolysis

was the same. In fact the values reported for fixed carbon multiplied for the solid yield gave the same values of fixed carbon for each entry. These data showed that cocking reactions were not preferentially promoted by Fe or carbon. At the same time volatiles were higher using Fe and lower when carbon was the MW absorber as already discussed in Section 8.1, even if the percentage of volatiles (Table 8.2) were multiplied for the solid yield.

A general trend could be observed on the three-dimensional Van Krevelen diagram (H/C, O/C, and LCV, Figure 8.2). H/C and O/C molar ratios jointly decreased when a MW absorber was employed and the conversion of WP was complete (entries WP5 - WP14). Lower calorific value (LCV) increased together with H/C and O/C reduction and all the values gathered in a narrow space as highlighted in Figure 8.2.

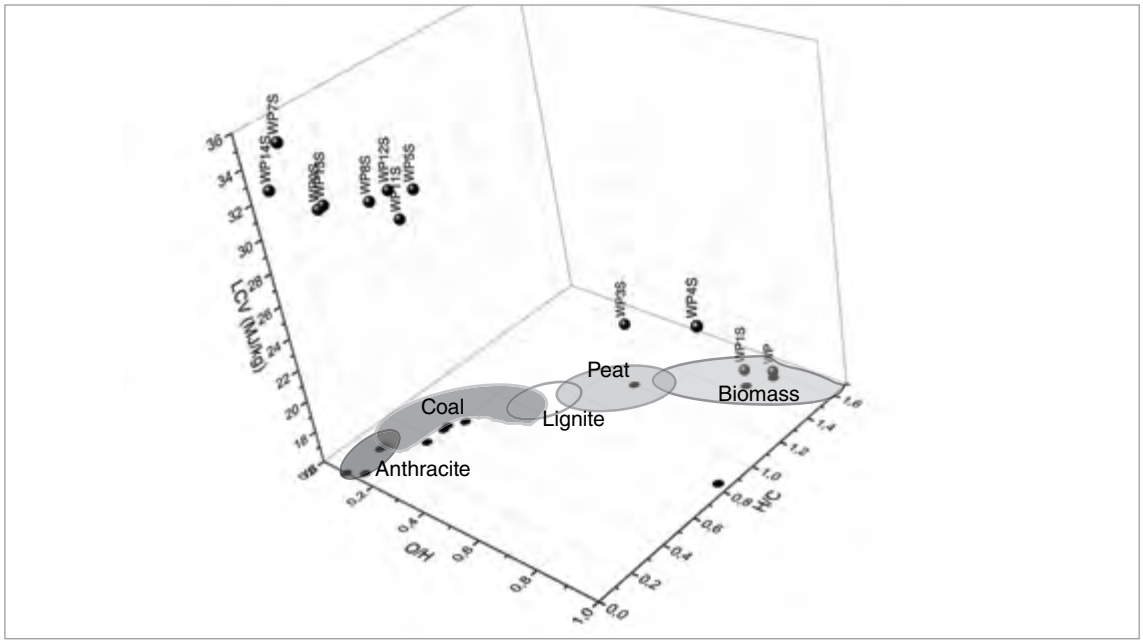

Figure 8.2. Three-dimension Van Krevelen diagram of char from MAP of WP.

An O/C molar ratio below 0.2 suggested a good stability of these solids in soil and a good substrate for carbon sequestration.[17]

LCV tended to an average value of 31 MJ/kg which was close to the value observed for char from wood pyrolysis and other carbon based material.[16,18-20]

The LCV of WP1S was 4% higher than LCV of not-pyrolyzed WP while the yield of char in entry WP1 was 96 wt%. This is an indication that there was no loss in heating capability after pellets irradiation. Anyway the reduction of moisture content made WP1S a better fuel than not-pyrolyzed WP.

8.2.2. FTIR of Char

FTIR spectra of char are reported in Figure 8.3. WP9S - WP14S did not show any remarkable absorption. Relative intensity of each peak for all the other char

is reported in Table 8.3.

Figure 8.3. FTIR spectra of: a) WP; b) WP1S; c) WP2S; d) WP3S; e) WP4S..

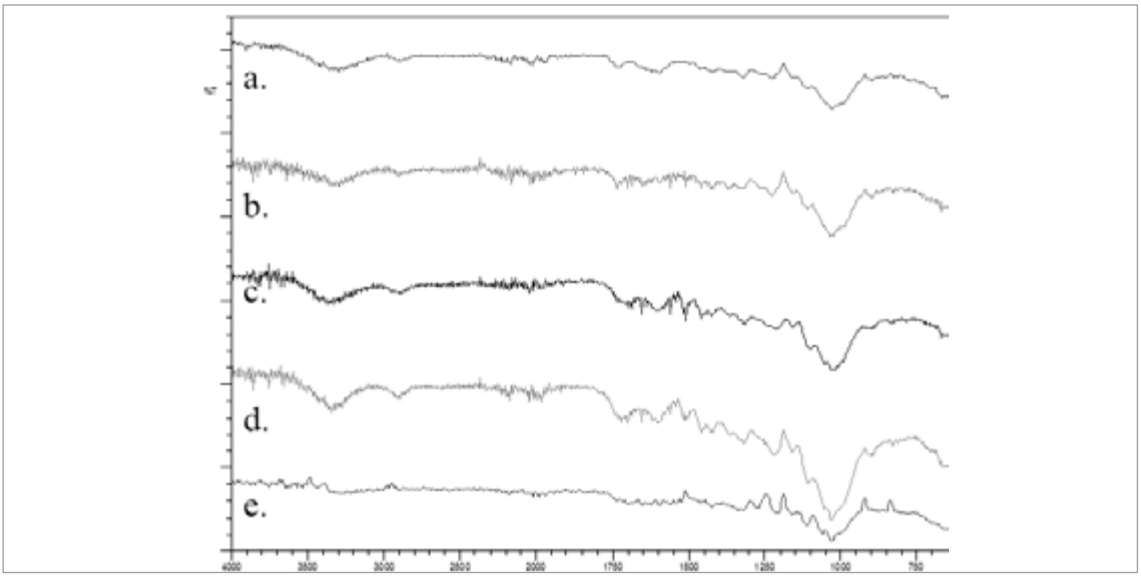

Table 8.3. IR absorptions of char from MAP of WPa.

Frequency (cm^{-1})	Attribution	WP	WP1S	WP2S	WP3S	WP4S	WP5S	WP6S	WP7S	WP8S
3300	H-bonded OH stretching	m	m	m	m	n.d.	n.d	n.d	n.d	n.d
2910/2860	Methylene C-H asym./ sym. stretching	w	w	m	m	n.d.	n.d	n.d	n.d	n.d
1926;1913; 1890	Aromatic combination band	w	w	w	w	w	n.d	n.d	n.d	n.d
1725 wide	C=O stretching	w	w	w	m	w	w	w	w	w
1610	Conjugated C=C stretching	m	m	m	m	m	s	s	s	s
1470	Methylene C-H bending	w	w	m	m	w	n.d	n.d	n.d	n.d
1410/1375	Methyl C-H asym./sym. bending	w	w	w	w	w	n.d	n.d	n.d	n.d
1316; 1270	Primary or secondary alcohol, OH in-plane bending	m	m	m	m	m	w	m	m	m
1250	Aromatic ethers, aryl-O stretching	w	w	w	w	w	w	m	m	m
1104	Secondary alcohol, C-O stretching	m	m	m	m	m	w	m	m	m
1000	Primary alcohol, C-O stretching (broad)	s	s	s	s	s	m	m	m	m
679	Alcohol, OH out-of-plane bending	m	w	w	w	m	n.d	n.d	n.d	n.d
651; 639; 618; 603	Alcohol, OH out-of-plane bending	m	w	w	w	m	n.d	n.d	n.d	n.d

a) Intensity reported as follow: s, strong; m, medium; w, weak; n.d. not detected.

IR spectra of WP and WP1S – WP3S showed similar absorptions and similar

relative intensities between peaks in each spectrum. Without a MW absorber the conversion of the polymeric matrix of WP was low and most of the functional groups remained stable into the matrix.

However when a MW absorber was present the intensity of each absorption was reduced. Char obtained in the presence of Fe (WP4S – WP6S) showed absorptions higher than those obtained in the presence of carbon (WP7S and WP8S). As highlighted in Section 8.1 carbon was able to envelop better the WP and promote a higher conversion of the polymeric matrix.

8.3. Liquid product

All liquids collected were separated in a two phase system. These phases were hardly separable, the lower phase stuck on the glass surface thus making difficult to handle it without significant mass loss during operation. Thus a quantification of yield for each phase was not performed. Anyway the amount of the lower phase was qualitatively reduced using a fractionating system (set-up B).

8.3.1. Physical properties

The main physical properties of liquid are reported in Table 8.4 (coded "WPnS_p" where "n" is the pyrolysis entry and "p" is referred to the phase: "UP", upper phase; "BOT", bottom phase). Only WP1L was a single phase liquid.

Viscosity, density, and HHV were measured only for upper phases (except HHV for WP8L_BOT) because it was not possible to obtain sufficient amount of the bottom phases.

Upper phases were transparent liquids with a color from pale yellow (when a MW absorber was not employed) to orange (when a MW absorber was employed).

Bottom phases were dark viscous sticky liquids which adhered to glass surface and made their handling problematical.

Water content was higher than in classical heating pyrolysis of woody feeds where it usually did not exceed 30 wt%.[16,21] However water content of upper phases was close to those reported by Shoujie et al. for MAP of Douglas fir sawdust pellet.[22] The heat transfer through MW was different from classical heating causing a different degradation of cellulose and hemicellulose promoting water formation. Anyway high amounts of water could not be only ascribed to the heating method, also quenching speed and efficiency of vapors collection from reactor might influence kinetics of secondary reactions involving cellulose and hemicellulose pyrolysis products.[21,23,24]

Viscosity was lower than those reported in several publications, even 200 times lower.[25-27] It was below the common reported viscosity range (25 – 1000 cSt).16 As outlined before MW heating and fractionating and collecting systems, might promote secondary pyrolysis reactions of cellulose and hemicellulose

giving smaller molecules (up to water) and it was not surprising the low values for viscosity. Density was close to 1 g/cm^3, and no significant differences were highlighted among samples collected.

Table 8.4. Liquid from MAP of WP

Entry	Viscosity (cP)	Density (g/cm^3)	Water content (wt%)	C (wt%)	H (wt%)	N (wt%)	O[a] (wt%)	C/H molar ratio	Empirical formula	HHV (MJ/kg)	LHV (MJ/kg)
WP1L_UP	n.d.	n.d.	48.6	n.d.	n.d.	n.d.	n.d.	n.d.	n.d.	n.d.	n.d.
WP2L_UP	1.96	1.053	n.d.	19.22	9.68	0.00	71.10	0.165	$CH_{6.00}O_{2.78}$	n.d.	n.d.
WP3L_UP	1.69	1.049	40.5	13.89	8.70	0.00	77.41	0.133	$CH_{7.46}O_{4.18}$	6.0	4.0
WP3L_BOT	n.d.	n.d.	n.d.	n.d.	n.d.	n.d.	n.d.	n.d.	n.d.	n.d.	n.d.
WP4L_UP	2.35	1.073	38.6	19.92	8.58	0.00	71.50	0.193	$CH_{5.13}O_{2.69}$	8.1	6.2
WP4L_BOT	n.d.	n.d.	n.d.	48.59	4.75	0.00	46.66	0.852	$CH_{1.16}O_{0.72}$	n.d.	n.d.
WP5L_UP	2.35	1.059	47.4	19.92	7.13	0.00	72.95	0.233	$CH_{4.27}O_{2.75}$	8.3	6.7
WP5L_BOT	n.d.	n.d.	n.d.	49.61	5.24	0.00	45.15	0.788	$CH_{1.26}O_{0.68}$	n.d.	n.d.
WP6L_UP	>4	1.076	n.d.	23.89	9.95	0.00	66.16	0.200	$CH_{4.96}O_{2.08}$	7.5	5.2
WP7L_UP	>4	1.086	n.d.	46.62	4.67	0.00	48.71	0.831	$CH_{1.19}O_{0.78}$	n.d.	n.d.
WP8L_UP	2.29	1.076	32.3	18.96	8.73	0.00	72.30	0.181	$CH_{5.49}O_{2.86}$	7.4	5.5
WP8L_BOT	n.d.	n.d.	n.d.	58.91	5.83	0.20	35.05	0.842	$CH_{1.18}N_{0.00}O_{0.45}$	25.0	
WP9L_UP	2.09	1.055	n.d.	23.01	9.41	0.00	67.58	0.204	$CH_{4.87}O_{2.20}$	n.d.	n.d.
WP10L_UP	2.00	1.060	n.d.	18.76	10.44	0.00	70.80	0.150	$CH_{6.63}O_{2.83}$	n.d.	n.d.
WP11L_UP	1.66	0.940	63.2	16.84	8.18	0.00	74.98	0.172	$CH_{5.78}O_{3.34}$	8.4	6.6
WP11L_BOT	n.d.	n.d.	n.d.	58.63	6.05	0.00	35.32	0.807	$CH_{1.23}O_{0.45}$	n.d.	n.d.
WP12L_UP	1.88	1.053	51.5	18.96	8.73	0.00	72.30	0.181	$CH_{5.49}O_{2.86}$	7.4	5.5
WP12L_BOT	n.d.	n.d.	n.d.	60.31	6.37	0.18	33.00	0.788	$CH_{1.26}N_{0.00}O_{0.41}S_{0.00}$	n.d.	n.d.
WP13L_UP	>4	1.067	n.d.	20.60	9.31	0.00	70.09	0.184	$CH_{5.39}O_{2.55}$	n.d.	n.d.
WP14L_UP	1.76	1.032	n.d.	23.10	9.91	0.00	66.99	0.194	$CH_{5.11}O_{2.18}$	n.d.	n.d.

a) by difference. n.d., not detected.

Only WP11L_UP showed a density below 1 g/cm^3 which was correlated to a strong pyrolysis as indicated by the highest water content (63.2 wt%). Fe as MW

absorber together with set-up B was the most efficient system to pyrolyze WP even if the reproducibility was not good.

HHV of upper phases was similar (within 6 and 8 MJ/kg) compared to reported data,[28] but lower than conventional liquid from fast pyrolysis due to the large presence of water.[21]

Otherwise the bottom phase showed a remarkable high value (25 MJ/kg) which was close to some reported values for liquids from woody biomasses.[28,29]

8.3.2. Thin layer chromatograph

Thin layer chromatography (TLC) is a quick, cheap, and powerful method to test qualitatively the nature of liquids. Elution performance of liquids were compared to those of selected standards to evaluate the affinity with the solvent mixture and to evaluate the possibility to analyze liquid via GC and HPLC.

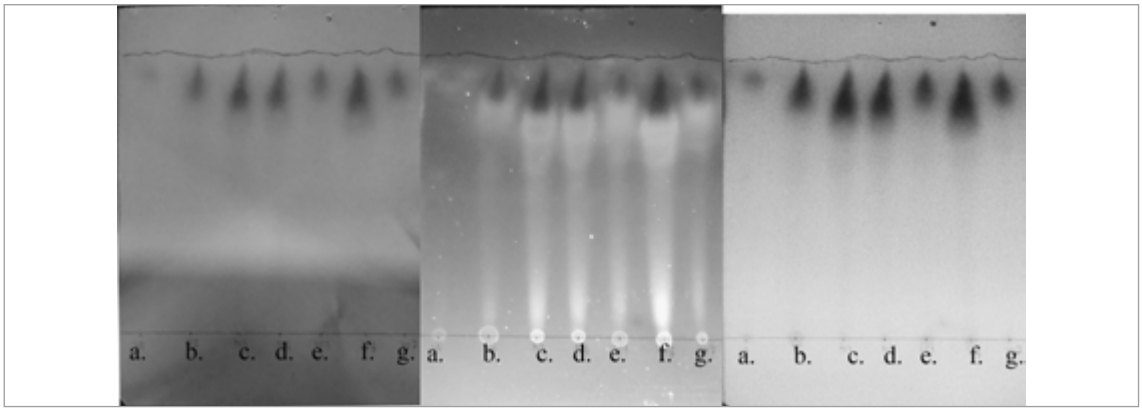

Figure 8.4. TLC using MeOH/AcN/H_2O, from left to right, TLC chromatograms examined under daylight and UV light, longwave and shortwave, of: a) WP1L_UP; b) WP3L_UP; c) WP4L_UP; d) WP5L_UP; e) WP11L_UP; f) WP8L_UP; g) WP12L_UP.

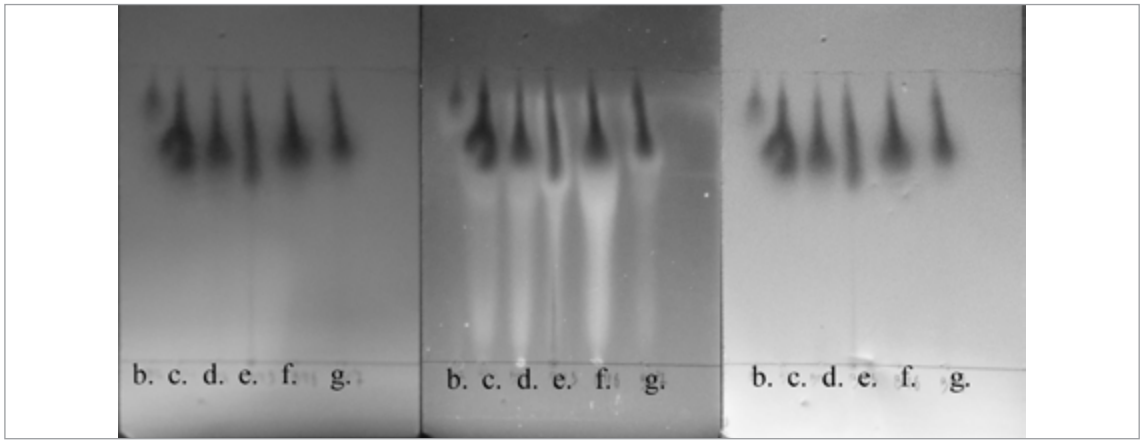

Figure 8.5. TLC using MeOH/AcN/H_2O, from left to right, TLC chromatograms examined under daylight and UV light, longwave and shortwave, of: b) WP3L_BOT; c) WP4L_BOT; d) WP5L_BOT; e) WP11L_BOT; f) WP8L_BOT; g) WP12L_BOT.

All liquids showed broad range of retention factors (Rf) from 0 to 1 with two solvent mixtures (MeOH/AcN/H_2O, Figure 8.4 and Figure 8.5, and CH_2Cl_2/H_2O,

Figure 8.6 and Figure 8.7). Compounds with a Rf below 0.5 (with both solvent mixtures) were not expected to be detectable in GC and HPLC. Compounds with a Rf between 0.5 and 0.9 were expected to be mainly detectable in HPLC, while compounds with a Rf over 0.9 were expected to be mainly detectable in GC and probably even in minor amount in HPLC.

Furthermore all samples were prepared with the same concentration (50.00 mg/mL) and contained compounds having similar structures so a semiquantitative analysis may be run by visual comparison of absorption intensities under UV lights. The liquids showed the strongest and prevalent absorption between 0.8 and 1. So they were suited for GC and HPLC investigation.

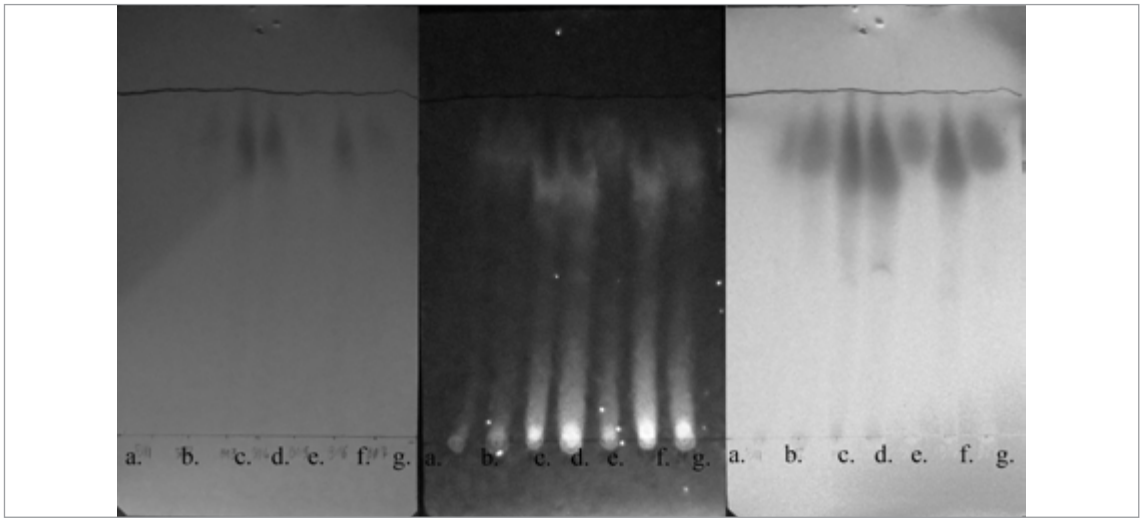

Figure 8.6. TLC using CH_2Cl_2/H_2O, from left to right, TLC chromatograms examined under daylight and UV light, longwave and shortwave, of: a) WP1L_UP; b) WP3L_UP; c) WP4L_UP; d) WP5L_UP; e) WP11L_UP; f) WP8L_UP; g) WP12L_UP.

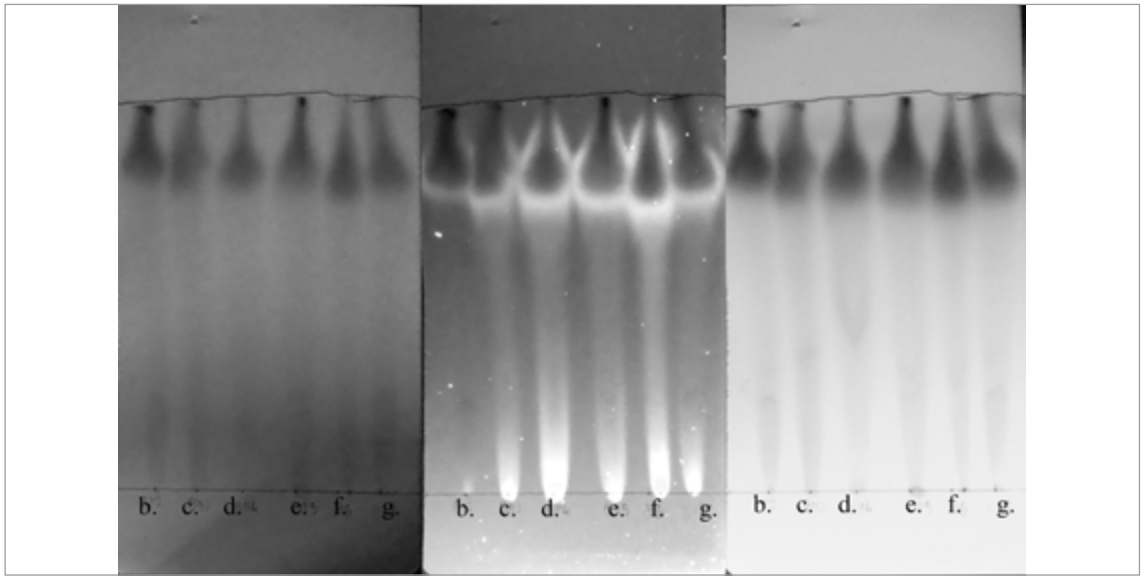

Figure 8.7. TLC using CH_2Cl_2/H_2O, from left to right, TLC chromatograms examined under daylight and UV light, longwave and shortwave, of: b) WP3L_BOT; c) WP4L_BOT; d) WP5L_BOT; e) WP11L_BOT; f) WP8L_BOT; g) WP12L_BOT.

8.3.3. GC/MS-FID

The gas chromatographic analyses were performed using a compound already found to be already present that worked as an internal standard. Guaiacol and furfural were two compounds chosen to act as internal standards because they were typical and reoccurring pyrolysis products of lignin, for guaiacol, and cellulosic materials, for furfural.[30-34] A calibration curve was prepared and used to quantify their concentration in tested samples (general equation is reported Eq. 8.1; guaiacol, slope: 70818, intercept: 0.00, R^2: 0.9959; furfural, slope: 46660, intercept: 0.00, R^2: 0.9952).

$$A_i = m_i \cdot C_i \qquad \textbf{8.1}$$

Where A_i is chromatographic peak area of analyte i; m_i, , is the slope of analyte i; C_i, is the concentration of analyte i in g/L.

The relative response factor (RRF), with respect to guaiacol or furfural, for references compounds detected by GC analysis, is reported in Table 8.7 (RRF_{found} column) and it was calculated using Eq. 8.2.

$$RRF_i = \frac{MW_i \cdot A_i \cdot C_S}{MW_S \cdot A_S \cdot C_i} \qquad \textbf{8.2}$$

Where subscript “i” refer to a target compound and “S” to standard; A, chromatographic area; MW, molecular weight; C concentration in g/L.

The following equation (Eq. 8.3) was obtained by substitution of Eq. 8.1 in Eq. 8.2.

$$RRF_i = \frac{MW_i \cdot A_i}{MW_S \cdot m_S \cdot C_i} \qquad \textbf{8.3}$$

The RRF allowed for a fast calculation of the concentration of any known compound (Eq. 8.4). This equation could be used regardless of the absence or presence of any internal standard in the bio-oil because the C_s was not necessary for calculations but just the slope of the calibration curve.

$$C_i = \frac{MW_i \cdot A_i}{MW_S \cdot m_s \cdot RRF_i} \qquad \textbf{8.4}$$

This procedure required to know the RRF of each compounds so their injection were necessary before its application. Since bio-oil produced from any kind of biomass could contain up to several hundred compounds of different classes and chemical functionalities, the expense in terms of time and money required to obtain individual data for so many compounds is seldom worthwhile. Consequently, a new route to determine the RRF was a mandatory issue.

The RRF_{found} might be correlated with the chemical composition and predicted, as reported by several authors.[35-39] Since none of the equations reported allowed for an unambiguous and effective prediction of all data required for Eq. 8.2, a new method to estimate RRF. It took into account the chemical composition of

the compounds (aromatic rings, double bonds C=C, ketones, carboxylic (acids, esters, anhydride), alcohols, aldehydes, and ethers) and a contribution factors for each atom present (carbon, hydrogen, and oxygen) in its molecular formula. Furthermore each contribution was modulated by a power function Z. These value was also connected with the molecular weight and chromatographic retention time. Therefore a new general equation to predict the RRF (RRFcalc) was proposed as reported below (Eq. 8.5).

$$RRF_{calc\,i} = \frac{rt_S \cdot MW_i \cdot \sum_k \left(P_k \cdot n_{kS}^{Z_k} + Q \right)}{rt_i \cdot MW_S \cdot \sum_k \left(P_k \cdot n_{ki}^{Z_k} + Q \right)} \quad \textbf{8.5}$$

Where subscript "i" refer to a reference compound, "S" refers to a given standard, and "k" refers to a type of atom or group present into the compound (Table 8.6); rrt, refers to the chromatographic retention time; MW, molecular weight; P, Z, and Q parameters refined for each n (Table 8.6); nn number of atom and groups into the reference and standard compound.

Considering the RRF for a specific compound such as vanillin, and guaiacol as standard (Table 8.5) as standard, Eq. 8.5 could be expressed as follow (Eq. 8.6):

$$RRF_{calc\,i} = \frac{rt_S \cdot 152.15}{rt_i \cdot 124.14} \cdot \frac{\left[\left(P_C 8^{Z_C} \right) + \left(P_H 8^{Z_H} \right) + \left(P_O 3^{Z_O} \right) + \left(P_{ring} 1^{Z_{ring}} \right) + \left(P_{C=C} 3^{Z_{C=C}} \right) + \left(P_{C=O} 1^{Z_{C=O}} \right) + \left(P_{OH} 1^{Z_{OH}} \right) + \left(P_{COC} 1^{Z_{COC}} \right) + Q \right]}{\left[\left(P_C 7^{Z_C} \right) + \left(P_H 7^{Z_H} \right) + \left(P_O 2^{Z_O} \right) + \left(P_{ring} 1^{Z_{ring}} \right) + \left(P_{C=C} 3^{Z_{C=C}} \right) + \left(P_{OH} 1^{Z_{OH}} \right) + \left(P_{COC} 1^{Z_{COC}} \right) + Q \right]} \quad \textbf{8.6}$$

Parameters P and Z and constant Q, in Eq. 8.5 and Eq. 8.6, were optimized using the RRF experimentally evaluated with Eq. 8.3 (RRF_{found}) for 30 reference compounds (Table 8.5). The RRF_{found} were compared with RRF_{calc} (calculated using the parameter reported in Table 8.6) in Table 8.7 and a visual comparison is shown in Figure 8.8.

Using this equation (Eq. 8.5) is possible to set-up quickly a new a set of parameters (P, Z, and Q) for different instrument and reference compounds using the data reported in Table 8.5. Indeed the program employed to refine the parameters P, Z, and Q gave more reliable results if the starting point for calculation was close to the final values. The initial values, before any calculation, were established equal to 1.

This method might be applied if the chemical structure of the target compound is known. It was possible to use Eq. 8.5 even if the structure was relatively uncertain and only one possible isomer was guessed.

Table 8.5. Standard compounds injected both in GC/MS and HPLC/MS

Formula	Traditional name	IUPAC name	Monoisotopic mass *(Da)*
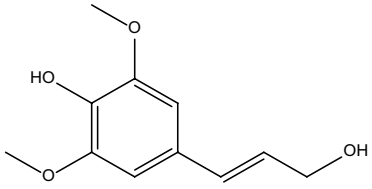	Sinapyl alcohol	4-(3-hydroxyprop-1-enyl)-2,6-dimethoxyphenol	210.089203
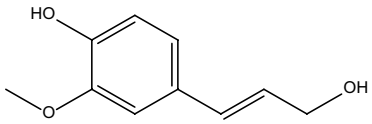	Coniferyl alcohol	4-(3-hydroxy-1-propenyl)-	180.078644
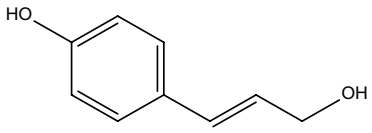	p-coumaryl alcohol	2-methoxyphenol	150.068085
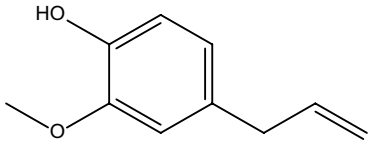	Eugenol	4-[(1E)-3-Hydroxy-1-propen-1-yl]phenol	164.083725
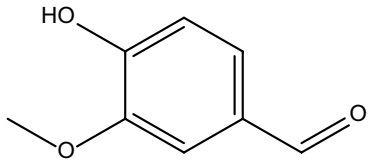	Vanillin	4-propen-2yl-2-methoxyphenol	152.047348
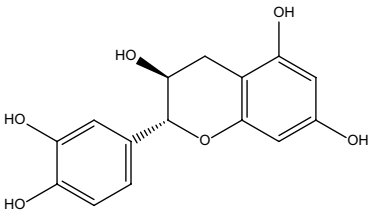	(+)-catechin	4-Hydroxy-3-methoxybenzaldehyde	290.079041
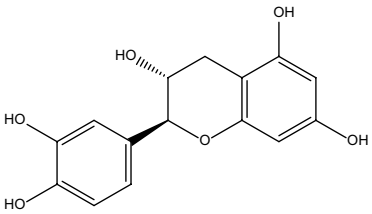	(-)-catechin	(2R,3S)-2-(3,4-dihydroxyphenyl)-3,4-dihydro-2H-chromene-3,5,7-triol	290.079041
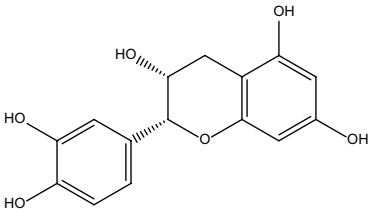	(-)-epicatechin	(2S,3R)-2-(3,4-Dihydroxyphenyl)-3,5,7-chromanetriol	290.079041
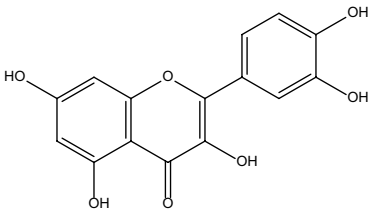	Quercitin	(2R,3R)-2-(3,4-Dihydroxyphenyl)-3,5,7-chromanetriol	302.042664

(continue)

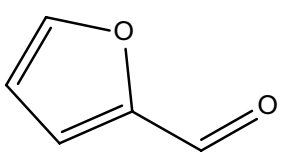	Furfural	2-(3,4-dihydroxyphenyl)-3,5,7-trihydroxy-4H-chromen-4-one	96.02113
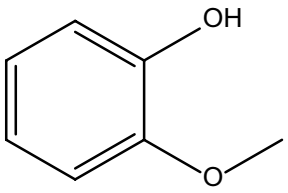	Guaiacol	Furan-2-carbaldehyde	124.052429
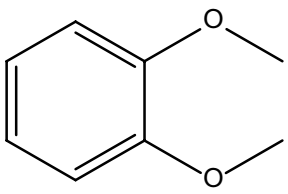	Veratrole	2-methoxyphenol	138.068085
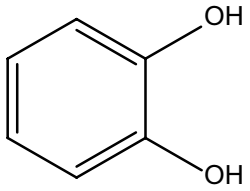	Catechol	1,2-dimethoxybenzene	110.036781
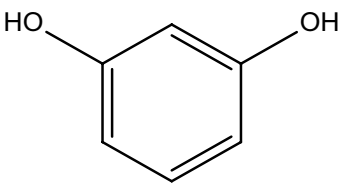	Resorcinol	1,2-dihydroxybenzene	110.036781
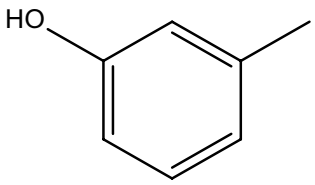	m-cresol	1,3-dihydroxybenzene-	108.057518
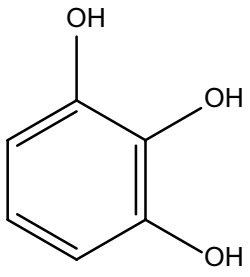	Pyrogallol	3-Methylphenol	126.031693
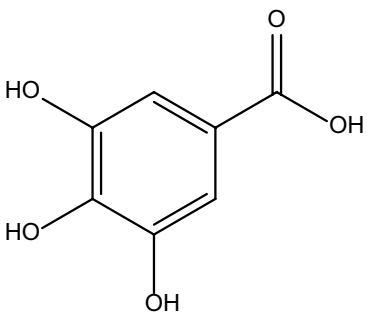	Gallic acid	1,2,3-trihydroxybenzene	170.02153

(continue)

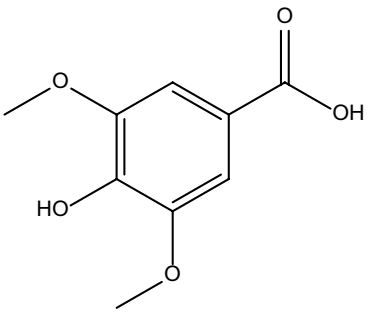	Syringic acid	3,4,5-trihydroxybenzoic acid	198.052826
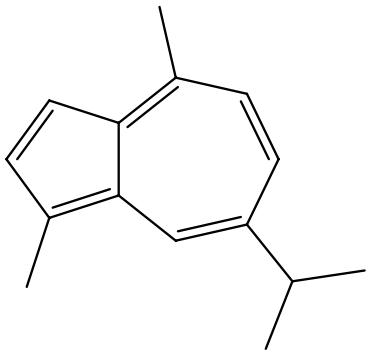	Guaiazulene	4-hydroxy-3,5-dimethoxybenzoic acid	198.140854
		1,4-dimethyl-7-isopropylazulene	74.073166
		2-methyl-2-propanol	86.10955
		Hexane	60.02113
		Acetic acid	74.073166
		2-methyl-1-propanol	78.046951
		Benzene	84.093903
		Cyclohexane	92.062599
		Toluene	84.057518
		Cyclopentanone	94.041862
		Phenol	120.093903
		2-ethyltoluene	120.093903
		1,2,4-trimethylbenzene	120.093903
		1,2,3-trimethylbenzene	108.057518
		Benzyl alcohol	122.036781
		Benzoic acid	128.062607
		Naphthalene	124.052429
		4-methoxyphenol	196.073563
		2,3,4-trimethoxy benzaldehyde	154.026611
		2,6-dihydroxy benzoic acid	154.026611
		2-naphtol	144.05751

Table 8.6. Parameters defined (P, Z, and Q) for Eq. 8.5 obtained using the experimental RRF from Table 8.7.

	Number referred to	Guaiacol	Furfural
P_C	Number of atom of carbon atoms	0.98	99.70
P_H	Number of atom of hydrogen atoms	-5.45	5.33E-06
P_O	Number of atom of oxygen atoms	-25.21	-12.21
P_{ring}	Number of aromatic ring	629.64	68.29
$P_{C=C}$	Number of C-C double bonds	-7.90	-0.03
PC=O	Number of ketones	394.61	70.55
PCO2R	Number of carboxylic	-1644.83	-181.85
POH	Number of alcohols	36.46	11.21
PCHO	Number of aldehyde	-161.68	-9.05
PCOC	Number of ethers	95.86	6.96
Q	Constant	-1195.74	-367.61
ZC	Number of atom of carbon atoms	2.821	0.416
ZH	Number of atom of hydrogen atoms	0.873	5.763
ZO	Number of atom of oxygen atoms	0.031	0.490
Zring	Number of aromatic ring	0.930	0.753
ZC=C	Number of C-C double bonds	2.911	4.426
ZC=O	Number of ketones	1.000	1.000
ZCO2R	Number of carboxylic	1.000	1.000
ZOH	Number of alcohols	1.111	0.825
ZCHO	Number of aldehyde	1.000	1.000
ZCOC	Number of ethers	0.091	1.424

Table 8.7. RRF_{found}, from experimental data, compared with the RRF_{calc} predicted with Eq. 8.5 and parameter reported in Table 8.6 for reference compounds.

	Compound	RRF_{found}	RRF_{calc}	RRF_{found}	RRF_{calc}
		Guaiacol		Furfural	
1	2-methyl-2-propanol	1.02	1.35	2.01	2.42
2	hexane	1.57	1.46	3.08	3.38
3	acetic acid	0.35	0.38	0.68	0.73
4	2-methyl-1-propanol	1.00	1.05	1.95	1.89
5	benzene	1.66	1.83	3.25	3.55
6	cyclohexane	1.51	1.14	2.96	2.39
7	toluene	1.84	1.53	3.61	3.08
8	cyclopentanone	0.92	0.89	1.80	1.78
9	furfural	0.51	0.53	1.01	1.00
10	phenol	0.64	-1.21	1.26	-2.96
11	2-ethyltoluene	2.80	2.83	5.49	5.51
12	1,2,4-trimethylbenzene	1.88	1.61	3.69	3.23
13	1,2,3-trimethylbenzene	1.28	1.52	2.50	3.04
14	benzyl alcohol	0.93	0.79	1.82	1.54
15	m-cresol	0.84	0.66	1.64	1.40

(continue)

16	guaiacol	0.93	1.00	1.82	1.65
17	veratrole	1.08	1.21	2.11	2.09
18	benzoic acid	0.31	0.18	0.60	0.40
19	catechol	0.39	0.59	0.77	1.08
20	naphtalene	1.70	1.68	3.34	3.33
21	4-methoxyphenol	0.61	0.82	1.19	1.36
22	resorcinol	0.42	0.53	0.82	0.96
23	eugenol	1.31	1.37	2.56	2.63
24	vanillin	0.81	0.73	1.58	1.36
25	2,3,4-trimethoxy benzaldehyde	1.72	1.72	3.37	3.36
26	2,6-dihydroxy benzoic acid	0.21	0.15	0.41	0.35
27	syringic acid	0.22	0.20	0.43	0.46
28	coniferyl alcohol	1.23	1.29	2.40	2.39
29	guaiazulene	4.87	4.86	9.55	9.60
30	sinapyl alcohol	4.86	4.84	9.54	9.55

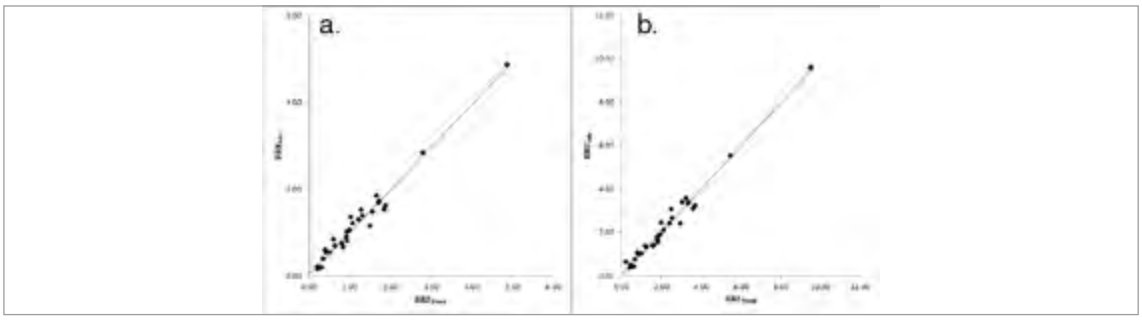

Figure 8.8. Comparison between RRF_{found} and $RRFc_{alc}$ reported in Table 8.7; a) for guaiacol, slope: 1.00, intercept: 7.82E-06, R^2: 0.9807; b) for furfural, slope: 1.00, intercept: 2.77E-07, R^2: 0.9907.

The ratio between retention times of the standard and the reference compound roughly related the chromatographic conditions (such as flows, split ratio, and so on) with the RRF. All these conditions are related to the amount of each compound which arrived to the detector and this ratio worked like an empirical correction factor. It was assumed, by using this ratio, that higher retention time corresponded to peak having a wide Gaussian shape that were harder to integrate.

The power function, Z, showed how much a variable influenced the RRF. Values closer to zero meant that the variable has a very low influence on the calculated RRF. Rising values of Z meant rising influence of the moiety on RRF.

These data gave reasonable values for compound similar chemical composition and structure to these reported in Table 8.5, however the date did not give reasonable values for polycyclic aromatic hydrocarbons (negative RRFs) and some tetra/penta substituted benzene.

The main compounds identified in the upper fractions are listed in Table 8.8, while those identified in the bottom fractions are listed in Table 8.9. The concentration of each compounds was calculated by averaging the values obtained using the

RRFs relative to guaiacol and furfural. The GC/FID of WP12L_UP and WP12L_BOT and total ion chromatogram (TIC) chromatograms of WP12L_BOT are reported in Figure 8.9.

Table 8.8. Concentration (g/L) of WP3L_UP, WP4L_UP, WP5L_UP, WP8L_UP, WP11L_UP, and WP12L_UP calculated using RRF_{found} or RRF_{calc}.

n	rt	Compound	a.c.	WP3L_UP	WP4L_UP	WP5L_UP	WP8L_UP	WP11L_UP	WP12L_UP
1	3.88	2-butanone	P	0.066	0.121	0.135	0.144	0.164	0.024
2	4.07	acetic acid	S	1.670	0.998	1.244	0.753	1.256	0.629
3	4.71	benzene	S	0.002	0.001	0.002	0.002	0.005	0.003
4	4.81	2-oxo-propanoic acid	U	0.000	0.004	0.006	0.006	0.010	0.007
5	4.90	1-hydroxy-2-propanone	U	0.098	0.144	0.177	0.131	0.171	0.155
6	5.07	3-Buten-2-one	U	0.032	0.032	0.032	0.029	0.060	0.044
7	5.45	4-Penten-2-one	P	0.017	0.022	0.009	0.020	0.011	0.021
8	5.67	2,3-Pentanedione	P	0.000	0.000	0.000	0.010	0.000	0.000
9	7.75	Toluene	S	0.000	0.000	0.001	0.018	0.001	0.000
10	7.86	1,4-diol-2-butene	U	0.054	0.042	0.077	0.058	0.061	0.046
11	7.97	Pyruvaldehyde	P	0.039	0.047	0.059	0.009	0.047	0.051
12	8.41	Tetrahydro-3-furanol	U	0.038	0.069	0.094	0.000	0.068	0.075
13	8.71	cyclopentanone	S	0.009	0.027	0.028	0.000	0.033	0.024
14	10.23	furfural	S	0.564	0.405	0.483	0.003	0.607	0.414
15	10.62	cyclohexanone	P	0.000	0.001	0.002	0.000	0.002	0.017
16	11.11	2-furanmethanol	P	0.005	0.023	0.037	0.000	0.003	0.004
17	11.31	etheylbenzene	U	0.003	0.012	0.022	0.001	0.008	0.007
18	11.68	1,4-dimethylbenzene	U	0.001	0.002	0.003	0.000	0.003	0.002
19	12.05	1,2-dimethylbenzene	U	0.001	0.002	0.003	0.000	0.003	0.002
20	12.36	1,3-dimethylbenzene	U	0.001	0.001	0.000	0.001	0.001	0.001
21	15.29	5-methyl-2-furancarboxaldehyde	P	0.032	0.044	0.067	0.054	0.051	0.036
22	15.84	phenol	S	0.000	0.042	0.058	0.000	0.049	0.038
23	16.45	3,4-dimethyl-2-Cyclopenten-1-one	P	0.000	0.003	0.003	0.006	0.004	0.002
24	16.60	benzofuran	P	0.004	0.009	0.012	0.012	0.008	0.008
25	16.92	tetrahydrofuran methanol	U	0.003	0.012	0.013	0.123	0.003	0.000
26	17.56	1,2,3-trimethyl benzene	U	0.008	0.047	0.072	0.000	0.030	0.036
27	18.55	o-cresol	P	0.000	0.024	0.033	0.000	0.031	0.023
28	19.30	m-cresol	S	0.000	0.024	0.046	0.000	0.021	0.023
29	19.79	Guaiacol	S	0.016	0.040	0.058	0.000	0.041	0.031
30	20.80	veratrol	S	0.001	0.007	0.013	0.000	0.003	0.003
31	24.05	4-methoxyphenol	S	0.002	0.023	0.025	0.012	0.000	0.000

(continue)

32	25.90	resorcinol	S	0.000	0.046	0.069	0.000	0.033	0.034
33	26.77	2-methylnaphtalene	U	0.000	0.000	0.000	0.001	0.000	0.000
34	28.04	2,6-dimethoxy-phenol	P	0.016	0.105	0.134	0.000	0.024	0.033
35	28.22	eugenol	S	0.006	0.001	0.007	0.000	0.001	0.000
36	30.69	1,2,4-Trimethoxy benzene	U	0.000	0.000	0.079	0.000	0.010	0.015
37	32.77	1,2,3-trimethoxy-5-methyl-benzene	P	0.002	0.008	0.011	0.000	0.002	0.002
38	35.97	benzophenone	P	0.000	0.007	0.012	0.000	0.000	0.002
39	36.19	levoglucosan	S	0.052	0.318	0.307	0.552	0.000	0.000
40	37.98	syringic acid	S	0.000	0.027	0.056	0.091	0.000	0.006
		TOTAL (%)[b]		5.5%	5.5%	7.0%	4.1%	5.7%	3.6%

a) a.c.: attribution confidence of identification with NIST:; P, probable, similarity index >91%; U, uncertain, similarity index with NIST <91% and S, standard, identified by retention time and MS spectrum; b) Total amount identified, calculated as follow: $\Sigma C_i/50$; where C_i is the concentration of each compound and 50 is the initial concentration of the vial.

Table 8.9. Concentration (g/L) of WP3L_BOT, WP4L_BOT, WP5L_BOT, WP8L_BOT, WP11L_BOT, and WP12L_BOT calculated using RRF_{found} or RRF_{calc}.

n	rt	compound	a.c.	WP3L_BOT	WP4L_BOT	WP5L_BOT	WP8L_BOT	WP11L_BOT	WP12L_BOT
1	3.82	2-methylpropanal	U	0.000	0.037	0.061	0.061	0.093	0.058
2	3.87	2-butanone	p	0.000	0.118	0.207	0.364	0.282	0.247
3	3.98	acetic acid	s	0.003	0.000	0.564	0.000	1.192	0.222
4	4.30	2-methyl-1-propanol	s	0.000	0.000	0.004	0.000	0.017	0.008
5	4.69	2-Butenal	p	0.000	0.003	0.018	0.025	0.070	0.047
6	4.81	benzene	s	0.001	0.002	0.022	0.032	0.059	0.063
7	4.92	2-oxo-propanoic acid	u	0.000	0.294	0.131	0.118	0.232	0.103
8	5.07	3-Buten-2-one	p	0.001	0.000	0.061	0.079	0.139	0.102
9	5.40	4-Penten-2-one	p	0.000	0.000	0.036	0.035	0.058	0.045
10	5.66	2,3-Pentanedione	p	0.000	0.003	0.009	0.012	0.031	0.014
11	5.82	2,5-dimethylfuran	p	0.001	0.000	0.014	0.025	0.028	0.014
12	7.74	Toluene	s	0.003	0.004	0.044	0.061	0.176	0.120
13	7.87	1,4-diol-2-butene	u	0.000	0.040	0.061	0.051	0.144	0.092
14	8.03	Acetic acid ethenyl ester	u	0.000	0.108	0.099	0.053	0.105	0.013
15	8.69	cyclopentanone	s	0.001	0.024	0.048	0.051	0.112	0.062
16	10.23	furfural	s	0.019	0.643	1.099	1.138	2.753	1.587
17	10.62	cyclohexanone	u	0.001	0.003	0.074	0.063	0.106	0.077
18	11.08	2-furanmethanol	u	0.000	0.000	0.123	0.193	0.121	0.114
19	11.32	etheylbenzene	p	0.002	0.012	0.034	0.056	0.093	0.069

(continue)

20	11.68	1,4-dimethylbenzene	p	0.003	0.022	0.071	0.112	0.202	0.162
21	12.05	1,2-dimethylbenzene	p	0.001	0.002	0.009	0.014	0.030	0.021
22	12.57	1,3-dimethylbenzene	u	0.004	0.004	0.029	0.036	0.182	0.097
23	12.91	2-methyl-2-cyclopenten-1-one	u	0.000	0.000	0.000	0.001	0.009	0.003
24	13.26	1-(2-furanyl)-ethanone	u	0.000	0.000	0.033	0.033	0.108	0.052
25	15.26	5-methyl-2-furancarboxaldehyde	p	0.006	0.084	0.230	0.262	0.959	0.394
26	15.83	phenol	s	0.034	0.121	0.312	0.278	0.938	0.533
27	16.43	3,4-dimethyl-2-Cyclopenten-1-one	u	0.000	0.006	0.011	0.040	0.098	0.053
28	16.50	1,2,4-trimethyl benzene	s	0.003	0.002	0.011	0.021	0.072	0.040
29	16.59	benzofuran	u	0.014	0.027	0.090	0.108	0.457	0.291
30	16.89	tetrahydrofuran methanol	u	0.000	0.005	0.021	0.026	0.024	0.023
31	17.54	1,2,3-trimethyl benzene	s	0.001	0.086	0.118	0.150	0.313	0.162
32	18.15	indene	p	0.007	0.029	0.057	0.057	0.235	0.116
33	18.54	o-cresol	p	0.037	0.090	0.235	0.223	0.825	0.419
34	18.78	1,2-diethylbenzene	u	0.001	0.002	0.006	0.008	0.025	0.014
35	18.86	1-(2-methylcyclopent-1-en-1-yl)ethan-1-one	p	0.003	0.006	0.021	0.031	0.066	0.040
36	19.16	Acetophenone	p	0.000	0.000	0.002	0.003	0.007	0.004
37	19.30	m-cresol	s	0.035	0.110	0.371	0.285	0.953	0.632
38	19.78	Guaiacol	s	0.040	0.107	0.318	0.319	0.973	0.525
39	20.62	2-methyl-benzofuran	u	0.018	0.014	0.074	0.074	0.363	0.155
40	20.97	4-methyl benzoic acid	u	0.005	0.000	0.034	0.067	0.153	0.121
41	21.38	2-ethylphenol	u	0.004	0.004	0.018	0.020	0.117	0.040
42	21.67	2,3-dihydro-1-methyl-1H-indene	p	0.001	0.000	0.005	0.011	0.031	0.017
43	21.80	veratrol	s	0.009	0.020	0.062	0.073	0.321	0.138
44	21.99	2-methyl-1H-indene	p	0.008	0.000	0.026	0.043	0.127	0.066
45	22.05	1-methyl-1H-indene	p	0.005	0.003	0.019	0.028	0.111	0.060
46	22.25	benzoic acid	s	0.022	0.004	0.065	0.099	0.541	0.234
47	22.40	4-ethylphenol	p	0.007	0.002	0.003	0.002	0.005	0.003
48	22.48	2,5-dimethylphenol	u	0.006	0.024	0.083	0.089	0.273	0.175
49	23.24	pyrocatechol	s	0.126	0.418	1.194	2.335	3.034	3.574
50	24.09	4-methoxyphenol	s	0.003	0.017	0.022	0.026	0.124	0.042
51	24.19	4,7-dimethyl benzofuran	p	0.009	0.003	0.024	0.023	0.188	0.061
52	24.30	5-(hydroxymethyl)-furfural	s	0.030	0.046	0.235	0.326	1.192	0.405
53	24.66	2-ethyl-6-methyl-phenol	u	0.005	0.008	0.036	0.052	0.190	0.088

(continue)

54	25.30	2-ethyl-4-methyl-phenol	u	0.000	0.040	0.114	0.151	0.157	0.083
55	25.65	2,6-Dimethoxytoluene	p	0.001	0.002	0.037	0.044	0.182	0.068
56	25.75	2-Methoxy-1,3-dimethylbenzene	u	0.000	0.001	0.018	0.022	0.074	0.028
57	25.89	resorcinol	s	0.022	0.077	0.320	0.328	1.698	0.695
58	26.08	4-methyl-1,2-benzenediol	p	0.001	0.001	0.003	0.004	0.002	0.002
59	26.75	2-methylnaphthalene	p	0.002	0.002	0.010	0.127	0.057	0.156
60	27.22	3-methylnaphtalene	p	0.002	0.001	0.012	0.073	0.060	0.093
61	28.03	2,6-dimethoxy-phenol	p	0.000	0.252	0.573	0.674	0.540	0.560
62	28.22	eugenol	s	0.003	0.050	0.101	0.086	0.194	0.132
63	28.28	4-(tert-butyl)benzene-1,2-diol	p	0.001	0.000	0.023	0.035	0.049	0.030
64	28.51	2-methoxy-4-propyl-phenol	u	0.007	0.028	0.111	0.100	0.416	0.215
65	29.50	Vanillin	s	0.001	0.002	0.001	0.001	0.001	0.001
66	30.69	1,2,4-Trimethoxy benzene	p	0.007	0.141	0.414	0.509	0.420	0.430
67	30.92	2-methoxy-4-(1-propenyl)-phenol	u	0.008	0.039	0.322	0.392	0.479	0.380
68	32.76	1,2,3-trimethoxy-5-methyl-benzene	u	0.001	0.024	0.081	0.111	0.106	0.101
69	34.17	2,3,4-trimethoxy benzaldehyde	s	0.000	0.001	0.012	0.023	0.020	0.017
70	35.51	p-coumaryl alcohol	s	0.010	0.000	0.039	0.170	0.056	0.059
71	35.98	benzophenone	p	0.000	0.014	0.123	0.183	0.144	0.093
72	36.24	syringaldehyde	s	0.000	0.030	0.075	0.099	0.108	0.068
73	37.27	2,6-dimethoxy-4-(2-propenyl)-phenol	u	0.000	0.014	0.197	0.277	0.138	0.049
74	37.97	syringic acid	s	0.000	0.052	0.168	0.147	0.213	0.114
75	39.67	9-methylene-9H-fluorene	p	0.000	0.000	0.033	0.804	0.050	0.586
76	51.35	sinapyl alcohol	s	0.004	0.000	0.000	0.001	0.002	0.001
		TOTAL (%)[b]		3.7	6.7	18.7	24.1	48.4	31.6

a) a.c.: attribution confidence of identification with NIST:; P, probable, similarity index >91%; U, uncertain, similarity index with NIST <91% and S, standard, identified by retention time and MS spectrum; b) Total amount identified, calculated as follow: $\Sigma C_i/50$; where C_i is the concentration of each compound and 50 is the initial concentration of the vial.

Levoglucosan, furfural, and acetic acid were formed by cellulose and hemicellulose pyrolysis[16,25,32,40-43] and they were present only in the upper fractions which were rich in water and they were not observed in the bottom fraction. Only WP11L_BOT showed large amount of acetic acid which remained present in this

liquid too.

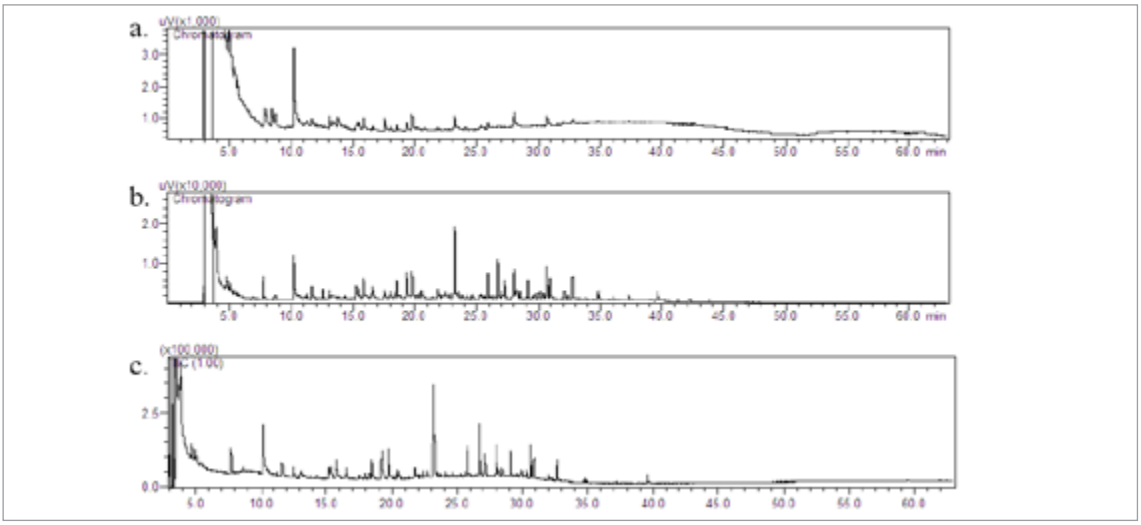

Figure 8.9. FID and TIC chromatograms of a) FID of WP12L_UP; b) FID of WP12L_BOT; c) TIC of WP12L_BOT.

The main phenolic compounds (phenol, m-cresol, guaiacol, veratrol, pyrocatechol, 4-methoxyphenol, resorcinol, and vanillin) were formed from lignin pyrolysis[30,32,34,44,45] and they were widely present in bottom fractions and in minor extent into water rich fractions. Their concentration rose when a MW absorber was employed suggesting that lignin was particularly transparent to MW radiation and an adsorber was required for its pyrolysis.

On the other hand concentration of furfural was steady, also in the absence of a MW absorber, in upper fractions and rose in bottom fraction due to the presence of phenolic compound able to dissolve it.

Some of monomers of lignin (such as syringaldehyde, syringic acid, coniferyl alcohol, and sinapyl alcohol), with a mass over 180 Da, were detected in very low concentration. They represent the upper limit of heavy compounds to be evaluated in the GC condition reported. Indeed other compounds with higher mass was not detected, such as catechin, quercitin, gallic acid methyl and ethyl esters.

8.3.4. HPLC/MS

HPLC analyses were performed over the standards with a mass over 100 Da, reported in Table 8.5, to validate the gradient technique employed and to record the actual mass spectrum and fragmentation of each compounds. The detected compound together with their fragmentation, in the positive and negative modes, are reported in Table 8.10.

Only a limited number of the analyzed standards were detected. Most of them were detected selectively in the positive or in the negative mode, thus the analysis in both mode was mandatory to detected the largest number of compounds.

Table 8.10. Standards detected in HPLC/MS analysis together with their retention time and fragmentation. ithin brac

Entry	Compound	MS experiment	rt	$(M\pm H)^{\pm a}$	$[(M\pm H)\text{-}nH_2O]^{\pm}$	$[(M\pm H)\text{-}nCO_2]^{\pm}$	$[(M\pm H)\text{-}nCO]^{\pm}$	$[(M\pm H)\text{-}nMeOH]^{\pm}$	$[(M\pm H)\text{-benzene}]^{\pm}$	$[(M\pm H)\text{-}nMe]^{\pm}$	$[(M\pm H)\text{-}n\ CO_2R]^{\pm}$
1	2-napthol	-MS	11.21	143,05019	125,06069 (7)						
		+MS		145,06469	127,07530 (0.1)						
3	2,6-dihydroxybenzoic acid	-MS	2.20	153,01912	135,00867 (22)	109,02960					
		+MS		155,03364	137,02308 (5)	111,02005 (1)					
4	2-ethyltoluene	+MS	10.77	121,10099							
5	2-methoxy-4-methylphenol	+MS	6.99	139,07518							
6	3',5'-dimethoxy-4'-hydroxy acetophenone	-MS	5.35	195,06656							
		+MS		197,08014			167,06986 (2)				
7	2,3,4-trimethoxy benzaldehyde	+MS	7.37	197,08005							
8	Benzoic acid	-MS	6.53	121,02954							
9	catechol	-MS	2.70	109,02948							
10	Ethyl gallate	-MS	4.40	197,04527							124,01666 (23)

(continue)

11	Eugenol	-MS	11.50	163,07607	145,05042 (51)		131,03470 (57)			
		+MS		165,09069	147,04394 (7)		133,06461 (8)			
12	Benzophenone	+MS	9.67	183,08007				105,03344 (4)		
13	Gallic acid	-MS	1.27	169,01412		125,02437 (84)				
14	Methyl gallate	-MS	3.33	183,02969		140,01132 (9)			168,00619 (2)	124,01652 (56)
15	Vanillin	-MS	4.25	151,03989					151,03989 (74)	
		+MS		153,05432						
16	resorcinol	-MS	2.29	109,02956						
17	Quercitin	-MS	10.52	301,03523						
18	Pyrogallol	-MS	1.50	125,02441						
		+MS		127,03899						
19	p-coumaryl alcohol	-MS	3.72	149,06073	131,05030 (28)					
20	guaiazulene	+MS	12.98	199,14789						
21	Guaiacol	+MS	6.04	125,05969						
22	napthalene	+MS	0.57	129,05200						

a) Relative intensity was 100 for each compounds.

Few of the standards were identified into selected liquids (WP4L_UP, WP4L_BOT, WP8L_UP, WP8L_BOT); a list of the presence or absence of them is reported in Table 8.11.

Table 8.11. Stadands identified into selected liquids (WP4L_UP, WP4L_BOT, WP8L_UP, WP8L_BOT). When identified the MS peak was of very weak intensity (below 1% of relative intensity). P: present; n.d.: not detected.

Entry	Compound	MS experiment	WP4L_BOT	WP4L_UP	WP8L_BOT	WP8L_UP
1	2-ethyltoluene	+MS	n.d.	n.d.	n.d.	p
2	2-methoxy-4-methylphenol	+MS	n.d.	n.d.	p	p
3	3',5'-dimethoxy-4'-hydroxy acetophenone	-MS	p	n.d.	n.d.	n.d.
		+MS	p	p	n.d.	n.d.
4	2,3,4-trimethoxy benzaldehyde	+MS	n.d.	p	p	p
5	Ethyl gallate	-MS	p	P	p	p
6	Eugenol	+MS	p	n.d.	P	P
7	Benzophenone	+MS	p	P	P	P
8	Gallic acid	-MS	n.d.	p	p	n.d.
9	Methyl gallate	-MS	n.d.	n.d.	p	p
10	Vanillin	+MS	p	p	p	p
11	Pyrogallol	+MS	p	n.d.	p	p
12	Guaiacol	+MS	n.d.	p	p	p
13	napthalene	+MS	n.d.	p	p	n.d.

Few of the standards identified were present in the liquids (Table 8.11), and even if they were identified, using both their rt and MS spectrum, the intensity of their base peak was below 1 % of relative intensity. Probably these compounds were more diluted than the standards, the sensitivity of the mass analyzer was low for these compounds, and they were mixed with the background noise which contribute with peaks in the range of 100 – 200 m/z. So far the HPLC did not work to its fullest potential with compounds with a masses below 300 Da which were the expected one in these liquids (see Sections 8.3.2 and 8.3.3). Furthermore several studies on liquids, which employed similar mass analyzer, limited the investigate masses range above 400 Da.[46-50]

However the HPLC analyses, even at this level, might give some information on the presence/absence of the reference compounds (Table 8.11) and the presence/absence of other relevant peaks over the 300 Da threshold. However no other relevant peaks were identified over 300 Da suggesting a prevalent mass distribution below 200 Da.

8.3.5. ^{1}H NMR

^{1}H NMR spectra of liquids (up and bottom phases) were a source of several informations. NMR was employed to evaluate water content by using an internal standard (see "Appendix II: Analytical Methods"). The nature of protons was assigned as follow (partially using ranges reported by Özbay et al.[51]): δ 13.0-12.0 (mobile proton of carboxylic acid); 10.0-9-0 (aldehyde); 9.0-6.5 (aromatic, furan, and C=CH-OCC); 6.5-5.0 (phenolic "OH" or C=CH olefins); 5.0-3.3 (CH_2-O-C; or CH_2-OOC; or ring-join methylene, Ar-CH_2-Ar); 3.3-2.0 (CH_3, CH_2, and CH on aromatic ring); 2.0-1.6 (CH, CH_2 of alkyl gropus; CH_2 and CH in β position to an aromatic ring); 1.6-1.0 (CH_2, CH_3 of alkyl groups, CH_3 in β position and CH_2 and CH in γ position to an aromatic ring or ether oxygen); 1.0-0-5 (CH_3 of alkyl groups or in γ position or further of an alkyl chain linked to an aromatic ring).

The ^{1}H NMR spectra of WP5L_UP, and their water subtracted spectra together with the integral region, are reported in Figure 8.10.

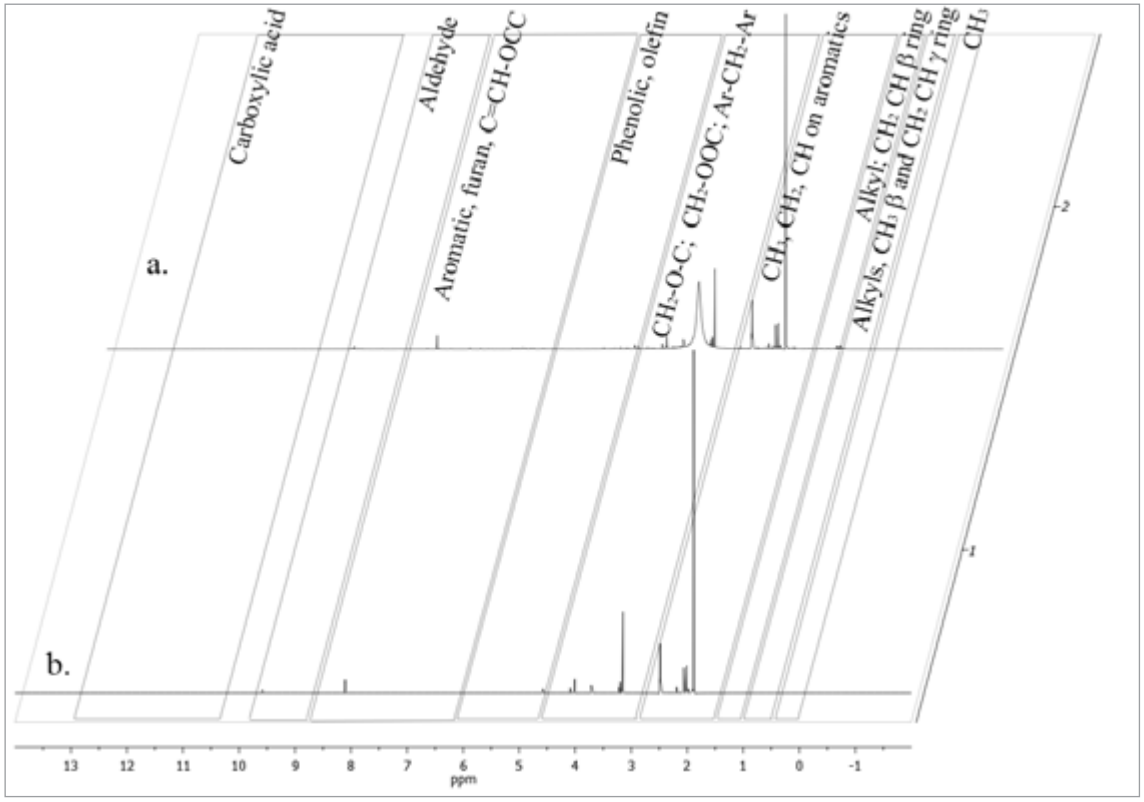

Figure 8.10. ^{1}H NMR spectra of WP5L_UP and their relative water subtract spectra together with the integral region.

Areas of residual spectra are reported in Table 8.12, they were calculated after subtracting the water peak, and then the sum of all areas was normalized to 100.0.

Table 8.12. Normalized areas of upper phase of liquids.

Hydrogen class	Mobile proton from carboxylic acids	Aldehydes	Aromatic, furan, and C=CH-OCC	Phenolic "OH" or C=CH olefins	CH_2-O-C; or CH_2-OOC; or ring-join methylene, Ar-CH_2-Ar	CH_3, CH_2, and CH on aromatic rings	CH, CH_2 alkyl gropus; CH_2, CH β to an aromatic ring	CH_2, CH_3 alkyl groups, CH_3 in β and CH_2, CH in γ to aromatic ring or ether oxygen	CH_3 of alkyl groups or in γ or further of an alkyl chain linked to aromatic ring
Chemical shift (ppm)	13.0-12.0	10.0-9.0	9.0-6.5	6.5-5.0	4.5-3.3	3.3-2.0	2.0-1.6	1.6-1.0	1.0-0.5
Entry									
WP1L_UP	0.00	2.12	1.92	0.00	0.00	35.65	48.88	7.46	3.98
WP3L_UP	10.36	0.31	5.28	11.67	0.47	2.58	60.98	3.93	4.42
WP4L_UP	6.58	1.31	4.78	6.55	2.87	19.83	43.59	9.27	5.21
WP5L_UP	1.97	0.69	8.09	16.10	15.28	5.36	42.49	6.01	4.02
WP8L_UP	1.31	0.90	6.88	14.08	8.57	27.44	30.97	6.27	3.58
WP11L_UP	0.64	0.78	5.38	9.59	20.34	23.60	32.53	3.67	3.46
WP12L_UP	2.79	1.49	8.42	16.63	7.35	5.08	47.05	6.20	4.99

The signal of acid protons was always present except for WP1L_UP. Probably acids were not formed in the first step of pyrolysis and they were pyrolyzed in the presence of a MW absorber. Indeed carboxylic acid areas were reduced when a MW absorber and a strong mixing protocol were employed. WP4L_UP, where no mixing was used, had a high value compared closer to WP3L_UP where there was no absorber. Aldehydes and aromatic/furan integrals were weakly present and negligible differences were shown. Phenolic protons and protons in β position to an oxygen were weakly present when no MW absorber or no mixing was used and they were improved when a MW absorber was employed. These data were in agreement with GC/MS-FID analysis (Section).

The ^{1}H NMR spectrum of W5L_BOT is reported in Figure 8.11.

The main group of signal (central peak) and their attribution are listed as follow together with their attribution and relative intensity (s, strong; m, medium; w, weak):

- 12.04 ppm (w): acids mobile protons.
- 9.60 ppm (w): aldehyde.
- 8.79, 8.25, 8.10, 7.98, 7.54, 7.19, 6.75, and 6.55 ppm (w): aromatic ring.
- 6.40 ppm (w): phenolic OH.
- 4.94, 4.72, 4.02, 3.81. 3.70 ppm (m): CH_2-OOC; or ring-join methylene, Ar-CH_2-Ar
- 3.55 ppm (m): CH_2-O-C.

- 3.34 ppm (s): water
- 3.14 (m) and 2.48, 1.18, and 2.06 ppm (s): CH_3, CH_2, and CH on aromatic ring.
- 1.98, 1.89, and 1.21 (w): CH_2, CH_3 of alkyl groups, CH_3 in b position and CH2 and CH in g position to an aromatic ring or ethereal oxygen.
- 0.96 and 0.91 ppm (w): CH_3 of alkyl groups or in g position or further of an alkyl chain linked to an aromatic ring.

These data were in agreement with GC/MS-FID analysis confirming the phenolic nature of the bottom phases.

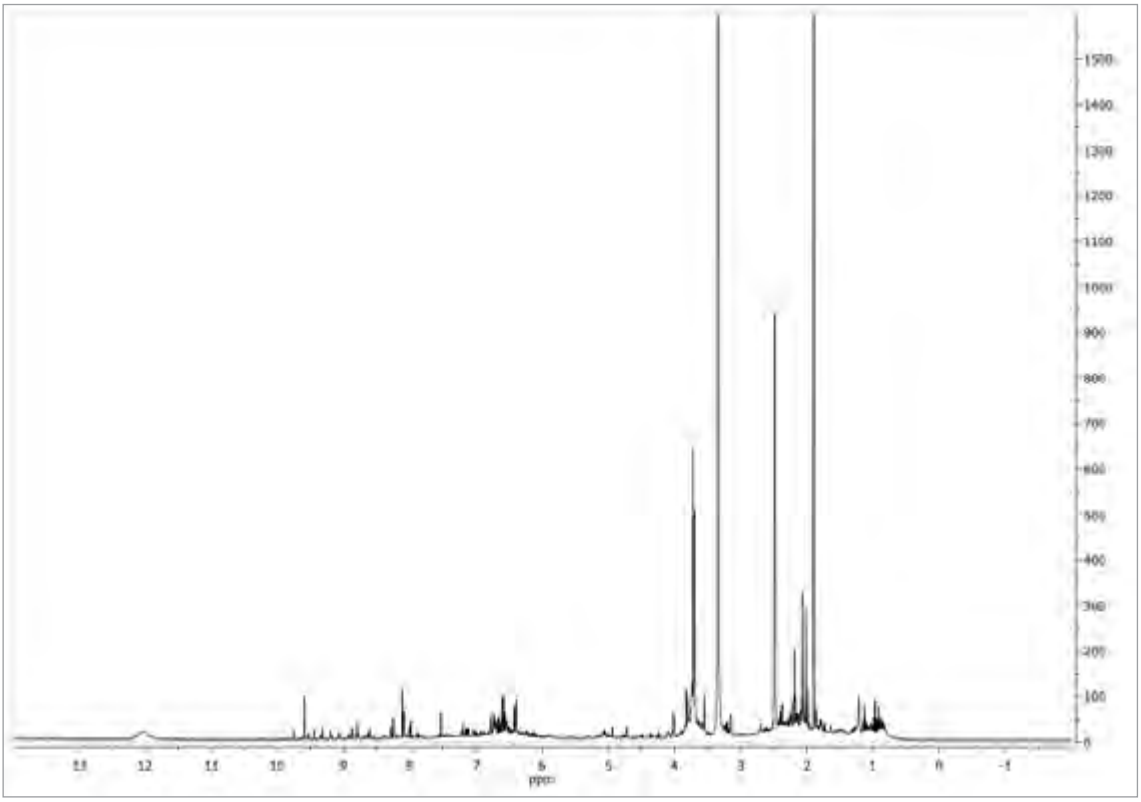

Figure 8.11. ^{1}H NMR spectra of W5L_BOT.

8.3.6. FTIR

FTIR analyses of both fractions supported the other data reported. Upper fractions were mainly composed of water and water spectrum was always subtracted. Bottom fractions had a low content of water anyway water spectrum was subtracted also from them. Water subtracted spectra of WP5L_UP and WP5L_BOT are reported in Figure 8.12. Relative intensity of each peak is reported in Table 8.13 for upper phase and listed for bottom phase. The relative intensities were referred to water subtracted spectra.

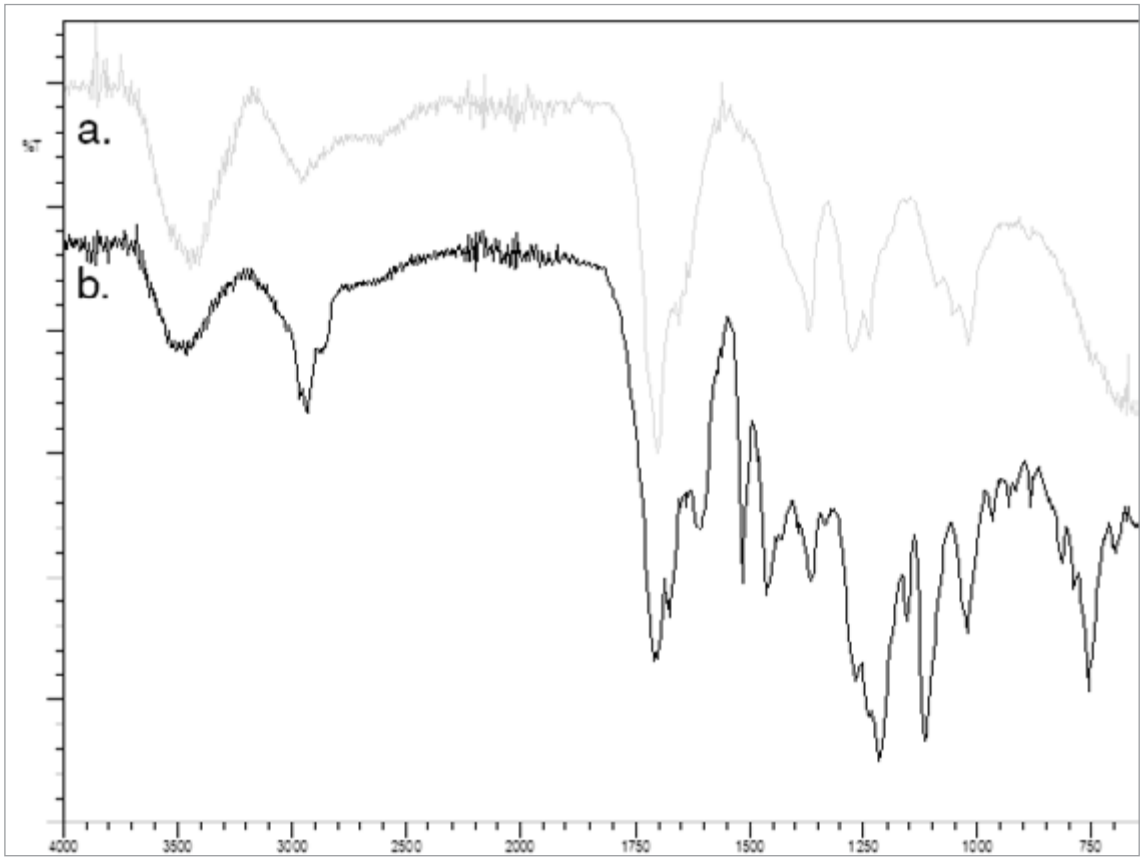

Figure 8.12. FTIR spectra of: a) WP12L_UP; b) WP12L_BOT.

All IR spectra had similar absorption and similar relative intensities between peaks in each spectrum. However some distinctive differences were highlighted. WP1L_UP spectrum perfectly overlapped WP3L_UP spectrum except for the overall intensity. All spectra from WP4L_UP to WP12L_UP had almost the same absorptions of WP3L_UP but stronger intensity below 1700 cm^{-1}.

Table 8.13. IR absorptions of upper phase of liquids from MAP of WP[a].

Frequency (cm^{-1})	Attribution	WP1L_UP	WP2L_UP	WP3L_UP	WP4L_UP	WP5L_UP	WP6L_UP	WP7L_UP	WP8L_UP	WP9L_UP	WP10L_UP	WP11L_UP	WP12L_UP	WP13L_UP	WP14L_UP
3400	H-bonded OH stretching	s	s	s	s	s	s	s	s	s	s	s	s	s	s
2964/2876	Methyl C-H asym./sym. stretching	m	m	m	m	m	m	m	m	m	m	m	m	m	m
2910/2860	Methylene C-H asym./sym. stretching	m	m	m	m	m	m	m	m	m	m	m	m	m	m
1710 wide	C=O stretching	s	s	s	s	s	s	s	s	s	s	s	s	s	s
1650	Alkenyl C=C stretching	w	w	w	w	w	w	w	w	w	w	w	w	w	w
1610	Conjugated C=C stretching	w	m	m	m	m	m	m	m	m	m	m	m	m	m
1515	C-C stretching (near oxygen)	w	w	w	w	m	m	m	m	w	w	w	n.d.	w	w
1470	Methylene C-H bending	w	w	w	w	w	w	w	w	w	w	w	w	w	w
1410/1375	Methyl C-H asym./sym. bending	m	m	m	m	m	m	m	m	m	m	m	m	m	m
1316; 1270	Primary or secondary alcohol, OH in-plane bending	m	s	s	s	m	m	m	m	s	s	s	s	s	s
1250	Aromatic ethers, aryl-O stretching	n.d.	n.d.	n.d.	n.d.	m	m	m	m	n.d.	n.d.	n.d.	m	n.d.	n.d.
1120	Tertiary alcohol, C-O stretching	w	w	w	w	m	m	s	m	w	w	w	w	w	w
1104	Secondary alcohol, C-O stretching	m	m	m	m	w	w	n.d.	w	m	m	m	m	m	m
1050	Primary alcohol, C-O stretching	m	w	w	w	m	m	m	m	w	w	w	w	w	w
720	Methylene $-(CH_2)_n$- rocking, n≥3	w	w	w	w	w	w	w	w	w	w	w	w	w	w
679	Alcohol, OH out-of-plane bending	s	s	s	s	s	s	s	s	s	s	s	s	s	s
651; 639; 618; 603	Alcohol, OH out-of-plane bending	s	s	s	s	s	s	s	s	s	s	s	s	s	s

a) Intensity reported as follow: s, strong; m, medium; w, weak; n.d. not detected.

The main absorptions frequencies identified in each bottom phase are reported as follow together with their attribution and relative intensity (s, strong; m, medium; w, weak):

- 3400 board cm^{-1} (m): H-bonded OH stretching.
- 2964 and 2865 cm^{-1} (m): Methyl C-H asym./sym. Stretching.

- 2931 and 2853 cm^{-1} (m): Methylene C-H asym./sym. Stretching.
- 1850-1750 multiple bands cm^{-1} (w): Aromatic combination bands.
- 1707 cm^{-1} (s): C=O stretching
- 1675 cm^{-1} (s): C=O stretching, conjugated.
- 1636 cm^{-1} (w): Alkenyl C=C stretching.
- 1610 cm^{-1} (m): Conjugated C=C stretching.
- 1515 cm^{-1} (s): C-C stretching (near oxygen).
- 1465 cm^{-1} (m): Methylene C-H bending.
- 1425 and 1365 cm^{-1} (m): Methyl C-H asym./sym. bending.
- 1265 cm^{-1} (w): Primary or secondary alcohol, OH in-plane bending.
- 1240 cm^{-1} (m): Aromatic ethers, aryl-O stretching.
- 1115 cm^{-1} (m): Tertiary alcohol, C-O stretching.
- 1020 cm^{-1} (w): Primary alcohol, C-O stretching.
- 1020 and 965-880 cm^{-1} (w): Aromatic bending.
- 750 cm^{-1} (m): Methylene $-(CH_2)_{n-}$ rocking, $n \geq 3$.
- 679 cm^{-1} (m): Alcohol, OH out-of-plane bending.
- 651; 639; 618; and 603 cm^{-1} (w): Alcohol, OH out-of-plane bending.

Both phases had similar absorption but different intensities. The broad absorption at 3400 cm^{-1} was stronger for the upper phase, confirming its larger water content while below 1600 cm^{-1} bottom phase had absorption with stronger intensities supporting the presence of large amount of organic materials.

8.4. Gas product

Gases were a mixture of CO, CO_2, H_2, aldehydes, ketones, and other short chain alkanes and alkenes. Gases were analyzed through FTIR for functional group identification and chemical trapping for aldehydes and ketones identification.

8.4.1. FTIR

Three fractions of selected pyrolyses were analyzed using FTIR. These fractions were collected at 3, 13 minutes, and the end of pyrolysis. Similar absorption were shown by the three fractions but different intensities were shown. A comparison between the three FTIR spectra of WP11G is reported in Figure 8.13.

CO_2 was predominant and except for WP1G the asymmetric stretching was always out-of-scale in all three collected fractions. Its formation started after the beginning of pyrolysis and its concentration increased during the course of pyrolysis. Indeed other absorption of CO_2 (at 3850 and 3750 cm^{-1}) increased their relative intensity from the first to the third fraction. CO formation was low if compared to CO_2, and it was maxim in the middle fraction. Water was always present but its concentration remained extremely low in any gas analyzed.

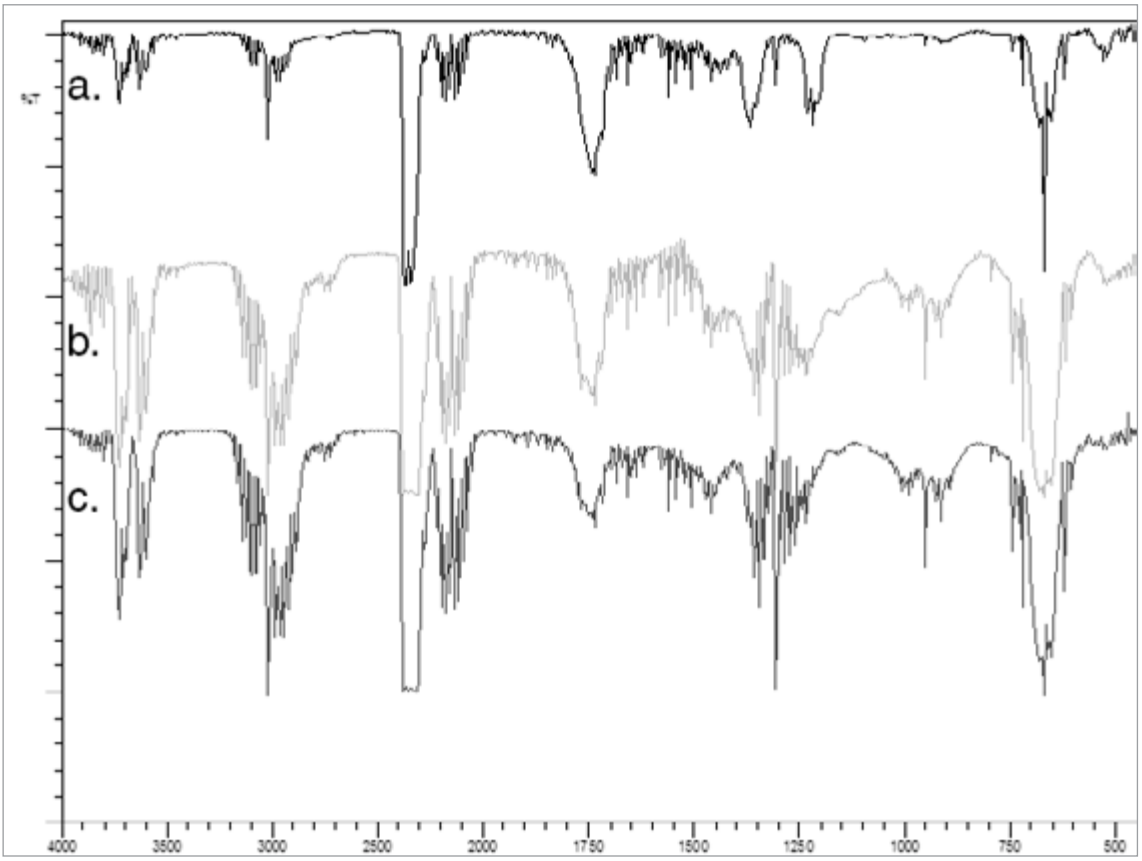

Figure 8.13. FTIR spectra of WP11G after 3, 13, and 26 min from the start of pyrolysis.

Identified peaks and their relative absorptions are reported in Table 8.14.

Carbonyl group and C-H absorptions were weak in the first fraction, increased in the second, and slightly decreased in the last. They were formed in small amount in first minutes of pyrolysis where mainly macromolecules were depolymerized. The last fraction had lower concentration of hydrocarbons than the middle one but higher than the first one; probably secondary reactions might take place. The nature of carbonyl compounds is discussed in the following Section.

Table 8.14. IR absorption of selected samples, second fraction of the gas stream[a].

Frequency (cm^{-1})	Attribution	WP1G	WP3G	WP4G	WP5G	WP8G	WP11G	WP12G
3853; 3750	CO_2 bands mixed with water vapors	m	m	m	m	s	m	s
3017	Aldehyde C-H stretching	n.d.	m	s	s	s	s	s
2951; 2872	Methyl CH asym./sym. Stretching	n.d.	w	w	m	m	m	m
2360; 2341	CO_2 asymmetric stretching	m	oos	oos	oos	oos	oos	oos
2179; 2120 multiple bands	CO	n.d.	m	m	m	s	m	s
1730; 1717	CO carbonyl stretching	n.d.	n.d.	n.d.	m	m	m	m
1653; 1559 multiple bands	Water gas phase	s	w	w	w	w	w	w
1457; 1373	Methyl CH asym./sym. bending	n.d.	n.d.	n.d.	w	w	w	w
720	Methylene $-(CH_2)_n-$ rocking, $n\geq3$	n.d.	n.d.	n.d.	w	w	w	w
668	CO2 bending modes	w	s	s	s	s	s	s
617	Alcohol, OH out-of-plane bending	n.d.	n.d.	n.d.	w	w	w	w

a) Intensity reported as follow: oos, out-of-scale; s, strong; m, medium; w, weak; n.d. not detected.

8.4.2. Chemical trapping

Gas formed in the course of WP6 and WP10 were bubbled in an acid solution of 2,4-dinitrophenylhydrazine (DNPH) in methanol in order to trap and characterize the hydrazones formed. Possible compounds formed between DNPH and simple aldehydes and ketones are reported in Figure 8.14.

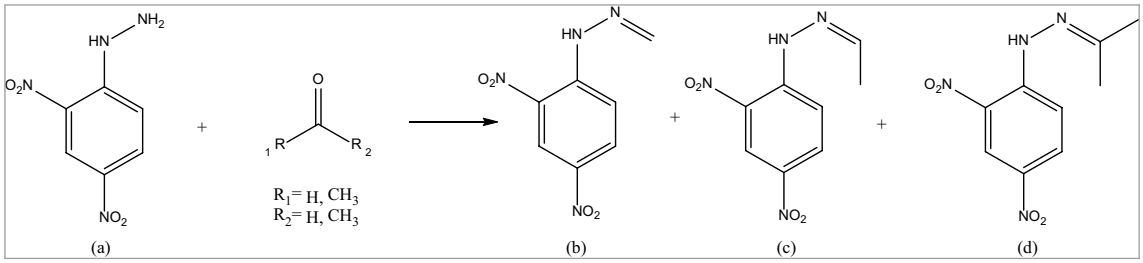

Figure 8.14. Hydrazine form DNPH (a) and formaldehyde, acetaldehyde, and acetone: b) 1-(2,4-dinitrophenyl)-2-methylenehydrazine; c) 1-(2,4-dinitrophenyl)-2-ethylidenehydrazine; d) 1-(2,4-dinitrophenyl)-2-(propan-2-ylidene)hydrazine.

An orange precipitate was always obtained, filtered, washed, and characterized via ^{1}H NMR, the spectrum from WP6G is reported in Figure 8.15.

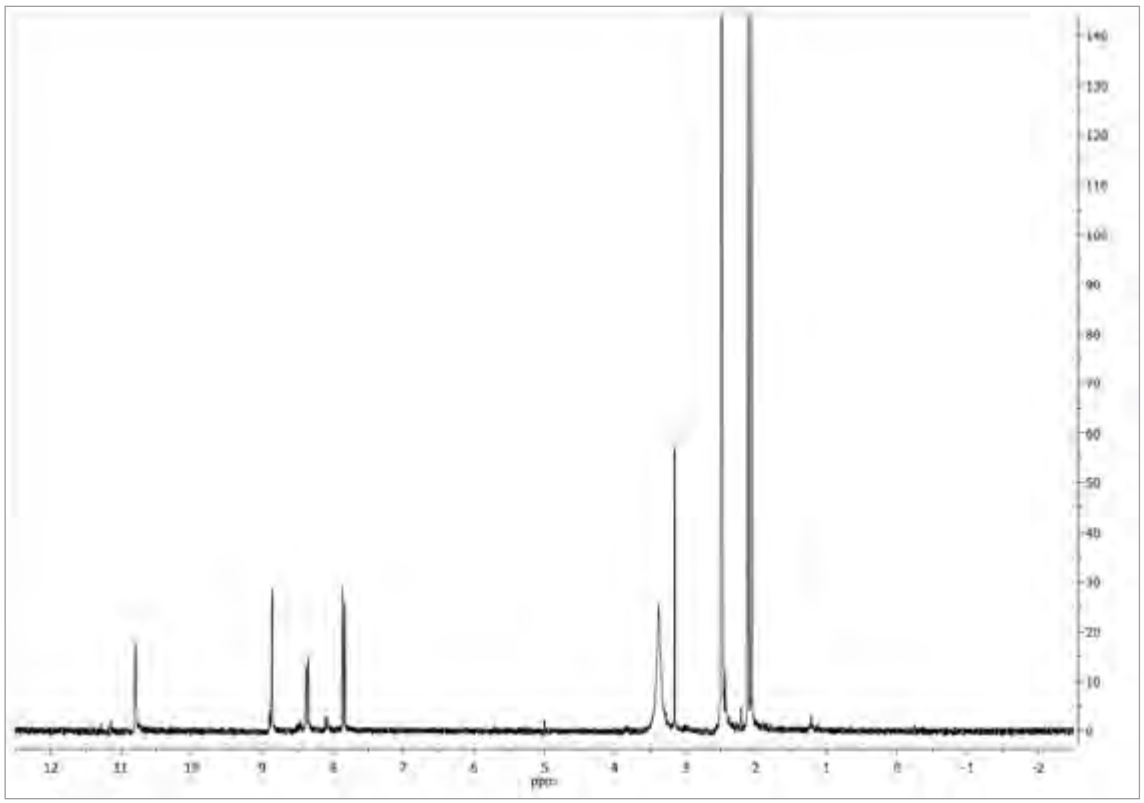

Figure 8.15. ^{1}H NMR spectrum of precipitate from WP6G.

^{1}H NMR peaks: δ 11.14 (s, 1H), 10.80 (s, 12.5H), 8.86 (d, J^{4} = 2.7 Hz, 13.5H), 8.36 (dd, J^{3} = 9.6, 2.7 Hz, 13.5H), 8.09 (d, J^{3} = 9.6 Hz, 2H), 7.85 (d, J^{3} = 9.6 Hz, 13.5H), 3.15 (s, 10.75H), 2.44 (s, 6,75H), 2.11 (s, 37.5H), 2.07 (s, 37.5H), 1.22 (m, 3H).

1-(2,4-dinitrophenyl)-2-(propan-2-ylidene)hydrazine was the only compound identified. Formaldehyde, acetaldehyde, and acetone were not identified via GC/MS-FID (Section 8.3.3) and probably they were overwhelmed by the solvent signal in GC. However only acetone went in gas phase and then was trapped.

8.5. Main achievements

Microwave assisted pyrolysis (MAP) of wood pellets (WP) was performed using different MW absorber (none, Fe, and carbon), mixing protocol of the MW absorber, apparatus set-up, and MW power.

MAP of WP might be run without a MW absorber but the pyrolysis could not be completed. MW absorber (Fe and carbon) were mixed with WP with three mixing protocol, none, mild, and strong, which affected the properties of solid and liquid only when Fe the MW absorber. Furthermore Fe was probably involved in coupling reaction within radical intermediates in the reactor which increased the yield of solid.

WP were converted into a char which preserved their former shape except when a MW absorber was not used.

The liquid obtained was separated in two phases, an upper and a bottom phase. These phases were characterized using an innovative chromatographic methodology. A single sample were prepared for thin layer chromatography, GC, and HPLC analyses. Quantitative analysis of liquid were performed using the relative response factor (RRF) referred to a compound present in the liquid. For the compound identified, but for which a RRF was not available, the RRF was predicted using an innovative formula.

The upper phases were composed of water and furans (such as furfural) and single ring phenols as minor compounds. The bottom phases were rich in phenols which were from lignin degradation.

MAP of WP showed the possibility to convert efficiently a biomass, non-thermoplastic, as all the other polymer tested (Sections 6 and 9), in products which might be employed in energy production (solid and liquid product), carbon sequestration (solid product), or source of chemicals (liquid product).

Reference

1. Undri, A.; Rosi, L.; Frediani, M.; Frediani, P. Efficient Disposal of Waste Polyolefins through Microwave Assisted Pyrolysis. *Fuel* **2013**, 116, 662-671.
2. Undri, A.; Rosi, L.; Frediani, M.; Frediani, P. Reverse Polymerization of Waste Polystyrene through Microwave Assisted Pyrolysis. *J. Anal. Appl. Pyrol.* **2013**, http://dx.doi.org/doi:10.1016/j.jaap.2013.10.001.
3. Miura, M.; Kaga, H.; Sakurai, A.; Kakuchi, T.; Takahashi, K. Rapid pyrolysis of wood block by microwave heating. *J. Anal. Appl. Pyrol.* **2004**, 71, 187–199.
4. Miura, M.; Kaga, H.; Yoshida, T.; Ando, K. Microwave pyrolysis of cellulosic materials for the production of anhydrosugars. *J. Wood Sci.* **2001**, 47, 502-506.
5. Farag, S.; Sobhy, A.; Akyel, C.; Doucet, J.; Chaouki, J. Temperature profile prediction within selected materials heated by microwaves at 2.45GHz. *Appl. Therm. Eng.* **2012**, 36, 360-369.
6. Vongpradubchai, S.; Rattanadecho, P. The microwave processing of wood using a continuous microwave belt drier. *Chem. Eng. Process.* **2009**, 48, 997-1003.
7. Undri, A.; Rosi, L.; Frediani, M.; Frediani, P. Upgraded Fuel from Microwave Assisted Pyrolysis of Waste Tire. *Fuel* **2014**, 115, 600-608.
8. Undri, A.; Meini, S.; Rosi, L.; Frediani, M.; Frediani, P. Microwave Pyrolysis of Polymeric Materials: Waste Tires Treatment and Characterization of the Value-Added Products. *J. Anal. Appl. Pyrol.* **2013**, 103, 149-158.
9. Robinson, J. P.; Kingman, S. W.; Barranco, R.; Snape, C. E.; Al-Sayegh, H. Microwave Pyrolysis of Wood Pellets. *Ind. Eng. Chem. Res.* **2010**, 49, 459-463.
10. Undri, A.; Sacchi, B.; Cantisani, E.; Toccafondi, N.; Rosi, L.; Frediani, M.; Frediani, P. Characterization of Carbon from Microwave Assisted Pyrolysis of Tires. *J. Anal. Appl. Pyrol.* **2013**, 104, 396-404.
11. Bolm, C.; Legros, J.; Le Paih, J.; Zani, L. Iron-Catalyzed Reactions in Organic Synthesis. *Chemical Reviews* **2004**, 104, 6217-6254.
12. Dongol, K. G.; Koh, H.; Sau, M.; Chai, C. L. L. Iron-Catalysed sp3–sp3 Cross-Coupling Reactions of Unactivated Alkyl Halides with Alkyl Grignard Reagents. *Advanced Synthesis & Catalysis* **2007**, 349, 1015-1018.
13. Hayashi, Y.; Shinokubo, H.; Oshima, K. Intramolecular Radical Cyclization of 2-Haloethanal Allyl Acetal and Allyl 2-Halophenyl Ether with a Grignard Reagent in the Presence of Iron(II) Chloride. *Tetrahedron Lett.* **1998**, 39, 63-66.
14. López, F. A.; Centeno, T. A.; Alguacil, F. J.; Lobato, B.; Urien, A. The GRAUTHERMIC-Tyres process for the recycling of granulated scrap tyres. *J. Anal. Appl. Pyrol.* **2013**, 103, 207–215.
15. López, F. A.; Centeno, T. A.; Alguacil, F. J.; Lobato, B.; López-Delgado, A.; Fermoso, J. Gasification of the char derived from distillation of granulated scrap tyres. *Waste Manage.* **2012**, 32, 743-752.
16. Mohan, D.; Pittman, C. U.; Steele, P. H. Pyrolysis of Wood/Biomass for Bio-oil: A Critical Review. *Energy Fuels* **2006**, 20, 848-889.
17. Spokas, K. A. Review of the stability of biochar in soils: predictability of O:C molar ratios. *Carbon Management* **2010**, 1, 289-303.
18. Ptasinski, K. J.; Prins, M. J.; Pierik, A. Exergetic evaluation of biomass gasification. *Energy* **2007**, 32, 568-574.
19. Crelling, J. C.; Hagemann, H. W.; Sauter, D. H.; Ramani, R. V.; Vogt, W.; Leininger, D.; Krzack, S.; Meyer, B.; Orywal, F.; Reimert, R.; Bonn, B.; Bertmann, U.; Klose, W.; Dach, G.: Coal. In Ullmann's Encyclopedia of Industrial Chemistry; Wiley-VCH Verlag GmbH & Co. KGaA, 2000.

20. Predel, H.: Petroleum Coke. In Ullmann's Encyclopedia of Industrial Chemistry; Wiley-VCH Verlag GmbH & Co. KGaA: Karlsruhe, Germany, 2000.
21. Bridgwater, A. V.; Peacocke, G. V. C. Fast pyrolysis processes for biomass. *Renew. Sust. Energ. Rev.* **2000**, 4, 1-73.
22. Ren, S.; Lei, H.; Wang, L.; Bu, Q.; Chen, S.; Wu, J.; Julson, J.; Ruan, R. Biofuel production and kinetics analysis for microwave pyrolysis of Douglas fir sawdust pellet. *J. Anal. Appl. Pyrol.* **2012**, 94, 163-169.
23. Bridgwater, A. V. Renewable fuels and chemicals by thermal processing of biomass. *Chem. Eng. J.* **2003**, 91, 87-102.
24. Ronsse, F.; Bai, X.; Prins, W.; Brown, R. C. Secondary reactions of levoglucosan and char in the fast pyrolysis of cellulose. *Environ. Prog. Sustain. Energy* **2012**, 31, 256-260.
25. Westerhof, R. J. M.; Brilman, D. W. F.; Garcia-Perez, M.; Wang, Z.; Oudenhoven, S. R. G.; van Swaaij, W. P. M.; Kersten, S. R. A. Fractional Condensation of Biomass Pyrolysis Vapors. *Energy Fuels* **2011**, 25, 1817-1829.
26. Nolte, M. W.; Liberatore, M. W. Viscosity of Biomass Pyrolysis Oils from Various Feedstocks. *Energy Fuels* **2010**, 24, 6601-6608.
27. Wang, X.; Chen, H.; Luo, K.; Shao, J.; Yang, H. The Influence of Microwave Drying on Biomass Pyrolysis. *Energy Fuels* **2007**, 22, 67-74.
28. Salehi, E.; Abedi, J.; Harding, T. Bio-oil from Sawdust: Effect of Operating Parameters on the Yield and Quality of Pyrolysis Products. *Energy Fuels* **2011**, 25, 4145-4154.
29. Salehi, E.; Abedi, J.; Harding, T. G.; Seyedeyn-Azad, F. Bio-oil from Sawdust: Design, Operation, and Performance of a Bench-Scale Fluidized-Bed Pyrolysis Plant. *Energy Fuels* **2013**, 27, 3332-3340.
30. Kibet, J.; Khachatryan, L.; Dellinger, B. Molecular Products and Radicals from Pyrolysis of Lignin. *Environ. Sci. Technol.* **2012**, 46, 12994-13001.
31. Mani, T.; Murugan, P.; Abedi, J.; Mahinpey, N. Pyrolysis of wheat straw in a thermogravimetric analyzer: Effect of particle size and heating rate on devolatilization and estimation of global kinetics. *Chem. Eng. Res. Des.* **2010**, 88, 952-958.
32. Branca, C.; Giudicianni, P.; Di Blasi, C. GC/MS Characterization of Liquids Generated from Low-Temperature Pyrolysis of Wood. *Ind. Eng. Chem. Res.* **2003**, 42, 3190-3202.
33. Wang, Y.; Li, X.; Mourant, D.; Gunawan, R.; Zhang, S.; Li, C.-Z. Formation of Aromatic Structures during the Pyrolysis of Bio-oil. *Energy Fuels* **2012**, 26, 241–247.
34. Ben, H.; Ragauskas, A. J. NMR Characterization of Pyrolysis Oils from Kraft Lignin. *Energy Fuels* **2011**, 25, 2322-2332.
35. Musumarra, G.; Pisano, D.; Katritzky, A. R.; Lapucha, A. R.; Luxem, F. J.; Murugan, R.; Siskin, M.; Brons, G. Prediction of gas chromatographic response factors by the PLS method. *Tetrahedron Computer Methodology* **1989**, 2, 17-36.
36. Tissot, E.; Rochat, S.; Debonneville, C.; Chaintreau, A. Rapid GC-FID quantification technique without authentic samples using predicted response factors. *Flavour Frag. J.* **2012**, 27, 290-296.
37. Jones, F. W. Estimation of Flame-Ionization Detector Relative Response Factors for Oligomers of Alkyl and Aryl Ether Polyethoxylates using the Effective Carbon Number Concept. *J. Chromatog. Sci.* **1998**, 36, 223-226.
38. Katritzky, A. R.; Ignatchenko, E. S.; Barcock, R. A.; Lobanov, V. S. Prediction of Gas Chromatographic Retention Times and Response Factors Using a General

Quantitative Structure-Property Relationship Treatment. *Anal. Chem.* **1994**, 66, 1799-1807.
39. de Saint Laumer, J.-Y.; Cicchetti, E.; Merle, P.; Egger, J.; Chaintreau, A. Quantification in Gas Chromatography: Prediction of Flame Ionization Detector Response Factors from Combustion Enthalpies and Molecular Structures. *Anal. Chem.* **2010**, 82, 6457-6462.
40. Bai, X.; Johnston, P.; Sadula, S.; Brown, R. C. Role of levoglucosan physiochemistry in cellulose pyrolysis. *J. Anal. Appl. Pyrol.* **2013**, 99, 58-65.
41. Zhou, C.-H.; Xia, X.; Lin, C.-X.; Tong, D.-S.; Beltramini, J. Catalytic conversion of lignocellulosic biomass to fine chemicals and fuels. *Chem. Soc. Rev.* **2011**, 40, 5588-5617.
42. Lin, Y.-C.; Cho, J.; Tompsett, G. A.; Westmoreland, P. R.; Huber, G. W. Kinetics and Mechanism of Cellulose Pyrolysis. *J. Phys. Chem. C* **2009**, 113, 20097-20107.
43. Ertas, M.; Alma, M. H. Pyrolysis of laurel (Laurus nobilis L.) extraction residues in a fixed-bed reactor: Characterization of bio-oil and bio-char. *J. Anal. Appl. Pyrol.* **2010**, 88, 22-29.
44. Zakzeski, J.; Bruijnincx, P. C. A.; Jongerius, A. L.; Weckhuysen, B. M. The Catalytic Valorization of Lignin for the Production of Renewable Chemicals. *Chem. Rev.* **2010**, 110, 3552-3599.
45. Jiang, G.; Nowakowski, D. J.; Bridgwater, A. V. Effect of the Temperature on the Composition of Lignin Pyrolysis Products. *Energy Fuels* **2010**, 24, 4470-4475.
46. Li, X.; Franke, A. A. Improved LC–MS Method for the Determination of Fatty Acids in Red Blood Cells by LC–Orbitrap MS. *Anal. Chem.* **2011**, 83, 3192-3198.
47. Pereira, A. S.; Bhattacharjee, S.; Martin, J. W. Characterization of Oil Sands Process-Affected Waters by Liquid Chromatography Orbitrap Mass Spectrometry. *Environ. Sci. Technol.* **2013**, 47, 5504-5513.
48. Zhurov, K. O.; Kozhinov, A. N.; Tsybin, Y. O. Evaluation of High-Field Orbitrap Fourier Transform Mass Spectrometer for Petroleomics. *Energy Fuels* **2013**, 27, 2974-2983.
49. Smith, E. A.; Lee, Y. J. Petroleomic Analysis of Bio-oils from the Fast Pyrolysis of Biomass: Laser Desorption Ionization–Linear Ion Trap–Orbitrap Mass Spectrometry Approach. *Energy Fuels* **2010**, 24, 5190-5198.
50. Cole, D. P.; Smith, E. A.; Lee, Y. J. High-Resolution Mass Spectrometric Characterization of Molecules on Biochar from Pyrolysis and Gasification of Switchgrass. *Energy Fuels* **2012**, 26, 3803-3809.
51. Özbay, N.; Pütün, A. E.; Pütün, E. Structural analysis of bio-oils from pyrolysis and steam pyrolysis of cottonseed cake. *J. Anal. Appl. Pyrol.* **2001**, 60, 89-101.

9. Bio-polymers

Microwave assisted pyrolysis (MAP) of two different classes of macromolecules obtained from natural resources: poly(lactic acid) (PLA) and corn-derived plastic bags (CDP) is herein reported. CDP was a mixture of different classes of polymer and lower molecular weight molecules meanwhile PLA is a pure commercial grade polymer.

9.1. Poly(lactic acid)

MAP of poly L-lactic acid (PLA) could be run only in the presence of a MW absorber. It was exploited by varying three parameters: set-up, MW absorber, and MW power.

9.1.1. Operating conditions and yields

The operating parameters employed, set-up, MW absorber, and MW power are reported in Table 9.1 (entries are named “PLAn” where “n” is an arbitrary ascending number for each experiment).

Table 9.1. MAP of PLA, operating parameters.

Entry	Set-up	MW Absorber	Power	PLA	MW Absorber	Time	Solid	Liquid	Gas
			(kW)[a]	*(g)*	*(g)*	*(min)*	*(wt%)*	*(wt%)*	*(wt%)*
T4	A	Tire M	3.0	-	233.3	35	43.2	42.6	14.1
PLA1	A	Tire M	3.0	151.1	303.6	30	38.2	44.2	17.6
PLA2	A	Carbon	3.0	150.3	70.2	30	2.6	28.4	69.0
PLA3	A	Carbon	1.2(25); 1.35(6); 1.5(59); 2.1(3); 2.4(9); 3.0(6)	101.9	32.2	107	2.7	48.4	48.9
PLA4	A	Fe	3.0	100.2	50.2	41	7.6	42.9	49.5
PLA5	B	Carbon	3.0	123.0	57.6	25	3.8	57.7	38.5
PLA6	B	Fe	3.0	100.0	50.4	70	29.6	18.2	52.2

a) within brackets the time for which each MW power was employed.

MAP of PLA produced large amount of gases and liquids with low formation of

solids when carbon was the MW absorber. Liquid yield was increased by reducing the MW power with detriment to gas production. In these condition pyrolysis time was incremented as a consequence of MW power reduction. Liquid yield was further increased by using set-up B. In these last conditions high boiling products remained in the oven for a longer time and pyrolyze. Furthermore cross reactions between degradation products might occur in the gas phase. Worthy of note was always the low formation of solid even using set-up B.

Fe as MW absorber increased the formation of solid (entry PLA4) moreover using set-up B the yield of solid was further increased to 29.6 wt% (entry PLA6). The effect of Fe as MW absorber was completely opposite to carbon. The gas formation was not influenced by set-up A or B, meanwhile liquid considerably decreased using set-up B. Fe seemed to be involved in condensation reactions to yield non-volatiles compound (which remained in the reactor as solid or high boiling compounds soaked in the solid) which were more effective than cross reactions when carbon was the MW absorber (entry PLA5). Indeed Fe salts are employed as catalyst in several coupling reactions for instance with Grignard reagents.[1] So far the Fe(0), used as MW absorber, or its oxidate form, could be involved in radical catalytic cycles as proposed for classical Grignard reactions.[2,3] This behavior was not surprisingly because bonds cleavage led to radical formation in pyrolysis reactors. Furthermore in a MW system the cleavage took place near the MW absorber which was Fe in this case. Fe in the presence of macromolecules promoted their pyrolysis meanwhile coupling of radicals formed was promoted.

MAP of tire alone (entries T4) were reported as referring pyrolysis to help results interpretation when tire was used as MW absorber. Indeed products from MAP of tire were mixed with those from PLA.

Separate considerations might be done when tire was the MW absorber. The amount of tire was higher than carbon or Fe because it contains more than 50 % of products unable to absorb MW. Liquids from MAP of PLA obtained in the presence of tire contained the same compounds formed in all other PLA pyrolysis together with those formed from MAP of tire. It is possible to evaluate the contribution of tire and PLA to the liquid formed. The amount of liquid from PLA was calculated assuming the same yields of entry PLA2 where carbon was the MW absorber while the yields of tire were assumed to be analogous to that reported in T4. These results (Table 9.2) were compared with the results obtained in PLA1.

Significant differences were highlighted suggesting cross reactions between products with a completely different behavior from those reported for MAP in the presence of carbon or Fe. Solid yield was surprisingly increased as well as liquid. Meanwhile gas was almost halved. The presence of tire degradation products probably enhanced cross reaction between products.

Table 9.2. Theoretical yield calculation for entry PLA1, together with the experimental values.

	Solid		Liquid		Gas	
	Tire	PLA	Tire	PLA	Tire	PLA
Relative amount calculated (g)[a]	131.2[b]	3.9[c]	129.3[b]	42.9[c]	43.1[b]	103.3[c]
Total amount calculated (g)	135.1		172.2		147.4	
Yield calculated (%)	29.5		37.9		32.4	
Experimental yield (%)	38.2		44.2		17.6	

a) Starting materials: tire 303.6 g, PLA 151.1 g; b) amount calculated from MAP of tire, T4; b) amount calculated from PLA2.

Moreover the pyrolysis time was reduced from T4 to PLA1, probably these interactions positively affected decomposition.

Probably tire pyrolysis gave liquid and gas products at the reaction temperature and these products worked as heat transfer agent more efficient than carbon or Fe. In this way pyrolysis was rapidly realized.

9.1.2. Collected lactide

After about one hour, from the end of some pyrolysis, crystals precipitated from solution. They were separated as white crystal after filtration over a Buchner funnel, washed with methanol, and dried. In Figure 9.6 is reported the ^{1}H NMR spectra of these crystals.

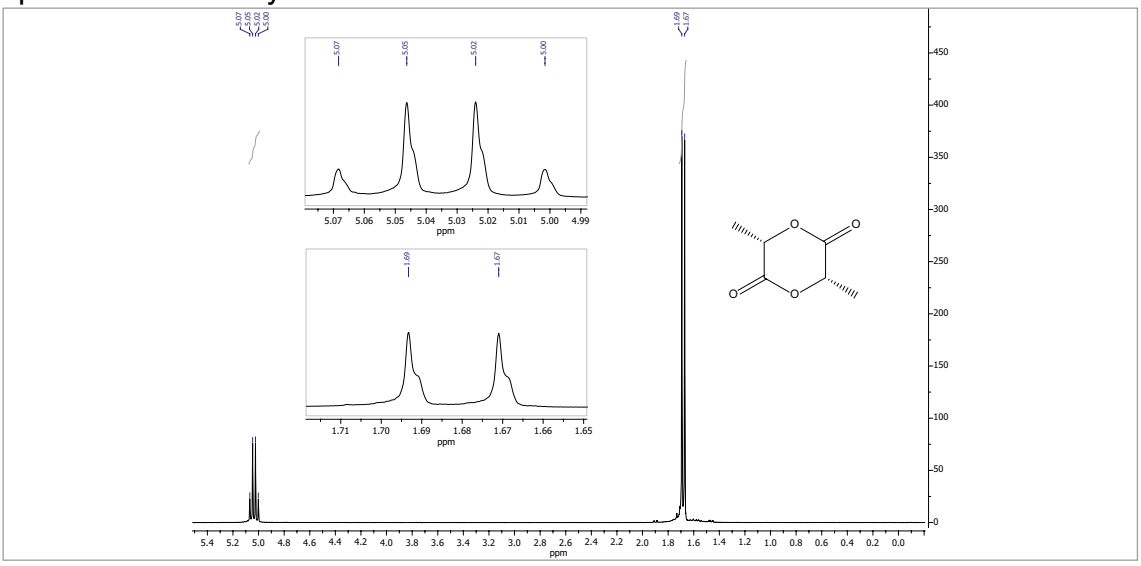

Figure 9.6. ^{1}H NMR spectrum of crystals collected from liquid.

^{1}H NMR ($CDCl_3$) peaks: δ 5.04 (q, J^3 = 6.8 Hz, 1H), 1.69 (d, J^3 = 6.8 Hz, 3H). These crystals were pure L-lactide (cyclic dimeric ester of lactic acid) in agreement with literature, where lactide was formed though a back biting process from PLA.[4] Furthermore racemization of L-lactide to its meso-form could be excluded, due to the presence of only one doublet at δ 1.69.[5] The amount of recovered lactide as weight, and yield % over the initial PLA and liquid collected are reported in Table

9.3.

Table 9.3. Lactide recovered from each pyrolysis experiment.

Entry	Set-up	MW Absorber	Lactide recovered *(g)*	Lactide recovered *(%)*[a]	Lactide recovered *(%)*[b]
T4	A	Tire M	0.0000	0.00	0.00
PLA1	A	Tire M	0.0000	0.00	0.00
PLA2	A	Carbon	7,6875	5.13	18.00
PLA3	A	Carbon	7.5747	7.43	15.36
PLA4	A	Fe	3.9692	3.96	9.23
PLA5	B	Carbon	11.0497	8.98	15.57
PLA6	B	Fe	0.0000	0.00	0.00

a) calculated from initial PLA; b) calculated from liquid collected.

Lactide precipitated form liquids only if it is a poor solvent for lactide itself because alcohols and linear alkanes were largely present while aromatics and chlorinated molecules were not present (see Section 9.1.3.2).[6]

This procedure could be a way to recover lactide from a waste PLA, even if it was contaminated with inorganics (such as carbon or Fe) but if other polymeric materials were mixed with it the overall recovery might be deeply affected. In the presence of tire pyrolysis compounds contained aromatics capable to solubilize efficiently the lactide and there was no formation of any precipitate (PLA1).

9.1.3. Liquid product

9.1.3.1. Physical properties

Physical properties of liquids, coded as “PLAnL” where “n” is an arbitrary ascending number for each experiment, are listed in Table 9.4. Liquid described in this section were partially depleted in lactide because it precipitated from liquid and it was analyzed separately (Section 9.1.2).

Table 9.4. Physical characteristics of liquid obtained by MAP of PLA.

Entry	Density	Ultimate analyses					C/H molar ratio
		C	H	N	S	O[a]	
	(g/cm³)	*(wt%)*	*(wt%)*	*(wt%)*	*(wt%)*	*(wt%)*	
T4	0.874	86.87	10.12	0.66	0.90	1.45	0.72
PLA1L	1.079	47.92	7.32	0.74	0.68	43.34	0.55
PLA2L	1.067	48.60	7.41	0.00	0.00	43.99	0.55
PLA3L	1.087	47.74	5.09	0.00	0.00	47.17	0.78
PLA4L	1.120	48.89	6.84	0.00	0.00	44.27	0.60
PLA5L	1.134	48.20	6.83	0.00	0.00	44.97	0.59
PLA6L	0.953	47.62	8.53	0.00	0.00	43.85	0.47

a) by difference.

Liquids showed a dark-yellow appearance except PLA1L which was dark due

to the presence of tire degradation products.

However the presence of tire degradation products did not affected the ultimate composition and very similar composition with PLA2L was observed. Different set-ups and MW absorber showed negligible effects over ultimate composition. Anyway for all liquids there was a reduction of carbon and oxygen content with respect to initial PLA (ultimate analysis,C: 49.32 %, H: 5.66 %, O: 45.03 %, C/H molar ratio: 0.73), connected with CO_2 formation. Only PLA6L showed a slightly lower C/H value and together with the lower density suggested a more efficient pyrolysis when Fe was the MW absorber and set-up B was employed.

Using set-up A and carbon or tire as MW absorber density was steady in a narrow interval, 1.067 – 1.087 g/cm^3. Surprisingly using set-up B and carbon as MW absorber the density was higher.

An opposite behavior was shown for Fe as MW absorber, a higher value of density was reported when using set-up A (1.120 g/cm^3) than set-up B (0.953 g/cm^3). This value was higher than those reported for carbon as MW absorber and set-up A.

9.1.3.2. GC/MS

All liquids contained a large number of compounds especially when tire pyrolysis products were present. In Table 9.5 are listed only the most representative compounds attributed to MAP of PLA. Abundances were evaluated by the TIC without any response factor correction. TICs of PLA3L and PLA4L are reported in Figure 9.7, while in Figure 9.8 are reported these of PLA5L and PLA6L for visual comparative purposes.

Table 9.5. Compounds in liquids from MAP of PLA.

	Entry		T4L[a]	PLA1L	PLA2L	PLA3L	PLA4L	PLA5L	PLA6L
	Set-up		A	A	A	A	A	B	B
	Absorber		Tire M	Tire M	Carbon	Carbon	Fe	Carbon	Fe
n	Substance	a.c.[b]							
1	acetaldehyde	C		2.04	2.53	2.56	2.94	1.07	7.75
2	2-Butene-trans	C	1.53	0.49	0.01				
3	butane	C	0.15		0.02				
4	ethanol	C		0.17	0.09		0.03		0.14
5	acetone	C		0.69	0.83	1.26	0.43		1.53
6	ethenyl acetate	C		0.18	0.60	0.24	0.12		0.82
7	2-butanone	P		1.95	2.56	1.30	0.71		3.64
8	acetic acid	P		0.46	2.39	5.68	1.18	1.25	3.20
9	tetrahydrofura	P			1.06				

(continue)

10	1-hydroxy-2-propanone	P		0.56	0.59	0.41	0.07	0.38	0.34
11	1-penten-3-one	P		0.21	0.36	0.21	0.09	0.12	
12	3-methyl-2-butanone	P		0.22	0.11	0.17	0.08	0.10	
13	3-pentanone	U		2.76	6.45	4.11	2.67	4.46	10.69
14	3-hydroxy-2-butanone	U		0.15	0.22		0.03	0.30	1.79
15	propanoic acid	P		6.82	10.50	9.65	8.03	11.23	17.73
16	2-methyl-2-butenal	U		0.44	0.76	0.12			
17	toluene	C	2.95	1.34	0.20	0.17			
18	paraldehyde	C		0.08	0.55	7.91	0.57		1.52
19	2-methylpentanal	U		0.69	0.33	0.30	0.12	0.55	0.41
20	1-propen-2-ol, acetate	P		0.80	1.45	0.78	0.18	0.65	0.29
21	1-(2-furanyl)-ethanone	U			0.18	0.29	0.11		0.08
22	methyl 2-methoxypropanoate	U		0.23	0.87				0.21
23	2-hydroxy-propanoic acid ethyl ester	C		0.56	0.19	2.85	1.31		4.98
24	5-methyl-1,4-dioxin-2(3H)-one	U		0.16	0.14				
25	2-cyclopent-1-one	U		0.19	0.66	1.73	0.08	0.42	
26	1-(acetyloxy)-2-propnanone	P		0.53	1.36	0.51	0.16	1.71	3.42
27	hydroxy ester ($C_5H_{10}O_3$)	U			0.82	0.65	0.11		0.36
28	Alcohol $C_7H_{12}O$	U			0.22	0.19	0.35		0.11
29	pentanoic acid	U		1.25	0.21	0.45	0.05	5.74	0.15
30	5,6-dihydro-2H-Pyran-2-carboxaldehyde	U			0.18	0.31	0.27		
31	C8 alkyne or C8 cyclic alkene	U			1.11	1.28	0.26	0.55	
32	1-(acetyloxy)-2-butanone	U			1.03	1.25		0.44	1.66
33	propanoic acid, ethenyl ester	P		0.47	0.36	0.30	1.57		1.59
34	aldheyde $C_6H_{12}O$	U			1.25	1.16		1.92	
35	2,3-dimethyl-2-cyclopenten-1-one	P			0.21	0.32	0.37		
36	octahydro-1H-Inden-1-one	U			0.15	0.19	0.12		
37	lactide	C		15.24	22.17	17.81	30.13	25.52	9.19
38	lactide	C		20.19	17.56	16.05	27.85	12.85	16.24
39	$C_{11}H_6O_7$ (m/z: 252)	U		0.58	1.46		3.09		
40	$C_{11}H_6O_7$ (m/z: 252)	U		3.58	0.17				0.25
41	$C_{11}H_6O_7$ (m/z: 252)	U						5.38	
42	$C_{11}H_6O_7$ (m/z: 252)	U			0.19	1.09	0.46	1.90	
43	$C_{11}H_8O_7$ (m/z: 254)	U				1.21		1.47	

(continue)

44	$C_{11}H_8O_7$ (m/z: 254)	U			0.17			0.92	
45	$C_{12}H_{12}O_7$ (m/z: 272)	U		0.14	0.60			1.20	
46	$C_{12}H_{12}O_7$ (m/z: 272)	U			1.17	1.23	0.13	1.83	
47	$C_{12}H_{12}O_7$ (m/z: 272)	U			0.87	0.70		1.24	0.03
48	$C_{12}H_{12}O_7$ (m/z: 272)	U		0.06	0.61	0.72		1.05	0.14
49	$C_{12}H_{16}O_7$ [2-((1-(5-methyl-3,6-dioxo-1,4-dioxan-2-yl)-3-oxobutan-2-yl) oxy)propanal]	U		0.07	0.15			0.17	0.20
TOTAL Alkanes, alkenes, and aromatics			4.63	1.83	1.34	1.45	0.26	0.55	0.00
TOTAL Alcohols			0.00	0.17	0.31	0.19	0.38	0.00	0.25
TOTAL Ketones			0.00	6.02	11.33	9.29	4.55	5.10	15.86
TOTAL Aldheyde			0.00	3.17	4.87	4.14	3.06	3.54	8.16
TOTAL Esters			0.00	0.65	0.96	0.54	1.69	0.00	2.41
TOTAL Ethers			0.00	0.08	1.61	7.91	0.57	0.00	1.52
TOTAL Acids			0.00	8.53	13.10	15.78	9.26	18.22	21.08
TOTAL Hydroxy ester			0.00	35.99	40.74	37.36	59.40	38.37	30.77
TOTAL Mixed			0.00	2.43	6.02	3.55	0.82	3.48	7.79
TOTAL PLA fragment			0.00	4.43	5.39	4.95	3.68	15.16	0.62
TOTAL			4.63	63.3	85.67	85.16	83.67	84.42	88.46

a) other compounds were present as reported in Table 5.7; b) a.c.: attribution confidence C, certain (>98%); P, probable (86-97%); U, uncertain (<85%).

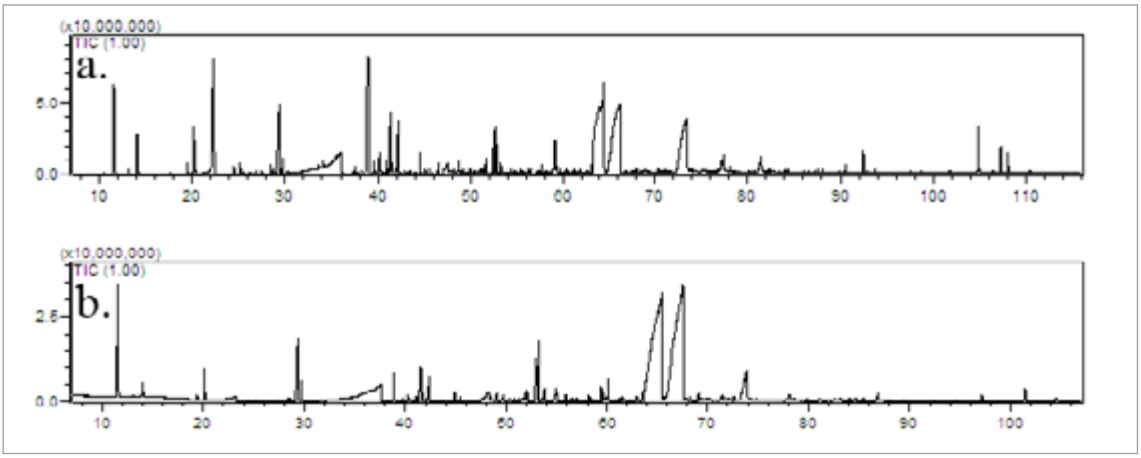

Figure 9.7. TIC of samples obtained from MAP of PLA with set-up A: PLA3L and PLA4L.

All liquid (except for T4L) contained large amount of lactide, even if this precipitated in large extent, in two forms, meso and enantiopure forms in agreement with data from literature.[7-13] However only L-lactide precipitated from solution as shown in Section 9.1.2. Probably the first peak attribute to lactide (entry 37, Table 9.5), in agreement with literature, was attributable to the meso form. Using carbon as MW absorber the meso lactide increased and the enantiopure form decreased

using set-up B with respect to set-up A. An opposite effect was observed for Fe, it reduced the amount of meso lactide and increased the enantiopure lactide working with set-up B instead of set-up A.

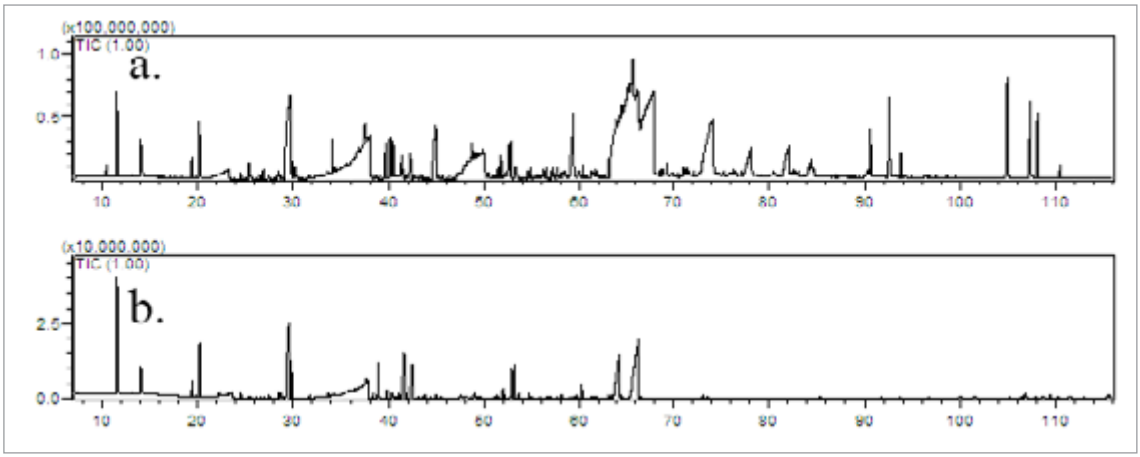

Figure 9.8. TIC of samples obtained from MAP of PLA with set-up B: PLA5L and PLA6L.

Using Fe and set-up B (PLA6) the pyrolysis of PLA was more efficient and less amount of lactide was formed. In fact there was no lactide precipitated (Table 9.3) and the area relative to lactide in Table 9.5 was the lowest and the acid was the highest.

The identification of some compounds was nearly impossible from their mass spectrum. Several compounds were separated in the GC but shared the same MS spectrum and similar structure because they were formed by partial cleavage of PLA backbone and followed analogous rearrangements (entries 39 – 49 Table 9.5). For entry 49 (Table 9.5) a structure might be proposed from its mass spectrum: 2-((1-(5-methyl-3,6-dioxo-1,4-dioxan-2-yl)-3-oxobutan-2-yl)oxy)propanal (Figure 9.9, following the peak attribution).

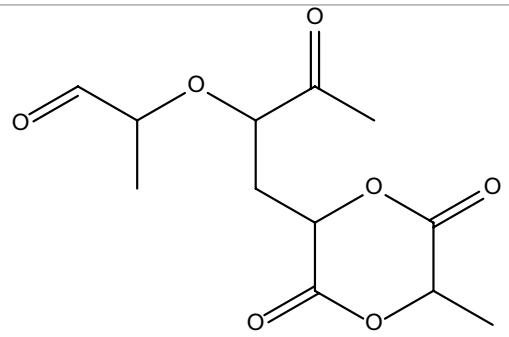

Figure 9.9. Proposed structure for entry 49 of Table 9.5.

9.1.3.3. FTIR

The FTIR spectra of liquids collected from MAP of PLA and depleted from precipitated lactide are reported in Figure 9.10.

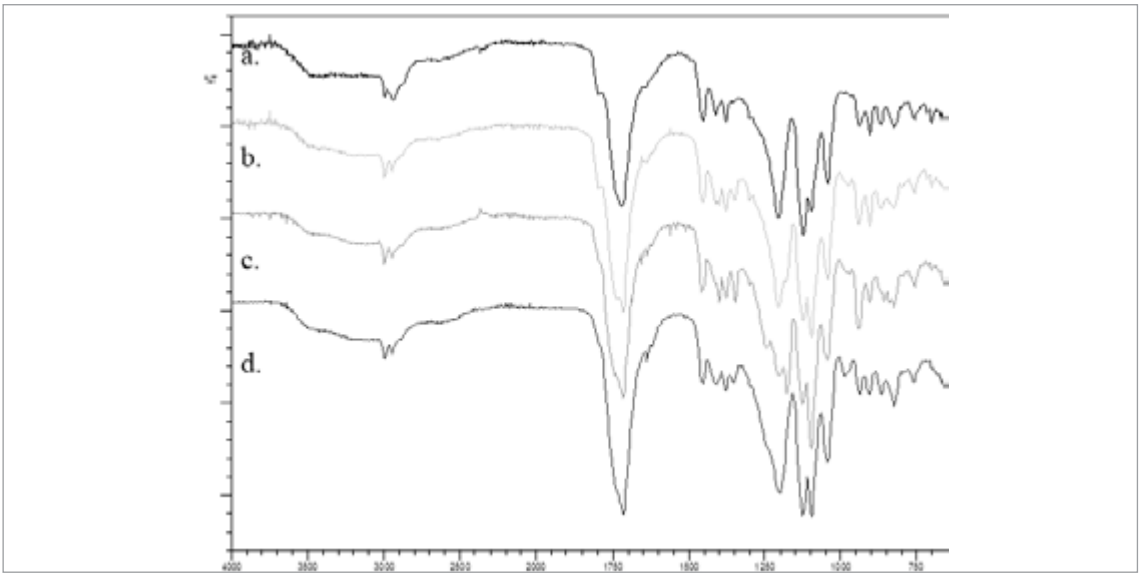

Figure 9.10. FTIR spectra of liquids from MAP of PLA: a) PLA1L; b) PLA2L; c) PLA3L; d) PLA5L.

All spectra showed the same absorptions with very close intensities. The main absorptions frequencies are reported as follow together with their attribution and relative intensities (s, strong; m, medium; w, weak):

- 3477, broad (m) cm^{-1}: H-bonded OH stretching.
- 3196 (w) cm^{-1}: normal polymeric OH stretching.
- 2993 (m) and 2883 (w) cm^{-1}: methyl C-H asym./sym. stretching.
- 2942 (m) cm^{-1}: methyne C-H stretching.
- 1735 (w) and 2743 (w) cm^{-1}: aldehyde and aldehydic C-H stretching, overlapped with ester.
- 1715 (s) cm^{-1}: carboxylic acid, ketone.
- 1452 (m) and 1377 (m) cm^{-1}: methyl C-H asym./sym. bending.
- 1410 (m) cm^{-1}: tertiary alcohol, OH in-plane bending.
- 1350 (m) cm^{-1}: secondary alcohol, OH in-plane bending.
- 1202 (m) cm^{-1}: secondary alcohol, CO stretching.
- 647, 639, 618,601 (m) cm^{-1}: primary or secondary alcohol, OH out-of-plane bending.

Only PLA1L showed few differences compared with other spectra because tire pyrolysis products were mixed with PLA one. Methyl and methyne absorptions were more intense and corresponding weak aromatic absorption were observed.

The data were in agreement with GC/MS analyses, the main component of liquid contained a mixture of simple organic acid, lactide, and substructure from PLA backbone cleavage. FTIR spectra also showed the absence of strong water absorption. The absence of water, or its low amount, suggested the negligible presence of dehydratation reactions.

9.1.4. Main achievements

Microwave assisted pyrolysis (MAP) of PLA was performed using different MW absorbers (tire, carbon, or Fe), apparatus set-up, and MW power, obtaining a liquid rich in lactide and other oxygenated hydrocarbons. The main achievements might be summarized in the following key points.

The meso-form of the lactide was found only in chromatogram from GC/MS analysis. Except for any form of lactide GC/MS analyses showed the presence of simple acids (such as acetic acid and propanoic acid), carbonyl compounds, and fragments from PLA backbone random cleavage for which were not possible to propose any definite structure.

FTIR spectra showed mainly the presence of alcohols and carbonyl groups confirming the GC/MS data.

The pyrolysis of PLA together with other polymers, which might pyrolyze to aromatic compounds, prevent the precipitation of lactide and moreover cross reactions between products took place affecting the yield and characteristics of liquid. MAP of PLA could not be performed in the presence of other polymers in order to recover lactide.

9.2. Corn-derived plastics

MAP of corn-derived plastic bags (CDP) might be run only in the presence of a MW absorber. It was exploited by varying three parameters: set-up, MW absorber, and MW power.

9.2.1. Operating conditions and yields

In Table 9.1 are reported the operating parameters employed (entries are named “CDPn” where “n” is an arbitrary ascending number for each experiment).

Table 9.1. MAP of corn-derived plastics, operating parameters.

Entry	Set-up	MW absorber	MW power *(kW)*[a]	MW abs. *(g)*	CDP *(g)*	CDP/ abs.	Time *(min)*	Solid *(wt%)*	Liquid[b] *(wt%)*	Liquid[c] *(wt%)*	Liquid[d] *(wt%)*	Gas *(wt%)*
CDP1	A	Carbon	3	127.7	56.4	2.26	30	13.3	47.5			39.2
CDP2	A	Carbon	1.2(23); 1.35(5); 1.5(22); 3(10)	126.2	56.6	2.23	60	18.3	22.3	5.7	18.1	35.6
CDP3	A	Fe	3	129.6	63.6	2.04	32	25.9	30.0	6.0	9.4	28.7
CDP4	B	Carbon	3	126.0	56.6	2.23	35	30.1	16.8	9.0	2.7	41.3
CDP5	B	Carbon	1.2(18); 1.35(3); 1.5(49); 3(26)	129.8	54.3	2.39	86	13.2	26.0	12.1	2.5	46.2
CDP6	B	Fe	3	132.9	65.7	2.02	41	32.7	11.3	8.5	2.5	45.0

a) within brackets the time for which each MW power was employed; b) upper fraction (U); c) middle fraction (M); d) lower fraction (L)

Pyrolysis could be performed in 30 minutes, but using set-up B the reaction time was slightly longer. The presence of a fractionating system increased the

residence time of products into the oven and the overall pyrolysis time in agreement with MAP of other polymeric materials (Section 6).[14-19]

MAP of CDP produced large amount of gases (28.7 – 46.2 wt%) and liquids (28.5 – 47.5 wt%) together with a significant amount of solids when carbon was the MW absorber. Liquid yield was increased by reducing the MW power (as a consequence pyrolysis time was increased) with detriment to gas formation. Anyway the liquid yield was decreased by using set-up B (an online fractionating system). Solid was formed in higher amount but it was reduced working with a lower MW power. Long reaction time and the presence of a fractionating system allowed further reactions between pyrolyzed products and solid or cocking reactions.

Fe as MW absorber increased the formation of solid (entry CDP4) moreover using set-up B the solid yield was further increased to 32.7 wt% (entry CDP6).

The gas formation was dramatically influenced by set-up; as a matter of fact using set-up B gas yield was 45.0 wt% instead or 28.7 wt% for set-up A. On the contrary liquid yield was reduced from 45.4 wt% using set-up A to 22.7 wt% with set-up B. Fe was involved in condensation reactions as highlighted for PLA pyrolysis in the presence of Fe (Section 9.1).

Apparently liquids were always collected as one phase. However after 30 minutes liquids separated in three phases. These three phases were thoroughly separated after centrifuging and they were weighted and analyzed separately.

The upper phase was always the predominant one. Its amount decreased working with set-up B and a MW power of 3 kW. On the contrary low MW power and the same set-up B increased the amount of this fraction. The bottom fraction was reduced by working with a MW power of 3 kW and further reduction was achieved by using set-up B. FTIR analysis (Section 9.2.2.3) showed for these two fractions, (upper and lower) the same FTIR spectra, so far the bottom fraction was probably a mixture of oligomers/plasticizers (heavy materials) which were not soluble in the other two fractions. Indeed using set-up B the lower fraction was dramatically reduced suggesting a more efficient pyrolysis of these oligomers.

Middle fraction yields was almost constant when varying any parameters. Only when a high yield of gas was obtained the yield of middle fraction was increased (CDP5), or more generally when set-up B was used. This fraction was mainly composed of water (Section 9.2.2.3) and when the pyrolysis was more efficient (that is when the ability to obtain small molecules was improved) gas collected was increased.

9.2.2. iquid product

9.2.2.1. Physical properties

Physical properties of liquids, coded as “CDPnL_f” where “n” is an arbitrary ascending number for each experiment and “f” is referred to one of the liquid fractions (U, upper; M, middle; L, lower), are listed in Table 9.2.

Table 9.2. Liquid from MAP of CDP.

Entry	Set-up	MW absorber	Density	Ultimate analyses				C/H molar ratio
				C	H	N	O[a]	
			(g/cm³)	*(wt%)*	*(wt%)*	*(wt%)*	*(wt%)*	
CDP1L_U	A	Carbon		61.95	5.75	1.44	30.86	0.897
CDP1L_M								
CDP1L_L			n.d.					
CDP2L_U	A	Carbon	1.0258	64.93	7.52	1.21	26.34	0.719
CDP2L_M			1.0317	8.89	6.29	0.00	84.82	0.118
CDP2L_L			n.d.	55.60	8.58	0.18	35.64	0.540
CDP3L_U	A	Fe	1.0249	59.37	7.90	1.39	31.34	0.626
CDP3L_M			1.0467	12.79	9.02	0.55	77.64	0.118
CDP3L_L			n.d.	57.67	8.69	0.48	33.16	0.553
CDP4L_U	B	Carbon	1.0048	61.13	7.28	0.40	30.89	0.699
CDP4L_M			1.0435	12.44	7.06	0.00	80.50	0.147
CDP4L_L			n.d.	59.91	6.92	2.37	30.80	0.721
CDP5L_U	B	Carbon	0.9905	51.73	8.76	0.00	39.51	0.492
CDP5L_M			1.0394	12.04	7.04	3.74	77.18	0.142
CDP5L_L			n.d.	58.03	6.58	0.44	34.95	0.734
CDP6L_U	B	Fe	0.9872	47.51	6.36	1.85	44.28	0.622
CDP6L_M			1.0388	10.90	8.59	0.00	80.51	0.106
CDP6L_L			n.d.	59.82	6.52	0.37	33.29	0.764

a) calculated by difference.

The lower fraction was a pale-yellow milky liquid, semi-solid a room temperature and it was not possible to evaluate its density. Probably this fraction was composed by the same products of the upper fraction but with compounds with high molecular weight.

The water content was very similar among each phase. Upper and bottom fractions had a water content between 4 and 10 wt % probably due to the presence of compounds which were able to solubilize water in these fractions. Middle fraction contained almost only water with about 75 wt % of water content.

Ultimate analyses confirmed the similarity between upper and lower phases, and the predominant presence of water in the middle fractions. Nevertheless ultimate analyses highlighted noticeable differences among CDP2L_U and CDP5L_U, CDP3L_U and CDP6L_U; using different reaction condition such as switching from

set-up A to set-up B or using different MW power or different MW absorber. Carbon and hydrogen content dropped; probably hydrocarbons not linked to oxygen were more reactive in the pyrolysis condition using the fractionating system.

Upper and lower fraction had a similar HHV which was about 28±3 MJ/Kg. Meanwhile the middle fraction showed very low values, below 4±0.4 MJ/Kg. The high water content of middle fractions hindered their use as energy sources, meanwhile upper and bottom fractions could be employed for energy production.

9.2.2.2. GC/MS

All the three fractions of liquids contained a large number of compounds but only upper and middle fractions were analyzed. Lower fraction was almost solid at room temperature thus it was not possible to analyze it by GC/MS. In Table 9.3 and Table 9.4 are listed the most representative compounds identified in upper and middle fractions respectively. Abundances were evaluated by the TIC without any response factor correction. In Figure 9.11 are reported TICs of CDP2L_U and CDP2L_M and in Figure 9.12 are reported TICs of CDP4L_U and CDP4L_M.

Table 9.3. GC/MS of liquid from MAP of CDP, upper fraction.

	Entry		CDP1L_U	CDP2L_U	CDP3L_U	CDP4L_U	CDP5L_U	CDP6L_U
	Set-up		A	A	A	B	B	B
	Absorber		Carbon	Carbon	Fe	Carbon	Carbon	Fe
No.	Substance	a.c.*						
1	acetaldehyde	C	1.6	0.5	1.1	0.6	0.6	0.5
2	1,3-butadiene	C	0.6	0.2	0.3	0.3	0.3	0.1
3	2-propenal	P	0.2	0.1	0.2			0.1
4	acetone	C	0.2	0.2	0.2	0.2	0.2	0.1
5	2,3-butadione	P		0.1	0.2		0.1	0.1
6	2-butanone	C		0.1	0.1	0.2	0.1	0.1
7	acetic acid	C		0.3	0.7	0.4	0.3	0.1
8	tetrahydrofuran	C	3.7	2.3	5.5	2.6	2.7	4.7
9	3-buten-1-ol	P	2.3	1.9	3.1	2.1	2.6	3.6
10	1-hydroxy-2-propanone	P	0.3	0.2	0.3	0.3	0.2	0.2
11	benzene	C	3.6	2.2	2.7	2.8	2.7	3.7
12	1-butanolo	C	0.5	0.1	0.1	0.2	0.2	0.2
13	3-methyl-3-buten-2-one	P		0.5	0.4	0.6	0.7	0.4
14	2,3-pentadienone	C	0.2	0.2	0.1	0.2	0.1	0.2
15	1-heptene	C	0.3	0.2	0.2	0.2	0.3	0.2
16	heptane	C	0.3	0.1	0.1		0.2	0.1
17	propanoic acid	C		0.7	0.2	1.6	0.5	1.3

(continue)

18	toluene	C	1.2	1.1	0.9	1.5	1.6	2.0
19	2-methylene-butanal	P	5.0	3.0	3.8	4.0	4.0	7.2
20	3-hepten-1-ol acetate	P	0.3	0.2	0.0	0.4	0.3	0.6
21	1-octene	C		0.2	0.0	0.3	0.4	0.3
22	octane	C		0.6	0.0	0.6	0.7	0.8
23	furfural	C	0.4	0.2	0.4	0.3	0.2	0.3
24	4-ethenyl-cyclohexene	P	0.3	0.3	0.0	0.3	0.4	0.2
25	ethylbenzene	C	0.4	0.4	0.2	0.5	0.6	0.5
26	2-Propenoic acid, 1,4-butanediyl ester	P		0.2	0.0	0.2	0.2	0.4
27	1,4-dimethylbenzene	C	0.3	0.3	0.2	0.4	0.5	0.4
28	cyclohexanone	U	0.5	0.2			0.2	0.2
29	1-penten-1-ol	P		0.2	0.3	0.3	0.3	0.7
30	styrene	C	0.9	1.0	1.1	1.6	1.2	1.8
31	5-methyl-1,3,5-heptatriene	U		0.2	0.1	0.2	0.2	0.2
32	1.2-dimethylbenzene	C		0.4	0.1	0.5	0.5	0.5
33	pentanoic acid	C		0.2		0.2		0.3
34	1-nonene	C		0.1	0.0	0.4	0.2	0.2
35	3-methylcyclopentanone	U		0.2	0.1	0.3	0.2	
36	nonane	C		0.1	0.1	0.2	0.2	0.1
37	2-methyl-2-pentanone	P		0.1	0.1	0.3	0.3	0.3
38	5-methyl-2-furancarboxaldehyde	U	0.6	0.6	0.5	0.9	0.8	1.2
39	benzaldeyhde	C	0.4	0.5	0.4	0.6	0.5	1.0
40	propylbenzene	P	0.4	0.2	0.1	0.3	0.3	0.4
41	1,2,3-trimethylbenzene	C		0.1	0.1	0.2	0.2	0.2
42	hexanoic acid	P	0.3	0.5	0.2	0.5	0.5	0.6
43	butanoic acid, 2-hexenyl ester	U		0.1	0.1	0.4	0.3	0.3
44	2-nornarbonone	U		0.4	0.0	0.3	0.4	0.5
45	a-methylstyrene	C	0.3	0.2	0.1	0.5	0.4	0.4
46	2-Buten-1-ol, formate	U		0.2	0.3	0.3	0.4	0.6
47	1-decene	C		0.1		0.2	0.2	0.3
48	Bicyclo[2.2.1]hept-5-ene-2-carboxaldehyde	P		0.2	0.1	0.3	0.3	0.1
49	3-methyl-1,2-cyclopentadienone	P		0.3	0.4	0.4	0.4	0.6
50	1-ethenyl-2-methylbenzene	U		0.2	0.0	0.3	0.3	0.2
51	2-methylphenol	P		0.2	0.1	0.2	0.2	0.1
52	indene	C		0.2	0.0	0.4	0.3	0.2
53	acetophenone	P	0.4	0.6	0.5	0.8	0.7	1.2
54	1-methylpropylbenzene	P		0.3	0.1	0.3	0.2	0.3
55	butylbenzene	P	0.4	0.1	0.0	0.2	0.2	0.1

(continue)

56	3-butoxy-propanenitrile	P	0.4	0.5	0.7	0.7	0.7	1.2
57	4-methylbenzaldehyde	U		0.7	0.1	0.7	1.0	0.6
58	1-hexanol	U	0.5	0.3	0.1	0.5	0.2	0.2
59	dihydro-2,5-furandione	P		0.7		0.8	0.7	1.1
60	2-oxepanone	U		0.1	2.0			0.1
61	1-ethyl-4-methylcyclohexene	U		0.1	0.0	0.2	0.1	0.4
62	1,2-diethenylbenzene	U	0.4	0.3	0.1	0.5	0.3	0.4
63	1,2-dihydronaphtalene	U		0.1		0.1	0.1	0.0
64	1-(3-methylphenyl)-ethanone	P		0.1			0.1	
65	2-dodecanone	P		0.1	0.1	0.1	0.1	0.4
66	benzoic acid	C	13.2	15.9	7.3	22.2	15.4	6.6
67	naphtalene	C		0.3	0.2	0.6		0.4
68	1-dodecene	C		0.2	0.0	0.1	0.2	0.2
69	1-naphtalenol	P		0.1				
70	n-hexyl acrylate	U	0.3	0.4	1.0	0.3		1.7
71	3-heptenoic acid, ethyl ester	U		0.3	0.2		0.4	0.4
72	undecylenic acid	P	3.2	0.2	0.1	0.7	0.2	
73	4-methylbenzoic acid	P	1.0	0.9	0.2	0.9	1.4	0.8
74	nonanoic acid	C		6.3	4.0	6.9	7.6	2.5
75	3-methylbenzoic acid	P		1.8	0.6	1.3	1.9	
76	nonanoic acid, ethyl ester	U		0.2	0.1	0.2	0.2	0.1
77	1-tridecene	C		0.1	0.0	0.2	0.2	0.1
78	2-methylnaphtalene	P	0.6	0.2	0.0	0.3	0.3	0.2
79	1-methylnaphtalene	P		0.3	0.2	0.3	0.3	0.1
80	1-phenyl-1-propanone	U		0.2	0.5		0.2	0.0
81	benzenecarbothioic acid	U	1.9	1.2	2.4	1.5	1.7	3.1
82	1,9-tridecadiene	U	0.7	0.5	0.5	0.8	0.7	1.0
83	decanoic acid			0.6	0.1	0.5	0.7	0.0
84	benzoic acid butyl ester	P	0.2	0.2	0.3	0.3	0.3	0.3
85	biphenyl	C	0.4	0.6	0.3	0.8	0.5	0.4
86	1-ethylnaphtalene	P	0.3	0.1	0.0			0.1
87	1,3-dibenzocarboxilic acid	U		0.2	0.1	0.2	0.3	0.0
88	diphenylmethane	P		0.1	0.2	0.2	0.2	0.2
89	9-heptadecanone	U	1.8	1.5	1.7	2.0	2.1	2.4
90	benzoic acid 4-methyl-, 2-methylpropyl ester	U	0.3	0.4		0.4	0.6	0.2
91	2-ethyl-1,3-hexadienol	U		0.1	0.1	0.2	0.2	0.1
92	3-methyl-1,1'-diphenil	P		0.1	0.1	0.2	0.2	0.1
93	2-methyl-1,1'-diphenil	P	2.1	0.5	0.3	0.6	0.6	0.8
94	1-pentadecene	P		2.6	2.2	1.1	2.7	0.1
95	tetradecanolo	U		0.3	0.1		0.3	0.1
96	fluorene	P		0.2	0.2	0.2	0.2	0.1

(continue)

97	benzophenone	C		0.2	0.4	0.3	0.2	0.1
98	11-hexadecenoic acid	U		0.2	0.1	0.2	0.2	
99	unknown acrylate	U	2.2	1.1	1.1	1.8	1.8	0.9
100	dodecandioic acid	U	0.7	5.5	5.6			0.1
101	1-phenyl-1-decanone	P		0.1	0.2			0.1
102	dibuthylphtalate	P	10.8	7.0	8.0	2.6	3.3	2.3
103	1,2-benzenedicarboxylic acid,monobuthyl ester	U	0.7	0.2		0.2	0.4	0.3
104	9-methylantracene	P		0.1	0.6			0.0
105	dodecyl acrylate	U	7.3	6.8	6.4	2.2	2.7	2.5
106	hexadecanoic acid	P		0.2	0.3	0.2	0.2	0.1
107	11-hptadecenoic acid	U	3.9	2.2	0.4	1.5	2.3	1.9
108	2-phenilnaphtalene	P		0.1	2.5			0.1
109	1,2-benzenedicarboxylic acid, buthyl octyl ester	P	0.4	0.4	4.6	0.2	0.3	0.3
110	2-propenoic acid, 1,4-butanediyl ester	U				1.6	2.3	3.0
	TOTAL Aldehyde		7.1	4.9	5.7	6.1	6.4	9.4
	TOTAL Ketones		3.1	5.2	5.0	5.4	6.0	6.7
	TOTAL Acids		24.2	36.7	22.3	38.6	33.1	17.4
	TOTAL Esters		22.4	18.3	24.1	11.7	14.3	14.9
	TOTAL Ethers		4.1	2.8	6.2	3.3	3.4	5.9
	TOTAL Alcohols		3.3	3.3	3.9	3.4	4.0	5.0
	TOTAL Aliphatic		2.2	5.7	3.7	5.0	7.1	4.2
	TOTAL Aromatics, not reported in previous classes		11.3	9.6	10.3	13.1	11.3	13.3
	TOTAL Mixed		1.3	1.0	1.2	1.6	1.2	1.7
	TOTAL		78.9	87.3	82.3	88.2	86.7	78.5

*a.c.: attribution confidence; C, certain (>98%); P, probable (86-97%); U, uncertain (<85%).

Table 9.4. GC/MS of liquid from MAP of CDP, medium fraction.

	Entry		CDP1L_M	CDP2L_M	CDP3L_M	CDP4L_M	CDP5L_M	CDP6L_M
	Set-up		A	A	A	B	B	B
	Absorber		Carbon	Carbon	Fe	Carbon	Carbon	Fe
No.	Substance	a.c.[a]						
1	acetaldehyde	C	8.7	5.0	2.2	4.5	4.9	4.0
2	ethanol	C	0.4	0.6	0.1	0.6	0.5	0.2
3	2-propenal	C	0.2	0.4	0.1	0.4	0.5	0.3
4	acetone	C	1.2	1.6	0.2	0.9	1.1	0.5
5	acetic acid ethenyl ester	P	1.8	0.7	0.1	0.5		0.1

(continue)

6	formic acid	C	0.6	0.4	0.1	0.6		0.4
7	2,3-butadione	P	0.8	0.7	0.2	0.8	0.7	0.6
8	2-butanone	C	0.4	0.2		0.3	0.2	
9	acetic acid	C	7.6	12.4	4.9	18.5	22.2	13.2
10	THF	C	4.3	4.2	3.4	4.5	4.7	6.4
11	3-buten-1-ol	P	4.0	4.8	2.2	4.0	6.9	9.3
12	1-hydroxy-2-propanone	P	0.5	2.5	1.1	3.6	2.7	2.4
13	3-methyl-3-buten-2-one	C	0.5	0.3	0.1	0.4	0.5	0.3
14	2,3-pentadienone	P	0.4	0.3	0.1	0.3	0.3	0.2
15	2-methoxy-ethanol acetate	U	0.3	0.2		0.3		0.1
16	2-propenoic acid	P	3.4	3.2	1.3	6.8	4.1	4.3
17	cyclopentanone	C	8.0	5.2	3.0	7.5	8.0	14.4
18	2-methyl propanoic acid	P	0.1	0.3	0.1			0.3
19	2-cyclopenten-1-one	P	0.8	0.5	0.2	1.0	0.8	1.1
20	furfural	P	0.3	0.3	0.1	0.6	0.5	0.4
21	1-acetyloxy-2-propanone	P	0.4	0.4	0.2	0.7	0.4	0.8
22	butyrolactone	P	0.1	1.1	0.2	0.5		0.3
23	propylene glycol	P	6.6	8.1	8.0	9.2	13.0	8.4
24	pentanoic acid	P		0.3				0.5
25	1-methyl-2-cyclopenten-1-one	P	0.2	0.2		0.8		0.4
26	2,5-hexadienone	P		0.2	0.2	0.3	0.4	0.4
27	cyclohexanone	U	0.5	0.5	0.2	1.2	0.7	0.8
28	2,4-pentadienone	U	0.2	0.3	0.2	0.5	0.4	0.4
29	4-methyl-5H-furan-2-one	P	0.3	0.4	0.4	0.7	0.8	1.1
30	benzoic acid	P	7.2	4.3	1.1	10.2	0.9	
31	heptanal	P			1.0	2.8	3.8	1.1
32	4-cyclopenten-1,3-diol	U	0.5	0.2	0.1		0.4	0.8
33	5-nonanol	U	0.1	0.5	0.3	0.8	0.3	0.3
34	5-hydroxymethyl-furancarboxylaldheyde	P		0.3	0.2	0.7	0.4	0.2
35	2-hydroxy-propionic acid ethyl ester	U	3.5	3.3	5.6	2.5	5.8	7.9
36	1,4-butandiol diacetate	U	0.1	0.5	0.3		0.5	
37	3-hepten-1-ol	U	0.1	3.3	0.1			
38	1,4-butanediyl ester-2-propenoic acid	U	0.4	8.6	0.1			
39	1-butanediyl-4-propyl ester, 2-propenoic acid	U		8.6	0.1			
40	hexadienoic acid	U	3.8	6.3	2.5	1.5	4.8	
41	Levoglucosan	C	11.5	3.8	22.1	1.7		5.8
42	4-pentanoic acid ethyl ester	U	0.5	0.4	0.4		0.3	0.2
43	4-butoxy-1-butanol	U	0.8	0.3	0.5		0.2	0.3

(continue)

44	1,2-benzenedicarboxylic acid, buthyl octyl ester	P			22.0			0.2
	TOTAL Aldehyde		8.9	5.4	3.2	7.7	9.1	5.3
	TOTAL Ketones		12.9	10.1	4.3	13.9	13.1	19.0
	TOTAL Acids		22.6	27.1	9.8	37.6	31.9	18.7
	TOTAL Esters		3.2	20.3	23.4	1.7	1.6	1.9
	TOTAL Ethers		4.3	4.2	3.4	4.5	4.7	6.4
	TOTAL Alcohols		11.7	17.4	10.8	14.6	21.1	18.9
	TOTAL Mixed		17.2	11.1	29.8	10.0	10.0	17.8
	TOTAL		80.8	95.6	84.7	90.0	91.6	88.1

*a.c.: attribution confidence; C, certain (>98%); P, probable (86-97%); U, uncertain (<85%).

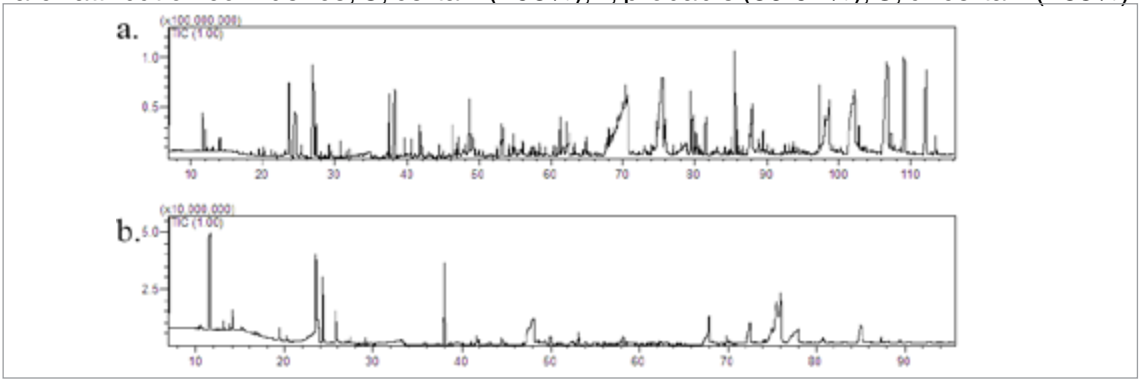

Figure 9.11. TIC of samples obtained from MAP of PLA with set-up A: a) CDP2L_U; b) CDP2L_M.

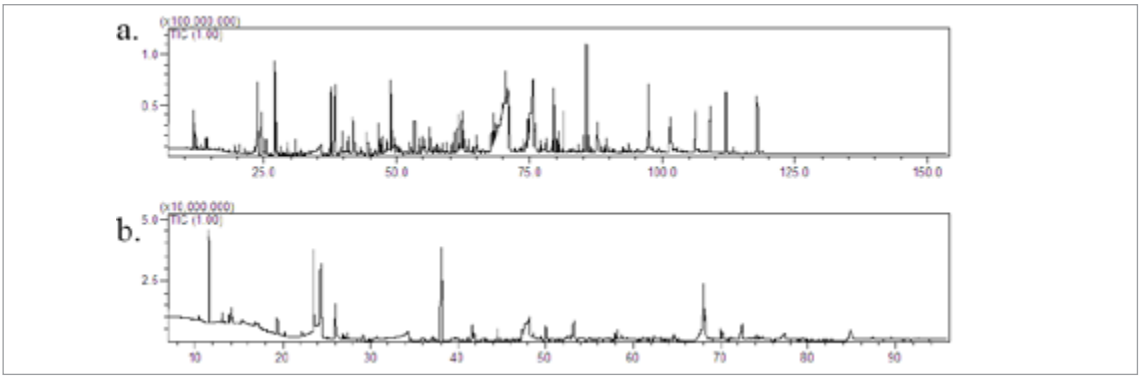

Figure 9.12. TIC of samples obtained from MAP of PLA with set-up B: a) CDP4L_U; b) CDP4L_M..

Most of the compounds identified were present in both upper and middle fractions except for non-oxygenated aromatics which were concentrated in the upper fraction.

Single ring aromatics (benzene, toluene, xylenes, and styrene) were identified together with indene, naphthalene, and their methyl derivatives. Large presence of aromatics, oxygenated or not, was attributed to pyrolysis of plasticizers. In point of fact several phthalates species were also found in both phases such as 1,2-benzenedicarboxylic acid, butyl octyl ester, also known as Plasticizer BOP, or 1,2-benzenedicarboxylic acid, monobutyl ester. Only CDP3L_U and CDP3L_M

showed an extremely large amount of phthalates (22.0 % of 1,2-benzenedicarboxylic acid, butyl octyl ester CDP3L_M), probably Fe (the MW absorber) promoted a fast pyrolysis together with a transportation of compounds which were usually further pyrolyzed in other reaction condition. Indeed in CDP3L_M the largest amount of Levoglucosan (22.1 %) was found suggesting a low efficiency of pyrolysis.[20-23] Also some acids were present and they might be correlated to plasticizer pyrolysis such as propionic, pentanoic, hexanoic, and benzoic acids. Actually the latter was observed in larger amount (up to 22.2 % in CDP4L_UP) when carbon was the MW absorber suggesting a higher efficiency in pyrolysis for carbon.

Nevertheless acetic acid was probably formed from pyrolysis of polysaccharide as well as Levoglucosan, acetone, and furan derivatives.[24-26]

The pyrolysis efficiency was increased using carbon and the fractionating system, as supported by the increasing amount of lower molecular weight compounds in the middle fraction, such as: acetic acid, 3-buten-1-ol, cyclopentanone, and propylene glycol.

9.2.2.3. FTIR

In Figure 9.13 are reported the FTIR spectra of liquids collected from MAP of CDP. A detailed description of absorption present in each series of liquid fractions is reported in Table 9.5, Table 9.6, and Table 9.7.

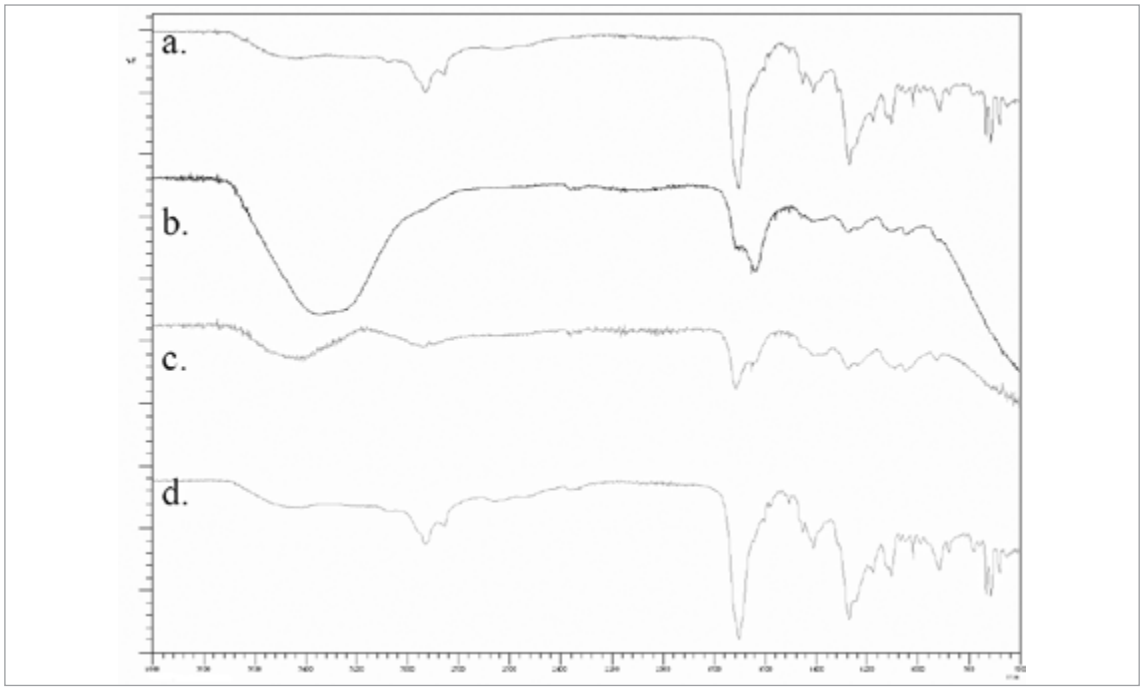

Figure 9.13. FTIR spectra of: a) CDPL1_U; b) CDPL1_M; c) CDP1L_M water subtracted; d) CDP1L_L.

All spectra from the three phases of the same fraction could be perfectly overlapped, and only one of them is reported. Upper fractions showed a broad

band centered at 3500 cm^{-1} of low intensity (Figure 9.13a). Middle fractions showed a strong and wide peak due to water absorption (Figure 9.13b). Pure water spectrum was subtracted to evidence other peaks (Figure 9.13c). Lower fractions showed very close absorption and intensities with respect to the upper fraction confirming the previous hypothesis that this fraction contains the same products of the upper phase but these compounds had a higher molecular weight than those present in upper phase.

Table 9.5. FTIR of liquid from MAP of CDP, upper fractiona.

Frequency *(cm^{-1})*	**Attribution**	**CDP1L_U**	**CDP2L_U**	**CDP3L_U**	**CDP4L_U**	**CDP5L_U**	**CDP6L_U**
3465	H-bonded OH stretching	m	m	m	m	m	m
3078	Aromatic C-H stretching	w	w	w	w	w	w
3030	Alkene C-H stretching	m	m	m	m	m	m
2956/2873	Methyl C-H asym./sym. stretching	m	m	m	m	m	m
2930/2857	Methylene C-H asym./sym. stretching	m	m	m	m	m	m
1701	Carboxylic acid C=O stretching	s	s	s	s	s	s
1642	Alkenyl C=C stretching	w	w	w	w	w	w
1604	Conjugated C=C stretching	w	w	w	w	w	w
1585	Aromatic ring stretching	w	w	w	w	w	w
1452/1380	Methyl C-H asym./sym. bending	m	m	m	m	m	m
1409	Phenol or tertiary alcohol, OH bending	m	m	m	m	m	m
1316; 1270	Primary or secondary alcohol, OH in-plane bending	s	s	s	s	s	s
1250	Aromatic ethers, aryl-O stretching	w	w	w	w	w	w
1178	Aromatic C-H in-plane bending	m	m	m	m	m	m
1120	Tertiary alcohol, C-O stretching	w	w	w	w	w	w
1104	Secondary alcohol, C-O stretching	w	w	w	w	w	w
1048	Primary alcohol, C-O stretching	w	w	w	w	w	w
1018; 990; 966; 959	Aromatic C-H in-plane bending	w	w	w	w	w	w
916; 876; 780	Aromatic C-H out-of-plane bending	w	w	w	w	w	w
732; 714	Methylene $-(CH_2)_n-$ rocking, $n \geq 3$	m	m	m	m	m	m
679	Alcohol, OH out-of-plane bending	m	m	m	m	m	m
651; 639; 618; 603	Alcohol, OH out-of-plane bending	w	w	w	w	w	w

a) Intensity reported as follow: s, strong; m, medium; w, weak; n.d. not detected.

Table 9.6. FTIR of liquid from MAP of CDP, middle fractiona.

Frequency *(cm^{-1})*	Attribution	CDP1L_M	CDP2L_M	CDP3L_M	CDP4L_M	CDP5L_M	CDP6L_M
3441	H-bonded OH stretching	s	s	s	s	s	s
2985/2895	Methyl C-H asym./sym. stretching	m	m	m	m	m	m
2940/2865	Methylene C-H asym./sym. stretching	m	m	m	m	m	m
1714	Ketones and carboxylic acid	s	s	s	s	s	s
1653	Conjugated ketones	w	w	w	w	w	w
1453/1363	Methyl C-H asym./sym. bending	w	w	w	w	w	w
1407	Tertiary alcohol, OH bending	m	m	m	m	m	m
1275	Primary or secondary alcohol, OH in-plane bending	m	m	m	m	m	m
1095	Secondary alcohol, C-O stretching	m	m	m	m	m	m
1050	Primary alcohol, C-O stretching	m	m	m	m	m	m
694	Alcohol, OH out-of-plane bending	m	m	m	m	m	m
651; 639; 618; 603	Alcohol, OH out-of-plane bending	w	w	w	w	w	w

a) Intensity reported as follow: s, strong; m, medium; w, weak; n.d. not detected.

Table 9.7. FTIR of liquid from MAP of CDP, bottom fractiona.

Frequency *(cm^{-1})*	Attribution	CDP1L_L	CDP2L_L	CDP3L_L	CDP4L_L	CDP5L_L	CDP6L_L
3465	H-bonded OH stretching	m	m	m	m	m	m
3078	Aromatic C-H stretching	w	w	w	w	w	w
3030	Alkene C-H stretching	m	m	m	m	m	m
2956/2873	Methyl C-H asym./sym. stretching	m	m	m	m	m	m
2930/2857	Methylene C-H asym./sym. stretching	m	m	m	m	m	m
1701	Carboxylic acid C=O stretching	s	s	s	s	s	s
1642	Alkenyl C=C stretching	w	w	w	w	w	w
1604	Conjugated C=C stretching	w	w	w	w	w	w
1585	Aromatic ring stretching	w	w	w	w	w	w
1452/1380	Methyl C-H asym./sym. bending	m	m	m	m	m	m
1409	Phenol or tertiary alcohol, OH bending	m	m	m	m	m	m
1316; 1270	Primary or secondary alcohol, OH in-plane bending	s	s	s	s	s	s
1250	Aromatic ethers, aryl-O stretching	w	w	w	w	w	w
1178	Aromatic C-H in-plane bending	m	m	m	m	m	m
1120	Tertiary alcohol, C-O stretching	w	w	w	w	w	w
1104	Secondary alcohol, C-O stretching	w	w	w	w	w	w
1048	Primary alcohol, C-O stretching	w	w	w	w	w	w
1018; 990; 966; 959	Aromatic C-H in-plane bending	w	w	w	w	w	w

(continue)

916; 876; 780	Aromatic C-H out-of-plane bending	w	w	w	w	w	w
732; 714	Methylene $-(CH_2)_n-$ rocking, n≥3	m	m	m	m	m	m
679	Alcohol, OH out-of-plane bending	m	m	m	m	m	m
651; 639; 618; 603	Alcohol, OH out-of-plane bending	w	w	w	w	w	w

a) Intensity reported as follow: s, strong; m, medium; w, weak; n.d. not detected

All spectra showed among each series very similar absorption intensities so far there was no a distinction based only on their relative intensities.

These results were in agreement with GC/MS results. The main absorptions were always related to carboxyl, carbonyl, and alcohol functional groups.

9.2.2.4. ^{1}H NMR

^{1}H NMR of upper and lower fractions gave the same spectra with the same peaks and only slightly difference of intensities of each peak. The overlapped spectra of CDP2L_U and CDP2L_L are shown in Figure 9.14.

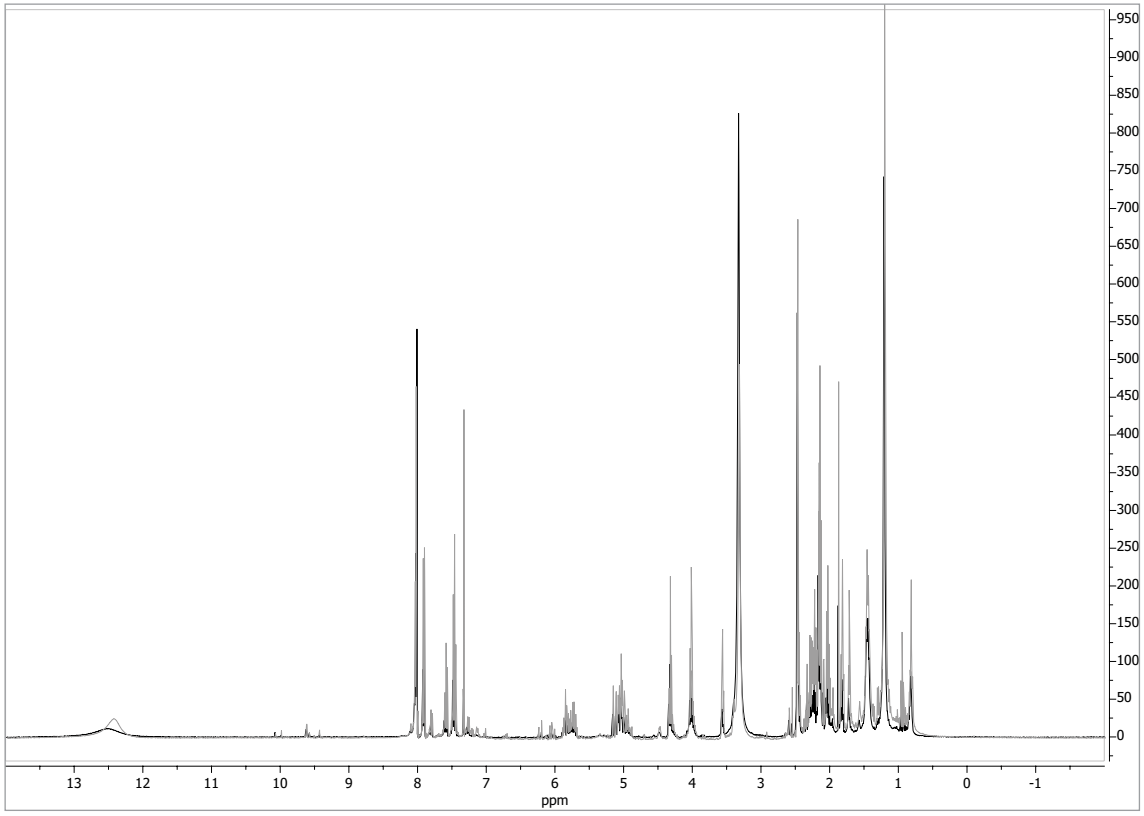

Figure 9.14. ^{1}H NMR spectra of CDP2L_U (gray line) and CDP2L_L (black line).

The main group of signal (central peak) and their attribution are listed as follow together with their attribution and relative intensity (s, strong; m, medium; w, weak):

- 12.45 ppm (w): acids mobile protons.
- 9.60 ppm (w): aldehyde.
- 8.04 and 7.94 ppm (s): aromatic ring, phthalates.

- 7.60, 7.40, and 7.35 ppm (m): aromatic ring.
- 5.80 ppm (w): phenolic OH.
- 5.00 (w), 4.30 (m), and 4.00 ppm (m): CH_2-OOC; or ring-join methylene, Ar-CH_2-Ar
- 3.58 ppm (m): CH_2-O-C.
- 3.34 ppm (s): water
- 2.20 – 2.40 (m) and 2.10 ppm (s): CH_3, CH_2, and CH on aromatic ring.
- 1.80, 1.74, and 1.46 (w), 1.89 (m), and 1.20 ppm (s): CH_2, CH_3 of alkyl groups, CH_3 in β position and CH_2 and CH in γ position to an aromatic ring or ethereal oxygen.
- 0.96 and 0.80 ppm (w): CH_3 of alkyl groups or in γ position or further of an alkyl chain linked to an aromatic ring.

These data were in agreement with both GC/MS and IR analyses confirming the close nature of upper and lower fractions and the wide presence of phthalates and their derivatives.

^{1}H NMR of middle fractions were overwhelmed by the peak of water, however some other absorption were present. The spectra of CDP2L_M is shown in Figure 9.15.

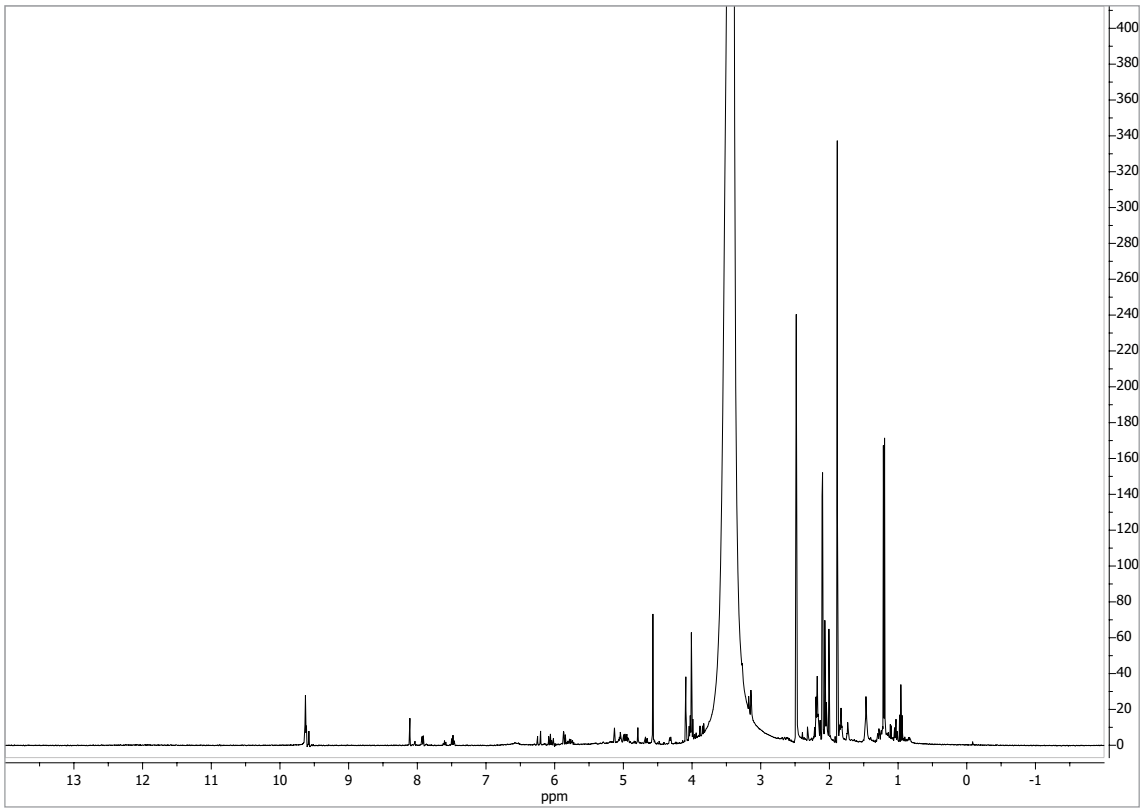

Figure 9.15. ^{1}H NMR spectra of CDP2L_M.

The main group of peaks (central peak) and their attribution are listed together with their attribution and relative intensity (s, strong; m, medium; w, weak):

- 9.60 ppm (m): aldehyde.
- 8.10 (w): aromatic ring, phthalates.
- 6.20 (w), 5.85 (w), 5.10 ppm (w): furan and phenolic OH.
- 4.79 (w) and 4.57 ppm (m):
- 4.00 ppm (m): esters.
- 2.10 ppm (m): alkyl group in β position to an aldehyde.
- 1.46, 1.89, and 1.20 ppm (s): CH_2, CH_3 of alkyl groups, CH_3 in β position and CH_2 and CH in γ position to an aromatic ring or ethereal oxygen.
- 0.96 ppm (s): CH_3 of alkyl groups or in γ position or further of an alkyl chain linked to an aromatic ring.

The peaks reported for middle fractions were close to these present in both upper and lower fractions even with strong differences in intensities. Especially in the range of δ 1.5 - 3.0 ppm the difference were stronger. Middle fractions, rich in water, was able to dissolve alkyl compounds in low extent.

9.2.3. Main achievements

Microwave assisted pyrolysis (MAP) of corn derived plastic bags (CDP) was performed using different MW absorbers (carbon or Fe), apparatus set-up, and MW power, obtaining a liquid and large amount of gas accordingly to the pyrolysis conditions. The main achievements might be summarized in the following key points.

The liquid after spinning was separated in three phases, upper, medium, and lower. Medium fractions were mainly composed of water (70 wt%), acids, alcohols, and anydrosugars and their pyrolysis products. Upper and lower fractions showed close properties and composition except that the lower fraction was a wax. Indeed the lower fraction was composed of oligomers and the upper phase was composed of the pyrolyzed form of these oligomers. The upper fractions contained large amount of aromatic acid and phthalates and their derivatives. Lower fraction was reduced working with set-up B together with an increasing of solid yield.

MAP of CDP might be performed to convert a material intended for compost porpouse into a source of chemicals or even fuel from the upper and lower phases.

Reference

1. Bolm, C.; Legros, J.; Le Paih, J.; Zani, L. Iron-Catalyzed Reactions in Organic Synthesis. *Chemical Reviews* **2004**, 104, 6217-6254.
2. Dongol, K. G.; Koh, H.; Sau, M.; Chai, C. L. L. Iron-Catalysed sp^3–sp^3 Cross-Coupling Reactions of Unactivated Alkyl Halides with Alkyl Grignard Reagents. *Advanced Synthesis & Catalysis* **2007**, 349, 1015-1018.
3. Hayashi, Y.; Shinokubo, H.; Oshima, K. Intramolecular Radical Cyclization of 2-Haloethanal Allyl Acetal and Allyl 2-Halophenyl Ether with a Grignard Reagent in the Presence of Iron(II) Chloride. *Tetrahedron Letters* **1998**, 39, 63-66.
4. Yoo, D.; Kim, D.; Lee, D. Synthesis of lactide from oligomeric PLA: Effects of temperature, pressure, and catalyst. *Macromol. Res.* **2006**, 14, 510-516.
5. Yoo, D.-K.; Kim, D. Production of optically pure poly(lactic acid) from lactic acid. *Polym. Bull.* **2009**, 63, 637-651.
6. Poly(Lactic Acid): Synthesis, Structures, Properties, Processing, and Applications; John Wiley & Sons, Inc.: Canada, 2010.
7. Kopinke, F.-D.; Remmler, M.; Mackenzie, K.; Milder, M.; Wachsen. Thermal decomposition of biodegradable polyesters -II. Poly(lactic acid). *Polym. Degrad. Stabil.* **1996**, 53, 329-342.
8. Mori, T.; Nishida, H.; Shirai, Y.; Endo, T. Effects of chain end structures on pyrolysis of poly(L-lactic acid) containing tin atoms. *Polym. Degrad. Stabil.* **2004**, 84, 243-251.
9. Nishida, H.; Mori, T.; Hoshihara, S.; Fan, Y.; Shirai, Y.; Endo, T. Effect of tin on poly(l-lactic acid) pyrolysis. *Polym. Degrad. Stabil.* **2003**, 81, 515-523.
10. Fan, Y.; Nishida, H.; Mori, T.; Shirai, Y.; Endo, T. Thermal degradation of poly(l-lactide): effect of alkali earth metal oxides for selective l,l-lactide formation. *Polymer* **2004**, 45, 1197-1205.
11. Fan, Y.; Nishida, H.; Shirai, Y.; Endo, T. Racemization on thermal degradation of poly(l-lactide) with calcium salt end structure. *Polym. Degrad. Stabil.* **2003**, 80, 503-511.
12. Fan, Y.; Nishida, H.; Hoshihara, S.; Shirai, Y.; Tokiwa, Y.; Endo, T. Pyrolysis kinetics of poly(l-lactide) with carboxyl and calcium salt end structures. *Polym. Degrad. Stabil.* **2003**, 79, 547-562.
13. Kopinke, F.-D.; Mackenzie, K. Mechanistic aspects of the thermal degradation of poly(lactic acid) and poly(β-hydroxybutyric acid). *J. Anal. Appl. Pyrol.* **1997**, 40-41, 43-53.
14. Undri, A.; Rosi, L.; Frediani, M.; Frediani, P. Upgraded Fuel from Microwave Assisted Pyrolysis of Waste Tire. *Fuel* **2014**, 115, 600-608.
15. Undri, A.; Meini, S.; Rosi, L.; Frediani, M.; Frediani, P. Microwave Pyrolysis of Polymeric Materials: Waste Tires Treatment and Characterization of the Value-Added Products. *J. Anal. Appl. Pyrol.* **2013**, 103, 149-158.
16. Undri, A.; Rosi, L.; Frediani, M.; Frediani, P. Efficient Disposal of Waste Polyolefins through Microwave Assisted Pyrolysis. *Fuel* **2013**, 116, 662-671.
17. Undri, A.; Rosi, L.; Frediani, M.; Frediani, P. Reverse Polymerization of Waste Polystyrene through Microwave Assisted Pyrolysis. *J. Anal. Appl. Pyrol.* **2013**, http://dx.doi.org/doi:10.1016/j.jaap.2013.10.001.
18. Frediani, P.; Rosi, L.; Frediani, M.; Undri, A.; Occhialini, S.; Meini, S. Production Of Hydrocarbons From Pyrolysis of Tyres WO2012110991.
19. Frediani, P.; Rosi, L.; Frediani, M.; Undri, A.; Occhialini, S. Production of Hydrocarbons from Copyrolysis of Plastic and Tyre Material with Microwave

Heating WO2012110990.
20. Miura, M.; Kaga, H.; Yoshida, T.; Ando, K. Microwave pyrolysis of cellulosic materials for the production of anhydrosugars. *J. Wood Sci.* **2001**, 47, 502-506.
21. Lin, Y.-C.; Cho, J.; Tompsett, G. A.; Westmoreland, P. R.; Huber, G. W. Kinetics and Mechanism of Cellulose Pyrolysis. *J. Phys. Chem. C* **2009**, 113, 20097-20107.
22. Ronsse, F.; Bai, X.; Prins, W.; Brown, R. C. Secondary reactions of levoglucosan and char in the fast pyrolysis of cellulose. *Environ. Prog. Sustain. Energy* **2012**, 31, 256-260.
23. Zhang, X.; Yang, W.; Blasiak, W. Kinetics of levoglucosan and formaldehyde formation during cellulose pyrolysis process. *Fuel* **2012**, 96, 383-391.
24. Patwardhan, P. R.; Satrio, J. A.; Brown, R. C.; Shanks, B. H. Product distribution from fast pyrolysis of glucose-based carbohydrates. *J. Anal. Appl. Pyrol.* **2009**, 86, 323-330.
25. Yang, Z.; Liu, X.; Yang, Z.; Zhuang, G.; Bai, Z.; Zhang, H.; Guo, Y. Preparation and formation mechanism of levoglucosan from starch using a tubular furnace pyrolysis reactor. *J. Anal. Appl. Pyrol.* **2013**, 102, 83-88.
26. Gómez-Martínez, D.; Barneto, A. G.; Martínez, I.; Partal, P. Modelling of pyrolysis and combustion of gluten–glycerol-based bioplastics. *Bioresour.Technol.* **2011**, 102, 6246-6253.

Conclusion

Microwave assisted pyrolysis (MAP) was exploited to convert several classes of waste polymers into a solid, a liquid, and a gas product with promising application as sources of chemicals, energy, and power production. The polymeric material tested were: tires, high density poly(ethylene) (HDPE), poly(propylene) (PP), poly(styrene) (PS), multilayer packaging beverage (WMP), wood pellets (WP), poly(lactic acid) (PLA), and corn-derived plastic bags (CDP).

Pyrolysis experiments were carried out in a batch laboratory scale reactor, using a microwave (MW) oven operating at 2.45 GHz, an energy output up to 6KW (set-up A), and for some pyrolysis a fractionating system, directly connected to the pyrolysis oven (set-up B). The presence of a fractionating system minimized the influence of different MW powers enhancing the residence time of the high boiling substances avoiding their stripping from the reactor and usually improving the quality of the liquid product. Pyrolysis were performed in an anoxic atmosphere without any carrier gas, avoiding mass transportation phenomena and increasing the residence time of the gas inside the oven. Furthermore the gas fraction was not diluted by the carrier.

MAP of different waste plastics might be transformed in a gas, a liquid, a solid. The gas fraction was usually constituted by H_2, CO, CO_2 (in some cases) and C1-C4 hydrocarbons. It might be used as energy source. The liquid was mainly constituted by hydrocarbons which might be used as source of chemicals or as a fuel. Finally the solid contained large amount of carbon and might be source of energy or after further transformation as carbon black for tire production or as activated carbon.

MAP of tire might be run without the addition of a MW absorber. The liquid showed a reduced density (from 0.92 to 0.88 g/cm^3), and viscosity (from 3.92 to 1.25 cP) when working with the fractionating system. Furthermore aromatic and olefinic compounds were formed in high amount. Different tire affected the MAP results: Tires containing a large amount of aromatics (styrene copolymers) were pyrolyzed faster than those containing large amount of natural rubber. X-ray diffraction of solid from MAP of tire showed two different crystalline forms of ZnS, spharelite or wurtzite due to the different reaction conditions. Their presence

suggested that tires were heated to a temperature higher than the usually accounted, over 1273 K, at last as hot spot points.

MAP of polyolefins, HDPE, PP, and PS was performed using different MW absorbers (tire, carbon, or Fe) and MW power, obtaining a high quality liquid fraction with tailoring properties. From HDPE a mixture of linear alkanes, the corresponding 1-alkenes, and a very low amount of aromatics was obtained. On the contrary liquids from MAP of PP contained a mixture of methyl branched alkanes and alkenes, some aromatics and dienes. From MAP of PS a clear and low viscosity liquids were always collected together with low amount of gas (3.0 wt %) and solid (0.9 wt %). Using a MW power of 3 KW the styrene in the liquid was increased up to 65.98 %. Tire and carbon could be assimilated to pollutant other than MW absorber, and they did not markedly affect the pyrolyses results, but almost only the products composition if some of these materials might be pyrolyzed. These results let us to affirm that MAP of HDPE, PP, and PS might be performed even when large amount of inorganic and polymeric compounds was present as contaminants.

MAP of WMP might by run with or without a MW absorber, and five products were always collected: char, gas, unscratched Al, and two liquid fractions. The organic liquid phase contained large amount of hydrocarbons, useful as fuel or the source of chemicals. The other liquid phase contained large amount of water and oxygenated organic compounds, such as acetic acid, 2-hydroxypropan-2-one and levoglucosan. Fe promoted a faster pyrolysis than the others MW absorbers, and avoided the formation of large amount of cyclic and aromatic compounds from PE layers. Furthermore Fe let a better pyrolysis of anydrosugars and acids from paper pyrolysis. Pyrolysis time with carbon as MW absorber was higher than using any other absorbers, and is allowed cross reaction between paper and PE degradation products enhancing aromatics formation.

MAP of WP might be run without a MW absorber but the pyrolysis could not be completed. WP were converted into a char which preserved their former shape and a two liquid phases. These latter phases were characterized using an innovative chromatographic methodology. A single sample were prepared for thin layer chromatography, GC, and HPLC analyses. Quantitative analysis of liquid were performed using the relative response factor (RRF) referred to a compound present in the liquid. For the compound identified, but for which a RRF was not available, the RRF was predicted using an innovative formula.

MAP of PLA was performed using different MW absorbers (tire, carbon, or Fe) and MW power, obtaining a liquid rich in lactide (the cyclic dimer of lactic acid) and other oxygenated hydrocarbons. The collected lactide was enantiopure and it was collected, separate, and purified directly from the liquid. Up to 9 wt% of initial PLA was recovered as L-lactide.

MAP of CDP was performed using different MW absorbers (carbon or Fe) and MW power, obtaining a liquid and large amount of gas accordingly to the pyrolysis conditions. The liquid was separated in three phases, upper, medium, and lower. Medium phases were mainly composed of water (70 wt%), acids, alcohols, and anydrosugars and their pyrolysis products. Upper and lower fractions showed close properties and composition except that the lower fraction was a wax. It was composed of oligomers and while the upper phase was composed of the pyrolyzed form of these oligomers. The upper fractions contained large amount of aromatic acid and phthalates and their derivatives.

This MAP process represent a very interesting way to transform a waste or contaminated plastics, otherwise hardly disposable, in the source of chemicals or energy.

Appendix I: Materials and Instruments

All materials used as feed for the microwave assisted pyrolysis and all solvents and reagents employed in this work are herein reported.

I. Tire

Two different tires were investigated in this work (Figure I.I). In Table I.I are reported the characteristics of both.

Figure I.I. Tire *M* and Tire *G*.

Table I.I. Characteristics of tire used in this work.

Brand	Michelin	BFGoodrich
Commercial model	Agilis 81–195/65 R16C	Touring t/a 205/60 R15
Commercial segment	Camping van	Car
ID for this work	Tire *M*	Tire *G*
Ash (wt%)	2.18	2.87
C (wt%)	88.19	87.48
H (wt%)	7.23	7.52
N (wt%)	0.23	0.35
S (wt%)	1.76	1.68

Both tires were chopped to 2 x 2 cm chips before pyrolysis.

II. High density polyethylene (HDPE)

HDPE was recovered from a waste solvent barrel (Figure I.II). It had an ultimate composition of, C: 85.10 %, H: 14.90 %, and ash: 0.02 %. It was chopped to 2 x 2 cm chips prior pyrolysis

Figure I.II. HDPE barrel and chopped HDPE.

III. PP

PP was recovered from a waste barrel (Figure I.III). It had an ultimate composition of, C: 81.35 %, H: 13.60 %, and ash: 5.50 %. It was chopped to 2 x 2 cm chips prior pyrolysis.

Figure I.III. PP barrel and chopped PP.

IV. PS

PS was recovered from waste expanded packaging used for freight of chemicals. It was heated a 388 K to de-foam and chopped it to 2 x 2 cm chips (Figure I.IV). It had an ultimate composition of, C: 92.10 %, H: 7.84 %, and ash: 0.76 %.

Figure I.IV. PS foam and PS chips.

V. PLA

PLA was supplied by NatureWorks LLC in pellets form (Figure I.V) and it was used without any other treatments. It had an ultimate composition of, C: 49.32 %, H: 5.66 %, O: 45.03 %.

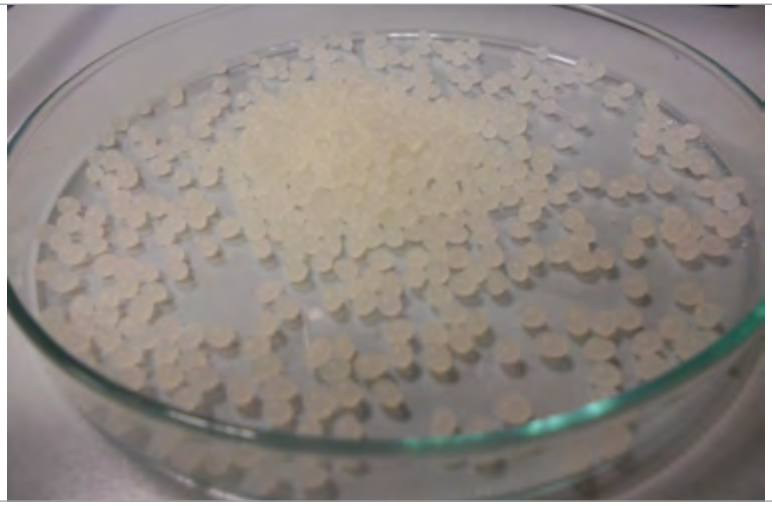

Figure I.V. PLA pellets from NatureWorks LLC.

VI. Wood pellets

WPs were bought in a local store. They were intended for wood stove usage. They were obtained by processing residual sawdust of beech to form 2 cm pellets (Figure I.VI). Their ultimate and proximate analyses are: C 44.81 %, H: 5.87 %, N: 0.59 %, O: 48.74 %; moisture: 8.68 %, volatiles: 80.93 %, fixed carbon: 9.01 %, ash: 1.38 %.

Figure I.VI. WP from beech.

VII. Crop derived plastic

CDP was obtained from shopping bags purchased from a local store (Figure I.VII). They were pyrolyzed as received. Their ultimate and proximate analyses are: C 58.68 %, H: 7.67 %, O: 33.65 %; moisture: 2.09 %, volatiles: 92.52 %, fixed

carbon: 4.50 %, ash: 0.90 %.

Figure I.VII. Shopping bags from CDP.

VIII. Multi-layer packaging

MLP was obtained from waste beverage carton. Bricks were thoroughly washed with demineralized water, dried in a ventilated oven at 373 K for at least 24 h and then chopped in 2 × 2 cm flakes (Figure I.VIII). Proximate analysis was: moisture: 5.25 %, volatiles: 72.46 %, fixed carbon: 15.89 %, ash: 6.40 %.

Figure I.VIII. MLP beverage carton.

IX. Reagents and Solvents

All the solid, liquid, and gas compounds used are listed below:

- Liquid nitrogen: Siad, purity 99.998%, dessicated prior use by flowing it over a column filled with Drierite.
- Drierite: Aldrich, composition 97% di $CaSO_4$ e 3% di $CoCl_2$.
- Hydrogen: Siad, purity 99. 8%.
- Acetone: Prolabio GPR Rectapur, purity 99.5%.
- Silicon oil: Fluka, temperature range 223-473 K.
- Cyclohexane: Aldrich, purity 99.5%.
- Chlorobenzene: Aldrich, purity 99.5%.
- 1,4-dimethylbenzene: Aldrich, purity 99%.
- Toluene: Aldrich, purity 99.5% (distilled over LiAlH4 prior use).
- Benzothiazole: Aldrich, purity 96%.
- 1-Benzothiphene: Aldrich, purity 98% (recrystallized from anhydrous toluene prior use).
- 2,4-Dinitrophenylhydrazine: Aldrich purity 97% (moistened with water).
- Methanol: Aldrich, anhydrous purity 99.8%.
- Sulfuric acid: Aldrich, purity 95%.
- Tetrahydrofuran: VWR international, HPLC grade.
- Hexane: VWR international, HPLC grade.
- 1,1,2,2-Tetrachloroethane-d2: Aldrich, purity 99.5%.
- Chloroform-d: Aldrich, purity 100%.
- Dimethyl sulfoxide-d6: VWR international, purity 100%.
- Acetonitrile: VWR international, HPLC grade.
- Water: VWR international, HPLC grade.
- Formic acid: Fluka, purity 99.8%.

Appendix II: Analytical Methods

All preparation methods for samples collection after any pyrolysis experiment together with all analytical methods employed to characterize and refine samples are herein reported.

I. Sample collection and storage

In the next section are briefly described the sample preparation and storage of the three products always collect in any pyrolysis experiment.

Liquid products were recovered straight after the end of each experiment and transferred into test tube. They were centrifuged at 2000 rpm for 10 min and then filtered to evaluate if any particulate was present. The filtered liquid was stored at 277 K prior any other analysis.

Liquids from MAP of corn derived plastic were three phases liquid. They were centrifuged, separated, and weighted to evaluate the yield in each fraction.

Liquids from MAP of multi-layer packaging were a two phases liquid and separation was achieved by using a separation funnel.

Liquids from MAP of WP were prepared as follow: about 50 mg of each sample were dissolved in AcN (about 1 mL) obtaining a concentration of 50.00 mg/mL. All samples were filtered through a Minispike GHP Acrodisk 13 mm syringe filter 0.2 μm filter Pall Life Sciences before HPLC analysis. No further treatments were employed in sample preparation.

Solid products were recovered directly from the reactor, and then they were milled and homogenized. They were stored in desiccator prior any other analysis. Eventual metal fragment and/or Al foil were removed and stored in plastic bags.

Gas products were collected in a gasometer and analyzed via GC-FID straight after the end of each experiment. Further analyses were performed on sample of gas stored in commercial tedlar gas sampling bags.

II. Density

Density was determined with a pycnometer thermostated at 298.14 K. Approximately 10 cm^3 of liquid were placed and weighted in a 10.01 cm^3 graduated picometer and immersed in a thermosated bath for at least 15 minutes and then

the volume was checked with the referring line.

Density was calculated with the following equation (Eq. II.I):

$$d_{\text{liquid}}^{298} = \frac{m_{liquid}}{V} \qquad \textbf{II.I}$$

Where m_{liquid} was the mass of the liquid placed into the graduated flask, expressed in grams (g); V the volume of graduated flask (10.01 cm^3). Density was reported as g/cm^3.

III. Viscosity

Kinematic viscosity (ASTM method D 2854–00) was detected with an Ostwald viscometer (Figure II.I) thermostated with a Julabo model ME-18V at 298.14 K. Kinematic viscosity was reported in centiPoise (cP).

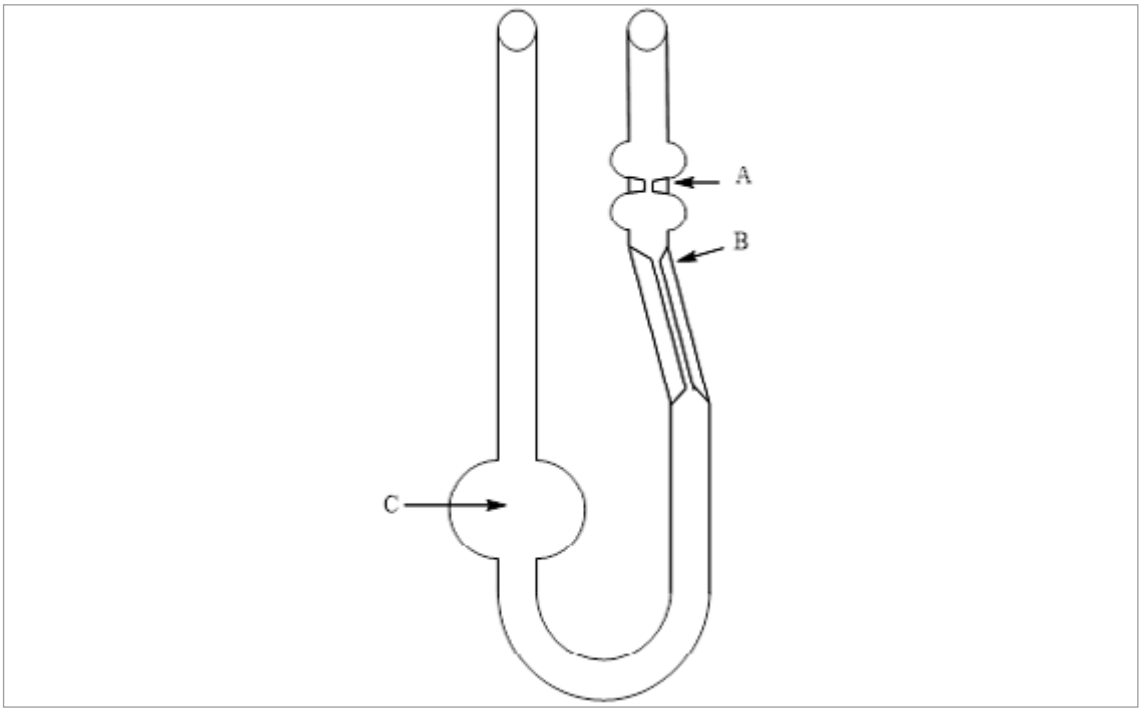

Figure II.I. Ostwald viscometer: a. starting point of measure; b. ending point for measure; c. reservoir.

Viscosity was measured with the following assumptions. The liquid that flowed into the capillary viscometer had a null velocity at walls and maximum in center. The flow rate (Q) could be defined by Eq. II.II:

$$Q = \frac{\partial V}{\partial t} \qquad \textbf{II.II}$$

Using the law of Poiselle it was possible to rewrite Eq. II.II as (Eq. II.III):

$$Q = \frac{4\pi r \Delta p}{8\eta l} \qquad \textbf{II.III}$$

Where Δp, difference of pressure at capillary extremes; l, length of capillary; r, radius of capillary; ν, kinematic viscosity.

From Eq. II.III, Q could be expressed as (Eq. II.IV):

$$V = \int_0^t Q(t)\,dt = \frac{\pi r^4}{8\eta l}\int_0^t \Delta p(t)\,dt \qquad \textbf{II.IV}$$

Where t was the time necessary to the liquid to flow through the capillary. A liquid with known kinematic viscosity could be used as referring standard (Eq. II.V and II.VI):

$$V_1 = \frac{\pi r^4}{8\eta_1 l}\int_0^{t_1} \Delta p_1(t)\,dt \qquad \textbf{II.V}$$

$$V_2 = \frac{\pi r^4}{8\eta_2 l}\int_0^{t_2} \Delta p_2(t)\,dt \qquad \textbf{II.VI}$$

It was possible to merge Eq. II.V and II.VI in Eq. II.VII:

$$\frac{1}{\eta_1}\int_0^{t_1} \Delta p_1(t)\,dt = \frac{1}{\eta_2}\int_0^{t_2} \Delta p_2(t)\,dt \qquad \textbf{II.VII}$$

So far the instantaneous difference in pressure could be expressed as (Eq. II.VIII):

$$\Delta p(t)\,dt = \delta g h(t)\,dt \qquad \textbf{II.VIII}$$

Where h(t) was the instantaneous level difference between the two free areas into the liquid. Eq. II.VIII could be inserted in Eq. II.VII (Eq. II.IX and II.X):

$$\frac{1}{\eta_1}\int_0^{t_1} \delta_1 g h_1(t)\,dt = \frac{1}{\eta_2}\int_0^{t_2} \delta_2 g h_2(t)\,dt \qquad \textbf{II.IX}$$

$$\frac{\delta_1}{\eta_1}\int_0^{t_1} g h_1(t)\,dt = \frac{\delta_2}{\eta_2}\int_0^{t_2} g h_2(t)\,dt \qquad \textbf{II.X}$$

By introducing the average level difference (h_x) Eq. II.X became (Eq. II.XI):

$$\frac{\delta_1}{\eta_1} t_1 \underline{h_1} = \frac{\delta_2}{\eta_2} t_2 \underline{h_2} \qquad \textbf{II.XI}$$

If measures were done in the same way h_1=h_2 and they could be simplified (Eq. II.XII and II.XIII):

$$\frac{\delta_1}{\eta_1} t_1 = \frac{\delta_2}{\eta_2} t_2 \qquad \textbf{II.XII}$$

$$\eta_2 = \frac{\delta_2 t_2}{\delta_1 t_1}\eta_1 \qquad \textbf{II.XIII}$$

Using Eq. II.XIII it was possible to measure the kinematic viscosity of liquids.

10.0±0.01 cm^3 of liquid were introduced into the reservoir. It was taken the time for the liquid to get from point a. to b. in Figure II.I. As referring standards was chosen: Cyclohexane, chlorobenzene and 1,4-dimethylbenzene.[1]

IV. Distillation curve

Distillation curve was tested with a Claisen's flask in nitrogen environment (Figure II.II). Distilled liquid was collected in single neck round bottom flask and after they were stored at 260 K after weighting. Distillation was performed at atmospheric and reduced pressure (1300 Pa) in order to test the largest range of temperature.

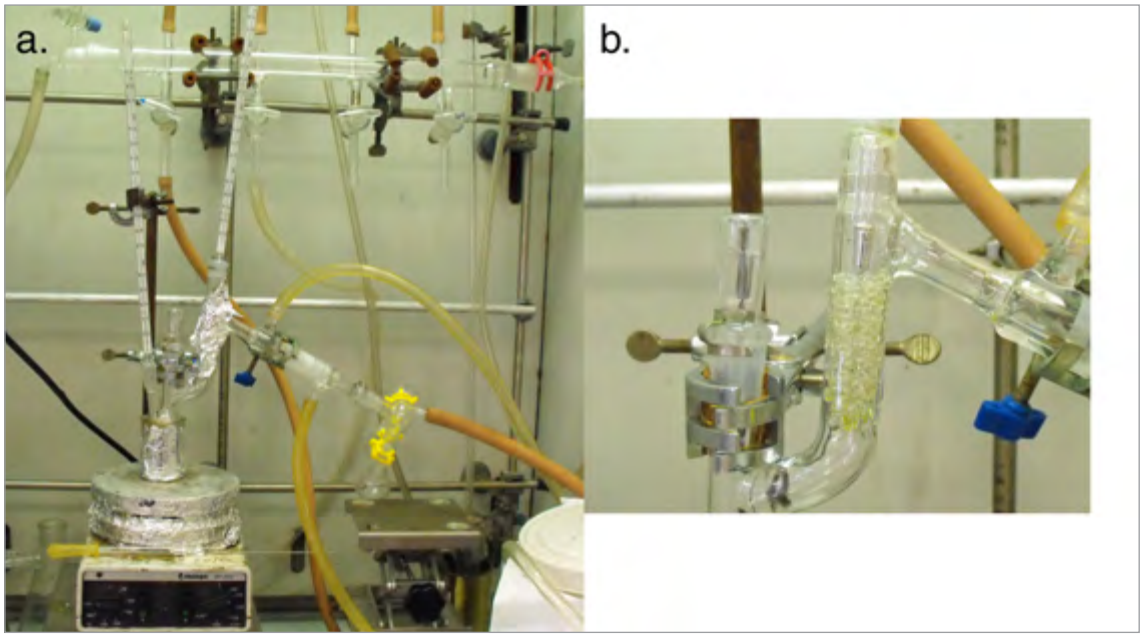

Figure II.II. a. Claisen's flask; b. detail of Claisen's flask distillation head.

V. Ultimate analysis

CHN analysis was performed using a Perkin-Elmer CHNS/O Analyzer model 2400 Series II. Sulfur content was evaluated through a calorimetric bomb, see Section VI.

VI. Calorific values

Higher heating values (HHV), for liquid, and gross calorific value (GCV), for solids, together with sulfur content of the products were detected by an external laboratory, ESSE.TI.A. srl, (Via dell'arte della paglia 3, Campi Bisenzio, Italy) using a homemade adiabatic bomb calorimeter.

LCV was calculated taking into account GCV and ultimate analysis. Lower heating value (LHV), for liquid, and lower calorific value (LCV), for solid were calculated taking into account HHV or GCV and ultimate analysis using the following Equation (Eq.):

$$LHV \cong HHV - 2500Kj / Kg\left(U + 9H\right) \qquad \textbf{II.XIV}$$

Where: 2500 kj/kg was the ΔH for water evaporation; W, water content of the sample; H hydrogen content of the sample.

VII. Thin layer chromatography

Thin layer chromatography (TLC silica gel 60 F254) plates were from EMD. They were cut in 10 × 20 cm and 3 drops for each solution of sample was spotted on the plates. Two solvent mixtures were used: MeOH, AcN, and H2O (6:3:1); CH_2Cl_2 and MeOH (9:1). TLC chromatograms were examined under daylight and UV light, longwave (365 nm) and shortwave (254 nm).

VIII. GC/MS

Gas chromatographic analyses were performed using a Shimadzu GC/MS QP5050A equipped with a capillary column Petrocol™ DH 24160-U, (100 m length, 0.25 mm diameter, 0.5 μm stationary phase, max temperature 593 K) using a 1:30 split ratio and a quadrupole mass (MS) detector, with an electron impact ions generator, operating in the mass range 40–450 m/z. The oven operated at 298 K for 15 min, then heated at 2.5 K/min up to 523 K and kept at this temperature for 15 min. For liquids from MAP of HDPE this latter hold time was 180 min. Other noteworthy peaks were not detected working at higher temperature. Total ion chromatography (TIC) was obtained with a signal/noise ratio of five, and composition was reported without any response factors correction. Compounds were identified using the NIST mass spectral library and commercial standards for selected compounds.

Liquids obtained from pyrolysis of WP where performed using a Shimadzu GC-2010 equipped with a capillary column Agilent DB-5MS, (30 m length, 0.25 mm diameter, 0.25 μm stationary phase, max temp 598 K) using a 1:25 split ratio, injected volume 1 μL. The oven operated at 303 K for 5 min, then heated at 5 K/min up to 553 K and kept at this temperature for 2 min, total run 55 min. Pressure was hold at 100 kPa with a column flow of 1.78 mL/min, and a total flow of 49.3 mL/min. The injection port and the interfaces were kept at 523 K. Two detectors were employed: a Shimadzu QP2010S quadrupole mass (MS) detector, with an electron impact ions generator with a voltage of 0.85 kV, operating in the mass range 35 – 650 m/z, scan speed 1428; and a flame ionization detector (FID) operating at 579 K.

Autotuning conditions: sensitivity adjustment over mass target of 264 m/z; adjustment of resolution with full width at half maximum of target mass of 0.6.

Compounds were identified using the NIST 05 mass spectral library when standards were not available.

IX. GC/FID and GC/TCD

Gas chromatographic analyses of gas product were performed using two different instruments equipped with a flame ionization detector (FID) or a thermal conductivity detector (TCD). The GC-FID analysis was carried out with a Shimadzu GC-2010 working with a capillary column Supelco SPB-5 (60 m length, 0.25 μm stationary phase, 0.25 mm diameter, column flow 0.98 mL/min.) The sample was injected using a 1:30 split ratio. The GC operated at 308 K for 20 min. The gaseous components were identified using pure standards. GC-TCD analysis was performed with a GC-HP model working with a capillary column Supelco Carbonex 1010 (30 m length, 0.53 mm diameter). The sample was injected using

a 1:30 split ratio. The GC operated at 308 K for 45 min. The quantitative analyses of gases were performed using a reference standard calibration curve obtained with standard gas mixtures at different concentrations.

X. FTIR

Infrared (FTIR) analyses were performed with a Shimadzu modelIRAffinity-1 (Figure II.III), using two methodologies. A transmission technique only for solid samples (using KBr disk) or a diamond Golden Gate single reflection attenuated total reflectance (ATR) accessory supplied by Specac. For FTIR-ATR spectra samples were directly placed on the diamond surface without any pretreatments.

Figure II.III. Shimadzu modelIRAffinity^{-1}.

XI. ICP/MS

Ion coupled plasma-mass spectroscopy (ICP-MS) analyses were determined by an external laboratory, Eureka srl, (Italy) using a MW mineralizer CEM Mars Xpress and ICP-MS Thermo Xseries2. Silicon was not quantified. Solid samples were not pretreated.

XII. NMR

^{1}H NMR spectra were recorded with an NMR Varian VXR 200, using various deuterated solvents accordingly to the investigated liquid. 1,1,2,2-tetrachloroethane-d_2 ($C_2Cl_4D_2$) was employed for tire derived liquid. Chloroform-d ($CDCl_3$) was employed for all liquids from synthetic polymer. Dimethyl sulfoxide-d_6 (C_2D_6SO, DMSO) was employed for liquids from wood and paper pyrolysis.

Hydrogen of the solvent was employed as internal standard and spectra were referred to TMS.

Water content in wood and paper derived liquid was evaluated by standard addition method. Three spectra were recorded for each tube: pure solvent; solvent plus weighted amount of sample; solvent, plus weighted amount of sample and

distilled water. Areas in each set of three spectra were calculated using the area of residual hydrogen of solvent as reference.

XIII. HPLC/MS

High performance liquid chromatography was performed with a Thermo Scientific LTQ Orbitrap Discovery MS 2.5.5, autosampler Accela AS 2.2.1, and pump Accela pump 1.04.05, equipped with a Thermo Scienctific column Syncronis C18, length 50 mm, I.D. 2.1 mm, and particle size 1.7 μm. A gradient technique was used at room temperature, solvent A AcN acidified with 0.1 vol% formic acid; solvent B water acidified with 0.1 vol% formic acid. Flow rate 0.3 mL/min. Initially solvent A was 5 vol %, increasing to 15 vol% at 1 min, increasing to 20 vol% at 8 min, increasing to 50 vol% at 10 min, increasing to 80 vol% at 13 min, decreasing to 5 vol% at 15 min, followed by 1 min of isocratic elution with 5% of solvent B (total eluition time 16 min).

LTQ Orbitrap MS was equipped with an ESI source operating in positive and negative ionization mode using the following operating parameters: electrospray voltage 3.1 kV, sheath gas flow rate 8 abu, auxiliary gas flow rate 1 abu, capillary temperature 543 K, capillary voltage -49.00 V, tube lens offset -148.43 V. Instrument calibration was performed externally prior to each sequence with a calibration solution: Thermo Scientic Pierce LTQ Velos ESI positive ion and ESI negative calibration solution. Accurate mass spectra of $[M+H]^+$ and $[M-H]^-$ ions were recorded from 100 to 1000 m/z, the mass resolution power of the mass analyzer was set to 30,000 (m/Δm). Nitrogen (99.95%) was used as sheath gas, aux gas and served as the collision gas in the HCD cell and the bath gas in the C-trap.

XIV. Proximate analysis

Moisture content was evaluated by heating weighted solid samples at 378 K for 4 hours.

Volatiles were evaluated by the weight loss after heating samples at 623 K under a reduced pressure of 80 Pa for 5h and in a stop up crucible at 900 K in a muffle furnace for 6 minutes.

Ash content was detected according to ASTM D 2866 – 94 method. Samples were placed in a crucible into a muffle furnace at 900 K (temperature reached in 4 hours) for 4 hours.

Fixed carbon was evaluated by difference using the following Equation (Eq. II.XV):

$$Fixed\ carbon = 100 - \left(M + V + A\right) \qquad \textbf{II.XV}$$

Where M, was the wt% of moisture; V, was the wt% of volatiles; A, was the wt% of ash.

XV. Apparent density of char

Apparent density was measured following the ASTM D 2854 – 00 method. Finely milled char were packed in a wide mouthed graduated cylinder by using a vibrating plate.

XVI. BET

Surface area of char samples (BET) was determined by isotherm nitrogen adsorption at 77 K using a Coulter SA3100 instrument. The BET area was evaluated either on collected samples or sample and degassed at 623 K, under a reduced pressure of 80 Pa for 5h. BJH method was used to provide information on the porous structure of char.

XVII. ESEM-EDX

Surface physical morphology and surface microanalyses were detected using an environmental scanning electron microscopy, ESEM Quanta-200 FEI, equipped with an X-ray energy dispersive spectroscopy (X-EDS) for microanalysis. Samples (granules of 0.3 – 0.5 mm) were mounted on a carbon tape and transferred into the analysis chamber; images and spectra were collected under reduced pressure (133 Pa).

XVIII. Powder XRD

X ray diffraction analysis was carried out using a PANalytical diffractometer X'Pert PRO with radiation $CuK_{\alpha 1}$= 1.545 Å, operating at 40 KV, 30 mA, 2θ range 3-120°, equipped with X'Celerator RTMS (Real Time Multiple Strip) X-ray detection technology, an High Score data acquisition and interpretation software. A zero background sample holder was used. Crystalline phases were identified using the ICDD database.[2]

XIX. Hydrodesulfurization

Hydrodesulfurization process was carried out in a 150 mL stainless steel Parr autoclave electrically heated (±1 K). The experiments were performed in H_2. The autoclave was loaded with the solid catalyst prior closing it in nitrogen flow to avoid oxygen presence during HDS process. Then vacuum was made into the autoclave to facilitate the introduction of the solution. The solution to be treated was prepared in a Schlenk tube in N_2 environment and then transferred into the autoclave.

The gas chromatographic analyses of liquids were performed using a Shimadzu GC MS QP5050A previuosly reported (Section VIII) using a 1:30 split ratio, a injection temperature of 523 K, and a quadrupole mass (MS) detector with electron ionization, operating in the mass range 40–450 m/z. The oven operated at 308

K for 15 min, then heated at 2.5 K/min up to 190 K. Other significative peaks were not detected at higher temperature. The total ion chromatography (TIC) was obtained with a signal-noise ratio of five, and the area percentage was reported without any response factors correction. The compounds were identified using the NIST mass spectra library.

The gas chromatographic analyses of liquids were also performed using a Shimadzu GC 2010 (Section IX) using helium as carrier gas, a 1:30 split ratio, injection port temperature of 563 K. The oven operated at 313 K for 10 min, then heated at 6 K/min up to 553 K.

XX. Chemical trapping of gas

Gas were bubbled in a solution of 2,4-dinitrophenylhydrazine (DNPH) for the qualitative analysis of aldehydes and ketones. About 1 g of moistened DNPH was placed in a gas-washing bottle, and then 200 mL of MeOH was added. While stirring 1 mL of H_2SO_4 was added drop-by-drop. The precipitate was recovered over a Buchner funnel and washed with MeOH, and then dried. Solid obtained were analyzed through ^1H NMR.

CO_2 in gas of pyrolysis was trapped in a 1M NaOH solution, and at the end of the experiment the residual NaOH was volumetrically titrated with a HCl solution.

Reference

1. Haynes, W. M., CRC Handbook of Chemistry and Physics. CRC Pr Inc: Colorado, USA, 2011.
2. The International Centre for Diffraction Data. http://www.icdd.com/ (Accessed: 15.03.2013).

Appendix III: Abbreviation

Abbreviation	
ABS	Acrylonitrile-butadiene-styrene
acac	Acetylacetonate
ASR	Automotive shredder residue
ATR	Attenuated total reflectance
BPA	2,2-bis(4-hydroxyphenyl)propane *or* Bisphenol A
BPA-PC	2,2-bis(4-hydroxyphenyl)propane poly(carbonate) *or* Bisphenol A poly(carbonate)
BT	Benzo[b]thiophene
BTZ	Benzothiazole
E	Electric field strength inside the material
ELV	End-of-life vehicles
EN	European Norm
EPS	Expanded Poly(styrene)
FID	Flame ionization detector
FTIR	Fourier transform infrared spectroscopy
GC	Gas chromatography
HDPE	High Density Poly(ethylene)
HDS	Hydrodesulfurization
HPLC	High performance liquid chromatography
L	Penetration depth
LDPE	Low Density Poly(ethylene)
LLDPE	Linear Low Density Poly(ethylene)
MAP	Microwave assisted pyrolysis
MLP	Multi-layer packaging
M_n	Number average molar mass
MS	Mass detector
M_w	Weight average molar mass
MW	Microwave
P	Power of heating
PAH	Polycyclic aromatic hydrocarbons

PC	Poly(carbonate)
PE	Poly(ethylene)
PET	Poly(ethylene terephthalate)
PLA	Poly(lactic acid)
PP	Poly(propylene)
PS	Poly(styrene)
PSD	Pore surface distribution
PUR	Poly(urethane)
PVC	Poly(vinylchloride)
PVD	Pore volume distribution
R	Reflected power
ROP	Ring opening polymerization
tan δ	Loss tangent
TCD	Thermal conductivity detector
t_g	Glass transition temperature
TGA	Thermal gravimetric analysis
THF	Tetrahydrofuran
TLC	Thin layer chromatography
VT	Total pore volume
WEEE	waste electric and electronic equipment
ε_0	Permittivity of free space
σ	Effective high-frequency conductivity
ε	Dielectric permittivity